

## 7.1 INTRODUCTION: FOUNDATIONS OF SATELLITE GEODESY AND THE CREATION OF WORLDWIDE GEODETIC REFERENCE SYSTEMS

### 7.1.1 Geometric and Geophysical Aspects in Satellite Geodesy

Artificial satellites in close-to-Earth orbits have contributed to the field of geodesy a new technique which, theoretically speaking, is capable of completely reorienting the methods and procedures of the geodetic discipline. Application of newly developed methods of precision measurements in satellite triangulation confirm early predictions of a reformation in the domain of classical geodetic field operations (Schmid, 1966a).

Without entering here into questions concerning the dividing line between geodesy and geophysics, it can be stated that the fundamental problem of geodesy is the mathematical description of the Earth's gravity field together with the determination of the geometry of the physical surface of the Earth, with unambiguous correspondence between the Earth-fixed coordinate systems or datums and the spherical coordinate system for a given epoch that serves as reference frame for metric astronomy. With satellite geodesy it is possible to find a solution to the fundamental problem on a synoptical basis, i.e., with reference to the whole Earth. Furthermore, triangulation with satellites, in conjunction with position and time determinations of satellite orbits, eventually provides the necessary link between the geometric and geophysical measuring concepts of geodesy.

Thus, with the aid of satellite geodesy it becomes possible to undertake the geometric description of the surface and the analytical description of the gravity field of the earth by means of worldwide measuring systems and to derive results in the form of three-dimensional models based on a minimum of a priori hypotheses.

These mathematical models then represent the frame of reference into which one can fit the existing geodetic results from the various local datums, as well as all geodetic measurements to be executed in the future. The relevant necessary adjustment should not confine itself to the limited, in practice, classical concept of the treatment of accidental errors, but must, with the aid of a generalization of the Gaussian algorithm, take advantage of the increasing knowledge derived from interdisciplinary research sources concerning the various geophysical parameters involved, with a meaningful inclusion of the corresponding covariance matrices.

From a formalistic mathematical point of view, the significance of artificial satellites for geodesy consists of the ability to express the time-position curve of the orbit of a close-to-Earth satellite in terms of functions of certain parameters, which give in turn information concerning geometric and geophysical properties of the earth and its surrounding space. In this development, the quantities describing the gravitational field are of prime importance to gravimetry; the remainder of the geophysical forces affecting the orbit or arising from the satellite itself are treated as perturbation sources.

The quantitative determination of the parameters appearing in the mathematical simulation of the satellite orbits is accomplished by setting up observation equations which functionally relate the measurements made for the orbit determination with the parameters describing the orbit. It is then apparent that, in addition to these orbital parameters, these equations will involve the position coordinates of the Earth-fixed observation stations which, in the geophysical content of the problem, represent the position of these stations relative to the Earth's mass center. If there is a sufficiently large number of observations, optimally distributed, it is possible to determine from the corresponding

adjustment not only the geophysical parameters affecting the orbit, but also the geocentric parameters of the observing stations. Thus presents itself the opportunity of a simultaneous solution of the geometric and gravimetric problems of geodesy in a worldwide frame.

This, from a purely theoretical standpoint, attractive train of thought has found great appeal, among astronomers and geophysicists in particular, and has already led to impressive results and new insights (Kozai, 1966a). Being more intimately connected with triangulation measurements proper, however, the measurement engineer and, in particular, the practicing geodesist will have certain reservations, based on the fact that the relatively large number of parameters appearing in the complex system of equations of such an adjustment are all more or less strongly correlated. In direct consequence of the simultaneous solution there exists, first of all, correlation among the various parameters of the same type, e.g., the coefficients of the harmonic functions describing the gravity field. In addition, statistical dependence exists between the gravimetric quantities and the geophysical parameters introduced to describe certain orbital perturbations. And, of course, the coordinates of the observing stations introduced into the solution and adjusted together with the other parameters are not only correlated among themselves but also with these nongeometric quantities. In practice, the number of observations, as well as their distribution in time and space, leaves much to be desired, which only serves to amplify these correlations.

Even when—as a consequence of using a larger capacity electronic computer—it is possible to unite a very large number of observations in a single solution, it may be that the geometry of the observing stations obtained from such a solution does not necessarily represent the actual spatial relations. Although the computed parameters in their entirety are well suited to describe, within the limits of accuracy of the original observations, the geometry of the satellite orbits, the possibility nevertheless exists that an iso-

lated group of such parameters (for example, the station coordinates) may have only limited accuracy. Their significance must be judged in the light of the underlying geophysical and astronomical hypotheses. In short, the geometry of the observation stations is prejudiced by the specific properties of the mathematical model chosen to simulate the geophysical-dynamic nature of the satellite orbit.

This in no way lessens the significance of the geophysical solution. On the contrary, dynamic satellite geodesy gains thereby. Once the three-dimensional geometry of a sufficiently large number of points of the Earth's surface has been established with a purely geometric solution, based only on Euclidean (flat space) geometry and the right ascension-declination system of metric astronomy, orbital observations from these stations can be used for the exclusive purpose of determining geophysical parameters. Such a system will be relieved of the problem of computing station coordinates in the adjustment.

Thus, the number of unknowns to be determined from a given available set of observations is reduced—in itself a desirable objective—and, in addition, correlation is eliminated between the geometry and the geophysics, at least with respect to the station coordinates and the orbital elements.

Given the results of the geometric solution, the opportunity presents itself, by way of a purely geometric orbit determination, to ascertain the geometrical shape of the surface of the oceans by applying laser and radar techniques to measure the distances between the satellite and the ocean surface. The influence of weather and tides on the measured profiles can be eliminated with measurements over a sufficiently long period of time. This would not only help to complete the presentation of the geometry of the physical surface of the Earth, but would also give a purely geometric, hence unconstrained by hypothesis, representation of a large portion of a surface which, though not quite rigorously, is a very good approximation to the geoid. The objection that with the preceding com-

ments concerning a purely geometric solution the information content of the dynamic solution is not completely exhausted, can be countered by seeing the eventual solution of the problem of satellite geodesy as a combination of the separate, individual geometric and dynamic solutions. In such a solution the station coordinates will no longer be treated as free variables for the dynamic solution, but will be introduced from the geometric adjustment together with their associated covariances.

This will be the real contribution of satellite geodesy to the principal geodetic mission. The problems of describing the Earth's gravity field and determining the geometry of the physical surface are solved in a consistent formulation; optimal results from a geophysical hypothetical as well as a metrological standpoint are yielded, the geometric and geophysical concepts mutually supporting each other. The amalgamation of the outputs of geometric and dynamic satellite geodesy must in the end be consummated, from the theoretical as well as the practical standpoint, by the inclusion of geodetic data measured on the surface of the Earth. This requirement seems necessary because, although the significant contribution of satellite geodesy to physical geodesy has been to open up the third dimension in the investigation of the Earth's gravity field, the fact still remains that the essential tasks of geodesy are the determination of the geometry of the physical surface of the Earth and the representation of the gravity field in detail and relatively close to the crust (Kaula, 1967a).

### **7.1.2 Development and Organization of a Geodetic Satellite Program for Creating a Worldwide Geodetic Reference System**

The history of satellite geodesy and its theoretical development began with the implementation of an idea that had been for decades an intermediary goal for scientists concerned with rocket development: to increase the cutoff velocity of the rocket to the point where it goes into orbit around the Earth.

The realization of this technical goal with the launch of the first Russian and, shortly thereafter, of the first American artificial satellite created renewed interest among experts in the fields of astronomy and aeronomy in the theoretical problems concerned with the description of the track of a body of small weight orbiting around an oblate mass, specifically around the Earth. The classical theories and procedures of physical geodesy being inadequate to the solution of all these problems, it has become the practice to apply almost exclusively the classical principles of celestial mechanics together with theories and results from the fields of aeronomy and related geosciences, which with the aid of rocket experiments have already made considerable advances in their studies on the subject.

This development explains the dominating influence of dynamic satellite geodesy to this day, reflected also in the planning and execution of the first American geodetic satellite program. The basic requirement for the satellite launched in the first American geodetic experiment, known as ANNA, and for the subsequent GEOS satellite program was compact construction and rotation-symmetric form to the highest possible degree. The resulting mass to cross-section ratio was designed to minimize the perturbing influence of the atmosphere and other geophysical forces, such as solar radiation pressure, in order not to complicate unnecessarily the adjustment of the orbit relative to the gravitational field.

In order to be able to sense the essential components of the Earth's gravitational field while keeping perturbing influences within bounds, a problem intimately connected with that of assuring the satellite a sufficiently long lifetime, the necessary experiments were executed at heights of 1000 to 1600 km above the Earth, and the nearly circular orbits were distributed over as wide a band of inclination as possible. The equipment for this type of satellite was characteristic of its purpose, the instruments on the satellite allowing, when operated together with instruments on the Earth's surface, measurements of the satel-

lite distance and direction, and the difference in distance to the satellite at two points in its orbit (or equivalently, the frequency of radio waves received from the satellite; see chs. 2 and 5 and sec. 7.2 of this chapter).

It is apparent that, viewed in the light of the present state of development, dynamic satellite geodesy in general faces two complexes of questions requiring further study in the planning for future geodetic satellite projects. From the theoretical side, for one, the question arises: To what extent are the concepts derived from classical celestial mechanics and applicable to spherical fields valid in the immediate vicinity of an oblate spheroidal mass? Of perhaps even greater significance are the questions regarding the validity of our concepts with respect to the various geophysical forces other than gravity that influence the orbit of an Earth satellite. So far as practical measuring techniques are concerned (assuming proper professional use of the equipment), there is little left to be desired with respect to data density and precision (internal accuracy) of data obtained by means of Doppler shift in radio frequency. However, even when care in the necessary time and spatial distribution of the measurements is exercised, there remains sufficient reason to suspect that even today occasional systematic errors creep in, not so much as the result of lack of reliability in the equipment but as of uncertainties in the corrections that are necessary to transform the velocity of light in vacuo into the wave propagation velocity existing at the time of observation. The frequencies in use at the present are particularly affected by periodic changes in the ionosphere.

The possibility of calibrating frequency-measuring equipment by comparison with data from laser-type DME, by way of position and time determination, offers little hope in a long-term program, if only for sighting reasons. Particularly ineffective in this connection have been the unsuccessful attempts to initiate an efficient and sufficiently extensive calibration program in which all the measuring methods to be used are systematically examined under typical observation con-

ditions by simultaneous orbit observations from previously and precisely surveyed observation sites. The method followed at present of judging the metric accuracy of the various procedures from the internal accuracy of, at times, very arbitrarily selected series of observations, or at any rate of deriving absolute accuracy from the differences between end results of measuring systems quite different in the techniques used in measuring and adjusting, is unsatisfactory for the metrological engineer in general and the geodesist in particular (see ch. 1).

In addition to the previously mentioned GEOS satellites, serving primarily the purposes of dynamic satellite geodesy, a balloon-type satellite (PAGEOS) was used exclusively for the purpose of geometric satellite triangulation within the framework of the NGSP (see ch. 5). The balloon, with a 30-meter diameter, is similar in material and construction to the balloon satellite ECHO-1 and has a casing 0.013 mm thick that specularly reflects sunlight, unlike the ECHO-2 satellite, whose somewhat thicker casing has a more diffusely reflecting surface. PAGEOS (passive geodetic satellite) was launched 23 June 1966, in a nearly circular, nearly polar orbit at a height of about 4200 km above the earth. With the launching was established an elevated target suitable for worldwide satellite triangulation. The U. S. Coast and Geodetic Survey (later the National Ocean Survey within the National Oceanic and Atmospheric Administration), together with National Aeronautics and Space Administration and the Department of Defense, set up a worldwide network of tracking stations to take advantage of PAGEOS. The coordinates of the stations are given in table 1.28; the network is shown graphically in figure 1.2 of chapter 1.

The compromise in the distribution of the stations necessitated by logistic and political considerations represents a good approximation to an optimal solution. The open mesh in the South Pacific Ocean is due to a lack of any kind of island, whereas the open space over central Asia obviously results from a political situation.

The triangulation method based on photogrammetric principles will be described in detail in section 7.4.

## 7.2 INSTRUMENTATION

### 7.2.1 Photogrammetric Camera

#### 7.2.1.1 General

The techniques used in the measurement of rocket trajectories, particularly because of their high accuracy requirements, had an early influence on the development of photogrammetric data acquisition and evaluation instrumentation. Characteristic in this field of application is the necessity to combine a great number of observations in a single photograph in which each individual observation is generally registered very accurately against a time or frequency standard. Consequently, there is a requirement on the photogrammetric instrumentation for great stability over extended periods of observation. This requirement led to the development of the so-called ballistic camera, which, on the whole, is based on the phototheodolite of terrestrial photogrammetry. In order to adapt the instruments to the unorthodox requirements of the geometry encountered in tracking rocket trajectories and at the same time increase the accuracy of the direction determination, cameras were developed that could be arbitrarily oriented and that had objectives with long focal lengths. A corresponding decrease in viewing angle is inevitable because of practical limitations on the size of the plate. Exact elements of exterior orientation are obtained with the use of elements from the classical geodetic angle-measuring instruments, such as precision spindles, circles, and hypersensitive levels.

The development of instrumentation reflecting these concepts reached a high point in the 1940's with the Askania phototheodolite (Lacman, 1950). This camera had a 370-mm focal length,  $f/5.5$ , 13- by 18-cm plate format, and a synchronous drive for the rotary shutters, producing 1.5, 3, 6, and 12 exposures per second with a synchronization

accuracy of  $10^{-3}$  sec. In addition, a louver shutter was available to block out certain exposures in the sequence or to generate time-related star trails. The horizontal and vertical circles could be set to within  $3''$ .

These instruments were used in Peenemünde for measuring the V-2 trajectory up to the point of engine cutoff. On the resumption of similar projects in the United States after 1945, interest in photogrammetric precision metrology faded because of, as it turned out, too-optimistic expectations from electronic approaches to the problem of trajectory measurements. When it became apparent that neither these electronic approaches nor the capability of the cinetheodolite could do justice to the developing rocket technique, the author had the opportunity, in connection with his assigned duties at the Ballistic Research Laboratories of the Aberdeen Proving Ground, Maryland, to initiate plans for improved precision theodolites, resulting, with the active and sympathetic cooperation of the Swiss firm Wild-Heerbrugg, in today's well-known BC-4 phototheodolite system. At the time, the experience gained in the various fields of experimentation created a demand for the development of a series of cameras with different angles of view, to be used interchangeably to a great extent on the same mount. In addition to the necessary variation in picture sequence over a wide range, the requirement for maximum accuracy in exposure synchronization was considered of utmost importance. The development of the complete system stretched out over a period of 10 years, and the general concept is described in Schmid (1962). The technical details of the BC-4 phototheodolite are explained in the literature of Wild-Heerbrugg.

In the early 1960's the idea of applying the photogrammetric technique for geometric satellite triangulation to the establishment of a continental net began to be seriously considered (U.S. Department of Commerce, 1965). The technical requirements for such a project differ from those of conventional trajectory mensuration in that first, the exterior orientation of the camera is not deter-

mined with graduated circles, but is determined from the photogram itself on the basis of the photographed control points (star images), and second, the unusually high accuracy demands require that the parameters needed for the reconstruction of the photogrammetric bundle (the generalized model of interior orientation) be recomputed for each individual plate. This makes it necessary to effect a compromise between focal length (increase of intrinsic accuracy) and a field of view large enough to enable the observer to record a sufficient number of available catalogued stars in any portion of the sky. Absolute synchronization between the widely separated stations is complicated, actually impossible in theory, in view of the unknown light travel time at the instant of observation. Hence, in satellite triangulation it is merely necessary to record the instants of satellite observation very accurately (to at least  $10^{-4}$  sec) against the frequency standard at each station. However, the station clocks (frequency standards) must be calibrated with respect to a basically arbitrary but uniquely defined time sequence. Synchronization of the clocks to within about  $10^{-5}$  sec is attained by periodic comparison at all stations with a traveling calibration clock, which in turn is compared at regular intervals with an atomic standard (e.g., that of the U.S. Naval Observatory). Stations with limited accessibility are additionally equipped with a cesium standard. The transmission, via satellites, of time signals for clock comparisons has proved quite satisfactory, with accuracies of from  $\pm 2$  to  $\pm 10$   $\mu$ sec, depending on the electronic equipment available at the receiving station. These procedures assure the elimination of the error source due to uncertainties in the propagation of light and reduce all other timing errors below the overall error level of the system. All other residual errors can therefore be neglected in the adjustment.

E. A. Taylor describes the BC-4 installation as modified to the specifications of the U.S. Coast and Geodetic Survey from the original missile trajectory instrumentation. The present BC-4 phototheodolite differs from the installation described by E. A. Tay-

lor mainly in the optic now in use, a special objective designed by Dr. Bertele and constructed by the Wild-Heerbrugg Co., which, taking all theoretical and practical considerations into account, represents an optimal solution for satellite triangulation. The Cosmotar objective has a focal length of 450 mm with a relative opening of 1:3.4, its chief advantage lying in the fact that it has minimal change of radial distortion within the visible spectrum. This practically eliminates differences in radial distortion for the centroids of images of stars of various colors and of the sun's image reflected from the satellite. Figure 7.1 shows a camera with the Cosmotar objective and the Henson capping shutter mentioned in the next section. Figure 7.2 shows a typical BC-4 station.

#### 7.2.1.2 Camera Shutters and Their Mechanical Drives

When continuously illuminated satellites are used for the triangulation, the tracks of

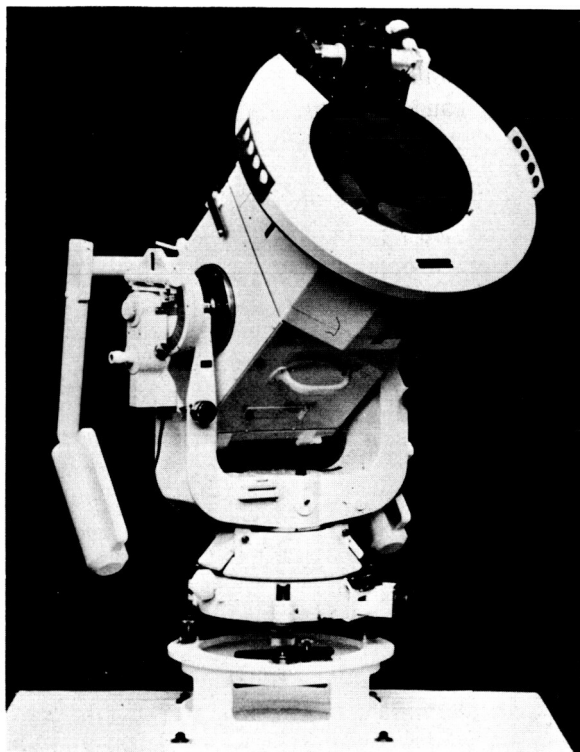


FIGURE 7.1.—Camera fitted with Cosmotar objective and Henson capping shutter.

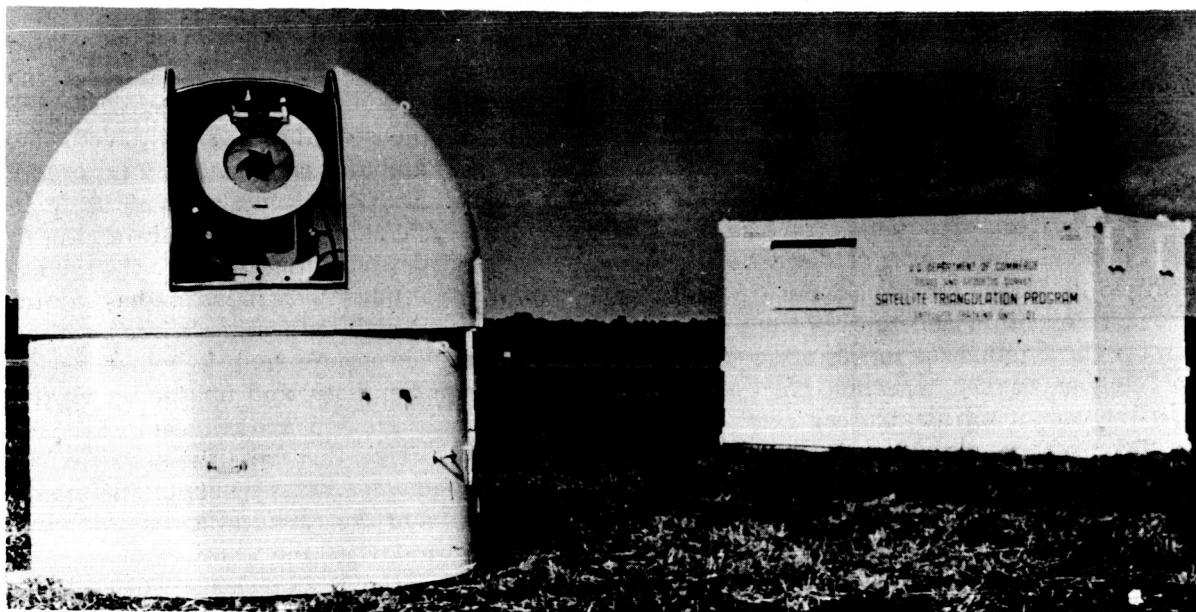


FIGURE 7.2.—Typical BC-4 installation.

the stars and of the satellites on the photograph must be chopped into a sequence of individual time-related images. The star trails are the result of the earth's rotation, shared by the Earth-fixed camera, whereas the track of the satellite is largely due to its own motion, although of course the Earth's rotation during the satellite pass contributes a component to the track. The track interruptions on the plate are effected in the BC-4 camera by three rotating disk shutters inserted between the lens elements, approximately in the principal plane of the lens system. Two of the disks rotate at equal rates in opposite directions to achieve maximum symmetry in the exposure and a high degree of efficiency (about 70%) of the shutter. The third disk subdivides the primary image sequence generated by the rotation velocity of the first two disks, which in addition fixes the exposure interval of the individual images. The most useful combinations of primary image sequence or exposure interval and actual exposure sequence in satellite triangulation, within the technical limitations of the BC-4, are given in table 7.1.

The shutter is activated by a synchronous motor specially developed for a frequency of 500 Hz. Registration of the image centroid

is initiated by an adjustable magnetic pickup. Further technical details of the shutter drive, developed and manufactured by Fred C. Henson Co., Pasadena, California, are given in the literature of that company.

Corresponding to the combination selected from table 7.1, the rotating disk shutter generates a chronologically regular sequence of images. In order to create arbitrary groupings in this sequence for the purpose of identification or to further subdivide the primary image sequence, an additional iris-type shutter is installed in front of the exchangeable filter element of the BC-4 (also made by the Henson Co. and known in the trade as a capping shutter). This shutter is activated through solenoids, and thus it is possible to open or close the shutter between two successive exposures generated by the rotating shutters. Technical details of the shutter operation are given in the manufacturer's literature.

Although it would be desirable from the photogrammetric standpoint to register the stars, as well as the satellite, by means of a shutter located in the principal plane of the lens system—i.e., by means of, say, the rotating disks—a compromise is imposed by the limitations of the f-stop. Although it is



are recorded by the oscillograph tape together with the station clock signals. This record determines time for the star exposures. The arrangement of the console, which at this time is part of all the BC-4 systems, is shown in figure 7.3

### 7.3 DATA

The survey coordinates of the stations whose observations were used are given in table 7.2. The distribution of the stations is shown in figures 7.4 and 7.5 through 7.10.

The set of interstation directions derived from the observations was associated with a scalar by including eight interstation distances computed from ground survey (fig. 7.11). These distances are given in table 7.3; the sources for the distances are listed in table 7.4.

Table 7.5 gives the number of photograms taken and processed for each station. The geographic distribution of the observations (location and direction of subsatellite points) is shown in figures 7.5 through 7.10.

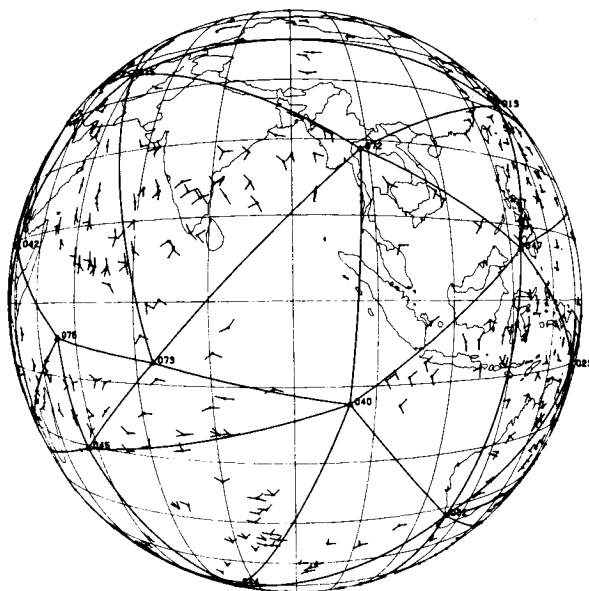


FIGURE 7.5.—Geographic distribution of stations and observations. Center of view: latitude 0°, longitude, 90° east.

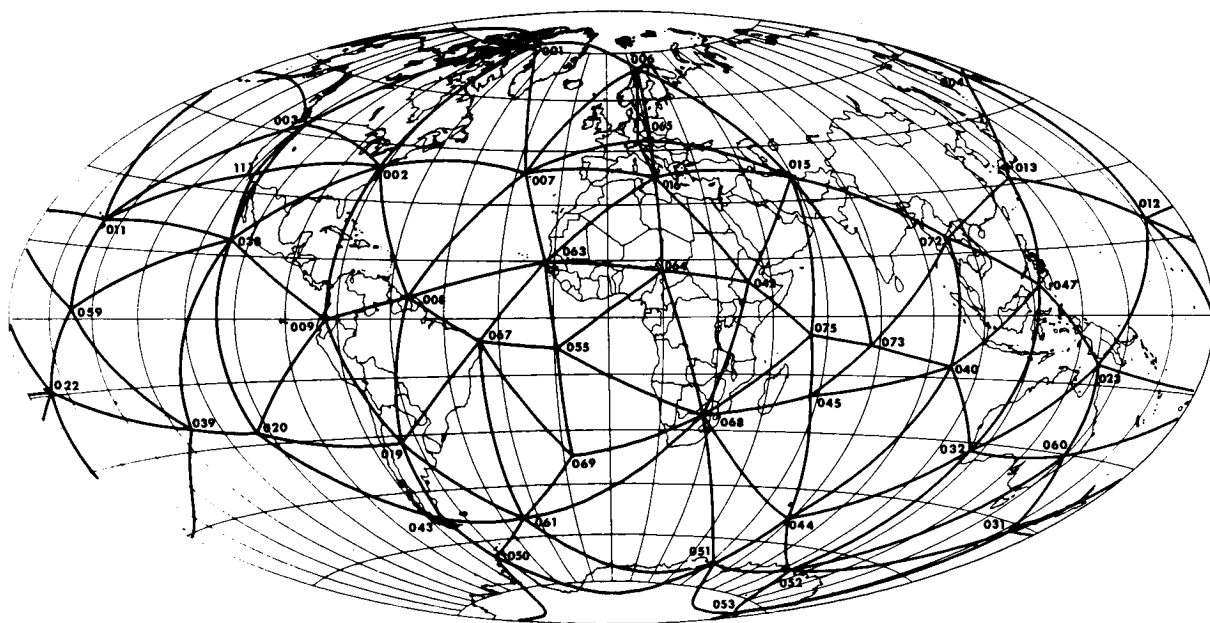


FIGURE 7.4.—Forty-five-station, worldwide, BC-4 photogrammetric satellite triangulation network. (Aitoff-Hammer equal area projection.)

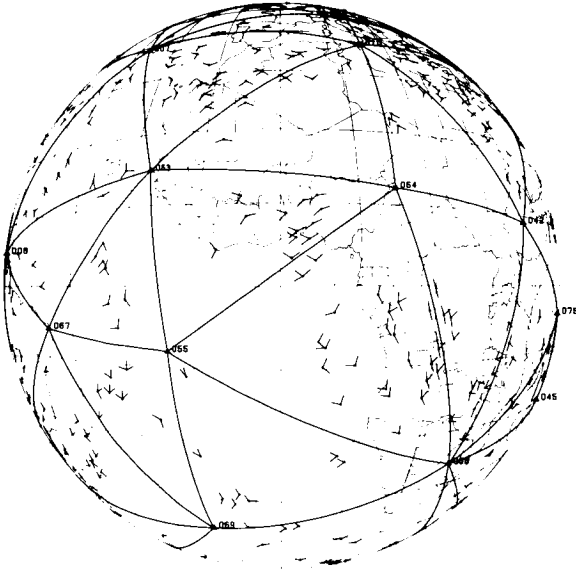


FIGURE 7.6.—Geographic distribution of stations and observations. Center of view: latitude  $0^\circ$ , longitude  $0^\circ$ .

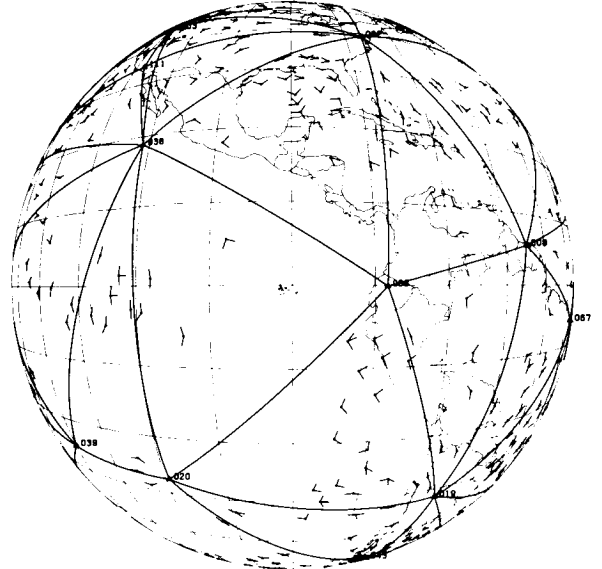


FIGURE 7.8.—Geographic distribution of stations and observations. Center of view: latitude  $0^\circ$ , longitude  $90^\circ$  west.

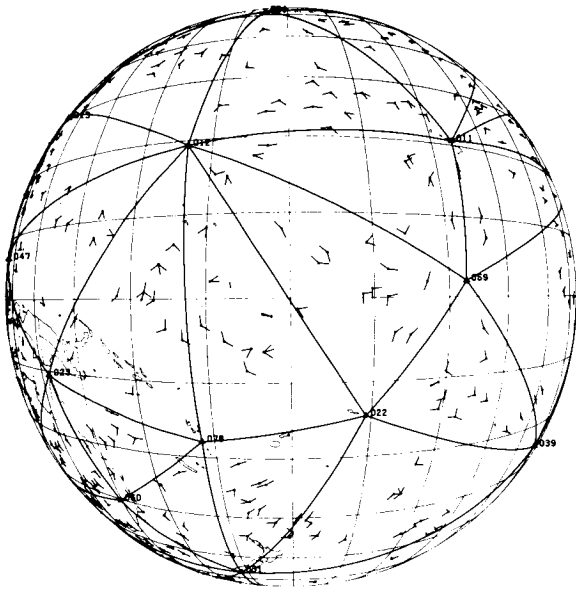


FIGURE 7.7.—Geographic distribution of stations and observations. Center of view: latitude  $0^\circ$ , longitude  $180^\circ$ .

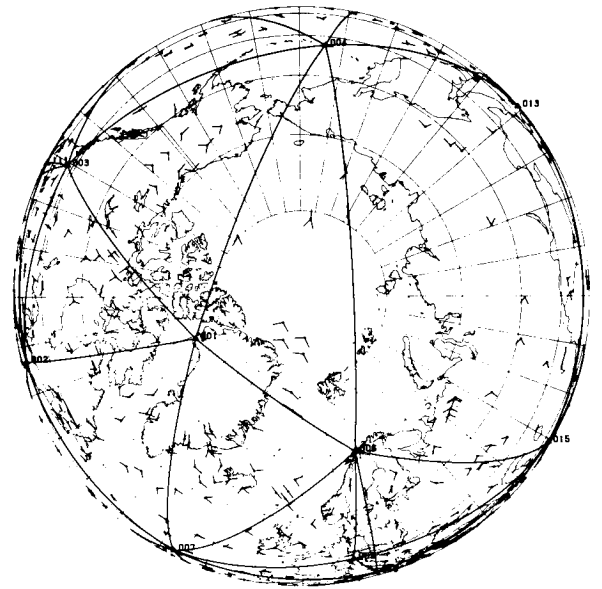


FIGURE 7.9.—Geographic distribution of stations and observations. Center of view: North Pole.

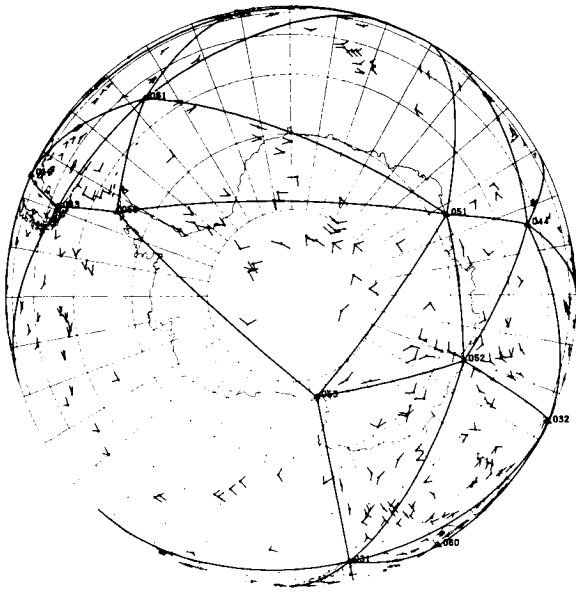


FIGURE 7.10.—Geographic distribution of stations and observations. Center of view: South Pole.

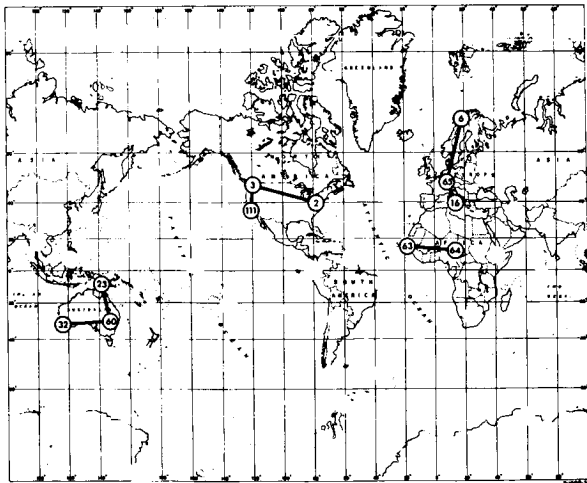


FIGURE 7.11.—Base lines used in adjustment.

### 7.3.1 Photogrammetric Registration

The size of the effective photographic area of the BC-4 plates is  $18 \times 18$  cm. The plates are either 6 or 10 mm thick, and those of best

quality have a flatness of  $3 \mu\text{m}$ . A good compromise between sensitivity and grain size is found in the Eastman Kodak emulsion 103-F. After accurately controlled developing of the plate, particular care must be exercised in the drying process: the plate must be turned continuously. The essential information content of an individual photogram consists of the point-shaped star images and the satellite trail. For star registration a sequence of five successive individual images is necessary, for statistical reasons. In order to obtain uniform star images independent of star magnitude, it is necessary to expose several such sequences with various shutter speeds. The selection of optimal exposure time is, in addition, dependent on the range in declination of the stars. Star photography, using the capping shutter, is executed before as well as after the satellite pass. During the satellite pass, additional images of the brighter stars in the field of view are generated by appropriate programming of the rotating disk shutters. These stellar images are of particular importance for the exterior orientation, since they are recorded simultaneously with the satellite trail. With suitable choice of exposure interval it is possible to obtain a presentation of both stars and the satellite in a series of similar point-shaped images.

In measuring the negative itself, one is presented with the problem of centering a black measuring mark within a dark point-shaped image. (To date—1973—ring-shaped measuring marks with a diameter of 20 to  $30 \mu\text{m}$  are not available.) A series of experiments has shown that the plate measurement process is faster and more reliable if a diapositive is first produced, so that the black measuring mark can be set within a white round image.

The negatives are copied in almost monochromatic blue light under vacuum onto a 6-mm-thick glass plate covered with an exceedingly fine-grained emulsion. Statistical tests have shown that the copying process introduces no marked deterioration in accuracy. Figure 7.12 shows the star and satellite images schematically. The sequences A, B, C, and D, E, F represent five star images, each taken with the capping shutter and various

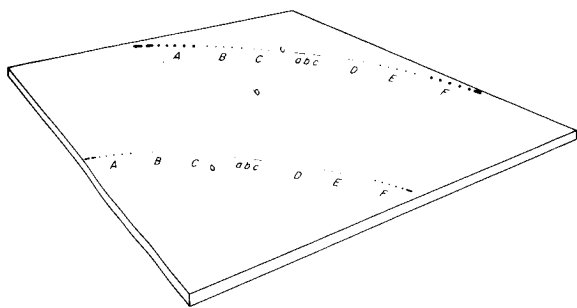


FIGURE 7.12.—Schematic presentation of star and satellite images.

shutter speeds, before and after the satellite pass, the upper star trails representing a brighter star. The sequences *a*, *b*, *c* symbolize images of the satellite and of stars recorded simultaneously by means of the rotating disk shutter. Because of the limited resolution of the objective and emulsion, only a single approximately point-shaped star image *b* corresponds to the three satellite images designated *abc*, whereas the star imagery corresponding to the satellite exposure intervals *a* and *c* appear as star trails, unresolved into individual images. Stars that are insufficiently bright produce no measurable image *b*, and those of higher magnitude are not recorded at all through the rotating disk shutter. Figure 7.13 is a magnified portion of a plate, showing trails of the balloon satellites ECHO-1 and ECHO-2 generated by the rotating disk shutter.

### 7.3.2 Coordinate Measurements on the Comparator and Their Reduction

Measurement of the photograms, either of the original negative or of a diapositive copy, produces rectangular coordinates in the plate plane with a basically arbitrary origin. The comparator used does not have to operate necessarily on this principle, but can, for example, measure polar coordinates instead (D. C. Brown, unpublished). These must, however, be transformed to the *x*, *y* coordinates needed later in the adjustment, and the corresponding weight matrix, correlated in this case, must be computed. Since the meas-

urement of photograms is one of the most essential phases of analytical photogrammetry and as such has been discussed in detail in the literature, and since, furthermore, the specific measuring method used depends not only on the type of comparator used but also on the organizational and environmental conditions, only those phases that are typical for the problem in question but do not necessarily have applicability for other more or less conventional working procedures will be discussed.

If a high degree of accuracy in the end results of geometric satellite triangulation is to be achieved, it is necessary to bear in mind from the outset the fact that a large number of points (600 to 750 star images and up to 600 satellite images) must be measured on each photogram, and consequently that 5 to 8 hours are required for the measurement. Special care must therefore be exercised in the selection of the type of comparator, the environmental conditions, and the arrangement of working procedures, so that systematic error influences can be held to a minimum or can be corrected computationally. A description of the current procedures at the U. S. National Ocean Survey (NOS) follows.

The measurements are made on comparators equipped with independent *x* and *y* screws with a working length of about 225 mm each. The instruments, manufactured by the firm of David Mann, Lincoln, Massachusetts, are equipped with a direct binocular microscope, magnification adjustable in steps up to 40 $\times$ , and a circular measuring mark (dot) with a diameter of about 30  $\mu$ m. The comparators are operated in a controlled environment (temperature 22 $^{\circ}$  C  $\pm$  0.5 $^{\circ}$ , humidity 50%  $\pm$  5%) and tested about every 2 months for linear and periodic scale errors in the *x* and *y* screws as well as for orthogonality of the motions. Calibrated grid plates in each of four positions are measured for this purpose by each of three observers. The measured coordinates to the nearest micron are registered electronically on a typewriter, punched tape, or card. The initial operations revealed the fact that the operator's body heat generated an unacceptably

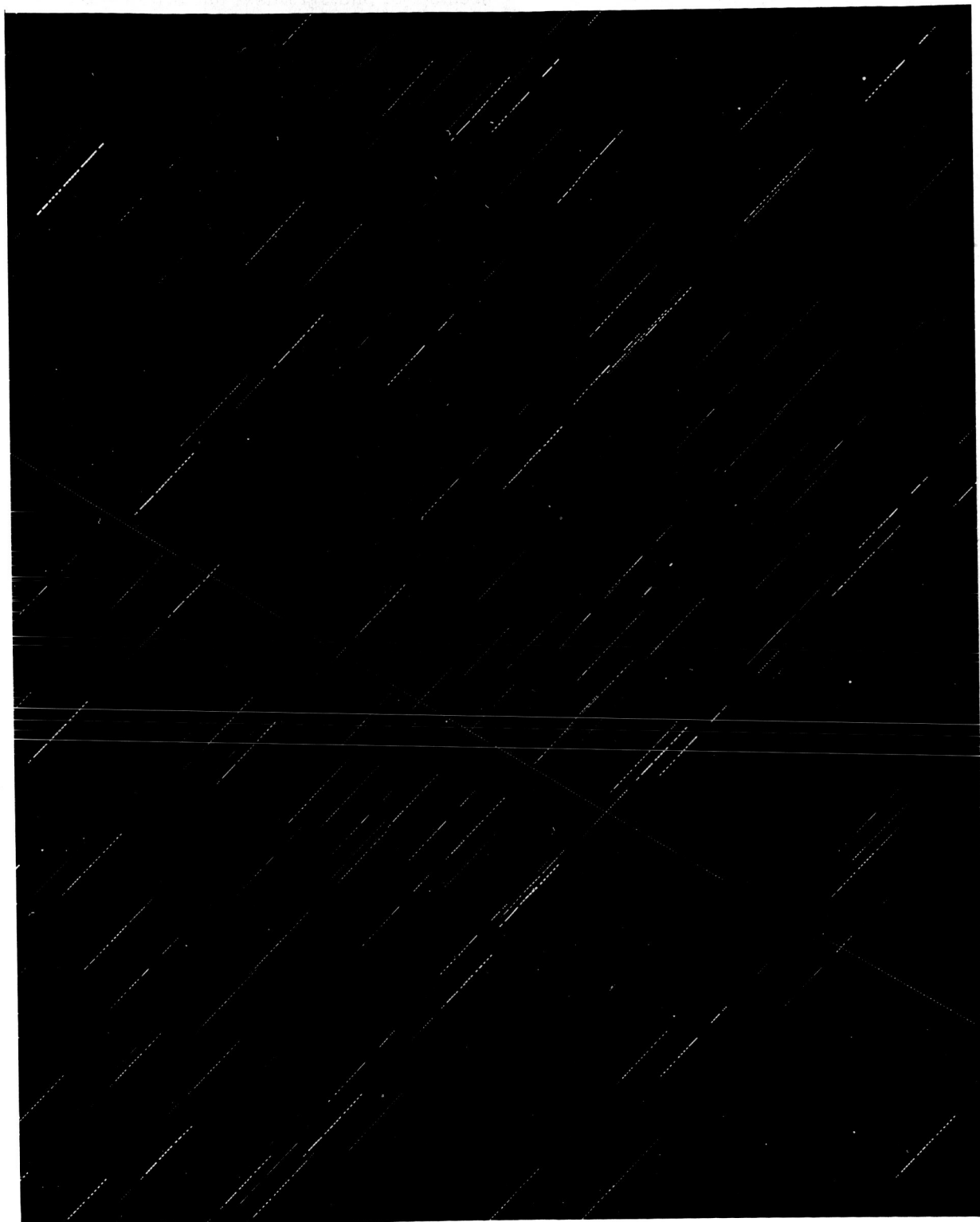


FIGURE 7.13.—Star plate.

large systematic error in the measurements, because the optics of the comparator was not constructed in accordance with the Abbe principle. It was necessary, therefore, to modify the construction to project the measuring mark into the plane of measurement. Extensive tests have shown that the comparators now are stable for operating periods of from 2 to 3 hours. However, it is still necessary to subdivide the measurement of a plate into several such periods.

The first step is to drill eight circular holes into the emulsion, approximately 40 to 50  $\mu\text{m}$  in diameter. These are located at the four corners, the extremities of the legs of the conventional fiducial marks pointing toward the center, and at the approximate center of each edge. These drill holes are measured at the beginning and end of each measuring session, and the differences are used to check the stability of the instrument during that period. Before continuing with the description of the measuring procedure, some essentials on the preparation for plate measurement must be mentioned.

The readings on the circles in the field give an orientation of the camera in azimuth and elevation to within 10 to 20'. With the time of observation and approximate station coordinates, a range in right ascension and declination on the celestial sphere can be computed. The computer searches the star catalog tape for all stars in this portion of the sky, and their coordinates together with the nominal camera constants and the approximated orientation data are used to compute plate coordinates for these stars. These points are projected on a cathode-ray tube associated with the electronic computer and are photographed to the scale of the photogram to produce a star chart. The stars are subdivided into three groups of magnitudes and labeled accordingly. Another symbol designates a group of at least eight stars as bright as possible and located in a circular ring 3 cm wide near the edges of the plate. Since the registration on the original photogram or diapositive varies according to magnitude, it is easy to bring the photogram and the "computed star chart" into coincidence on a

light table. At the same time, a grid template is superimposed, dividing the plate format into 100 equal squares. The photogram is now examined under the binocular magnification of the comparator. In each of the squares a star of the series, before and after the satellite pass, that coincides with an image on the star chart is selected and marked. In addition, all stars recorded during the satellite pass (cf. fig. 7.12) and the specially selected bright stars near the edge of the plate are marked with an identification symbol.

After this preparation, the plate is placed in the comparator. In order to eliminate as far as possible the influence of unknown systematic errors, a subgroup of stars and satellite images covering the whole extent of the plate is measured at each of the two or three sessions required. At the completion of the measurements all premarked stars and satellite images will have been measured. In connection with the satellite trail it should be added that it crosses the plate within at most a few millimeters of the center and its images are measured to a maximum distance of 6 cm from the center, in order to avoid edge effects in the emulsion. To combine in a consistent system the reading obtained from the two or three necessary comparator sittings, the individual sets are translated, rotated, and stretched with two scale corrections in adjustment, in accordance with the coordinates of the relevant drill holes to best fit the configuration of drill holes, showing the smallest mean error. The residuals of the reference points after these transformations are typically 0.3  $\mu\text{m}$ . The entire measuring process is then repeated with the plate turned through approximately 180 degrees. Both results are then meaned by fitting the latter result to the first, again by means of an adjustment (determination of two components of translation, a rotation, and two scale factors). From the residual differences between corresponding double measurements in this adjustment, a characteristic mean error of 1.6  $\mu\text{m}$  results as a measure of precision of the measured coordinates.

In addition, the plate coordinates of all premarked star and satellite images are referred

to the plate center as determined by the fiducial marks. The coordinates of the above-mentioned bright stars near the edges of the plate that are easily identifiable in the catalog are now used to compute an approximate orientation. With this result, right ascensions and declinations are computed from the image coordinates of all measured stars (cf. sec. 7.4.6). The same program compares these values with the tape containing the star catalog, identifies the stars, and updates them to the observation epoch and true equinox (cf. sec. 7.4.3, eqs. 7.1–7.15).

The step in the overall adjustment procedure of satellite triangulation under discussion represents a mutually interacting combination of human effort and electronic computing. The contributions from the human element, such as the execution of the measurements and evaluation of the statistical intermediate results, are the critical operations; the computing system prepares star charts, presents catalogued data, and makes the necessary computations.

After completion of this operation, measured coordinates for all selected stars and satellite images are available, as well as the star coordinates reduced up to a certain point. These data are now further reduced in a numerical adjustment to be discussed in section 7.4.6.

## 7.4 THEORY

### 7.4.1 Introductory Considerations

In the classical treatment of geometric geodesy, i.e., the part of geodesy that concerns itself with the derivation of rigorous geometric results, difficulties arise from the fact that the measured quantities cannot be rigorously related to the geometric model that is to be established. Physical influences are responsible for this dilemma. The so-called measurements of horizontal and vertical angles are vitiated to an unknown extent by systematic influences such as anomalies in the gravity field and refraction. The reduction of baseline measurements is in principle similarly affected.

In addition, the classical method of triangulation is forced to adopt a number of complex postulates whose geometric content is based on certain hypotheses. Typical examples are the present-day correction methods generally known as "isostatic reduction procedures." The physical principle underlying these procedures is the assumption of homogeneity and hydrostatic equilibrium of the masses within the Earth's crust. The resulting corrections to all geodetic observations will prejudice the end result in favor of Clairaut's theory. Aside from the physical assumptions, an unavoidable characteristic of classical geodetic triangulation consists of the practical limitation of sight length between points on or near the surface of the Earth. Not only are such geodetic triangulations incapable of making intercontinental connections, but the first-order nets must be pieced together with an excessive number of individual arcs. The disadvantage of this method arises not so much from the relatively large number of stations involved as from the fact that accuracy is impaired, especially in extensive nets, by error propagation.

As a consequence, geodetic theory has developed complex methods of adjustment designed to eliminate the contradictions in the data by iteration, permitting the results of partly geometric and partly geophysical adjustment operations to interact until all results become internally consistent. Although they are attractive from a theoretical standpoint, such methods have practical limitations. For this reason a purely geometrically defined, three-dimensional worldwide geodetic reference system is desired in order to transcend the shortcomings of the classical geodetic triangulation method. Moreover, such a worldwide geometric solution is superior to a mere connection of the various geodetic datums, which has at times been called the purpose of satellite geodesy.

The significance of a three-dimensional triangulation method, emphasized repeatedly in the recent history of geodesy, becomes especially apparent in connection with the field of satellite geodesy, which because of its geometric and geophysical aspects demands a three-

dimensional solution. Perhaps the greatest significance of geometric satellite triangulation, however, lies in the fact that with this method there exists, for the first time in the history of geodesy, the possibility for the creation of a worldwide three-dimensional reference system that is supported by a minimum of a priori hypotheses, in particular without reference to either the magnitude or the direction of the force of gravity.

Establishing geometric correspondence among a number of selected nonintervisible points of the physical surface of the Earth can be accomplished with spatial triangulation by means of auxiliary targets elevated sufficiently above the Earth's surface.

The generation of light signals visible over large distances is possible by means of artificial satellites. Because of the high velocity of such targets, observation of directions to them can at present be made only with photogrammetric precision cameras. Owing to the physical and chemical properties of the photogrammetric measurement components, the absolute accuracy as well as the reproducibility of the observation conditions in this method is limited. To obtain observational results with maximum absolute accuracy, the adjustment of the photogrammetric measurements must be based on a method of interpolation.

A suitable reference system into which an elevated target can be intercalated is obviously the right ascension-declination system of metric astronomy. This system is all the more attractive from the geodetic point of view because one of its axes is parallel to the Earth's axis of rotation. A large number of fixed stars are available whose coordinates are tabulated in catalogs. These control points being practically at an infinite distance, it follows that their direction coordinates are insensitive to a parallel displacement of the observer and hence cannot be used for scale determination. It is therefore necessary to determine the scale of the satellite triangulation independently: for example, by measuring the distance between two adjacent stations. As will be shown later (sec. 7.4.3), it is necessary to carry out such

scale determinations in several portions of the worldwide triangulation net.

#### 7.4.2 Geometric Foundations

We turn our attention now to a three-dimensional method of triangulation that is based on direction measurement and designed to determine the coordinates of nonintervisible triangulation stations.

The relevant geometric solution is not new. In fact, there is little room for originality in the field of the application of photogrammetry to ballistic and related problems. The use of star photography for the calibration of photogrammetric cameras is a proven method, especially with astronomers. The use of star images to orient photogrammetric cameras and the corresponding triangulation of additionally photographed target points was used successfully in the 1930's by Hopmann and Lohmann (1943) in the tracking of missiles before the method was applied in the development of the V-2 rocket at Penne-münde, Germany, and subsequently in various other countries.

There are several ways to present the geometric principles of this triangulation method. Väisälä's proposal contains a lucid geometric explanation. Two rays issuing from the end-points of a given baseline and directed at a common point define a plane in space whose orientation can be determined from the direction cosines of the rays. When two such planes have been fixed, the direction in space of the baseline can be computed as the intersection of the two planes. The principle involved is shown in figures 7.14 and 7.15.

After two directions  $AB$  and  $AC$  issuing from station  $A$  have been determined in this fashion, the shape and spatial orientation of the station triangle  $ABC$  is fixed by intersecting  $AB$  and  $AC$  with a plane whose orientation is known from observing the satellite position  $S_s$  from  $B$  and  $C$ . Thus, five planes are necessary and sufficient to fix the shape and orientation of a station triangle. Each of these planes contains two stations and one point of the satellite orbit; therefore, there

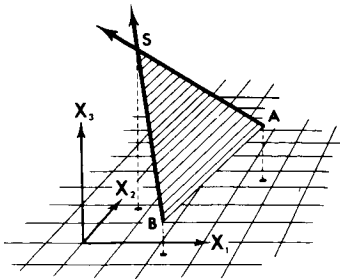


FIGURE 7.14

are five positions of the orbit, together with the positions of the three stations *A*, *B*, *C*, or  $(5+3) \times 3 = 24$  unknowns to be determined.

Since each pair of simultaneous observations of a satellite position—or, in other words, the determination in space of two intersecting lines—gives rise to four equations, there are, in all,  $5 \times 4 = 20$  equations available. Hence,  $24 - 20 = 4$  additional independently determined geometric quantities are required for a complete solution of the triangle. The most obvious of the many theoretically available choices are the three coordinates of one of the stations, which, in principle, can be assumed arbitrarily, for example, as the origin of the coordinate system. It is equally logical to choose as the fourth assumption the length of one of the sides of the triangle, which fixes the scale for the whole triangulation. For purposes of explaining the principle of satellite triangulation it is sufficient to introduce this side-length as the unit of length.

It is interesting to note that three of the five necessary planes can be determined with a single pass of the satellite, if the satellite subpoint lies near the middle of the triangle

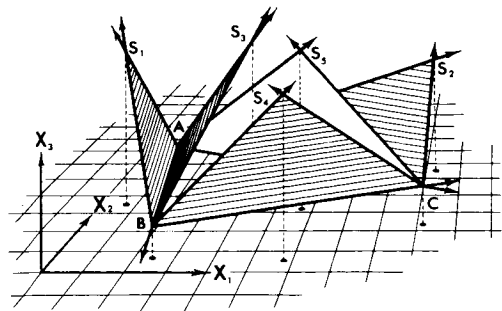


FIGURE 7.15

of stations (see fig. 7.16). For this case, a unique solution can be obtained with the determination of  $(3+3) \times 3 = 18$  unknowns from  $7 \times 2 = 14$  available condition equations. Again, four additional independently determined parameters must be introduced.

From the viewpoint of analytical photogrammetry, the geometric principle of satellite triangulation can be explained by identifying the unknown positions of the triangulation stations and the unknown orientations of the observing cameras with the corresponding conditions in classical aerial photogrammetry. The unknown orbital positions of the satellite correspond to the relative control points, with the restriction that they cannot furnish scale, since they lie at an infinite distance.

The geometric concept of photogrammetric satellite triangulation must, however, be interpreted in the light of the fact that at each station the stars (absolute control points) are used for the determination of the elements of the interior orientation necessary for the reconstruction of the photogrammetric bundle,

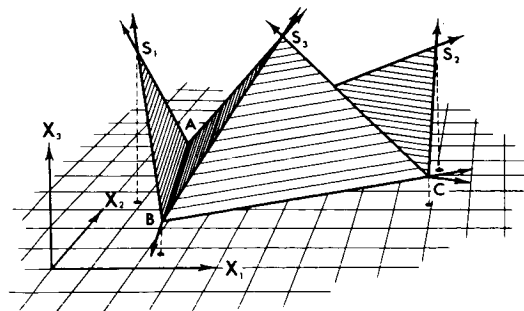


FIGURE 7.16

together with the determination of the three rotation elements of the exterior orientation. The condition of intersection of the rays resulting for each satellite image observed from more than one station is used exclusively to determine the three elements of translation of the exterior orientation. This circumvents the unfavorable correlation between the elements of rotation and translation that is typical in aerial triangulation, an advantage that is reflected in the favorable error propagation characteristics of satellite triangulation (see sec. 7.3.3).

The geometric content of satellite triangulation, in complete agreement with the corresponding concepts in the general field of analytical photogrammetry, is thus based on a multitude of individual rays whose directions must be determined from the relevant photographs. Hence, the idealized conditions must be satisfied: that the three points—objective (satellite), center of projection (triangulation station), and image (photographed satellite image)—lie on one straight line. This condition is the geometric basis for satellite triangulation, just as it is the necessary and sufficient criterion for any photogrammetric triangulation (Schmid, 1958, 1959).

It is obvious that after fixing the first station triangle in space nothing prevents the addition of further stations as vertices of triangles adjacent to the first. Postulating the possibility of scale determination, either by direct measurement of a side of one of the space triangles or, for example, by simultaneous distance measurement from at least four stations to a satellite position, the positions of a number of points on the physical surface of the Earth can be determined in a homogeneous three-dimensional reference system. In practice, the arrangement of the stations, and hence the shape of the configuration, is to a great extent dictated by the geographical distribution of islands over the oceans.

Aside from using the method to determine a worldwide geodetic reference system, the same technique can be applied to establish the frames for continental triangulations. On

the basis of accuracies in the determination of directions attained even today and of the basically favorable error propagation characteristic of satellite triangulation, these frames are equivalent or superior to classical first-order nets, particularly where such nets cover extensive areas (see fig. 7.17).

Judging by present technical standards, it seems unlikely that, because of their limited life span, satellites with a height above the earth of under 1000 km will be used. Therefore, as a consequence of the nearly linear decrease in accuracy of the triangulation results with increased height (see sec. 7.4.3), the practically acceptable shortest average distance between points of a continental satellite triangulation net should be 500 to 1000 km. Without changing in any way the geometric principle—although the influence of the physical parameters is different and not necessarily more favorable from the standpoint of measuring technique—the described method of satellite triangulation becomes a type of three-dimensional triangulation with elevated targets, taking into account present-day capabilities to generate a large number of light flashes or to burn pyrotechnic signals on airplanes, which may in the near future be

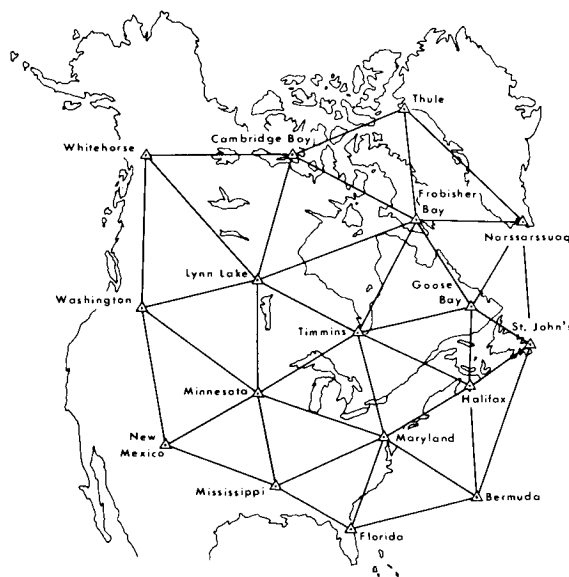


FIGURE 7.17.—Satellite-triangulation network in North America.

expected to fly at heights of 20 to 25 km. In addition to the theoretically desirable three-dimensional character of the triangulation method, it will be a question of economic feasibility whether the development of such a technique will, in part, replace classical first-order triangulation in certain areas of the Earth.

Quite independently of the measurements of the individual spatial triangulation figures, the basic geometrical concept underlying the method of satellite triangulation requires, at least in principle, simultaneously executed observations of directions to the target (in our case the satellite) from at least two stations. Clearly, the requirement to measure directions rather than merely angles implies the necessity of orienting the observed bundle in each case relative to a uniquely defined system of reference. This is otherwise self-evident in view of the fact that our end result is to represent a consistent spatial reference system.

A spatial coordinate system to which a direction to a target sufficiently elevated above the horizon can be referred is the right ascension-declination system. This reference system, surrounding the whole Earth, is qualitatively as well as quantitatively suitable, a great number of precisely measured reference points being readily available. Of especial significance to the photogrammetric mensuration principle is the abundance of such absolute control points, since because of the physical and chemical nature of its numerous components and procedures the photogrammetric method can satisfy the requirements for highest accuracy only if the corresponding observational and adjustment procedures are executed in a close-interval interpolation process.

We emphasize here, therefore, that the claim of satellite triangulation, that it produces results without the aid of physical hypotheses and practically free of systematic errors, derives chiefly from the fact that photogrammetric direction determination in satellite triangulation not only operates with the aid of geometric interpolation within the reconstructed photogrammetric bundle but rep-

resents equally an interpolation into the physical process of astronomic refraction (see sec. 7.4.5). This also means that the absolute accuracy of photogrammetric satellite triangulation depends primarily on the quality of the right ascension-declination system, particularly on its freedom from systematic errors. On account of the importance of the astronomic reference system to satellite triangulation, some relevant remarks will be made in the next section, specifically as they apply to the data processing in satellite triangulation.

### 7.4.3 Astronomical Reference System<sup>1, 2</sup>

In satellite triangulation, photographing the fixed stars serves to reconstruct and to uniquely orient in space the photogrammetric bundle. The problem of reconstructing the bundle is fundamentally identical with the problem of calibrating a photogrammetric camera. The geometric interpretation of the relevant parameters is independent of the orientation of the camera. It would therefore suffice to have given the relative geometric arrangement of the images of the stars on a particular plate in an arbitrary coordinate

<sup>1</sup> For the proper interpretation of the computations in this section it is recommended that the reader first study sections 7.4.6 and 7.4.8.

<sup>2</sup> The symbolism used in this chapter is common in photogrammetric practice, and the author did not wish it changed. Some of the symbols are used with different meanings outside of photogrammetry (in particular in geodesy and astronomy) and even occur in this chapter with two or more meanings. Therefore, care should be exercised in interpreting the equations in this chapter. For this reason, the following ambiguities are indicated by footnotes: (1)  $\alpha$  is used in this chapter to denote one of the angles defining the orientation of a camera and to denote right ascension; the latter sense is that used in the rest of the volume. (2) The symbol  $c$  is used to denote one or (with subscripts) more of the characteristics of a camera and to denote the velocity of light; only the latter convention is used in the rest of this volume. Where used in this chapter in the former sense and where confusion may occur, the exceptions are noted by (1) a dagger ( $\dagger$ ) for  $\alpha$  denoting one of the angles defining the orientation of the camera, and (2) a double dagger ( $\ddagger$ ) for  $c$  denoting a characteristic of the camera. Editor.

system. However, the determination of an unambiguous orientation for all the bundles of rays serving the triangulation is predicated on the fact that all given control points (the totality of fixed stars used) are given in a uniquely defined reference system, which furthermore can be uniquely transformed to an Earth-fixed coordinate frame. The right ascension-declination system of metric astronomy, as was previously mentioned, furnishes the metric basis for geometric satellite triangulation. The point of departure is the apparent position coordinates of stars tabulated for a given epoch in star catalogs such as *Apparent Places of 1535 Fundamental Stars*, published by the Astronomisches Rechen-Institut, Heidelberg; the *General Catalogue* (Boss, 1936), with approximately 33 000 apparent star positions; or in probably the most complete catalog to date, issued by the Smithsonian Astrophysical Laboratory, in which over 250 000 stars with their apparent places are tabulated (see chs. 1 and 9).

The choice of stars selected for the purpose of satellite triangulation depends primarily on the accuracy of their coordinates. Stars with large proper motions should be avoided and double stars should not be used at all.

To counteract the influence of spectral differences of the stars, a special lens was used (see sec. 7.2). Finally, the selection was limited by the magnitude registered by the specific optical system and emulsion used. With the BC-4 system and the Eastman-Kodak emulsion 103-F in use today, stars of the seventh and eighth magnitude still produced good, measurable images over the entire plate. Using very bright stars at the same time raised the question concerning the influence of relative systematic errors in locating the centroid of the image. With the focal lengths in use at present for satellite triangulation purposes, the existence of a magnitude effect, which is not negligible in astronomical measurements, has not as yet been quantitatively demonstrated.

In Bossler (1966), the distribution over the celestial sphere with respect to right ascension and declination of the Smithsonian

catalog stars is described from the standpoint used in the selection.

Geometric satellite triangulation can at best, therefore, attain the accuracy of the astronomical reference system (see sec. 7.3.1). Hence, for a critical study of the theoretical accuracy of satellite triangulation, the observation and adjustment procedures used in metric astronomy to establish star catalogs are of fundamental importance. Within the frame of this presentation it must suffice to refer to the literature on these highly specialized and complex procedures: Clemence, 1963; Scott, 1957, 1963; Vasilevskis, 1963; Dieckvoss, 1963; Woolard and Clemence, 1966.

To understand geometric satellite triangulation, it is necessary to interpret correctly the qualitative (geometric) and quantitative (statistical) data listed in the star catalogs in order to grasp the reductions necessary to transform the time- and space-dependent geometry of the individual photogrammetric exposures into a homogeneous geometric system. The problems arising in this connection are basically the same as those faced in the reduction of astronomic geodetic field observations.

The star catalogs list for apparent places a pair of spherical coordinates for a specified epoch, right ascension  $\alpha$  and declination  $\delta$  (see ch. 1). The specification that the cataloged values refer to a given epoch (generally the beginning of the tropical year 1950.0 in the newer catalogs) means that time-dependent corrections must be added to the star coordinates before they represent the actual position at the instant of observation, in our case the time of exposure.

The reason for these corrections is chiefly to be found in the dynamics of the universe, although purely physically based corrections must also be taken into consideration. Theoretical explanations are described in detail in standard works on geodetic astronomy (e.g., König, 1962; Clemence, 1966; Wayman, 1966; Fricke and Kopff, 1963; Morgan, 1952; Gliese, 1963; Kopff *et al.*, 1964). Nevertheless, it seems useful to outline here, in terms of formulas, the sequence of corrections used.

For one thing, such a presentation will present a computerized method designed to reduce a large number of star places, including circumpolars, that are needed in geometric satellite triangulation. For another, it helps to clarify the contribution of the individual corrections to the overall adjustment procedure of satellite triangulation and to judge the technical and economical aspects involved.

The following computations are made for the purpose of deriving, from the star catalog data for a specific epoch, that unit vector which designates the apparent geocentric direction of a star with reference to the true equinox at the instant  $T$  of observation. The solution shown here is based on the method now in use at the U. S. Naval Observatory. The lower indices to the right of the matrices designate first, the equinox to which the coordinates are referred, and second, the epoch. To begin with, the heliocentric unit vector  $\mathbf{x}_{00}$ , referred to the epoch and equinox of the catalog used, is computed with the catalog entries  $\alpha$  and  $\delta$ .

$$\mathbf{x}_{00} \begin{bmatrix} x_1 \\ x_2 \\ x_3 \end{bmatrix}_{00} = \begin{bmatrix} \cos \delta \sin \alpha \\ \cos \delta \cos \alpha \\ \sin \delta \end{bmatrix}_{00} \quad (7.1)$$

Then the star coordinates are corrected for the proper motion of the star. The corresponding correction vector  $\mathbf{u}_r$  is computed by using the proper motion components in right ascension  $\mu_\alpha$  and in declination  $\mu_\delta$  listed in the catalog and by differentiating the vector in equation 7.1), since  $\mathbf{u}_r = d\mathbf{x}/dt$  by definition,

$$\mathbf{u}_r = \begin{bmatrix} -\cos \delta \sin \alpha & -\sin \delta \cos \alpha \\ \cos \delta \sin \alpha & -\sin \delta \cos \alpha \\ 0 & \cos \delta \end{bmatrix}_{00} \begin{bmatrix} \mu_\alpha \\ \mu_\delta \end{bmatrix}_{00} \\ = \begin{bmatrix} -x_2 & -x_3 x_1 (1-x_3^2)^{-1/2} \\ x_1 & -x_3 x_2 (1-x_3^2)^{-1/2} \\ 0 & (1-x_3^2)^{1/2} \end{bmatrix}_{00} \begin{bmatrix} \mu_\alpha \\ \mu_\delta \end{bmatrix}_{00} \quad (7.2)$$

with  $\mu_\alpha$  and  $\mu_\delta$  in radians.

A second differentiation yields the components of the secular variations. The corresponding vector  $\mathbf{u}_r$  is then

$$\dot{\mathbf{u}}_r = -\mu^2 \mathbf{x}_{00} \text{ with } \mu^2 = \mu_{x_1}^2 + \mu_{x_2}^2 + \mu_{x_3}^2 \quad (7.3)$$

If the radial velocity of the stars is to be applied, equation (7.3) is augmented to

$$\mathbf{u} = -\mu^2 \mathbf{x}_{00} - 0.000205\pi V \mathbf{u}_r \quad (7.4)$$

in which  $\pi$  is the parallax of the stars in seconds of arc and  $V$  is the radial velocity of the star in kilometers per second. The second term in (7.4) is quite small and needs to be considered for only a few stars.

With (7.1), (7.2), and (7.3) or (7.4) the unit vector  $\mathbf{x}_{0T}$  referred to epoch  $T$  and the catalog equinox is

$$\mathbf{x}_{0T} = \mathbf{x}_{00} + \begin{bmatrix} \mu x_1 & \dot{\mu} x_1 \\ \mu x_2 & \dot{\mu} x_2 \\ \mu x_3 & \dot{\mu} x_3 \end{bmatrix} \begin{bmatrix} T \\ \frac{1}{2} T^2 \end{bmatrix} \quad (7.5)$$

Expression (7.5) is obviously the Taylor-Maclaurin expression of vector  $\mathbf{x}$  in time to second order. The time interval  $T$  is in tropical years or centuries, depending on the interval for which  $\mu_\alpha$ ,  $\mu_\delta$  are listed in the particular catalog used;  $T$  includes the fraction  $\tau$  of the year in which the observation is made. Values for  $\tau$  are taken from the volume of the *American Ephemeris and Nautical Almanac* in question. The result (7.5) can be transformed for convenience in programming to

$$\mathbf{x}_{0T} = \left( 1 - \frac{\mu^2 T^2}{2} \right) \mathbf{x}_{00} + (T - 0.0001025\pi VT) \mathbf{u}_r \quad (7.6)$$

The next step rotates the vector  $\mathbf{x}_{0T}$  from (7.5) or (7.6) in accordance with precession, so that the transformed rectangular coordinates will be referred to the mean equinox for the beginning of the Besselian year  $T'$  nearest the date of observation. The transformation is

$$\mathbf{x}_{T'T} = \underline{R} \begin{pmatrix} -\zeta & 0 & -z \\ 3 & 2 & 3 \end{pmatrix} \mathbf{x}_{0T} \quad (7.7)$$

in which the rotation matrix has the following meaning:

$$\begin{aligned} \underline{R}(-\zeta, \theta, -z) &= \underline{R}(-z) \underline{R}(\theta) \underline{R}(-\zeta) \\ &= \begin{bmatrix} \cos z & -\sin z & 0 \\ \sin z & \cos z & 0 \\ 0 & 0 & 1 \end{bmatrix} \\ &\begin{bmatrix} \cos \theta & -\sin \theta & 0 \\ 0 & 1 & 0 \\ \sin \theta & \cos \theta & 0 \end{bmatrix} \begin{bmatrix} \cos \zeta & -\sin \zeta & 0 \\ \sin \zeta & \cos \zeta & 0 \\ 0 & 0 & 1 \end{bmatrix} \end{aligned} \tag{7.8}$$

The indices under the angles in the rotation matrices designate the axis around which the rotation takes place (for direction of rotation see sec. 7.4.6.2.2). When Newcomb's constants are used, the rotation angles are

$$\begin{aligned} \zeta &= (2304''250 + 1'396T_0) + 0''302T^2 \\ &\quad + 0''018T^3 \\ z &= \zeta + 0''791T^2 \\ \theta &= (2004''682 - 0''853T_0)T - 0''426T^2 \\ &\quad - 0''042T^3 \end{aligned} \tag{7.9}$$

The geometric meaning of the angles is given in *Explanatory Supplement to the Astronomical Ephemeris and the American Ephemeris and Nautical Almanac*.  $T_0$  (in tropical centuries) is the interval between 1900.0 and the epoch of the catalog used;  $T$ , also in tropical centuries, is the difference between the Besselian year  $T'$  nearest the date of observation and the epoch of the catalog.

The vector of (7.7) is next corrected for annual aberration, for which daily values are listed in the *American Ephemeris and Nautical Almanac*. Since these tabulated values are computed from the true motion of the Earth with reference to the mean equinox at the beginning of the Besselian year nearest the date for which they are published, they can be applied directly to this vector. The annual aberration corrections must be interpolated with first and second differences to the date of observation. The resulting constants  $-D$ ,  $C$ , and  $C \tan \epsilon$  in radian measure may be regarded as displacements of the rectangular coordinates. Thus, the position

vector of a star for the epoch  $T$ , referred to the mean equinox of  $T'$  and including the aberration, is

$$\mathbf{x}_{(TT)} = \mathbf{x}_{T'T} + \begin{bmatrix} -D \\ +C \\ C \tan \epsilon \end{bmatrix} \tag{7.10}$$

with the mean inclination of the ecliptic

$$\begin{aligned} 23^\circ 26' 44'' 840 - 46'' 850T - 0'' 003T^2 \\ + 0'' 002T^3 \end{aligned} \tag{7.11}$$

with  $T$  as above.

The transformation (7.7) accounts for precession up to the beginning of the Besselian year nearest the date of observation. An additional rotation is necessary to transform the position coordinates from the corresponding mean equinox to the true equinox at the time  $T$  of observation.

With allowable neglect of terms of second and higher order that do not contain the factor  $\tan \delta$  one obtains

$$\mathbf{x}_{(TT)} = \underline{R}(B, A, -f) \mathbf{x}_{(T'T)} \tag{7.12}$$

where  $A$ ,  $f$ , and  $B$  in radians are taken from the *American Ephemeris and Nautical Almanac* and interpolated to second differences. The rotation matrix (7.12) has the meaning

$$\begin{aligned} \underline{R}(B, A, -f) &= \underline{R}(-f) \underline{R}(A) \underline{R}(B) \\ &= \begin{bmatrix} \cos f & -\sin f & 0 \\ \sin f & \cos f & 0 \\ 0 & 0 & 1 \end{bmatrix} \\ &\begin{bmatrix} \cos A & 0 & -\sin A \\ 0 & 1 & 0 \\ \sin A & 0 & \cos A \end{bmatrix} \begin{bmatrix} 1 & 0 & 0 \\ 0 & \cos B & \sin B \\ 0 & -\sin B & \cos B \end{bmatrix} \end{aligned} \tag{7.13}$$

or, with sufficient accuracy,

$$\underline{R}(B, A, -f) = \begin{bmatrix} 1 & -f & -(A+Bf) \\ f & 1 & (B-Af) \\ A-B & & 1 \end{bmatrix} \tag{7.14}$$

The rectangular coordinates used up to this point are heliocentric, and it is necessary to transform them to geocentric coordinates whenever the absolute parallax  $\pi$  appearing in the *General Catalogue of Trigonometric Stellar Parallaxes* (Jenkins, 1952) exceeds 0".010. This last correction is obtained with

$$\mathbf{x}_{TT} = \mathbf{x}_{(TT)} + \begin{bmatrix} -C \sec \epsilon \\ -D \cos \epsilon \\ -D \sin \epsilon \end{bmatrix} \frac{\pi}{k} \quad (7.15)$$

with  $C$ ,  $D$ , and  $\epsilon$  as in (7.10). The aberration constant  $k = 20".496$ . The  $\mathbf{x}_{TT}$  vector indicates the apparent geometric direction to a star for the observation epoch and the corresponding true equinox. The corresponding apparent right ascension and declination are obtained with the inversion of (7.1) from (7.15) as

$$\begin{aligned} \alpha &= \arctan x_2/x_1 \\ \delta &= \arctan x_3/(x_1^2 + x_2^2)^{1/2} \end{aligned} \quad (7.16)$$

For a computer program a convenient sequence of operations is obtained by combining the individual steps chosen in (7.6), (7.7), (7.10), (7.12), and (7.15). In connection with (7.1), (7.2), (7.3), (7.8), (7.9), (7.11), and (7.13) or (7.14), auxiliary computations are required based on tabulated or, where necessary, interpolated values. The geocentric directions computed with the rectangular coordinates (7.15) or the orthogonal spherical coordinates (7.16) can be adopted without change as topocentric directions, since the stars are sufficiently remote; i.e., no additional parallax correction is needed. The situation is shown in figure 7.18a, where the basically geometric astronomical reference system  $x_{1,2,3}$  is shown in parallel displacement to an arbitrary point of the earth's surface on a unit sphere surrounding this point.

The orientation of this assumed spatially stationary astronomical system differs, therefore, from the orientation of a geocentric coordinate system  $y_{1,2,3}$  that rotates with the Earth by an angle  $\theta_{Gr}$  that corresponds to this

rotation and is formed by the plane of the Earth-fixed null meridian of longitude ( $\lambda' = 0$ ) and the plane of the astronomic null meridian ( $\alpha = 0$ ). The geometrical meaning of the angle  $\theta_{Gr}$  is apparent from figure 7.19. It is the sidereal time of the null meridian and is computed from Universal Time (UT) (mean Greenwich time) by converting mean to Sidereal Time (i.e., by multiplication with the ratio 366.2427/365.2427 or 1.002 737 91) and adding to  $\theta_{0Gr}$ . The angle  $\theta_{0Gr}$  is listed in the *American Ephemeris and Nautical Almanac* for 0<sup>h</sup> UT of each day. The introduction of Universal Time for the instant of observation makes it necessary to raise certain questions in connection with the measurement of time. This train of thought is presented in section 7.4.4.

By studying the further steps in the reduction it will become apparent that it is advantageous to change the spatial orientation of the astronomical reference system  $x_{1,2,3}$  in a way to simplify the form of certain corrections.

The first is diurnal aberration. In consequence of the daily rotation of the earth-fixed observation stations with respect to the right ascension-declination system, assumed stationary, we must, in addition to the annual aberration caused by the Earth's movement around the Sun, consider a so-called diurnal aberration. This is a function of the true position ( $\phi'$ ,  $\lambda'$ ) of the observation site on the Earth and the angle  $\theta_{Gr}$  (see fig. 7.18a), as well as of the direction of observation, i.e., of the  $\alpha$  and  $\delta$  of the star. After the  $x$  system of figure 7.18a is turned through the angle  $\theta$  about the  $x_3$  axis (see fig. 7.19), the resulting  $x'_1$  direction lies in the meridian plane of the observation site and  $x'_2$  points to the east, i.e., in the direction of the linear velocity vector  $\mathbf{v}_\phi$  of the Earth's rotation.

Figure 7.20a shows a unit circle in the plane that contains the unit vector  $\mathbf{x}'_0$  (direction to the star) and its  $x_2$  component, and hence also the  $\mathbf{v}_\phi$  vector.

From this the length of the aberration vector  $\Delta$  is

$$|\Delta| = \frac{v_{\phi'}}{c} \cos \gamma \quad (7.17)$$

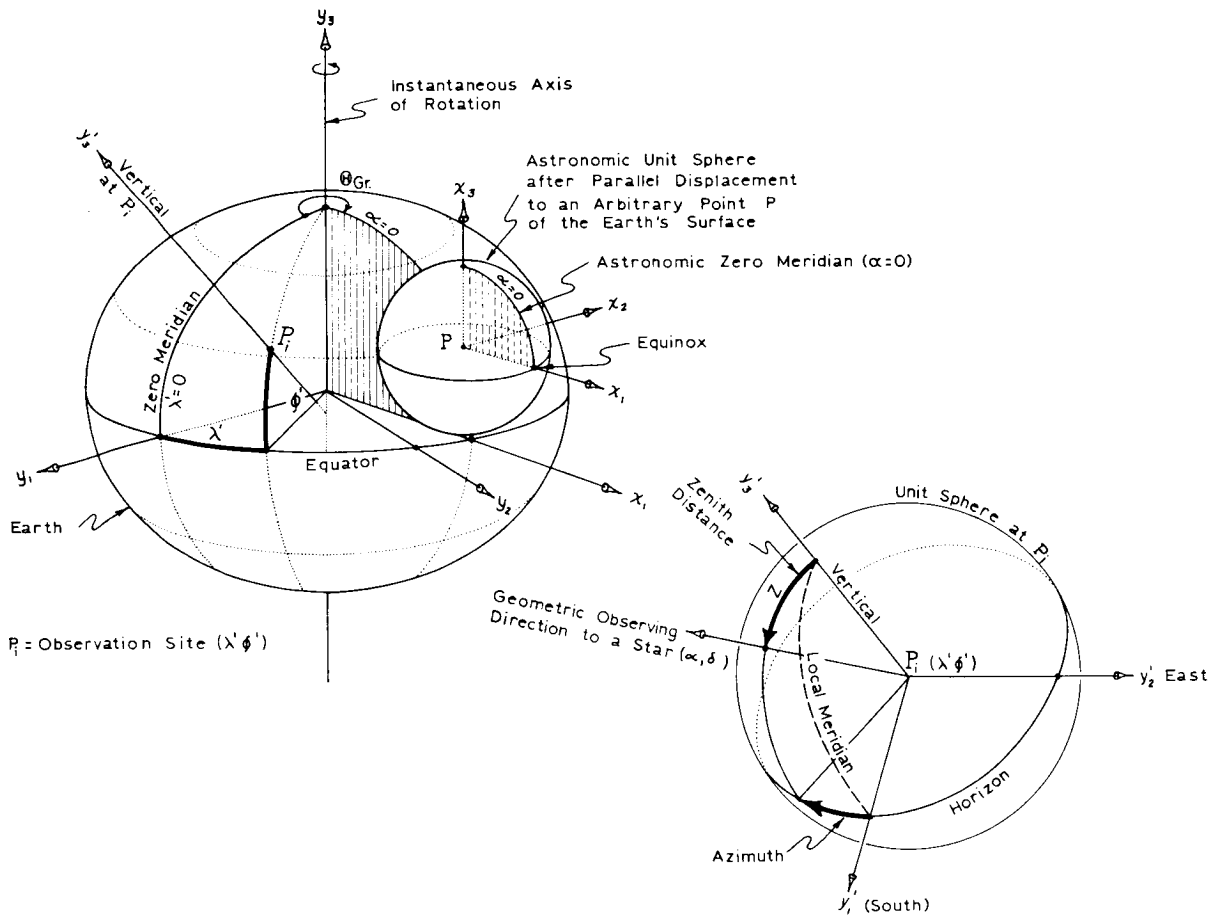


FIGURE 7.18.—Coordinate systems.

in which  $v_\phi$  is the linear velocity of the Earth's rotation in latitude  $\phi'$  and  $c$  is the velocity of light.

The components of  $\Delta$  in the  $x'_{1,2,3}$  directions (see fig. 7.20 and eq. 7.73) are

$$\Delta = \begin{bmatrix} -x'_1 x'_2 \\ (1 - x'^2_2) \\ -x'_3 x'_2 \end{bmatrix} \cdot k' \quad (7.18)$$

with  $k' = v_\phi/c$ , or sufficiently close for the purpose,

$$k' = 0.319 \cos \phi' \quad (7.19)$$

To compute (7.18), we must rotate the  $x$  system to which the  $x_{TT}$  vector (7.15) is

referred through the angle  $\theta$ . This results in

$$\mathbf{x}'_{TT} = \underline{R}(\theta) \mathbf{x}_{TT} \quad (7.20)$$

where

$$\underline{R}(\theta) = \begin{bmatrix} \cos \theta & \sin \theta & 0 \\ -\sin \theta & \cos \theta & 0 \\ 0 & 0 & 1 \end{bmatrix} \quad (7.21)$$

The unit vector  $\mathbf{x}'_{TT}$  corrected for diurnal aberration is, with (7.18) and (7.19),

$$\mathbf{x}'_{(TT)} = \mathbf{x}'_{TT} + \begin{bmatrix} -x'_1 \cdot x'_2 \\ (1 - x'^2_2) \\ -x'_3 \cdot x'_2 \end{bmatrix} k' \quad (7.22)$$

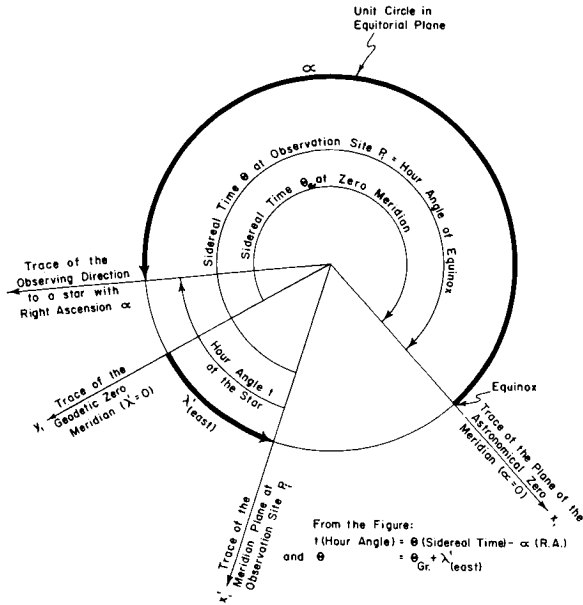


FIGURE 7.19.—Relation of local times to other times.

To account for astronomic refraction, a further correction is necessary. Since astronomic refraction is most conveniently computed as a function of the geometric zenith distance  $\zeta$  of the observed direction, the  $x'_{TT}$  system (7.20) is rotated through  $(90^\circ - \phi')$  about its  $x'_2$  axis into the local rectangular  $y'$  system (see fig. 7.20b). The resulting unit vector from (7.22) is

$$y' = \frac{R}{2} (90^\circ - \phi') x'_{(TT)} \quad (7.23)$$

with

$$\frac{R}{2} (90^\circ - \phi') = \begin{bmatrix} \sin \phi' & 0 & -\cos \phi' \\ 0 & 1 & 0 \\ \cos \phi' & 0 & \sin \phi' \end{bmatrix} \quad (7.24)$$

and, correspondingly, with (7.16) from (7.23) the azimuth  $A$  (from south over west) and zenith distance  $\zeta$  are

$$\begin{aligned} A &= \arctan \frac{y'_2}{y'_1} \\ \zeta &= \arctan \frac{(y'^2_1 + y'^2_2)}{y'_3} \end{aligned} \quad (7.25)$$

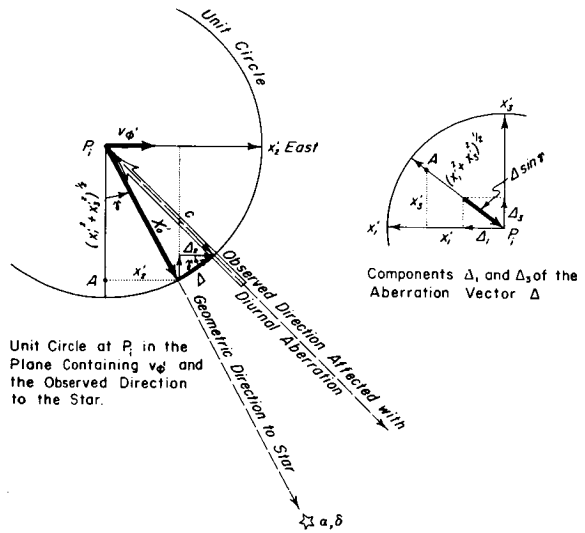


FIGURE 7.20

The astronomic refraction  $r_\infty$  is next computed, on the basis of the mathematical model described in section 7.4.5, as functions of the weather data obtained during the observation (air temperature, pressure, relative humidity, etc.). The vector  $y'$  of (7.23) is corrected for this refraction in accordance with (7.74) of section 7.4.6.2 (cf. also eq. (7.42)), giving

$$y'_r = y' + \begin{bmatrix} -\cos\left(\zeta - \frac{r_\infty}{2} \cos A\right) \\ \cos\left(\zeta - \frac{r_\infty}{2} \sin A\right) \\ \sin\left(\zeta - \frac{r_\infty}{2}\right) \end{bmatrix} 2 \sin \frac{r_\infty}{2} \quad (7.26)$$

When  $r_\infty$  is small in a differential sense in relation to the expected limit of accuracy, (7.26) simplifies in accordance with (7.73) to:

$$y'_r = y' + \begin{bmatrix} -y'_1 y'_3 \\ -y'_2 y'_3 \\ (1 - y'^2_3) \end{bmatrix} r_\infty (1 - y'^2_3)^{-1/2} \quad (7.27)$$

where  $r_\infty$  is in radians.

Corresponding spherical coordinates can be obtained from (7.26) or (7.27) with (7.25).

More suitable for further development of our problem are the rectangular coordinates  $\xi$  and  $\eta$  in the plane tangent at the zenith of the observer to a unit sphere, as shown in figure 7.27 of section 7.4.6.2. These coordinates are commonly designated as standard coordinates in astronomy and are computed with the expressions on the left of (7.26) or (7.27) in accordance with (7.66) and (7.67) of section 7.4.2.6:

$$\begin{aligned}\xi_r &= y'_1/y'_3 \\ \eta_r &= y'_2/y'_3\end{aligned}\quad (7.28)$$

Hence (cf. eq. (7.64) and (7.65) of sec. 7.4.6.2):

$$\begin{aligned}A &= \arctan \eta_r/\xi_r \\ \zeta_r &= \arctan (\xi_r^2 + \eta_r^2)^{1/2}\end{aligned}\quad (7.29)$$

The correction steps of the preceding paragraphs can again be combined in a sequence of steps convenient for programmed computation. From (7.20), (7.22), (7.23), and (7.26) or (7.27) results the direction vector  $y'_r$  in the local coordinate system as derived from the  $x_{T'}'$  vector (7.15) in the astronomic  $x$  system. These directions represent a stationary oriented bundle of rays at the point of observation for the instant  $T$ , expressed in UT, of the observation. The rays forming this bundle pierce the tangent plane of the unit sphere at the zenith of the observing station in points whose locations are defined by their coordinates  $\xi_r, \eta_r$ . The  $\xi\eta$  system corresponds in its orientation to the  $y'$  system. By obtaining the coordinates  $\xi_r, \eta_r$ , therefore, we have transformed the spherical coordinates, originally tabulated in a star catalog for a specified epoch, into three-dimensional rectangular coordinates such that all the reference points lie in a plane tangent to the unit sphere. The coordinates assigned to these points with reference to the center of the sphere as origin and axes parallel to the directions  $y'_{1,2,3}$  are therefore  $\xi_r, \eta_r, +1$ .

The images of the stars corresponding to these control points lie in the plane of the

photographic plate on which their position is determined with reference to an arbitrarily oriented plane rectangular coordinate system  $(x, y)$  introduced into the plate plane (see fig. 7.32 of sec. 7.4.6.2). There remains the problem of establishing the projective correspondence between the two sets of points on the two planes, one set defined by coordinates  $(\xi_r, \eta_r)$ , the other by corresponding image coordinates  $(x, y)$ . This principal problem of the photogrammetric measuring technique is solved by the application of the principles of generalized central perspective. The mathematical model for this solution is described in detail in section 7.4.6.3. For the present, it is necessary only to accept the fact that this step establishes, either directly or indirectly, the orientation of the photogram with respect to the coordinate system in which the control points are given, in our case with reference to the local  $y'$  system. Similarly, all the derived rays from this oriented bundle, such as the directions to the additionally photographed individual satellite positions (see sec. 7.4.6.5.1), are obtained in this coordinate system. Since in the subsequent triangulation (see sec. 7.4.7.2) all directions from the various stations must be referred to a common coordinate system, one can rotate the locally introduced coordinate systems so as to make their axes parallel to those of the common system chosen for the spatial triangulation before the photogrammetric reduction of the individual single cameras. This rotation can also be effected after the reduction of the single camera. The rotation matrices which determine the orientation of the photogrammetric exposure, and which, as was mentioned, refer to the local  $y'$  systems, are transformed for this purpose so that they refer with their elements of orientation to the common coordinate system chosen for the triangulation. Hence, the next step in the computation is the transformation of either the local  $y'$  system established at the point of observation  $P$  ( $\phi', \lambda'$ ) or the local orientation matrix  $\underline{R}'_y$  ( $\alpha, \omega, \kappa$ )<sup>†</sup> obtained in the photogrammetric reduction to  $z$  system selected for the subsequent triangulation (see sec. 7.4.6.2.6). First, the local  $y'$

system is transformed to the corresponding geocentric  $y$  system. The necessary rotations are through the angle  $(270^\circ + \phi)$  about the  $z$  axis, and then through the angle  $(-\lambda_{\text{east}})$  about the turned 3 axis. This gives

$$y = \underset{3}{R}(-\lambda'_{\text{east}}) \underset{2}{R}(270^\circ + \phi) y'_r$$

$$= \begin{bmatrix} \cos \lambda' & -\sin \lambda' & 0 \\ \sin \lambda' & \cos \lambda' & 0 \\ 0 & 0 & 1 \end{bmatrix} \begin{bmatrix} \sin \phi' & 0 & \cos \phi' \\ 0 & 1 & 0 \\ -\cos \phi' & 0 & \sin \phi' \end{bmatrix} y'_r \tag{7.30}$$

or analogously,

$$\underset{y}{R}_y(\alpha, \omega, \kappa) = \underset{3}{R}(-\lambda'_{\text{east}}) \underset{2}{R}(270^\circ + \phi')$$

$$\underset{y}{R}'_y(\alpha, \omega, \kappa) \tag{7.31} \dagger$$

where  $\underset{y}{R}_y(\alpha, \omega, \kappa) \dagger$  corresponds in the  $y$  system to the photogrammetric orientation matrix.

Basically, the aim of the reductions so far discussed is to refer all the photographically registered directions to stars—observed from different stations and, in general, at different times—to a consistent stationary coordinate system. The computations would produce a rigorous geometric solution only if we could assume that the direction of the Earth's axis of rotation, i.e., the  $y_3$  direction of figure 7.18a labeled instantaneous axis of rotation, remains invariant in space. We know, however, that the poles describe more or less irregular loops in a period of approximately 430 days about a mean position which itself possibly has a secular displacement. From a geometrical point of view it is immaterial whether this so-called polar motion is treated as an additional motion relative to the astronomic reference system (a sort of additional precession and nutation) or whether one accepts the direction of the rotation axis as invariant and ascribes the phenomenon to a displacement of the crust. However, in addition to this purely geometric and computable effect, the influence of polar motion is coupled with the problem of time determination at the observation site. For this reason the discussion of these corrections

will be combined with the questions of time determination in the following section.

#### 7.4.4 Meaning and Measurement of Time

The significance of time determination for the problem of geometric satellite triangulation is twofold. First, because of the dynamic characteristics of the universe, i.e., because of the Earth's motion in space, we must determine the instant of the photographic exposure of the star image within an interval based on astronomic observations. In addition, because of the motion of the satellite itself, the instants of observation of the satellite at all stations observing the pass must be correlated with respect to an otherwise arbitrary measuring frequency, which amounts to a relative time determination.

With this, one interpolates points along the satellite track whose images, from a geometric standpoint, represent basically arbitrary but uniquely defined points on the orbit. In registering the pass of a satellite whose track is marked by short-duration light flashes this requirement is not necessary. Because of the finite speed of light, part of the photons emitted in the flash will, in general, not arrive at the different observation sites simultaneously, but for that very reason they will produce images whose positions on the various photograms correspond to a single point in space, the origin of the flash, and thus fulfill automatically the "geometric condition of simultaneity." Following is a discussion of those problems concerned with the impact on satellite triangulation of the time of observation needed for star imagery. We emphasize again the fact that the requirement for time correlation in star observations is, in principle, of a purely geometric nature. This conclusion follows from the fact that the spatial position of the Earth with its observation stations changes with time, relative to the astronomic reference system. The measurement of time, therefore, serves to refer the spatial orientation of the Earth at the instant of observation back to an orientation assumed as a normal position and corresponding at a specified epoch.

For the motion of the Earth around the Sun it is necessary to refer the Julian day and fraction of a day, as represented by UT for the instant of observation, to the beginning of the corresponding tropical year, the latter representing a point of time independent of all calendar reckoning and the same for all meridians (cf. Jordan/Eggert, 1939). The interval  $T$  so determined is needed for all the reductions described in section 7.4.3. The interval derived from the time of day serves as the basis for determining local sidereal time in accordance with the steps given in the previous section. There now arises in satellite triangulation the problem of the geometrical meaning of the measure of time known as Universal Time (UT).

As is well known, the time of day is transmitted by radio signals broadcast from numerous stations distributed all over the world. Abstracting the delays due to physical causes in the transmitters and receivers and their antennas and to variations in the propagation velocity of light caused by atmospheric influences, these time signals represent a sequence of extremely regular intervals. They are monitored by atomic clocks with great and long-term stability ( $\pm 10^{-10}$  sec over a period of months with daily variations of  $< 10^{-11}$  sec).

In principle, these transmitted signals do not represent a time referred to the Earth's rotation, but to a definite signal sequence. For most daily and public purposes, however, it can be considered directly as the "time of day." By means of stellar observations at a group of observatories linked in an international service, the relation between these time signals and time referred to the Earth's rotation is established. In addition, this international working group concerns itself with the determination of the instantaneous position of the pole. These figures are published in the form of preliminary and later definitive values. One set lists the position of the instantaneous pole with respect to a selected null position; other tables give time corrections for converting the transmitted signals to Universal Time 1 (UT1) and Universal Time 2 (UT2). The results from the

various observations (58 are participating at this time) are combined at the Bureau International de l'Heure (BIH) into a "mean observatory" value. This eliminates neglected influences such as refraction anomalies, secular polar motions, and irregular changes in the Earth's rotation statistically, at least to some extent. It also smooths out the errors in the determination of time due to systematic biases caused by the assumed nominal longitudes of the various observations and long-term refraction influences. Universal Time 2 in this system refers to a fictitious Earth that is practically independent of periodic, chiefly seasonally dependent, changes in the rate of the Earth's rotation.

UT1 is characterized by the fact that it, like the original observation, contains the periodic, seasonal variations of the Earth's rotation and therefore represents a measure of the instantaneous rate of rotation. Hence, it is a more suitable time for the present purpose, even though it is not uniform, and the time interval so determined can, as was indicated above, be converted into the corresponding sidereal interval by multiplication with 1.002 737 91. Since 24 hours of sidereal time represents exactly one revolution of the earth relative to the right ascension-declination system, the so-computed sidereal time is proportional to an angle of rotation, the geometric equivalent of our time coordinate, and is represented in figure 7.19 in a form convenient to the purpose, as sidereal time of the null meridian (see also fig. 7-18a). By introducing two great circles to include this angle, one obtains a definition valid for all instantaneous positions of the pole. One great circle is the meridional trace of the plane containing the instantaneous axis and pole of the Earth's rotation and the point of the celestial equator that represents the equinox of the observational period. The other great circle is the null meridian, which is the trace of a plane again containing the instantaneous axis of rotation plus an arbitrary but uniquely defined point of the Earth's surface. This point, by international convention, has the coordinates longitude  $\lambda_0 = 0$  and latitude  $\phi_0 = 0$  referred to the mean position of the pole for

the period 1900–1905. Unfortunately, this point lies in the Atlantic Ocean, and no direct observations are possible from it. This situation is regrettable from a geodetic standpoint, but conceivably reveals the foresight of the specialists involved in the extraordinarily complex and difficult problem of reducing astronomical observations made for the purpose of time determination.

The ultimate refinements in time determination are not of decisive importance in the method of geometric satellite triangulation treated here, since the accuracy required in timing the instant of star exposures is at most  $\pm 3$  msec. Consequently, UT1 furnishes geometric satellite triangulation with a time coordinate whose geometric equivalent, when it is transformed into a sidereal interval, is compatible with the coordinate transformation (7.20) of the previous section.

In the past the situation described above was complicated by the fact that UT1 and UT2 were not referred to the conventional 1900–1905 pole, but were until 1958 referred to a pole which dropped periodically, and thereafter these times had as a reference pole a periodically displaced pole with a so-called secular motion. Since for all these various positions of the pole the corresponding null meridian passed through Greenwich, its intersection with the conventional equator was correspondingly displaced. As a consequence, for the period from 1958 to 31 December 1967, UT1 cannot be used as a rigorous measure for rotation. After 1 January 1968 the time pole is stationary and identical with the 1900–1905 conventional pole (CIO) as recommended by the International Astronomical Union 1967.

It should be noted, however, that the classical null meridian of Greenwich should be replaced by either a correspondingly rotated geodetic meridian or an equivalent discontinuity introduced into universal time on 1 January 1968 (see sec. 1.4). After that, the situation is clarified, our basic considerations have validity, and UT1 can be accepted as a measure of the Earth's rotation. Under these assumptions, the  $y$  system obtained with (7.30) represents a reference system

corresponding to an instantaneous position of the Earth to which, therefore, the photogrammetric rotation matrix  $\underline{R}_y(\alpha, \omega, \kappa)$  † computed with (7.31) is referred as well. From the geometric considerations above, it follows readily that for the eventual geometric normalization of the observation results, i.e., for the transformation of these data into the system chosen for the triangulation of the station coordinates, it will be necessary to rotate the  $y$  system referred to the observation period into the  $z$  system of the epoch selected for the spatial triangulation.

From figure 7.20 it is apparent that only two rotational components are needed. First the  $y$  system must be turned about its 2 axis through the angle  $-a$ , and then this turned system must be turned about its 1 axis through the angle  $-b$ . The 3 axis thus obtained will then define the direction of the rotation axis for the epoch chosen; the intersection of the 1 axis with the sphere will represent the origin of the system of time measurement adopted by international agreement, its meridian corresponding to the classical Greenwich meridian. From figure 7.21, this transformation is

$$\mathbf{z} = \underline{R} \begin{pmatrix} -a & -b \\ 2 & 1 \end{pmatrix} \mathbf{y} \tag{7.32}$$

with

$$\begin{aligned} \underline{R} \begin{pmatrix} -a & -b \\ 2 & 1 \end{pmatrix} &= \underline{R} \begin{pmatrix} -b \\ 1 \end{pmatrix} \underline{R} \begin{pmatrix} -a \\ 2 \end{pmatrix} \\ &= \begin{bmatrix} 1 & 0 & 0 \\ 0 & \cos b & -\sin b \\ 0 & \sin b & \cos b \end{bmatrix} \begin{bmatrix} \cos a & 0 & \sin a \\ 0 & 0 & 0 \\ -\sin a & 0 & \cos a \end{bmatrix} \end{aligned} \tag{7.33}$$

The rotation angles  $a$  and  $b$  are small and equal to the differential displacements  $x$  and  $y$  published by the BIH for defining the instantaneous pole with respect to the conventional origin (the 1900–1905 pole in our case). The rotation (7.33) becomes

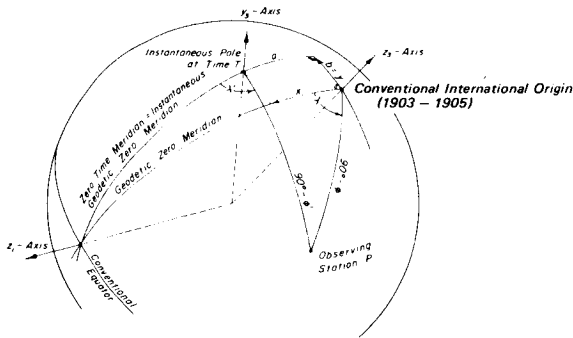


FIGURE 7.21.—Relations between instantaneous pole and conventional pole (1903-1905).

$$\underline{R} \begin{pmatrix} -x \\ -y \\ 1 \end{pmatrix} = \begin{bmatrix} 1 & 0 & x \\ 0 & 1 & -y \\ -x & y & 1 \end{bmatrix} \quad (7.34)$$

$\underline{R}_y$  of (7.31) transforms into the corresponding photogrammetric rotation matrix

$$\underline{R}_z(\alpha, \omega, \kappa) = \underline{R} \begin{pmatrix} -x \\ -y \\ 1 \end{pmatrix} \underline{R}_y(\alpha, \omega, \kappa) \quad (7.35) \dagger$$

When the satellite triangulation is adjusted within a local rectangular coordinate system, a process which could be entirely practical within a given geodetic datum, expression (7.35) must be further rotated. If, for example, the rectangular Cartesian coordinate system to be used in the final triangulation is to be erected at the point  $P(\lambda_{east}, \phi, h=0)$ , we will have, analogous to the preceding transformations,

$$\mathbf{z}' = \underline{R}[\lambda_{east}, (90^\circ - \phi)] \mathbf{z} \quad (7.36)$$

with

$$\begin{aligned} \underline{R}[\lambda_{east}, (90^\circ - \phi)] &= \underline{R}(90^\circ - \phi) \underline{R}(\lambda_{east}) \\ &= \begin{bmatrix} \sin \phi & 0 & -\cos \phi \\ 0 & 1 & 0 \\ \cos \phi & 0 & \sin \phi \end{bmatrix} \\ &\quad \begin{bmatrix} \cos \lambda & \sin \lambda & 0 \\ -\sin \lambda & \cos \lambda & 0 \\ 0 & 0 & 1 \end{bmatrix} \end{aligned} \quad (7.37)$$

and similarly for the transformation of the photogrammetric orientation matrix

$$\underline{R}'_z(\alpha, \omega, \kappa) = \underline{R}[\lambda_{east}, (90^\circ - \phi)] \underline{R}_z(\alpha, \omega, \kappa) \quad (7.38) \dagger$$

### 7.4.5 Additional Geometric and Physical Influences

The preceding section has treated all the coordinate transformations needed (based on the given star catalog data) to reconstruct analytically the photogrammetric bundle of rays and orient it in space. The analytical reconstruction is determined by means of those parameters which simulate interior orientation and distortion, whereas the elements of exterior orientation express the orientation in space of the bundle with respect to a uniquely defined Earth-fixed coordinate system. To reproduce the oriented bundle, a mathematical model is used (see secs. 7.4.6.4 and 7.4.7 for a more detailed description).

For the present, it will be assumed that this problem has been solved, and we will pass on to an explanation of the corrections necessary to derive, from the image coordinates of the satellite points together with the parameters from bundle reconstruction, those directions needed later in the triangulation of the station coordinates. It will be assumed further that the measured images of the satellite trail have, by means of the parameters obtained in the bundle reconstruction, been made to conform to the mapping principle of a rigorous central perspective. Then, the direction in space corresponding to any point image computed with the corresponding elements of interior and exterior orientation will be tangent at the center of projection to the ray of light representing the physical light bundle. The center of projection in the present case is the center of the unit sphere. The unit vector  $\mathbf{y}'_o$ , in this direction is derived, as will be shown in section 7.4.6.2 with (7.81), from the photogrammetric bundle vector  $\mathbf{p}$ . In section 7.4.3 it

was explained that this direction refers to the same coordinate system as the photogrammetric rotation matrix in use. Hence, by use of the  $\underline{R}_y(\alpha, \omega, \kappa)$ † matrix mentioned there, one obtains the unit vector  $y'_{0,r}$  corresponding to an arbitrary image, where in accordance with (7.61),

$$y_{0,r} = \begin{bmatrix} y'_1 \\ y'_2 \\ y'_3 \end{bmatrix}_r \equiv y'_r \quad (7.39)$$

(The subscript 0 used to designate a unit vector will be omitted in what follows, unless its use is necessary for better understanding.)

This observed direction must first be corrected for refraction. The problem of refraction is pictured schematically in figure 7.22 for both star and satellite images. Astronomical refraction  $r_\infty$  for zenith distances up to 85 degrees can be computed to sufficient accuracy with, for example, Garfinkel's (1944, 1967) formula:

$$r_\infty = \underline{T}^{1/2} W \left( \tau_1 \tan \frac{\beta}{2} + \tau_2 \tan^3 \frac{\beta}{2} + \tau_3 \tan^5 \frac{\beta}{2} + \tau_4 \tan^7 \frac{\beta}{2} \right) \quad (7.40)$$

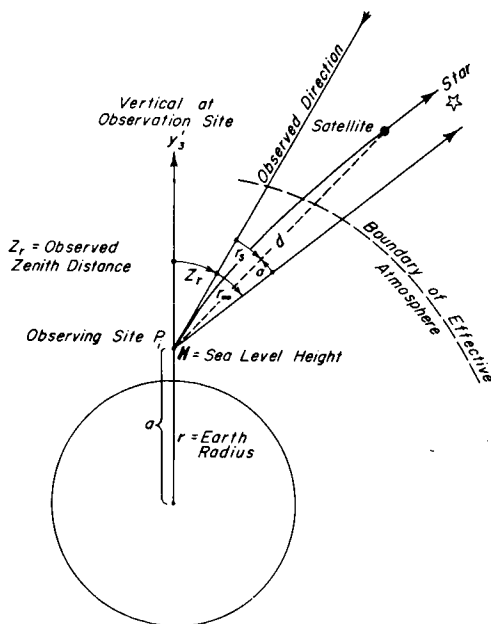


FIGURE 7.22.—Schematic presentation of star and satellite refraction.

in which

$$\begin{aligned} \underline{T} &= T/T_0, \text{ where } T_0 = 273.16^\circ \text{ K} \\ W &= P/T_0, \text{ where } P = p/p_0 \text{ and } p_0 = 760 \text{ mm Hg} \end{aligned}$$

$\tan \beta = (\underline{T}^{1/2}/\gamma) \tan z_r$ , where  $\gamma = 8.7137$  and  $z_r$  is the observed zenith distance.

If the coefficients  $\tau_1$  to  $\tau_4$  are referred to geometric zenith distances, then an iteration loop must be provided for the computation of refraction from observed zenith distances.

Refraction for a satellite observation  $r_s$  is

$$r'_s = r''_s \left( 1 - \frac{a \cdot s}{d \cos z_r} \right) \quad (7.41)$$

where

$a = r + H$ , i.e., the Earth radius plus the height above sea level of the observing site  
 $s = RT_0/r$ , where  $R = 29.2745$ , the pressure height of a homogeneous atmosphere, and hence  $s = 0.001255$

$d$  = distance between satellite and station in meters

The unit vector corrected for refraction is obtained from (7.39) by using (7.25), (7.26), or (7.27) as

$$y' = y'_r - \begin{bmatrix} -\cos \left( z_r + \frac{r_s}{2} \right) \cos A \\ \cos \left( z_r + \frac{r_s}{2} \right) \sin A \\ \sin \left( z_r + \frac{r_s}{2} \right) \end{bmatrix} 2 \sin \frac{r_s}{2} \quad (7.42)$$

or, with (7.73) in section 7.4.6,

$$y' = y'_r + \begin{bmatrix} y'_1 y'_3 \\ y'_2 y'_3 \\ -(1 - y'^2_3) \end{bmatrix} r_s (1 - y'^2_3)^{-1/2} \quad (7.43)$$

where  $r_s$  is expressed in radians.

To compute the refraction  $r_s$  for the direction to the satellite in (7.41), the distance  $d$  between the station and satellite is needed. This quantity is also necessary for the computation of subsequent corrections. However, only a good approximation for the distance is



The distance between the observer and the satellite  $d$  is large in relation to the balloon radius, and hence in relation to  $a$ , so that to a sufficient degree of approximation

$$d\mathbf{m} = - (a/d)\mathbf{n} \quad (7.48)$$

or, with (7.45),

$$d\mathbf{m} = - \frac{a}{d \sin \gamma} (\mathbf{l} + \cos \gamma \mathbf{m}) \quad (7.49)$$

The displacement  $a$  from the center for a reflecting satellite with radius  $\xi_b$  is, from figure 7.23,

$$a = \xi_b \sin (\gamma/2) \quad (7.50)$$

For a balloon with a diffusively reflecting surface it can be argued that the centroid of the satellite image corresponds to the centroid of the illuminated portion of the balloon surface as seen from the observation site. In this case, we have

$$a = \frac{\xi_b}{2} (1 - \cos \gamma) \quad (7.51)$$

Finally, with (7.50) or (7.51), as the case may be,

$$\mathbf{m}^* = \mathbf{m} + d\mathbf{m} \quad (7.52)$$

To compute (7.49), the unit vectors  $\mathbf{l}$  and  $\mathbf{m}$  are needed. Up to this point we have assumed only that they are referred to an arbitrary but consistent coordinate system. We set, therefore, with (7.43),

$$\mathbf{m} = \mathbf{y}' \quad (7.53)$$

With the right ascension and declination values of the Sun  $\alpha_\odot$  and  $\delta_\odot$  interpolated for the time of observations, the  $\mathbf{x}_\odot$  vector is computed with (7.1), neglecting refraction and other corrections, and then the  $\mathbf{x}'_\odot$  vector is computed by using local sidereal time  $\theta = 1.002\,739\,91 \text{ (UTI)} + \lambda'_{east}$  and (7.20), (7.21). Finally the  $\mathbf{y}'_\odot$  vector is derived with (7.23) and (7.24). Then,

$$\mathbf{y}'_\odot = \mathbf{l} \quad (7.54)$$

Similarly, with equation (7.52) the unit vector  $\mathbf{y}'$  in the direction of the balloon center is

$$\mathbf{y}' = \mathbf{m}^* \quad (7.55)$$

A detailed explanation of the phase correction is given in Schmid (1971).

In order to interpret the direction of (7.55) correctly in a geometric sense, it is necessary to bear in mind that the satellite serving as a target and the station site are subject to independent motions. The satellite, in orbiting the Earth, shares the motion of the Earth around the Sun, so that the annual aberration effect is canceled. However, because of the Earth's rotation, the linear velocity component of the observation stations creates a displacement of the observed directions corresponding to diurnal aberration. In addition, the relative spatial relation between the satellite and the observing station changes in the time required for the light to travel from the satellite to the station. This situation is shown schematically in figure 7.24 for a flash emitted from the satellite. The position of the observing station ( $\phi', \lambda'$ ) and its Earth-

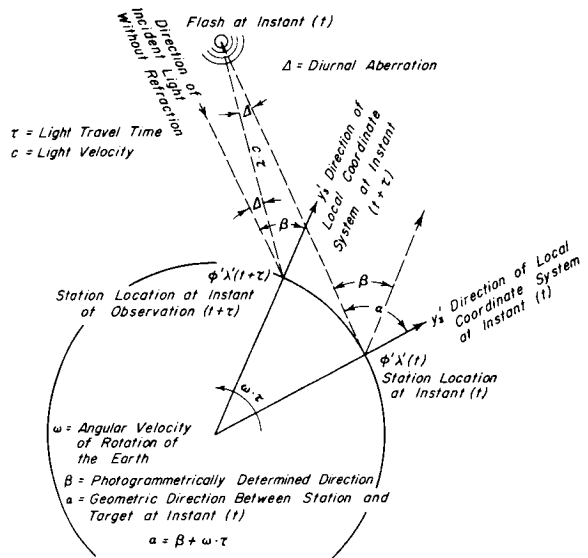


FIGURE 7.24.—Influence of diurnal aberration and earth rotation when recording light flashes originating at satellite.

fixed  $y'$  reference system (symbolized by the  $y_3$  direction) is shown at the instant  $t$  of the emission. Let the geometric direction at time  $t$  from the station to the flash be indicated by the direction angle  $\alpha$ . Owing to its finite propagation velocity  $c$ , the light requires an interval  $\tau$  to reach the station by traversing the distance  $d$ :

$$\tau = d/c \tag{7.56}$$

During the interval  $\tau$ , however, the station has reached a position differing from the initial position by the angle  $\omega\tau$ , where  $\omega = 15''/\text{sec}$  is the Earth's angular velocity. From the aberration theory (cf. Schaub, 1950), it follows that the apparent direction of observation differs from the corresponding geometrical direction by the aberration angle  $\Delta$ . The latter direction is parallel to the geometrical direction existing between the station and the satellite at the instant  $t$ . This statement is rigorous to the order to which the Earth's rotational velocity may be considered linear and constant. It follows that the flash is observed at the directional angle  $\beta$  relative to the local coordinate frame. The angle  $\alpha$  needed in the subsequent treatment of the problem is therefore obtained from

$$\alpha = \beta + \omega \cdot \tau \tag{7.57}$$

The situation is complicated somewhat for the case in which satellite triangulation is carried out not by means of flashes but by means of a continuously illuminated satellite. The shutter mechanism of the observing camera permits the chopping of the satellite trail into a series of separate images. Thus, the individual images are formed at times  $t_1, t_2, \dots, t_n$ , to which appertain corresponding light travel durations  $\tau_1, \tau_2, \dots, \tau_n$ . The images corresponding to instants  $t_1 + \tau_1, t_2 + \tau_2, \dots, t_n + \tau_n$  must now be interpolated into the image sequence. Strictly speaking, according to figure 7.25, the interpolation should be for the instants  $t_1 + \tau_1^*, t_2 + \tau_2^*, \dots, t_n + \tau_n^*$ , where

$$\tau_1^* = \tau_1 + \frac{\tau_2 - \tau_1}{t_2 - t_1} \tau_1, \text{ etc.}$$

The difference  $\tau_1^* - \tau_1$  is, however, negligible. To effect the interpolation, a time-related function of position is set up, expressing the photographic image sequence.

Figure 7.25 shows the relations existing between the recorded time, the satellite position, and the observation station, the symbols used having the same meaning as in figure 7.24. The principle of interpolation is shown, in considerably simplified form, for only two observations occurring at instants  $t$  and  $t + \Delta t$ . As before, the needed direction angle  $\alpha$  is obtained from the interpolated observed direction  $\beta$  by means of (7.57).

The direction  $\alpha$  thus obtained reproduces the geometry between station and satellite existing at the instant  $t$ . From a similar treatment of the observations at other stations observing the same pass, directions to the satellite position at the instant  $t$  can be computed. These, then, are geometrically coherent directions with which the eventual

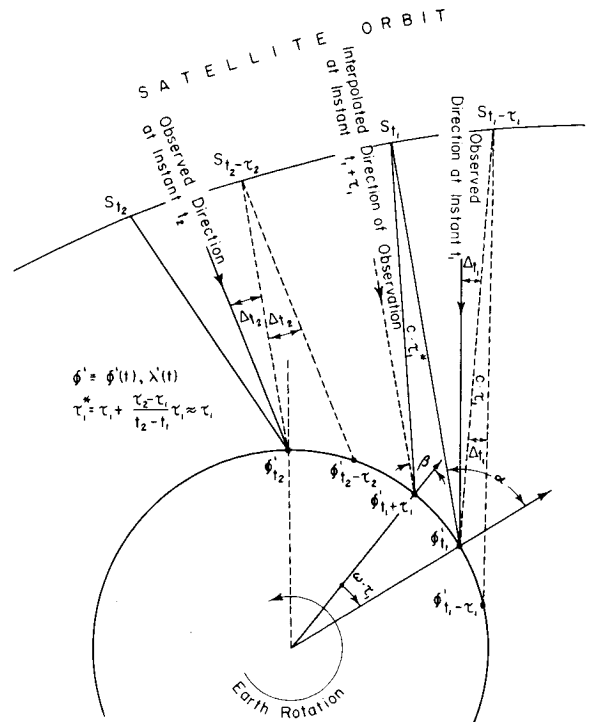


FIGURE 7.25.—Influence of diurnal aberration and earth rotation when recording a continuously illuminated satellite.

space triangulation of the observing stations will be carried out. The interpolation of fictitious satellite images referred to above also serves the purpose of taking into account the time differences between the station clocks at the various sites (see sec. 7.3). The time differences can be considered as shifts in the origins of the time bases at the several observation stations at the same time.

In order to execute the various reductions just described, it is necessary to derive the corresponding image coordinates  $\bar{x}$ ,  $\bar{y}$  with (7.85) and (7.86) referred to the vector  $y'$  of (7.55). On the assumption that the exposure sequence has been carefully monitored (the practice with the BC-4 system is to monitor to within better than 50  $\mu$ sec), the following polynomials can be set up as interpolation functions:

$$\begin{aligned} \bar{x} &= a_0 + a_1 t + a_2 t^2 + a_3 t^3 + a_4 t^4 + a_5 t^5 + \dots \\ \bar{y} &= b_0 + b_1 t + b_2 t^2 + b_3 t^3 + b_4 t^4 + b_5 t^5 + \dots \end{aligned} \tag{7.58}$$

The coefficients  $a_0, a_1, \dots, a_n$  and  $b_0, b_1, \dots, b_n$  are obtained from an adjustment (see section 7.4.6.2.1). The degree assumed for the polynomial depends chiefly on the length of the recorded satellite trail, i.e., more or less on the aperture of the camera used. With the BC-4 system a polynomial of the fifth degree, at least for the component in the direction of the trail, is necessary (see sec. 7.4.1). Several hundred satellite images are used to compute the polynomial. The adjustment effects a smoothing that is of decisive importance for the accuracy of satellite triangulation, since it eliminates the influence of scintillation. Regardless of its amplitude, which, depending on local meteorological conditions, can attain several seconds of arc, scintillation is always characterized by a nearly ideal normal distribution and hence can be eliminated practically completely with a Gaussian adjustment, provided a sufficiently large number of satellite images is available. This condition is not met by the use of present-day light flashes.

The polynomials (7.58) are now used to interpolate fictitious satellite images. Image

coordinates  $\bar{x}$ ,  $\bar{y}$  are computed for the instant (in station time) that corresponds to the satellite position at time  $T$ . Since, as was indicated above, the times assigned to the various observing stations are not necessarily referred to the same null point, the local  $t_i + \tau_i$  values must be reduced to a consistent clock time by the addition of  $\Delta T_i$  (represented schematically in fig. 7.26).

To repeat, the station times  $t_i + \tau_i, t_j + \tau_j, t_k + \tau_k, \dots$  used for interpolation at station  $i, j, k, \dots$  do not represent the same instant  $T$  at the clock, but fix image coordinates which are geometrically consistent; i.e., they satisfy the "geometric condition of simultaneity" mentioned in section 7.4.4.

With the image coordinates  $\bar{x}, \bar{y}$  thus obtained, the corresponding  $y'$  vector is recomputed from the corresponding bundle vector  $p$  of (7.81). The last correction modifies the orientation of this vector to account for the Earth's rotation during the light travel time  $\tau$ . Theoretically, this is accomplished by rotating the local  $y'$  system about its 2 axis through an angle  $-(90^\circ - \phi')$ , which brings the 3 axis into coincidence with the Earth's rotation axis. Next, the system is rotated about this latter axis through the angle  $-\omega\tau$ . This rotation cancels the effect of the Earth's rotation. Finally, the twice-rotated 2 axis is turned through the angle  $(90^\circ - \phi)$ , resulting in a system with the unit vector  $y_s$ . The necessary computations are, therefore,

$$\begin{aligned} y' &= \underline{R}(90^\circ - \phi') \underline{R}(-\omega\tau) \underline{R}-(90^\circ - \phi') y \\ &= \begin{bmatrix} \sin \phi' & 0 & -\cos \phi' \\ 0 & 1 & 0 \\ \cos \phi' & 0 & \sin \phi' \end{bmatrix} \begin{bmatrix} \cos \omega\tau & -\sin \omega\tau & 0 \\ \sin \omega\tau & \cos \omega\tau & 0 \\ 0 & 0 & 1 \end{bmatrix} \begin{bmatrix} \sin \phi' & 0 & \cos \phi' \\ 0 & 1 & 0 \\ -\cos \phi' & 0 & \sin \phi' \end{bmatrix} y' \end{aligned} \tag{7.59}$$

Since  $\omega\tau$  is small, (7.59) simplifies to

$$y'_s = y' + \begin{bmatrix} -y'_2 \sin \phi' \\ y'_1 \sin \phi' + y'_3 \cos \phi' \\ -y'_2 \cos \phi' \end{bmatrix} \cdot \omega\tau \tag{7.60}$$

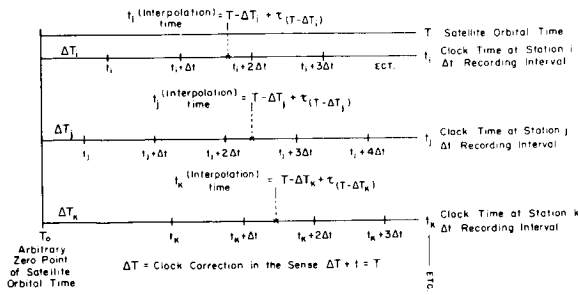


FIGURE 7.26.—Principle of time interpolation for the “geometrical condition of simultaneity.”

The transformation of the direction of the unit vector  $y'_s$  into the chosen  $z$  or  $z'$  system can now be effected in accordance with (7.30) and (7.32) or (7.36), as the case may be.

This completes the discussion of all the steps needed in preparing for the satellite triangulation proper.

### 7.4.6 Numerical Adjustment

#### 7.4.6.1 Introductory Remarks

In this section the attempt will be made to present the mathematical concept of the method of geometric satellite triangulation, considering the problem, so far as possible, from the standpoint of analytical photogrammetry. The principle of the photogrammetric measuring method is most conveniently identified with the concept of a direction fixed within a certain coordinate system. It is therefore reasonable to expect a clear and computationally economical solution with a vectorial presentation. In this connection it should be borne in mind that the mathematical expression for a direction in space can be changed either by rotating the coordinate system to which the direction is referred or by making a change in direction within the fixed reference frame. The latter can be accomplished either by rotating the given vector or by adding a correction vector. From a mathematical standpoint, rotating the coordinate system and changing the direction are equivalent. However, in associating this generally valid geometric concept with a specific measuring process by forming a mental pic-

ture of the direction and the related coordinate system in object space, definite advantages can be derived from such a specific interpretation, at any rate, to explain the measuring process geometrically. One difference between the two cited operations is that a rotation of the coordinate system does not affect the geometry existing between the object points. The concept of a linear coordinate transformation, including, if necessary, translations, therefore seems meaningful. A change in direction within a given coordinate system, on the other hand, effects a change of the spatial position of this direction in object space. The designation “change in direction” will therefore be reserved for this operation.

Finally, as simple a representation as possible will be given of the photogrammetric measuring method, whose concept rests on the principles of a central perspective. For this purpose it is necessary merely to get a mental picture of a unit vector  $x_0$  assigned to a specified direction in object space, with reference to an arbitrary but uniquely defined coordinate system. With the assumption that the starting point of this vector coincides with the center of projection of the central perspective (e.g., at the center of the unit sphere), the photogrammetric bundle vector  $p$  in object space, reduced to unit length, is, geometrically speaking, identical with the vector  $x_0$ , mentioned above. The photogrammetric bundle vector  $p$  being referred to the coordinate system  $\bar{x}, \bar{y}, c$  of the camera, merely a rotation of the coordinate system is required to transform the vector  $x_0$  into vector  $p$  or vice versa. This step, described above as a coordinate transformation, represents the fundamental analytical operation of the photogrammetric measuring method (see sec. 7.4.6.2.1). It remains now only to consider those displacements of the image from the central perspective concept that are the result of the physical photographic process. Before an adjustment algorithm is developed from this line of thought, the more important mathematical aids needed in this discussion will be listed in logical order.

7.4.6.2 Mathematical Aids

7.4.6.2.1 VARIOUS MATHEMATICAL EXPRESSIONS FOR THE UNIT VECTOR

From figure 7.27 directly,

$$\begin{aligned} \mathbf{x}_0 &= \begin{bmatrix} x_1 \\ x_2 \\ x_3 \end{bmatrix} = \frac{\mathbf{x}}{|\mathbf{x}|} \\ &= \begin{bmatrix} X - X_0 \\ Y - Y_0 \\ Z - Z_0 \end{bmatrix} \\ &\quad \times [(X - X_0)^2 + (Y - Y_0)^2 + (Z - Z_0)^2]^{-1/2} \\ &= \begin{bmatrix} \xi \\ \eta \\ 1 \end{bmatrix} (\xi^2 + \eta^2 + 1^2)^{-1/2} \end{aligned} \tag{7.61}$$

where either

$$\mathbf{x} = \begin{bmatrix} (X - X_0) \\ (Y - Y_0) \\ (Z - Z_0) \end{bmatrix} \quad \text{or} \quad \mathbf{x} = \begin{bmatrix} \xi \\ \eta \\ 1 \end{bmatrix} \tag{7.62}$$

Furthermore,

$$\mathbf{x}_0 = \begin{bmatrix} \cos \beta \cos \alpha \\ \cos \beta \sin \alpha \\ \sin \beta \end{bmatrix} \tag{7.63}$$

where from figure 7.27

$$\tan \alpha = \frac{x_2}{x_1} = \frac{\eta}{\xi} \tag{7.64}$$

$$\tan \beta = \frac{x_3}{(x_1 + x_2)^{1/2}} (\xi^2 + \eta^2)^{-1/2} \tag{7.65}$$

$$\xi = \frac{(X - X_0)}{(Z - Z_0)} = \frac{x_1}{x_3} \tag{7.66}$$

$$\eta = \frac{(Y - Y_0)}{(Z - Z_0)} = \frac{x_2}{x_3} \tag{7.67}$$

7.4.6.2.2 COORDINATE TRANSFORMATION

$$\mathbf{x}' = \underline{R} \begin{matrix} (\gamma_1 \gamma_2 \gamma_3) \\ 1 \ 2 \ 3 \end{matrix} (\mathbf{x} + \Delta \mathbf{x}) \tag{7.68}$$

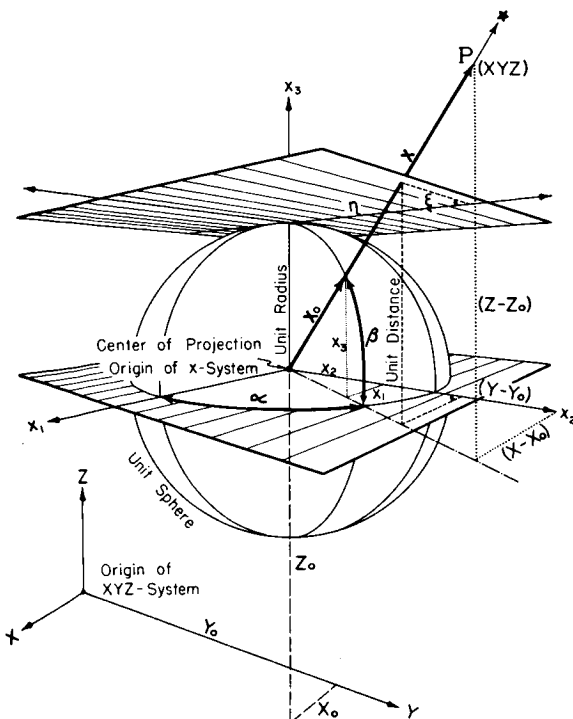


FIGURE 7.27

where the rotation matrix has the following meaning:

$$\underline{R} \begin{matrix} (\gamma_1 \gamma_2 \gamma_3) \\ 1 \ 2 \ 3 \end{matrix} = \underline{R} \begin{matrix} (\gamma_3) \\ 3 \end{matrix} \underline{R} \begin{matrix} (\gamma_2) \\ 2 \end{matrix} \underline{R} \begin{matrix} (\gamma_1) \\ 1 \end{matrix} \tag{7.69}$$

The  $\gamma$  designates the angles through which rotation takes place in the indicated order, the indices under the angle showing the axis around which rotation takes place. Counter-clockwise rotation (as seen from above) is positive.

7.4.6.2.3 CHANGE OF DIRECTION

From figure 7.28

$$\mathbf{x}'_0 = \mathbf{x}_0 + \Delta \mathbf{x} \tag{7.70}$$

The differential  $d\mathbf{x}_0$  of a unit vector  $\mathbf{x}_0$  is a vector of infinitesimal length with a direction perpendicular to  $\mathbf{x}_0$ , since the length of the unit vector is constant by definition. The vector  $\mathbf{x}_0$  can therefore turn only through an

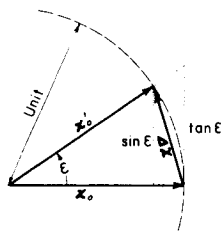


FIGURE 7.28

infinitesimal angle  $\epsilon$ , whose measure in radians is equal to the length of the linear displacement  $dx_0$ . For small displacements the following equalities follow, therefore, from figure 7.28:

$$|\Delta \mathbf{x}| = |d\mathbf{x}_0| = \epsilon = \sin \epsilon = \tan \epsilon \quad (7.71)$$

and hence

$$\mathbf{x}'_0 = \mathbf{x}_0 + d\mathbf{x}_0 \quad (7.72)$$

For the special case where  $d\mathbf{x}_0$  is coplanar with one of the coordinate axes, e.g., with  $x_3$ , it follows from figure 7.29 that

$$d\mathbf{x}_0 = \begin{bmatrix} -x_1 \cdot x_3 \\ -x_2 \cdot x_3 \\ + (1 - x_3^2) \end{bmatrix} \epsilon (1 - x_3^2)^{-1/2} \quad (7.73)$$

in radians. Then  $\mathbf{x}_0$  follows from (7.72).

Similar expressions for the other axes are obtained by cyclic permutation of the subscripts and the vector components in (7.73) in the order (1)  $\rightarrow$  (2)  $\rightarrow$  (3)  $\rightarrow$  (1)

For larger values of  $\epsilon$ , one obtains from (7.63)

$$\mathbf{x}'_0 = \begin{bmatrix} \cos(\beta + \epsilon) \cos \bar{\alpha} \\ \cos(\beta + \epsilon) \sin \bar{\alpha} \\ \sin(\beta + \epsilon) \end{bmatrix} \quad (7.74)$$

#### 7.4.6.2.4 CENTRAL PERSPECTIVE

From figure 7.30 the photogrammetric bundle vector  $\mathbf{p}$  is

$$\mathbf{p} = \bar{x} \cdot \mathbf{i} + \bar{y} \cdot \mathbf{j} + c \cdot \mathbf{k} = \begin{bmatrix} \bar{x} \\ \bar{y} \\ c \end{bmatrix} \quad (7.75) \ddagger$$

and, with (7.61),

$$\mathbf{p}_0 = \frac{\mathbf{p}}{|\mathbf{p}|} \quad |\mathbf{p}| = (\bar{x}^2 + \bar{y}^2 + c^2)^{1/2} \quad (7.76)$$

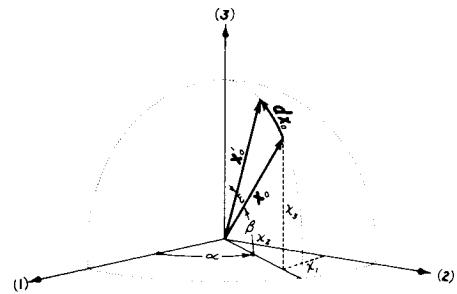


FIGURE 7.29

From (7.68), with  $\Delta \mathbf{x} = 0$ , follows the fundamental equation of analytical photogrammetry

$$\mathbf{p}_0 = \underline{R}(\alpha, \omega, \kappa) \mathbf{x}_0 \quad (7.77) \ddagger$$

where

$$R(\alpha, \omega, \kappa) = R(\kappa) R(\omega) R(\alpha) = \begin{bmatrix} r_{11} & r_{12} & r_{13} \\ r_{21} & r_{22} & r_{23} \\ r_{31} & r_{32} & r_{33} \end{bmatrix} \quad (7.78)$$

The  $r_{ij}$  in the orthogonal matrix (7.78) are actually the direction cosines—in other words, the components of the corresponding unit vectors—in the  $x$  coordinate system of the corresponding axes after the indicated rotations through angles  $\alpha$ ,  $\omega$ , and  $\kappa$  shown in figure 7.31. They are found to be

$$\begin{aligned} r_{11} &= \cos \alpha \cos \kappa + \sin \alpha \sin \omega \sin \kappa \\ r_{12} &= \cos \omega \sin \kappa \\ r_{13} &= -\sin \alpha \cos \kappa + \cos \alpha \sin \omega \sin \kappa \\ r_{21} &= -\cos \alpha \sin \kappa + \sin \alpha \sin \omega \cos \kappa \end{aligned}$$

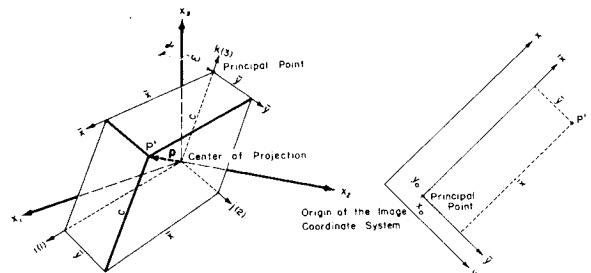


FIGURE 7.30.—(Left) The photogrammetric bundle vector  $\mathbf{p}$ . (Right) Diapositive as seen from center of projection.

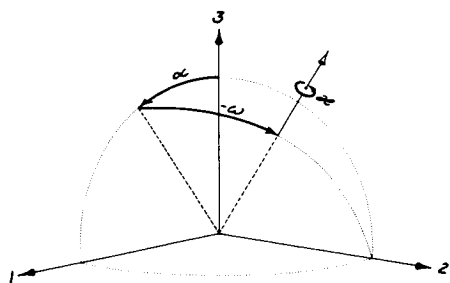


FIGURE 7.31.—Sense of direction of exterior elements of orientation.

$$\begin{aligned}
 r_{22} &= \cos \omega \cos \kappa \\
 r_{23} &= \sin \alpha \sin \kappa + \cos \alpha \sin \omega \cos \kappa \\
 r_{31} &= \sin \alpha \cos \omega \\
 r_{32} &= -\sin \omega \\
 r_{33} &= \cos \alpha \cos \omega
 \end{aligned}
 \tag{7.79}$$

For the orthogonal matrix  $R(\alpha, \omega, \kappa)$

$$\underline{R}^{-1}(\alpha, \omega, \kappa) = \underline{R}^*(\alpha, \omega, \kappa) \tag{7.80}$$

so that with (7.77), (7.78), and (7.79),

$$\mathbf{x}_0 = \frac{\mathbf{x}}{|\mathbf{x}|} = \underline{R}^*(\alpha, \omega, \kappa) \frac{\mathbf{p}}{2 \ 1 \ 3} \frac{|\mathbf{p}|}{|\mathbf{x}|} \tag{7.81}$$

Furthermore, from (7.77) with (7.78), (7.61) and (7.65),

$$\begin{bmatrix} \bar{x} \\ \bar{y} \\ c \end{bmatrix} = \begin{bmatrix} r_{11} & r_{12} & r_{13} \\ r_{21} & r_{22} & r_{23} \\ r_{31} & r_{32} & r_{33} \end{bmatrix} \begin{bmatrix} (X-X_0) \\ (Y-Y_0) \\ (Z-Z_0) \end{bmatrix} \frac{|\mathbf{p}|}{|\mathbf{x}|} \tag{7.82}$$

so that

$$\frac{\bar{x}}{c} = \frac{r_{11}(X-X_0) + r_{12}(Y-Y_0) + r_{13}(Z-Z_0)}{r_{31}(X-X_0) + r_{32}(Y-Y_0) + r_{33}(Z-Z_0)} = \frac{m}{q} \tag{7.83}$$

$$\frac{\bar{y}}{c} = \frac{r_{21}(X-X_0) + r_{22}(Y-Y_0) + r_{23}(Z-Z_0)}{r_{31}(X-X_0) + r_{32}(Y-Y_0) + r_{33}(Z-Z_0)} = \frac{n}{q} \tag{7.84}$$

Finally, for (7.83) and (7.84),

$$\bar{x} = cm/q \tag{7.85}$$

$$\bar{y} = cn/q \tag{7.86}$$

### 7.4.6.2.5 DEVIATIONS FROM THE CENTRAL PERSPECTIVE BUNDLE

Refraction effects a displacement in direction which with equation (7.73) (see eqs. 7.26 and 7.27) can be applied to the unit vector in the direction in question, or which with (7.74) leads directly to the unit vector corrected for refraction.

We consider next those influences which displace the image from its central perspective position and which are due to the constructive properties of the camera. It is known from experience that the image of the object point  $P$  is formed not at  $P'$  but at  $P^*$ , which is displaced relative to  $P'$  by a vector  $\Delta$  lying in the plane of the photogram.

From figure 7.32 we have

$$\bar{x} = x - x_0 - \Delta x \tag{7.87}$$

$$\bar{y} = y - y_0 - \Delta y \tag{7.88}$$

in which  $\Delta x$  and  $\Delta y$  are the components of  $\Delta$ .

The coordinates  $x$  and  $y$  are obtained from the corresponding comparator coordinates, corrected for the nonorthogonality  $\epsilon$  of the comparator spindles as shown in figure 7.32, from

$$\bar{x} = x_{meas} + \bar{y} \epsilon \tag{7.89}$$

$$\bar{y} = y_{meas} \tag{7.90}$$

Since the vector  $\Delta$  is always small, a sufficiently accurate linear scale correction re-

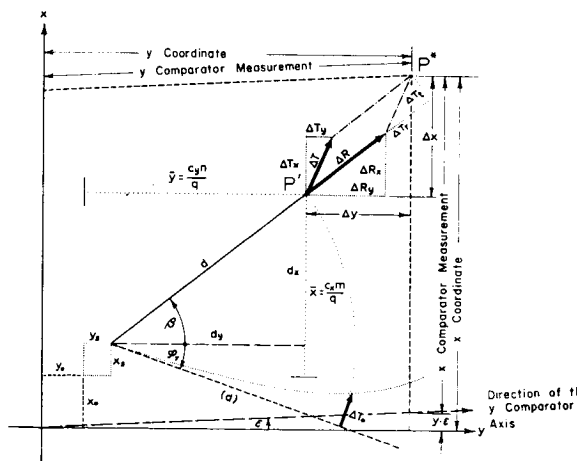


FIGURE 7.32.—Diapositive as seen from projection center.

sults from replacing the scale factor  $c$  in (7.85) and (7.86) by  $c_x$  and  $c_y$ . Thus,

$$\bar{x} = c_x m / q \quad (7.91)$$

$$\bar{y} = c_y m / q \quad (7.92)$$

The required expressions for  $\Delta x$  and  $\Delta y$  are, from figure 7.32,

$$\Delta x = \Delta R_x + \Delta T_x \quad (7.93)$$

$$\Delta y = \Delta R_y + \Delta T_y \quad (7.94)$$

The symmetric radial distortion  $\Delta R$  is, as usual, expressed as a polynomial in odd powers of the distance  $d$ . Omitting the first power, which is equivalent to a scale correction, one obtains

$$\Delta R = K_1 d^3 + K_2 d^5 + K_3 d^7 \quad (7.95)$$

where

$$d = [(\bar{x} - x_s)^2 + (\bar{y} - y_s)^2]^{1/2} \quad (7.96)$$

$$\Delta R_x = \frac{\Delta R (\bar{x} - x_s)}{d} (\bar{x} - x_s) (K_1 d^2 + K_2 d^4 + K_3 d^6) \quad (7.97)$$

$$\Delta R_y = \frac{\Delta R (\bar{y} - y_s)}{d} (\bar{y} - y_s) (K_1 d^2 + K_2 d^4 + K_3 d^6) \quad (7.98)$$

A model for the distortion due to the unavoidable residual errors in entering the individual elements of the lens system was given by Conrady, 1919 (see also Brown, 1966). In figure 7.32 the minimal component of this distortion is purely tangential and is designated  $\Delta T_0$ . For high-quality objectives,  $\Delta T_0$  can be expressed sufficiently accurately with two terms of an even polynomial in  $d$ :

$$\Delta T_0 = K_4 d^2 + K_5 d^4 \quad (7.99)$$

According to Conrady, the components of this nonsymmetric distortion are, using the designations in figure 7.32, in the tangential direction

$$\Delta T_t = \Delta T_0 \cos(\phi_T + \beta) \quad (7.100)$$

and in radial direction

$$\Delta T_r = 3\Delta T_0 \sin(\phi_T + \beta) \quad (7.101)$$

Hence,

$$\Delta \mathbf{T} = \begin{bmatrix} \Delta T_x \\ \Delta T_y \end{bmatrix} = \begin{bmatrix} \cos \beta & \sin \beta \\ -\sin \beta & \cos \beta \end{bmatrix} \begin{bmatrix} \Delta T_t \\ \Delta T_r \end{bmatrix} \quad (7.102)$$

Finally, with (7.99), (7.100), and (7.101) one obtains from (7.102)

$$\Delta \mathbf{T} = \begin{bmatrix} \Delta T_x \\ \Delta T_y \end{bmatrix} = (K_4 + K_5 d^2) \begin{bmatrix} 2(\bar{x} - x_s)(\bar{y} - y_s) & 3(\bar{x} - x_s)^2 + (\bar{y} - y_s)^2 \\ 3(\bar{y} - y_s)^2 + (\bar{x} - x_s)^2 & 2(\bar{x} - x_s)(\bar{y} - y_s) \end{bmatrix} \begin{bmatrix} \sin \phi_T \\ \cos \phi_T \end{bmatrix} \quad (7.103)$$

Figure 7.33 shows schematically the components for radial and decentering distortion for a certain distance  $d$ .

Finally, one obtains with (7.89), (7.90), (7.97), (7.98), and (7.103), in accordance with (7.87), (7.88), and (7.93), (7.94) and Figure 7.32

$$\bar{x} = x + y \cdot \epsilon - (\bar{x} - x_s) (K_1 d^2 + K_2 d^4 + K_3 d^6) - (K_4 + K_5 d^2) \{ 2(\bar{x} - x_s)(\bar{y} - y_s) \sin \phi_T + [3(\bar{x} - x_s)^2 + (\bar{y} - y_s)^2] \cos \phi_T \} - x_0 \quad (7.104)$$

$$\bar{y} = y - (\bar{y} - y_s) (K_1 d^2 + K_2 d^4 + K_3 d^6) - (K_4 + K_5 d^2) \{ [3(\bar{y} - y_s)^2 + (\bar{x} - x_s)^2] \sin \phi_T + 2(\bar{x} - x_s)(\bar{y} - y_s) \cos \phi_T \} - y_0 \quad (7.105)$$

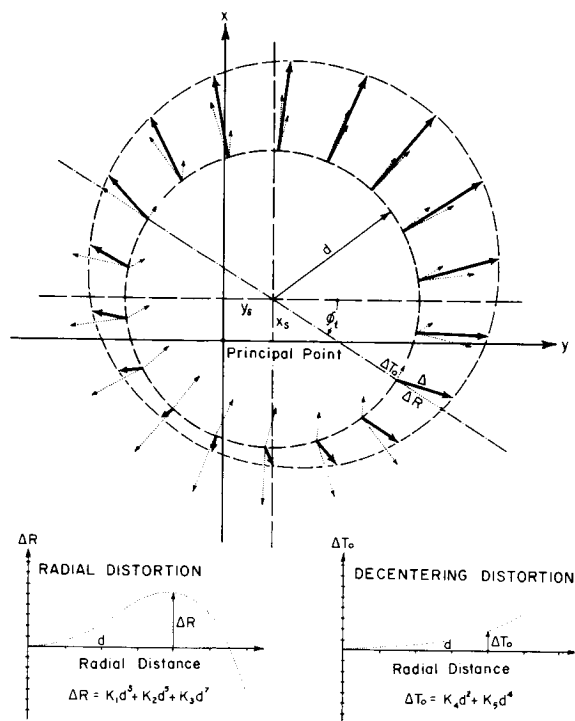


FIGURE 7.33.—Components of distortion.

where the meaning of  $d$  is defined by (7.96) and  $x$  and  $y$  are the comparator coordinates measured on the photogram.

#### 7.4.6.2.6 DESCRIPTION OF THE RECTANGULAR COORDINATE SYSTEMS

In order to make the computations for the adjustment of geometric satellite triangulation as clear and synoptic as possible, three rectangular coordinate systems are used. Each of the three systems has a subgroup. The three principal systems are designated  $x$ ,  $y$ , and  $z$  systems, and the corresponding subsystems are  $x'$ ,  $y'$ , and  $z'$ . The  $x$  system corresponds to the astronomic reference system, in that the  $x_3$  axis points to the celestial north pole and the  $x_1$  axis intersects the equator at the vernal equinox. The origin of this system is the center of the unit sphere which circumscribes the Earth's center (origin of the rectangular geometric coordinates) or any arbitrary point of observation.

Turning the  $x$  system about its  $x_3$  axis through the hour angle  $\theta$  of the equinox (local sidereal time at observation site  $P$ ) results in the  $x'$  system

$$\mathbf{x}' = \underline{R}(\theta) \mathbf{x} \quad (7.106)$$

(See also (7.20) and (7.21).)

The  $y$  system (see fig. 7.18a) designates the rectangular geocentric coordinate system, which corresponds to the orientation of the earth for a specific epoch and in which the  $y_3$  axis points to the instantaneous north pole. The intersection of the instantaneous null meridian with the instantaneous equator determines the direction of the  $y_1$  axis. The instantaneous null meridian is defined on the reference ellipsoid as the trace of the plane containing the instantaneous axis of rotation of the Earth and that point whose coordinates in the reference system (1900–1905 pole) are  $\phi = 0, \lambda = 0$  (see sec. 7.4.4). At an arbitrary point of observation in the  $y$  system, the corresponding instantaneous coordinates are  $\phi'$  and  $\lambda'_{cast}$ . If the  $y$  system is rotated first through the angle  $\lambda'_{cast}$  about its  $y_3$  axis, the local  $y'$  system is obtained. In this system the  $y'_3$  axis points to the station zenith, while the  $y'_1$  axis lies in the plane of the meridian as well as of the horizon, and hence points south. Therefore:

$$\mathbf{y}' = \underline{R}(90^\circ - \phi') \underline{R}(\lambda'_{cast}) \mathbf{y} = \underline{R}(90^\circ - \phi') \mathbf{x}' \quad (7.107)$$

See also (7.23) and (7.30), the latter being the inverse transformation.

Finally, we have the  $z$  and  $z'$  systems, which coincide essentially with the  $y$  and  $y'$  systems, except that the  $z$  systems are referred to the conventional (1900–1905) pole (CIO). If the displacement of the instantaneous pole relative to the conventional pole is given, as is the practice, by the components  $x$  and  $y$  (see sec. 7.4.4 and fig. 7.21), the transformation is effected by

$$\mathbf{z} = \underline{R}(-y) \underline{R}(-x) \mathbf{y} \quad (7.108)$$

and

$$z' = \frac{R}{2} (90^\circ - \phi) \frac{R}{3} (\lambda_{cast}) z \quad (7.109)$$

(see also (7.32), (7.34), (7.36), and (7.37)).

Coordinates corresponding to the  $z$  system are designated  $\phi$  and  $\lambda$ .

7.4.6.2.7 TRANSFORMATION OF GEODETIC COORDINATES  $\phi, \lambda, h$  INTO RECTANGULAR COORDINATES AND CONVERSELY

The astronomical systems  $x$  and  $x'$  introduced in the previous section are, with respect to their informational content, essentially two-dimensional, defining merely directions in three space. On the other hand, the  $y, y', z, z'$  systems are used in the three-dimensional positioning of points on the Earth's surface (station coordinates) (e.g., see figs. 7.18a and 7.18b). In the course of reducing the satellite triangulation it is therefore necessary to transform coordinates into three-dimensional rectangular coordinates and vice versa. It is also necessary to make provisions for the introduction of given coordinates with their weights into the adjustment of the spatial triangulation. This brings up the problem of a purely geometric solution for transformations. Finally, the problem of determining ellipsoid constants arises when one desires to refer the rectangular station coordinates resulting from an extended satellite triangulation to a best-fitting ellipsoid for this area. In consequence of our assumption that electronic computers are being used, such computations are rigorously performed with closed formulas rather than the differential transformation of classical geodesy.

The designations for the constants of the reference ellipsoid are taken from figure 7.34:

$$\begin{aligned} a &= \text{semimajor axis} \\ b &= \text{semiminor axis} \\ e &= \text{eccentricity} = \left( \frac{a^2 - b^2}{a^2} \right)^{1/2} \end{aligned} \quad (7.110)$$

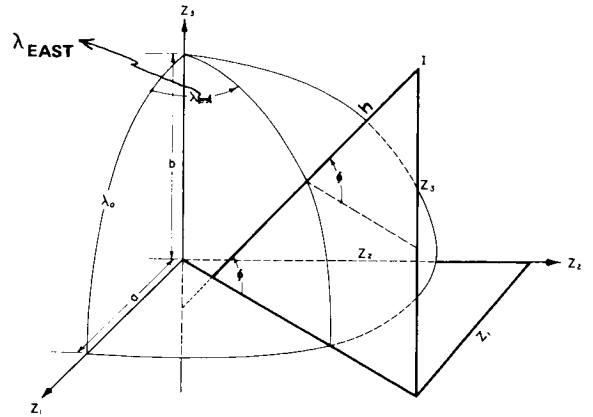


FIGURE 7.34

Figure 7.35 represents the plane of the meridian  $\lambda$ .

To transform the  $\phi, \lambda, h$  into geocentric rectangular coordinates  $z_1, z_2, z_3$  (see sec. 7.4.6.2.6 and fig. 7.34), the following formulas are used:

$$z_1 = [a^2 (a^2 + b^2 \tan^2 \phi)^{-1/2} + h \cos \phi] \cos \lambda \quad (7.111)$$

$$z_2 = [a^2 (a^2 + b^2 \tan^2 \phi)^{-1/2} + h \cos \phi] \sin \lambda \quad (7.112)$$

$$z_3 = (a^2 + b^2 \tan^2 \phi)^{-1/2} b^2 \tan \phi + h \sin \phi \quad (7.113)$$

For the inverse transformation,

$$\tan \lambda = z_2 / z_1 \quad (7.114)$$

$$\tan \beta_0 = z_3 (z_1^2 + z_2^2)^{-1/2} a \cdot b^{-1} \quad (7.115)$$

$$\Delta\beta = \frac{\tan \beta_0 - a e^2 (z_1^2 + z_2^2)^{-1/2} \sin \beta_0 - a^{-1} b z_3 (z_1^2 + z_2^2)^{-1/2}}{1 + \tan^2 \beta_0 - a e^2 (z_1^2 + z_2^2)^{-1/2} \cos \beta_0} \quad (7.116)$$

$$\beta = \beta_0 + \Delta\beta \quad (7.117)$$

$$\tan \phi = a b^{-1} \tan \beta \quad (7.118)$$

$$h = [(z_1^2 + z_2^2)^{1/2} - a \cos \beta] \sec \phi \quad (7.119)$$

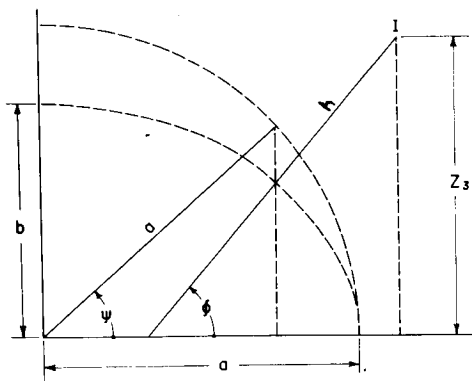


FIGURE 7.35

Equations 7.116 and 7.117 are introduced to avoid the alternative of solving the fourth-degree equation.

$$\tan \beta - ae^2 (z_1^2 + z_2^2)^{-1/2} \sin \beta - a^{-1}bz_3 (z_1^2 + z_2^2)^{-1/2} = 0$$

Their use requires an iteration loop. Transforming  $\phi$  to reduced latitude  $\beta$  accelerates the convergence of the process.

To transform, if necessary, the geocentric rectangular coordinates into local rectangular or vice versa, use (7.68) in appropriate connection with (7.30) or (7.36). Such a transformation represents the link between the  $y$  and  $y'$  or  $z$  and  $z'$  systems of section 7.4.6.2.6. For example, with the  $z$  systems

$$z' = \underline{R} \begin{bmatrix} \lambda_0 \\ 3 \\ 2 \end{bmatrix} (90^\circ - \phi_0) (z - z_0) \quad (7.120)$$

where the  $z_0$  vector is computed from (7.111), (7.112), and (7.113) with  $\phi_0, \lambda_0, h_0$ , the coordinates of the selected origin of the  $z'$  system.

In introducing certain coordinates

$$\phi = \begin{bmatrix} \phi \\ \lambda \\ h \end{bmatrix} \quad (7.121)$$

with their given weights

$$P_\phi = \begin{bmatrix} P_\phi & P_{\phi,\lambda} & P_{\phi,h} \\ P_{\phi,\lambda} & P_\lambda & P_{\lambda,h} \\ P_{\phi,h} & P_{\lambda,h} & P_h \end{bmatrix} \quad (7.122)$$

into the adjustment of the spatial satellite triangulation as additional conditions, it should be noted that

$$z' = \begin{bmatrix} z_1' \\ z_2' \\ z_3' \end{bmatrix} \quad (7.123)$$

can be represented as a vector function of  $\phi$ . Hence we can compute

$$\frac{dz'}{d\phi} = \underline{T}_\phi = \begin{bmatrix} \frac{\partial z_1'}{\partial \phi} & \frac{\partial z_1'}{\partial \lambda} & \frac{\partial z_1'}{\partial h} \\ \frac{\partial z_2'}{\partial \phi} & \frac{\partial z_2'}{\partial \lambda} & \frac{\partial z_2'}{\partial h} \\ \frac{\partial z_3'}{\partial \phi} & \frac{\partial z_3'}{\partial \lambda} & \frac{\partial z_3'}{\partial h} \end{bmatrix} \quad (7.124)$$

and

$$\Delta z' = \underline{T}_\phi \Delta \phi \quad (7.125)$$

Since, furthermore,

$$\frac{d\phi}{dz'} = \underline{T}_\phi^{-1} \quad (7.126)$$

we have

$$\Delta \phi = \underline{T}_\phi^{-1} \Delta z' \quad (7.127)$$

From similar considerations we have, in addition,

$$\underline{P}_{z'} = (\underline{T}_\phi^{-1})^* \underline{P}_\phi \underline{T}_\phi^{-1} \quad (7.128)$$

The partial derivatives in the  $\underline{T}_\phi$  matrix (7.124) are computed with the coordinates  $\phi_0, \lambda_0$  of the origin of the local system:

$$\underline{T}_\phi = \underline{R} \begin{bmatrix} \lambda_0 \\ 3 \\ 2 \end{bmatrix} (90^\circ - \phi_0) \frac{dz}{d\phi} \quad (7.129)$$

where  $dz/d\phi$  is computed by differentiation of the expressions (7.111), (7.112), and (7.113) as follows

$$\frac{dz}{d\phi} \begin{bmatrix} -I \cos \lambda & -II \sin \lambda & \cos \phi \cos \lambda \\ -I \sin \lambda & II \cos \lambda & \cos \phi \sin \lambda \\ I \cot \phi & 0 & \sin \phi \end{bmatrix} \quad (7.130)$$

where

$$I = \{a^2 b^2 \tan \phi [\cos^2 \phi (a^2 + b^2 \tan^2 \phi)^{3/2}]^{-1} + h \sin \phi\} \rho^{-1} \quad (7.131)$$

$$II = [a^2 (a^2 + b^2 \tan^2 \phi)^{-1/2} + h \cos \phi] \rho^{-1} \quad (7.132)$$

with  $\rho = 206\,264''8$ .

The  $\Delta\phi$  ( $\Delta\phi$ ,  $\Delta\lambda$ ,  $\Delta h$ ) vector computed with (7.127) is in seconds of arc for  $\Delta\phi$  and  $\Delta\lambda$  and in meters for  $\Delta h$ ; corresponding values are substituted in (7.125).

The classical coordinates of the triangulation stations, referred at times—especially in the world net—to different datums, are most conveniently recomputed on a common reference ellipsoid before they are introduced into the spatial triangulation as initial approximations, as is described later on. These purely geometric ellipsoid transformations can be accomplished with the formulas above by (1) computing from the given coordinates  $\phi$ ,  $\lambda$ ,  $h$  with (7.111), (7.112), (7.113), geocentric coordinates pertaining to a specific ellipsoid; (2) translating, if necessary, the origin—the ellipsoid center—of these rectangular coordinates; and (3) transforming these rectangular coordinates into coordinates  $\phi$ ,  $\lambda$ ,  $h$ , using (7.114) to (7.119), taking into account the parameters of the new reference ellipsoid.

This type of transformation is common, especially in connection with comparison of the final results of satellite triangulation with classical geodetic surveys.

The determination of the constants of a reference ellipsoid which best fits the results of an extended satellite triangulation is discussed in the sections immediately following. Such solutions must include the results of dynamic satellite geodesy, and the formulas so far developed serve as the basis for such a solution, since with (7.110) and (7.119) the geoid undulation  $N$  can be written, after suitable transformation, as

$$N = (h - H) = -H - (z_1^2 + z_2^2)^{1/2} \sec \phi - a(1 - e^2 \sin^2 \phi)^{-1/2} \quad (7.133)$$

If the leveling height  $H$  is assumed to be free of error, the other partial derivatives are

$$\begin{aligned} \frac{\partial N}{\partial z_1} &= \cos \phi \cos \lambda \\ \frac{\partial N}{\partial z_2} &= \cos \phi \sin \lambda \\ \frac{\partial N}{\partial z_3} &= \sin \phi \\ \frac{\partial N}{\partial a} &= -W \\ \frac{\partial N}{\partial f} &= b \sin^2 \phi W^{-1} \end{aligned} \quad (7.134)$$

with

$$W^2 = (1 - e^2 \sin^2 \phi) \quad (7.135)$$

By means of an adjustment, three translation components  $\Delta z_1$ ,  $\Delta z_2$ ,  $\Delta z_3$  and new ellipsoid parameters  $a$  and  $f = 1 - (b/a)$  can be computed, subject to the condition  $\Sigma v_N^2 = \min$ . The fundamental concepts for such a solution are treated in Schmid and Schmid (1971).

#### 7.4.6.3 Setting Up the General Photogrammetric Observation Equations

The general photogrammetric observation equations are obtained through combination of the expressions given in (7.91), (7.92), (7.104), and (7.105), with reference to the relations (7.79), (7.83), (7.84), and (7.96).

The mathematical model is

$$\begin{aligned} F &= \bar{x} - y_e + (\bar{x} - x_s) (K_1 d^2 + K_2 d^4 + K_3 d^6) \\ &+ \{2(\bar{x} - x_s) (\bar{y} - y_s) \sin \phi_T + [3(\bar{x} - x_s)^2 \\ &+ (\bar{y} - y_s)^2] \cos \phi_T\} (K_4 + K_5 d^2) \\ &+ x_0 - l_x = 0 \end{aligned} \quad (7.136)$$

$$\begin{aligned} G &= \bar{y} + (\bar{y} - y_s) (K_1 d^2 + K_2 d^4 + K_3 d^6) \\ &+ \{[3(\bar{y} - y_s)^2 + (\bar{x} - x_s)^2] \sin \phi_T \\ &+ 2(\bar{x} - x_s) (\bar{y} - y_s) \cos \phi_T\} (K_4 + K_5 d^2) \\ &+ y_0 - l_y = 0 \end{aligned} \quad (7.137)$$

where, according to figure 7.32 and (7.91), (7.92), and (7.96),

$$\bar{x} = \frac{c_j m}{q} \quad (7.138)$$

$$\bar{y} = \frac{c_y n}{q} \tag{7.139}$$

$$d^2 = \left( \frac{c_x m}{q} - x_s \right)^2 + \left( \frac{c_y n}{q} - y_s \right)^2 \tag{7.140}$$

and  $l_x, l_y$  are the measured values of  $x$  and  $y$ .

The meaning of  $m, n,$  and  $q$  is apparent from (7.83), (7.84), the direction cosines  $r_{ij}$  being obtained from (7.79).

Substituting (7.138), (7.139), and (7.140) in (7.136) and (7.137), taking into account (7.83), (7.84), and (7.79), results in expressions for the equations  $F$  and  $G$  which represent the mathematical model for the generalized central perspective.

Since, however, especially at the beginning of the adjustment, the approximation values for the exterior orientation parameters are not necessarily good ones, it is better to adopt the following computational procedure, which, in general, converges more rapidly and leads to a simpler solution with sufficiently close approximation. It should be noted that the radial distortion (7.95), and particularly the decentering distortion  $\Delta T_o$  (7.99), as functions of  $d$ , are small and vary relatively little with a change in  $d$ .

At the beginning of each iteration step of the adjustment,  $\bar{x}$  and  $\bar{y}$  are computed by using the comparator coordinates  $x$  and  $y$ , neglecting the influence of their measuring error, in accordance with figure 7.32 and (7.87), (7.88), (7.89), (7.90), (7.93), and (7.94). Since the coordinates  $x$  and  $y$  are replaced by the actual measurements  $l_x$  and  $l_y$ , the designations  $l_{\bar{x}}$  and  $l_{\bar{y}}$  will now be introduced for  $\bar{x}$  and  $\bar{y}$ .

$$l_{\bar{x}} = l_x + l_y \cdot \epsilon - x_o - \Delta R_x - \Delta T_x \tag{7.141}$$

$$l_{\bar{y}} = l_y - y_o - \Delta R_y - \Delta T_y \tag{7.142}$$

With this,

$$(\bar{x} - x_s) = (l_{\bar{x}} - x_s) = d_x \tag{7.143}$$

$$(\bar{y} - y_s) = (l_{\bar{y}} - y_s) = d_y \tag{7.144}$$

$$d^2 = d_x^2 + d_y^2 \tag{7.145}$$

The radial and Conrady components of distortion,  $\Delta R_x, \Delta R_y, \Delta T_x,$  and  $\Delta T_y$  in (7.141) and (7.142) are computed with (7.97), (7.98), and (7.103). Since the mathematical models of the distortion, and hence also the distance  $d$  with its components  $d_x$  and  $d_y$ , refer to the geometry of the central perspective (see fig. 7.32), an iteration loop must be designed for computing all the distortion components used in (7.141) and (7.142). In (7.97), (7.98), and (7.103),  $\bar{x}$  and  $\bar{y}$  are first replaced by

$$\bar{x} = l_{\bar{x}} \approx l_x + l_y \cdot \epsilon - x_o \tag{7.146}$$

$$\bar{y} = l_{\bar{y}} \approx l_y - y_o \tag{7.147}$$

The  $\Delta R_x, \Delta R_y, \Delta T_x,$  and  $\Delta T_y$  so computed are substituted in (7.141) and (7.142) to give new  $l_{\bar{x}}, l_{\bar{y}}$  values, with which distortion components are again computed, followed by new  $l_{\bar{x}}$  and  $l_{\bar{y}}$  values. This iteration is continued until the difference between successive  $l_{\bar{x}}$  and  $l_{\bar{y}}$  becomes less than a prescribed tolerance.

Introduction of  $l_x$  and  $l_y$  and substitution for  $m, n,$  and  $q$  in accordance with (7.83) and (7.84) changes (7.136) and 7.137) to

$$F = -l_y \cdot \epsilon + \frac{c_x [r_{11}(x-x_o) + r_{12}(y-y_o) + r_{13}(z-z_o)]}{r_{31}(x-x_o) + r_{32}(y-y_o) + r_{33}(z-z_o)} + x_o + (l_{\bar{x}} - x_s)(K_1 d^2 + K_2 d^4 + K_3 d^6) + \{2(l_{\bar{x}} - x_s)(l_{\bar{y}} - y_s) \sin \phi_T + [3(l_{\bar{x}} - x_s)^2 + (l_{\bar{y}} - y_s)^2] \cos \phi_T\} (K_4 + K_5 d^2) - l_x = 0 \tag{7.148}$$

$$G = \frac{c_y [r_{21}(x-x_o) + r_{22}(y-y_o) + r_{23}(z-z_o)]}{r_{31}(x-x_o) + r_{32}(y-y_o) + r_{33}(z-z_o)} + y_o + (l_{\bar{y}} - y_s)(K_1 d^2 + K_2 d^4 + K_3 d^6) + \{[3(l_{\bar{y}} - y_s)^2 + (l_{\bar{x}} - x_s)^2] \sin \phi_T + 2(l_{\bar{x}} - x_s)(l_{\bar{y}} - y_s) \cos \phi_T\} (K_4 + K_5 d^2) - l_y = 0 \tag{7.149}$$

with

$$d^2 = (l_{\bar{x}} - x_s)^2 + (l_{\bar{y}} - y_s)^2 \tag{7.150}$$

The meaning of the  $r_{ij}$  is apparent from (7.78) and (7.79), and the  $l_{\bar{x}}, l_{\bar{y}}$  are computed iteratively with (7.141) and (7.142).

Equations 7.148 and 7.149 are analytical expressions for the generalized central perspective principle. The influences requiring generalization are:

(1) Skewness  $\epsilon$  of the comparator carriage; its effect is simulated by the term  $\epsilon l_y$  in (7.148).

(2) Linear scale error, in the measuring screws of the comparator; their influence is adequately accounted for with the scale factors  $c_x$  and  $c_y$  in (7.148) and (7.149), respectively.

(3) Distortion; the two last terms in each of (7.148) and (7.149) simulate the components of the distortion vector  $\Delta$  as the sum of radial and decentering distortion. In addition, the actual conditions are more closely approximated by displacing the origin  $(x_s, y_s)$  of the distortion from the principal point  $(x_0, y_0)$ . These relations are shown schematically in figures 7.32 and 7.33.

For the further treatment of expressions 7.148 and 7.149, it is necessary only to note that the direction cosines (see (7.62), (7.83), and (7.84)) in the third term of (7.148) and in the second term of (7.149) refer to refracted corrections.

The next step is to set up the observation equations. In the adjustment, a generalized adjustment algorithm described in Schmid (1965b) and Schmid and Schmid (1965) is used. The mathematical model is given with the two functions  $F$  and  $G$  of (7.148) and (7.149), and the general observation equations are obtained by expanding these functions in Taylor series and neglecting terms of the second and higher order as

$$\frac{\partial F}{\partial \mathbf{u}} \Delta \mathbf{u} + F_0 = 0 \quad (7.151)$$

$$\frac{\partial G}{\partial \mathbf{u}} \Delta \mathbf{u} + G_0 = 0 \quad (7.152)$$

in which  $\mathbf{u}$  is the vector of all parameters in the mathematical model, including the measured quantities. Table 7.6 lists the symbols designating the various partial derivatives of  $F$  and  $G$ , where

$$\begin{aligned} J_x &= D_x & K_x &= -E_x & L_x &= -F_x \\ J_y &= -D_y & K_y &= -E_y & L_y &= -F_y \end{aligned} \quad (7.153)$$

The corresponding analytical expressions, including the necessary auxiliary quantities, are

$$\begin{aligned} \textcircled{1} &= (\bar{x} - x_0) / c_x & \textcircled{5} &= \textcircled{1} F - r_{13} \\ \textcircled{2} &= (\bar{y} - y_0) / c_y & \textcircled{6} &= \textcircled{2} D - r_{21} \\ \textcircled{3} &= \textcircled{1} D - r_{11} & \textcircled{7} &= \textcircled{2} E - r_{22} \\ \textcircled{4} &= \textcircled{1} E - r_{12} & \textcircled{8} &= \textcircled{2} F - r_{23} \\ \textcircled{9} &= \textcircled{2} r_{12} - \textcircled{1} r_{22} \end{aligned} \quad (7.154)$$

$$\begin{aligned} A_x &= c_x (\textcircled{1} \cdot \textcircled{9} + \textcircled{7}) & A_y &= +c_y \textcircled{2} \cdot \textcircled{9} \\ B_x &= +c_x [(1 + \textcircled{1}^2) \sin \kappa + \textcircled{1} \cdot \textcircled{2} \cos \kappa] & B_y &= +c_y [(1 + \textcircled{2}^2) \cos \kappa + \textcircled{1} \cdot \textcircled{2} \sin \kappa] \\ C_x &= +c_x \textcircled{2} & C_y &= -c_y \textcircled{1} \\ D_x &= \frac{c_x}{q} \textcircled{3} & D_y &= \frac{c_y}{q} \textcircled{6} \\ E_x &= \frac{c_x}{q} \textcircled{4} & E_y &= \frac{c_y}{q} \textcircled{7} \\ F_x &= \frac{c_x}{q} \textcircled{5} & F_y &= \frac{c_y}{q} \textcircled{8} \\ G_x &= \textcircled{1} & G_y &= \textcircled{2} \\ H_x &= 1 + P_x & H_y &= P_y \\ I_x &= Q_x & I_y &= 1 + Q_y \\ M_x &= d_x d^2 & M_y &= d_y d^2 \\ N_x &= d_x d^4 & N_y &= d_y d^4 \\ O_x &= d_x d^6 & O_y &= d_y d^6 \end{aligned}$$

$$\begin{aligned} P_x &= -\frac{\Delta R}{d} - d_x^2 D_r - d_x D_w \cos \phi_T \\ &\quad - 4d_x [K_4 + (2d_x^2 + d_y^2) K_5] \cos \phi_T \\ &\quad - 2d_y [K_4 + (d_x^2 + 3d_y^2) K_5] \sin \phi_T \\ P_y &= -d_x d_y D_r - d_x D_w \sin \phi_T - 2d_y \{ [K_4 \\ &\quad + (3d_x^2 + d_y^2) K_5] \cos \phi_T + 2d_y K_5 \sin \phi_T \} \\ Q_x &= -d_x d_y D_r - d_y D_w \cos \phi_T - 2d_x \{ [K_4 \\ &\quad + (d_x^2 + 3d_y^2) K_5] \sin \phi_T \} \\ Q_y &= -\frac{\Delta R}{d} - d_y D_r - d_y D_w \sin \phi_T - 2d_x [K_4 \\ &\quad + (d_x^2 + 2d_y^2) K_5] \cos \phi_T - 4d_y [K_4 \\ &\quad + (d_x^2 + 2d_y^2) K_5] \sin \phi_T \end{aligned} \quad (7.155)$$

where

$$\begin{aligned}
 d_x &= (l_x - x_s) & d_y &= (l_y - y_s) \\
 D_r &= [2K_1 + 4K_2 d^2 + 6K_3 d^4] \\
 D_w &= [2K_4 + 4K_5 d^2] \\
 d^2 &= d_x^2 + d_y^2 \\
 R_x &= d^2 \cos \phi_T + 2(d_x^2 \cos \phi_T + d_x d_y \sin \phi_T) \\
 R_y &= d^2 \sin \phi_T + 2(d_y^2 \sin \phi_T + d_x d_y \cos \phi_T) \\
 S_x &= d^4 \cos \phi_T + 2d^2(d_x^2 \cos \phi_T + d_x d_y \sin \phi_T) \\
 S_y &= d^4 \sin \phi_T + 2d^2(d_y^2 \sin \phi_T + d_x d_y \cos \phi_T) \\
 T_x &= -\sin \phi_T (K_4 d^2 + K_5 d^4) \\
 &\quad + 2(K_4 + K_5 d^2)(d_x d_y \cos \phi_T - d_x^2 \sin \phi_T) \\
 T_y &= \cos \phi_T (K_4 d^2 + K_5 d^4) \\
 &\quad + 2(K_4 + K_5 d^2)(d_y^2 \cos \phi_T - d_x d_y \sin \phi_T) \\
 U_z &= l_y & U_y &= 0 \\
 Z_x &= -1 & Z_y &= -1
 \end{aligned}
 \tag{7.155a}$$

With an arbitrarily selected mean error of unit weight  $m_0$  before adjustment the weight matrix (see (7.196)) assigned to the observation equations (7.151) and (7.152) is computed. The adjustment then determines the  $\Delta \mathbf{u}$  vector subject to the condition

$$\Delta \mathbf{u}^* \underline{P} \Delta \mathbf{u} = \min \tag{7.156}$$

The required parameters are then

$$\mathbf{u} = \mathbf{u}_0 + \Delta \mathbf{u} \tag{7.157}$$

where  $\mathbf{u}_0$  are the approximations for the parameters (see (7.208) to (7.210)).

#### 7.4.6.4 Mathematical Model for the Photogrammetric Camera

Each of the various different applications of the photogrammetric measurement method requires the development of an appropriate analytical expression from the general formulation. A special application will now be shown as the first step in satellite triangulation. As was outlined initially in section 7.4.3, the parameters needed for the reconstruction of the bundle from the star images (in this

case,  $\epsilon, c_x, c_y, x_0, y_0, x_s, y_s, K_1, K_2, K_3, K_4, K_5, \phi_T$ ) and of the exterior orientation ( $\alpha, \omega, \kappa$ ) are to be computed.

Since the directions to the fixed stars refer to the center of the unit sphere at the center of projection, the coordinates  $X_0, Y_0, Z_0$  of (7.148) and (7.149) are set equal to zero. Furthermore, it was shown toward the end of section 7.4.3 that the coordinates expressing the direction to a star can be transformed to standard coordinates  $\xi_r, \eta_r, +1$  (see fig. 7.27 and eqs. (7.66), (7.67) with (7.61)). This changes (7.148) and (7.14) into

$$\begin{aligned}
 F &= -l_x - l_y \cdot \epsilon + \frac{c_x(r_{11}\xi_r + r_{12}\eta_r + r_{13})}{r_{31}\xi_r + r_{32}\eta_r + r_{33}} \\
 &\quad + x_0 + (l_x - x_s)(K_1 d^2 + K_2 d^4 + K_3 d^6) \\
 &\quad + \{2(l_x - x_s)(l_y - y_s) \sin \phi_T + [3(l_x - x_s)^2 \\
 &\quad + (l_y - y_s)^2] \cos \phi_T\} (K_4 + K_5 d^2) = 0
 \end{aligned}
 \tag{7.158}$$

$$\begin{aligned}
 G &= -l_y + \frac{c_y(r_{21}\xi_r + r_{22}\eta_r + r_{23})}{r_{31}\xi_r + r_{32}\eta_r + r_{33}} \\
 &\quad + y_0 + (l_x - y_s)(K_1 d^2 + K_2 d^4 + K_3 d^6) \\
 &\quad + \{[3(l_y - y_s)^2 + (l_x - x_s)^2] \sin \phi_T \\
 &\quad + 2(l_x - x_s)(l_y - y_s) \cos \phi_T\} (K_4 + K_5 d^2) = 0
 \end{aligned}
 \tag{7.159}$$

We note, first of all, that right ascension  $\alpha$  and declination  $\delta$ , together with their mean errors, are given quantities. Consequently, it is necessary to minimize the sum of the  $(v_\alpha v_\alpha + v_\delta v_\delta)$ , weighted in accordance with the weight matrix  $\underline{P}_{\alpha, \delta}$  given for the stars, not the sum of squares of the  $v_\xi$  and  $v_\eta$  residuals. To accomplish this, the  $\xi_r$  and  $\eta_r$  are differentiated with respect to  $\alpha$  and  $\delta$ , and the coefficients in the observation equations used to compute the  $\Delta \xi$  and  $\Delta \eta$  are multiplied accordingly. After appropriate arrangement, coefficients are obtained in the observation equations which do not refer to the corrections  $\Delta \xi$  and  $\Delta \eta$ , but to  $v_\alpha$  and  $v_\delta$ . Using (7.66) and (7.67), one obtains in the  $y'$  system

$$\xi_r = y'_1 / y'_3 \tag{7.160}$$

$$\eta_r = y'_2 / y'_3 \tag{7.161}$$

from which, when the index  $r$  is omitted,

$$d\xi = \frac{y'_3 dy'_1 - y'_1 dy'_3}{y'^2_3} \quad (7.162)$$

$$d\eta = \frac{y'_3 dy'_2 - y'_2 dy'_3}{y'^2_3} \quad (7.163)$$

From (7.1) with (7.20), (7.23) and figure 7.19, it follows that

$$\begin{aligned} \mathbf{x}' &= \begin{bmatrix} x'_1 \\ x'_2 \\ x'_3 \end{bmatrix} = \begin{bmatrix} \cos \delta & \cos t \\ -\cos \delta & \sin t \\ \sin \delta \end{bmatrix} \\ &= \begin{bmatrix} \sin \phi' & 0 & \cos \phi' \\ 0 & 1 & 0 \\ -\cos \phi' & 0 & \sin \phi' \end{bmatrix} \begin{bmatrix} y'_1 \\ y'_2 \\ y'_3 \end{bmatrix} \end{aligned} \quad (7.164)$$

Differentiating (7.164), noting that  $dt = -d\alpha$ , gives

$$d\mathbf{x}' = \begin{bmatrix} -x'_2 & -\sin \delta \cos t \\ x'_1 & \sin \delta \sin t \\ 0 & \cos \delta \end{bmatrix} \begin{bmatrix} d\alpha \\ d\delta \end{bmatrix} \quad (7.165)$$

From (7.23),

$$d\mathbf{y}' = \underline{R}(90^\circ - \phi') d\mathbf{x}' \quad (7.166)$$

which with (7.165) gives

$$d\mathbf{y}' = \begin{bmatrix} -x'_2 \sin \phi' - (x'_3 \cos t \sin \phi' + \cos \delta \cos \phi') \\ x'_1 & x'_3 \sin t \\ -x'_2 \cos \phi' (-x'_3 \cos t \cos \phi' + \cos \delta \sin \phi') \\ \left[ \begin{matrix} d\alpha \\ d\delta \end{matrix} \right] \end{bmatrix} \quad (7.167)$$

With the relations found in (7.160), (7.161), and (7.164), the application of (7.167) with (7.162) and (7.163) yields

$$\begin{aligned} \frac{d\xi}{d\alpha} &= \frac{-y'_2 \sin \phi'}{y'_3} + \xi_r \frac{y'_2 \cos \phi'}{y'_3} \\ &= \eta_r (\xi_r \cos \phi' - \sin \phi') \end{aligned} \quad (7.168)$$

$$\begin{aligned} \frac{d\eta}{d\alpha} &= \frac{y'_1}{y'_3} + \eta_r^2 \cos \phi' \\ &= \xi_r \sin \phi' + (1 + \eta_r^2) \cos \phi' \end{aligned} \quad (7.169)$$

and, similarly, the intermediate steps having been omitted,

$$\frac{d\xi}{d\phi} = -\cos t (1 + \xi_r^2 + \eta_r^2) \quad (7.170)$$

$$\frac{d\eta}{d\delta} = \sin t \sin \phi' (1 + \xi_r^2 + \eta_r^2) \quad (7.171)$$

Other quantities needed are

$$\frac{\partial F}{\partial \alpha} = J_x^* = J_x \cdot \frac{d\xi}{d\alpha} + K_x \cdot \frac{d\eta}{d\alpha} \quad (7.172)$$

$$\frac{\partial F}{\partial \delta} = K_y^* = J_y \cdot \frac{d\xi}{d\delta} + K_y \cdot \frac{d\eta}{d\delta} \quad (7.173)$$

$$\frac{\partial G}{\partial \alpha} = J_y^* = J_y \cdot \frac{d\xi}{d\alpha} + K_y \cdot \frac{d\eta}{d\alpha} \quad (7.174)$$

$$\frac{\partial G}{\partial \delta} = K_y^* = J_y \cdot \frac{d\xi}{d\delta} + K_y \cdot \frac{d\eta}{d\delta} \quad (7.175)$$

in which  $d\xi/d\alpha$ ,  $d\xi/d\delta$ ,  $d\eta/d\alpha$ , and  $d\eta/d\delta$  are given with (7.168) through (7.171) and  $J_x$ ,  $J_y$ ,  $K_x$ , and  $K_y$  are computed from (7.153) through (7.155).

If one accepts the coordinates corrected for refraction  $\xi_r$  and  $\eta_r$ , the corresponding linearized observation equations can be set up directly with (7.158), (7.159) and the introduction of (7.172) to (7.175). Just as the central perspective bundle was altered by additional physical influences, the direction given with the coordinates  $\xi_r$ ,  $\eta_r$  can be subjected to a further refraction correction by further improving the  $\tau$  constants used for the original refraction correction.

In consonance with (7.40) one can therefore write

$$\begin{aligned} \Delta r_x &= T^{1/2} W \left( \tan \frac{\beta}{2} \Delta \tau_1 + \tan^3 \frac{\beta}{2} \Delta \tau_2 \right. \\ &\quad \left. + \tan^5 \frac{\beta}{2} \Delta \tau_3 + \tan^7 \frac{\beta}{2} \Delta \tau_4 \right) \end{aligned} \quad (7.176)$$

Assuming further that refraction does not affect azimuth, we have  $\xi_r/\eta_r = \text{constant}$ , and therefore

$$\Delta \xi / \Delta \eta = \xi_r / \eta_r \quad (7.177)$$

and, in analogy with (7.66) and (7.67),

$$\xi_r^2 + \eta_r^2 = \tan^2 z_r = \frac{y_1'^2 + y_2'^2}{y_3'^2} \quad (7.178)$$

Differentiating (7.178) gives

$$\xi_r \Delta \xi + \eta_r \Delta \eta = \tan z_r (1 + \tan^2 z_r) \Delta z \quad (7.179)$$

Substituting (7.171) in (7.179) gives

$$\Delta z = \Delta r_x \quad (7.180)$$

$$\begin{aligned} \Delta \xi &= \xi_r \frac{(1 + \tan^2 z_r)}{\tan z_r} \Delta r_x \\ &= \frac{2\xi_r}{\sin 2z_r} \Delta r_x \\ &= \frac{y_1'}{y_3'^2} (y_1'^2 + y_2'^2)^{-1/2} \Delta r_x \end{aligned} \quad (7.181)$$

$$\begin{aligned} \Delta \eta &= \eta_r \frac{(1 + \tan^2 z_r)}{\tan z_r} \Delta r_x \\ &= \frac{2\eta_r}{\sin 2z_r} \Delta r_x \\ &= \frac{y_2'}{y_3'^2} (y_1'^2 + y_2'^2)^{-1/2} \Delta r_x \end{aligned} \quad (7.182)$$

in which  $\Delta r_x$  is given with (7.176).

When (7.176), (7.181), and (7.182) are taken into consideration and the designations of table 7.6 are used, the partial derivatives of the functions  $F$  and  $G$  needed in the refraction correction are now introduced, giving

$$\frac{\partial F}{\partial \tau} = \begin{bmatrix} V_x \\ W_x \\ X_x \\ Y_x \end{bmatrix} = \begin{bmatrix} \tan \beta/2 \\ \tan^3 \beta/2 \\ \tan^5 \beta/2 \\ \tan^7 \beta/2 \end{bmatrix} \cdot \tau_x \quad (7.183)$$

$$\frac{\partial G}{\partial \tau} = \begin{bmatrix} V_y \\ W_y \\ X_y \\ Y_y \end{bmatrix} = \begin{bmatrix} \tan \beta/2 \\ \tan^3 \beta/2 \\ \tan^5 \beta/2 \\ \tan^7 \beta/2 \end{bmatrix} \cdot \tau_y \quad (7.184)$$

where

$$\tau_x = T^{1/2} W \frac{(J_x y_1') + (K_x y_2')}{y_3'^2 (y_1'^2 + y_2'^2)^{1/2}} = T^{1/2} W \frac{2(J_x \xi_r + K_x \eta_r)}{\sin 2z_r} \quad (7.185)$$

$$\tau_y = T^{1/2} W \frac{(J_y y_1') + (K_y y_2')}{y_3'^2 (y_1'^2 + y_2'^2)^{1/2}} = T^{1/2} W \frac{2(J_y \xi_r + K_y \eta_r)}{\sin 2z_r} \quad (7.186)$$

with  $T$  and  $W$  as in (7.40).

The observation equations (7.151), (7.152) for the single camera are therefore set up in accordance with (7.158), (7.159), table 7.3, (7.153) to (7.155), and with (7.172) to (7.175), (7.183), and (7.184). Since the skewness  $\epsilon$  of the comparator axes is always small, the term  $v_{1y}\epsilon$  is negligible. We thus have the system of observation equations

$$A v_u + l = 0 \quad (7.187)$$

with the weight matrix,  $P_u = m_o^2 \sigma_u^{-1}$ , where, in general, we have for each pair of observation equations

$$A = \begin{array}{c} \begin{array}{c} \overbrace{\begin{array}{c} v_u^* \\ \Delta^* \\ \Delta_o^* \end{array}} \\ \underbrace{\begin{array}{c} v_{1x,y}^* \\ v_{\alpha,\delta}^* \end{array}} \end{array} \\ \begin{array}{c} \begin{array}{c} l_x \quad l_y \\ -1 \quad - \\ - \quad -1 \end{array} \\ \begin{array}{c} \alpha^1 \quad \delta \\ J_x^* \quad K_x^* \\ J_y^* \quad K_y^* \end{array} \end{array} \begin{array}{c} \begin{array}{c} v \quad \omega \quad x \quad c_x \quad c_y \quad x_0 \quad y_0 \quad K_1 \quad K_2 \quad K_3 \quad x_s \quad y_s \quad K_4 \quad K_5 \quad \gamma \tau \quad \epsilon \quad \tau_1 \quad \tau_2 \quad \tau_3 \quad \tau_4 \end{array} \\ \begin{array}{c} A_x \quad B_x \quad C_x \quad G_x \quad - \quad H_x \quad I_x \quad M_x \quad N_x \quad O_x \quad P_x \quad Q_x \quad R_x \quad S_x \quad T_x \quad U_x \quad V_x \quad W_x \quad X_x \quad Y_x \\ A_y \quad B_y \quad C_y \quad - \quad G_y \quad H_y \quad I_y \quad M_y \quad N_y \quad O_y \quad P_y \quad Q_y \quad R_y \quad S_y \quad T_y \quad - \quad V_y \quad W_y \quad X_y \quad Y_y \end{array} \end{array} \quad (7.188) \\ \begin{array}{c} \underbrace{-A_1} \\ \underbrace{B_{\alpha,\delta}} \\ \underbrace{B_0} \\ B \end{array} \end{array}$$

$\alpha^1$  being right ascension.

$l$  is computed (see (7.151), (7.152)) from the approximation and measured values as

$$l = \begin{bmatrix} F_0 \\ G_0 \end{bmatrix}_i \quad (7.189)$$

$$P_u = \begin{bmatrix} P_{l_x, l_y} & 0 & 0 & 0 \\ 0 & P_{\alpha, \delta} & 0 & 0 \\ 0 & 0 & P_0 & 0 \\ 0 & 0 & 0 & P_\tau \end{bmatrix} \quad (7.190)$$

The  $P_u$  matrix (7.190) theoretically could be completely filled, but it is necessary to normalize all weights with respect to a selected value for  $m_0$ , and, in addition, the mean errors of the rotation parameters must be in radians. Thus, it becomes possible to account for all existing correlations. In practice, however, as is indicated in (7.190), there are uncorrelated groups, since no correlation exists between the  $\sigma_l$  matrix specifying the accuracy of comparator measurements, the  $\sigma_{\alpha, \delta}$  matrix specifying the accuracy of the star coordinates, the  $\sigma_0$  matrix specifying the accuracy of the other, chiefly photogrammetric, parameters, and the  $\sigma_\tau$  matrix specifying the accuracy of the refraction determination.

Since in what follows it will be repeatedly necessary to compute accuracy criteria, the meaning of the various designations used will now be explained.

**Measures of Accuracy Before Adjustment.**—The mean error of unit weight arbitrarily fixed before the adjustment is  $m_0$ . The mean error of a measurement  $i$  is designated  $m_i$ . Hence

$$p_i = m_0^2 / m_i^2 \quad (7.191)$$

The corresponding weight matrix, e.g., for the comparator measurements  $l_x, l_y$ , is

$$P_{l_i} = \begin{bmatrix} pl_x & pl_{x,y} \\ pl_{x,y} & pl_y \end{bmatrix} = m_0^2 \begin{bmatrix} \sigma_{l_x}^2 & \sigma_{l_x, y} \\ \sigma_{l_x, y} & \sigma_{l_y}^2 \end{bmatrix}^{-1} = m_0^2 \sigma_{l_i}^{-1} \quad (7.192)$$

with  $\sigma_{l_x, y} = \rho_{x,y} \sigma_{l_x} \sigma_{l_y}$ ;  $\rho_{x,y}$  denotes the correlation coefficient which equals 0 for comparator measurements when the comparator has independent mechanisms for measuring  $x$  and  $y$ .

**Measures of Accuracy After Adjustment.**—The mean error of unit weight after the adjustment is

$$s_0 = \left( \frac{\mathbf{v}^* P \mathbf{v}}{n - u} \right)^{1/2} \quad (7.193)$$

and the mean error of an observation after the adjustment is

$$s_i = \frac{s_0}{m_0} m_i \quad (7.194)$$

With respect to the unknowns  $u$  computed in the adjustment there exists the relation

$$s_0^2 N_u^{-1} = \mathbf{s}_u^2 = \underbrace{\begin{bmatrix} s_{u_1 u_1} & s_{u_1 u_2} & \cdot & \cdot & s_{u_1 u_n} \\ & s_{u_2 u_2} & \cdot & \cdot & s_{u_2 u_n} \\ & & \cdot & \cdot & \cdot \\ & & & \cdot & \cdot \\ & & & & s_{u_n u_n} \end{bmatrix}}_{\text{Covariance matrix}} \quad (7.195)$$

in which  $s_{u_i u_j} = \rho_{ij} s_{u_i} s_{u_j}$ . With (7.193) and (7.195) we obtain

$$P_u = m_0^2 \mathbf{s}_u^{-1} = \frac{m_0^2}{s_0^2} N_u \quad (7.196)$$

Omitting the index  $u$  in order to simplify the notation, we have  $s_{ij} = \rho_{ij} s_i s_j$ , and the dimensionless correlation matrix that corresponds to (7.195) is then



(7.188),  $A_i$  is always a unit matrix. If we introduce, for the moment,  $P_{\alpha,\delta}$  as a null matrix with  $P_i$  from (7.192), the normal equations system corresponding to the observation equations (7.187) is

$$\sum_{i=1}^m [B^* P_i B]_i \Delta + \sum_{i=1}^m [B^* P_i l]_i = 0 \quad (7.201)$$

where  $m$  is the number of star images.

Each pair of observation equations for an individual star image  $i$  contributes to the normal equations system (7.201) in the following manner:

$$B_i^* P_{ii} B_i \Delta + B_i^* P_{ii} l_i = 0 \quad (7.202)$$

Subdividing the  $B$  matrix further by using the notations introduced in (7.188) results in the following scheme for (7.202):

$$\begin{array}{c} v_{\alpha,\delta} \quad \Delta_0 \\ \left[ \begin{array}{c|c} (B_{\alpha,\delta}^* P_i B_{\alpha,\delta})_i & (B_{\alpha,\delta}^* P_i B_0)_i \\ \hline (B_{\delta}^* P_i B_{\alpha,\delta})_i & (B_{\delta}^* P_i B_0)_i \end{array} \right] + \left[ \begin{array}{c} (B_{\alpha,\delta}^* P_i l)_i \\ \hline (B_{\delta}^* P_i l)_i \end{array} \right] = 0 \end{array} \quad (7.203)$$

The accuracy of the given  $\alpha, \delta$  values expressed with the  $P_{\alpha,\delta}$  matrix is, in accordance with the concepts developed in Schmid (1965b), taken into consideration by replacing the term  $(B_{\alpha,\delta}^* P_i B_{\alpha,\delta})_i$  in (7.203) with

$$(B_{\alpha,\delta}^* P_i B_{\alpha,\delta} + P_{\alpha,\delta})_i \quad (7.204)$$

Elimination of the  $v_{\alpha,\delta}$  vector reduces the normal equation system to

From (7.205), finally, the vector  $\Delta_0$  of parameter corrections is obtained as

$$\Delta (7.206)_0 = \underline{N}^{-1} \Delta l$$

and

$$\underline{0} = \underline{0}_0 + \Delta_0 \quad (7.207)$$

In consequence of the fact that in linearizing the original functions  $F$  and  $G$ , terms of the second and higher order were neglected, the result of an adjustment must be iterated until the change in  $v^* P v$  in successive iterations becomes equal to or less than a prescribed tolerance.

The treatment of given right ascension and declination values in the above manner allows the determination of unknown stellar coordinates by simply introducing the  $P_{\alpha,\delta}$  matrix as a null matrix. It is, of course, necessary to find in this case adequate approximation values  $(\alpha_0, \delta_0)$  to replace the normally given  $\alpha, \delta$  values.

Although the determination of unknown stellar coordinates is merely incidental to the problem at hand, it should be stated here that the use of uncataloged stars contributes to the calibration of the camera whenever the uncataloged star is photographed at sufficiently large intervals of time, but at least twice. By means of the associated instants of time the corresponding angle of the Earth's rotation can be introduced into the adjustment to help fix the geometry. Thus, the images of such stars furnish additional data and contribute in a small way to the determination of the parameters of interior orientation. In satellite triangulation it is scarcely possible to gain any advantage from this, because the total period of observation of an event, i.e., the elapsed interval between the

$$\begin{array}{c} \overbrace{\sum_i [B_0^* P_i B_0 - B_{\delta}^* P_i B_{\alpha,\delta} (B_{\alpha,\delta}^* P_i B_{\alpha,\delta} + P_{\alpha,\delta})^{-1} B_{\alpha,\delta} P_i B_0]_i \Delta_0}^N \\ + \underbrace{\sum_i [B_{\delta}^* P_i l - B_{\delta}^* P_i B_{\alpha,\delta} (B_{\alpha,\delta}^* P_i B_{\alpha,\delta} + P_{\alpha,\delta})^{-1} B_{\alpha,\delta}^* P_i l]_i}_{-\Delta l} = 0 \end{array} \quad (7.205)$$

pre- and post-satellite pass star recordings, is deliberately held to a minimum in order to minimize the chance of changes in environmental conditions. Experience has shown that elimination of these changes is not always possible, especially when the requirements for accuracy are high.

For that reason an observation technique was developed, designed to detect small variations in camera orientation occurring during the normal 20- to 30-min period of observation. The method provides for stellar observations during the actual period of transit of the satellite, as well as before and after. Since it is reasonable to assume (actually there is no other choice) that the elements of interior orientation do not vary significantly within the period of observation, a mathematically closer simulation of the actual situation is obtained by computing three separate and independent exterior orientations, one for each of the three periods—before, after, and during the transit of the satellite across the field of view of the camera. The single camera observation equations (7.187) are therefore augmented to include three sets of corrections to the exterior orientation  $\Delta\alpha$ ,  $\Delta\omega$ ,  $\Delta\kappa$ , instead of just one subset. The first term in (7.205), schematically represented, will then have the form shown in figure 7.36.

In order to increase the internal accuracy of the photogrammetric measuring process,

$\Delta_0^*$

$(\alpha_{ex})_1$	$(\alpha_{ex})_2$	$(\alpha_{ex})_3$	$c_x$	$c_y$	$x_0$	$y_0$	$K_1$	$K_2$	$K_3$	$x_B$	$y_B$	$K_4$	$K_5$	$\theta_T$	$\epsilon$	$\tau_1$	$\tau_2$	$\tau_3$	$\tau_4$
	0	0																	
0		0																	
0	0																		

FIGURE 7.36

particularly to minimize the influence of the emulsion and shimmer, it is the practice to measure, for each star, sequences of generally five consecutive single images. This means that each of these  $l_x, l_y$  coordinate measurements has its individual residuals, but only one pair of corrections to the right ascension and declination values of the star may be postulated. Hence, for a star recorded  $n$  times it is necessary first to construct the partial normal equations system (7.203) as the sum of the corresponding  $n$  subsystems, followed by the addition, in accordance with (7.204), of  $\underline{P}_{\alpha,\delta}$  just once before continuing the computations with the elimination of the  $v_\alpha$  and  $v_\delta$  to set up the final normal equations (7.205). If  $\Delta\tau$  corrections are to be computed, it is advisable to first carry out a solution without the  $\Delta\tau$  to avoid the unfavorable influence of existing correlations on the numerical adjustment. In a final iteration step the  $\Delta\tau$  will then be included as additional unknowns to produce the end result. If measurements of unknown stars are included in the system, it is best not to set up coefficients for refraction corrections in the relevant observation equations, because of the limited geometrical content of such equations.

For example, whenever values for certain photogrammetric parameters, as determined from an independently executed camera calibration  $e$ , are to be introduced together with their measures of accuracy into the adjustment, the corresponding weight matrix  $\underline{P}_{0_e}$  (cf. eq. 7.196).

$$\underline{P}_{0_e} = \frac{m_0^2}{s_{0_e}^2} \underline{N}_{0_e} \quad (7.208)$$

must be added to the normal equations system (7.205). It must be borne in mind that this  $\underline{P}_{0_e}$  matrix has reference to the given values which are appropriately used as approximation values in the first iteration. Since in the course of the iteration, however, the approximation for the  $0_0$  vector undergoes changes, a modification of the vector of absolute terms in the normal equations system is necessary at each iteration step, in that a vector

$$\underline{P}_{o_c} \Delta \underline{l}_{o_c} \quad (7.209)$$

is added to the  $\Delta \underline{l}$  vector for that iteration, where

$$\Delta \underline{l}_{o_c} = \underline{0}_{o_c} - \underline{0}_c \quad (7.210)$$

The purpose and effect of this operation is to initialize the  $\underline{0}_c$  components of the  $\underline{0}_o$  vector to their given values before proceeding with the next iteration step. For parameters that are not given, the  $\Delta \underline{l}_{o_c}$  vector has zero components.

It can be argued that the determination of three different sets of orientation parameters does not lead to an optimum solution in cases where the exterior orientation of the camera does not change at all during the entire observation, so that only one or two sets of  $\alpha, \omega, \kappa$  are justified. For this reason, we first compute directions in space for a number of fictitious images along the plate diagonal, using the results of the present solution. For each of the fictitious point images whose coordinates  $x, y$  are assumed free of error, three unit vectors corresponding to the three orientations are computed by use of (7.81) in the  $y'$  system:

$$\underline{y}'_{j=1,2,3} = \underline{R}'_{y_{j=1,2,3}}(\alpha, \omega, \kappa) \frac{\underline{p}}{|\underline{p}|} \quad (7.211) \dagger$$

where

$$\underline{p} = \begin{bmatrix} \bar{x} \\ \bar{y} \\ c \end{bmatrix} \begin{bmatrix} c_x \\ c_r \\ c_y \end{bmatrix} \quad (7.212)$$

$$|\underline{p}| = \left[ \bar{x}^2 + \left( \bar{y} \frac{c_r}{c_x} \right)^2 + c_x^2 \right]^{1/2} \quad (7.213)$$

Premultiplication of the  $\underline{y}'_{j=1,2,3}$  vectors with  $\underline{R}(270^\circ + \phi')$  yields, in accordance with (7.107), the corresponding  $\underline{x}'_{j=1,2,3}$  vectors. With  $\underline{y}'$  or  $\underline{x}'$  vectors, as the case may be, one computes with (7.28) the corresponding  $\xi$  and  $\eta$  values, and with (7.29) the azimuths and zenith distances or hour angles and declinations.

Next, one computes for each pair from the  $\underline{y}'_{j=1,2,3}$  or  $\underline{x}'_{j=1,2,3}$  the small angle  $\epsilon_{jk}$  between the computed directions. For the combination 1, 2 in an  $x'$  system, one obtains, for example,

$$\epsilon_{1,2} = |\underline{x}'_2 - \underline{x}'_1| \quad (7.214)$$

or, in radians,

$$\epsilon_{1,2} = [(x'_{21} - x'_{11})^2 + (x'_{22} - x'_{12})^2 + (x'_{23} - x'_{13})^2]^{1/2} \quad (7.215)$$

If the differences between corresponding right ascensions and declinations or azimuths and zenith distances, so computed from the three orientations, exceed their confidence limits, a timing error or camera motion may be the cause. Before one can decide whether these computed differences in direction are significant, one must find the mean errors either of the direction components  $(\alpha, \delta)$  and  $(A, z)$ , or at least of the angles  $\epsilon_{jk}$ , which can be looked upon as combinations in pairs of the computed  $(\alpha, \delta)$  or  $(A, z)$ .

Since  $\alpha$  and  $\delta$  are parameters of the mathematical model on which the adjustment is based, the following solution offers itself. Using (7.204) and taking into account the considerations leading to (7.202) and (7.203), we can schematically represent the first term of the normal equations system (7.201) as

$$\begin{bmatrix} (\underline{B}_{\alpha, \delta}^* \underline{P}_1 \underline{B}_{\alpha, \delta} + \underline{P}_{\alpha, \delta})_1 & \underline{0} & \underline{0} & (\underline{B}_{\alpha, \delta}^* \underline{P}_1 \underline{B}_0)_1 \\ \underline{0} & \underline{0} & & \\ \underline{0} & \underline{0} & (\underline{B}_{\alpha, \delta}^* \underline{P}_l \underline{B}_{\alpha, \delta} + \underline{P}_{\alpha, \delta})_m & (\underline{B}_{\alpha, \delta}^* \underline{P}_l \underline{B}_0)_m \\ (\underline{B}_0^* \underline{P}_l \underline{B}_{\alpha, \delta})_1 & \dots & (\underline{B}_0^* \underline{P}_l \underline{B}_{\alpha, \delta})_m & \sum_{i=1}^{i=m} (\underline{B}_0^* \underline{P}_l \underline{B}_0)_i \end{bmatrix} \equiv \begin{bmatrix} \underline{A}_{11} & \underline{A}_{12} \\ \underline{A}_{12}^* & \underline{A}_{22} \end{bmatrix} \quad (7.216)$$

Designate the inverse of the matrix (7.216) as

$$\begin{bmatrix} \underline{A}_{11} & \underline{A}_{12} \\ \underline{A}_{12}^* & \underline{A}_{22} \end{bmatrix}^{-1} = \begin{bmatrix} \underline{Q}_{11} & \underline{Q}_{12} \\ \underline{Q}_{12}^* & \underline{Q}_{22} \end{bmatrix} \quad (7.217)$$

From (7.216) and (7.217) it is apparent that for the inverted normal equations system of (7.206)

$$[\underline{A}_{22} - \underline{A}_{12}^* \underline{A}_{11}^{-1} \underline{A}_{12}]^{-1} = \underline{N}^{-1} = \underline{Q}_{22} \quad (7.218)$$

Furthermore, since

$$\begin{bmatrix} \underline{A}_{11} & \underline{A}_{12} \\ \underline{A}_{12}^* & \underline{A}_{22} \end{bmatrix} \begin{bmatrix} \underline{Q}_{11} & \underline{Q}_{12} \\ \underline{Q}_{12}^* & \underline{Q}_{22} \end{bmatrix} = \underline{E} \quad (7.219)$$

it follows from (7.217) that

$$\underline{Q}_{11} = \underline{A}_{11}^{-1} + \underline{A}_{11}^{-1} \underline{A}_{12} \underline{N}^{-1} \underline{A}_{12}^* \underline{A}_{11}^{-1} \quad (7.220)$$

From the schematic shown in (7.216) it follows that the computation indicated with (7.220) can be performed in independent steps for each individual pair  $i$  of values  $\alpha, \delta$ . Hence we can write

$$\begin{aligned} s_{(\alpha,\delta),i}^2 &= s_0^2 [ (\underline{D}_{\alpha,\delta}^* \underline{F}_i \underline{B}_{\alpha,\delta} + \underline{F}_{\alpha,\delta})_i^{-1} \\ &+ (\underline{B}_{\alpha,\delta}^* \underline{P}_i \underline{B}_{\alpha,\delta} + \underline{P}_{\alpha,\delta})_i^{-1} (\underline{B}_{\alpha,\delta}^* \underline{P}_i \underline{B}_0)_i \underline{N}^{-1} \\ &(\underline{B}_{\alpha,\delta}^* \underline{P}_i \underline{B}_{\alpha,\delta})_i (\underline{B}_{\alpha,\delta}^* \underline{P}_i \underline{B}_{\alpha,\delta} + \underline{P}_{\alpha,\delta})_i^{-1} ] \end{aligned} \quad (7.221)$$

With (7.221) we obtain the covariance matrix for the corrected values of  $\alpha, \delta$  for the stars originally selected for the adjustment. If the star in question was originally unknown, it is merely necessary to set the relevant  $\underline{P}_{\alpha,\delta}$  equal to a null matrix and to introduce the corresponding  $\underline{P}_i$  matrix, which must, of course, relate to the initially chosen  $m_0$  value. In the present case a further simplification is present, since the  $\underline{B}_{\alpha,\delta}$  matrix is quadratic and nonsingular, hence invertible. The covariance matrix for an originally unknown star is, therefore, from (7.221)

$$s_{\alpha,\delta} = s_0 ( \underline{B}_{\alpha,\delta}^{-1} \underline{P}_i^{-1} \underline{B}_{\alpha,\delta}^{-1*} + \underline{B}_{\alpha,\delta}^{-1} \underline{B}_0 \underline{N}^{-1} \underline{B}_0^* \underline{B}_{\alpha,\delta}^{-1*} ) \quad (7.222)$$

Finally, to compute the accuracy of a direction defined by a fictitious, errorless point, the  $\underline{P}^{-1}$  matrix in (7.222) becomes a null matrix, resulting in

$$s_{\alpha,\delta}^2 = s_0^2 ( \underline{B}_{\alpha,\delta}^{-1} \underline{B}_0 \underline{N}^{-1} \underline{B}_0^* \underline{B}_{\alpha,\delta}^{-1*} ) \quad (7.223)$$

Formula (7.223) is now applied for a selected fictitious point to the three orientations obtained from the solution of the system (7.205). The resulting covariance matrix  $s_{\alpha,\delta}$  is of the dimension  $6 \times 6$ . The three  $2 \times 2$  submatrices along the diagonal are the three covariances  $s^2(\alpha,\delta)_{j=1,2,3}$  associated with the three sets of  $\alpha, \delta$ . The analogous covariance matrices of the azimuth and elevation components are obtained with (7.107) as

$$\begin{aligned} s^2(\underline{A}, z)_{j=1,2,3} &= \underline{R} (90^\circ - \phi) s^2(\alpha,\delta)_{j=1,2,3} \\ &\quad \underline{2} \\ &\quad \times \underline{R}^* (90^\circ - \phi) \end{aligned} \quad (7.224)$$

Finally, the variances  $s_{21}^2, s_{32}^2, s_{31}^2$  of the three  $\epsilon$  angles of (7.215) are the diagonal terms of the covariance matrix

$$s_\epsilon^2 = \underline{F}^* s_{\alpha,\delta}^2 \underline{F} \quad (7.225)$$

where

$$\underline{F} = \begin{bmatrix} \frac{\partial \epsilon}{\partial \alpha_1} & 0 & \frac{\partial \epsilon}{\partial \alpha_1} \\ \frac{\partial \epsilon}{\partial \delta_1} & 0 & \frac{\partial \epsilon}{\partial \delta_1} \\ \frac{\partial \epsilon}{\partial \alpha_2} & \frac{\partial \epsilon}{\partial \alpha_2} & 0 \\ \frac{\partial \epsilon}{\partial \delta_2} & \frac{\partial \epsilon}{\partial \delta_2} & 0 \\ 0 & \frac{\partial \epsilon}{\partial \alpha_3} & \frac{\partial \epsilon}{\partial \alpha_3} \\ 0 & \frac{\partial \epsilon}{\partial \delta_3} & \frac{\partial \epsilon}{\partial \delta_3} \end{bmatrix} \quad (7.226)$$

In (7.226) for each combination  $j, k$

$$\begin{bmatrix} \frac{\partial \epsilon}{\partial \alpha_j} \\ \frac{\partial \epsilon}{\partial \delta_j} \\ \frac{\partial \epsilon}{\partial \alpha_k} \\ \frac{\partial \epsilon}{\partial \delta_k} \end{bmatrix} = \frac{1}{\epsilon_{jk}} \begin{bmatrix} x'_{j_1} x'_{k_2} - x'_{j_2} x'_{k_1} \\ x'_{j_1} x'_{k_1} x'_{k_3} (1 - x'^2_{k_3})^{-1/2} + x'_{j_2} x'_{k_2} x'_{k_3} (1 - x'^2_{k_3})^{-1/2} - x'_{j_3} (1 - x'^2_{k_3})^{1/2} \\ x'_{j_2} x'_{k_1} - x'_{j_1} x'_{k_2} \\ x'_{k_1} x'_{j_1} x'_{j_3} (1 - x'^2_{j_3})^{-1/2} + x'_{k_2} x'_{j_2} x'_{j_3} (1 - x'^2_{j_3})^{-1/2} - x'_{k_3} (1 - x'^2_{j_3})^{1/2} \end{bmatrix} \quad (7.227)$$

If all  $|\epsilon_{1,2,3}|$  exceed the corresponding quantity  $K \cdot s_{\epsilon_{1,2,3}}$  (where  $K$  is a constant selected on the basis of personal experience), then it must be assumed that the camera orientation has changed during the three observation periods. In this case the second solution indicated in the schematic of figure 7.36 will be accepted as definitive, this being the orientation corresponding to the stars recorded during the satellite transit.

On the other hand, if certain values of  $\epsilon$  are less than the corresponding  $K \cdot s_{\epsilon}$ , then these orientations can be combined. Thus, if

$$\epsilon_{12} < K s_{\epsilon_{12}} \quad (7.228a)$$

combine orientations 1 and 2; if

$$\epsilon_{23} < k s_{\epsilon_{23}} \quad (7.228b)$$

combine orientations 2 and 3; if

$$\epsilon_{13} < k s_{\epsilon_{13}} \quad (7.228c)$$

combine orientations 1 and 3.

The result is obtained as shown in Schmid and Schmid (1965) in the form

$$\Delta_0 = \frac{[N^{-1} - N^{-1}C^* (CN^{-1}C^*)^{-1} CN^{-1}]}{[\Delta I + N^{-1}C^* (CN^{-1}C^*)^{-1} I]} \quad (7.229)$$

where  $N^{-1}$  and  $\Delta I$  are from the last iteration in the solution of the original system (7.205) and

$$C = \begin{bmatrix} 1 & 0 & 0 & -1 & 0 & 0 & 0 & 0 & 0 \\ 0 & 1 & 0 & 0 & -1 & 0 & 0 & 0 & 0 \\ 0 & 0 & 1 & 0 & 0 & -1 & 0 & 0 & 0 \\ 0 & 0 & 0 & 1 & 0 & 0 & -1 & 0 & 0 \\ 0 & 0 & 0 & 0 & 1 & 0 & 0 & -1 & 0 \\ 0 & 0 & 0 & 0 & 0 & 1 & 0 & 0 & -1 \end{bmatrix} \quad (7.230)$$

where  $C$  is a  $6 \times 9$  matrix (0 being the number of components of the  $\Delta_0$  vector), the first nine columns being as indicated and the balance of the matrix consisting of zero entries. The form of the  $6 \times 9$  portion will vary according to the results of the criteria (7.228). The form in (7.230) corresponds to the case of combining all three orientations. For such a case, furthermore,

$$I = \begin{bmatrix} \alpha_2^0 - \alpha_1^0 \\ \omega_2^0 - \omega_1^0 \\ \kappa_2^0 - \kappa_1^0 \\ \alpha_3^0 - \alpha_2^0 \\ \omega_3^0 - \omega_2^0 \\ \kappa_3^0 - \kappa_2^0 \end{bmatrix} \quad (7.231)$$

The values with the superscript 0 are the approximation values used in the final iteration in the solution of the system shown in figure 7.36. The correction vector computed with (7.229) pertains to these approximations. The final result is then computed with (7.229) and (7.207).

The last phase of the computations covers the partial results, and a summary of these results now follows. Values for distortion at a prescribed interval, e.g., in 3-mm steps, are

computed to a maximal radial distance  $d_{max}$  dictated by the plate format. If the radial distortion for a prescribed distance  $d_0$  is to be made equal to 0, the corresponding camera constant  $c^*$  is computed with

$$c^* = \frac{c_x + c_y}{2} (1 - K_0) \quad (7.232)$$

in which

$$K_0 = - (K_1 d_0^2 + K_2 d_0^4 + K_3 d_0^6) \quad (7.233)$$

The radial distortion is then computed successively for the required distance  $d$  with (7.95). The transformed radial distortion corresponding to  $c^*$  is

$$(\Delta R) = d \cdot K_0 + \Delta R \quad (7.234)$$

Values for the decentering distortion are computed similarly with (7.99).

If it is desired to study the values of astronomic refraction within the range of the photogrammetric exposure, they can be computed from (7.40) as a function of  $z$  in suitable intervals, with either the given or the newly computed  $\tau$  values.

Computing distortion and refraction values is of particular significance when star observations are evaluated for the calibration of photogrammetric cameras or used in error studies of individual photographs. In satellite triangulation the computation of such data recommends itself strongly for the purpose of gaining insight into the behavior of all cameras in use, in view of the fact that the photogrammetric registration in a continental, and especially in a worldwide, net is exposed to extreme ranges of local and seasonal environmental conditions. It is therefore required, on the one hand, to be informed as to the reliability and metric quality of the instrumentation used; it is also expected that a systematic study of these results will allow the drawing of conclusions with respect to the individual photograms.

Finally, we must compute the corrections to the given values resulting from the adjustment, the statistical measures of accu-

racy, such as the mean error of unit weight, the mean errors of the computed quantities as well as mean errors of values, computed as functions of those quantities.

Corrections to the measured images are computed with (7.189). With the parameters obtained in the adjustment one has

$$\begin{aligned} v_{l_{xi}} &= F_i \\ v_{l_{yi}} &= G_i \end{aligned} \quad (7.235)$$

To get a better picture of the distribution of these residuals, it is useful to compute the radial and tangential components of these corrections. Computation of the corrections  $v_\alpha$  and  $v_\delta$  for each given star is carried out with (7.203) (7.204), where now  $\Delta_0$  is a zero vector:

$$v_{(\alpha,\delta)_i} = - (B_{\alpha,\delta}^* P_l B_{\alpha,\delta} + P_{\alpha,\delta})^{-1} (B_{\alpha,\delta}^* P_l l)_i \quad (7.236)$$

Wherever quantities introduced by means of approximations into the adjustment differ from free variables, in that corresponding entries in the  $P_u$  matrix (7.190) (cf. also eq. (7.208)) represent a priori given weights, relevant corrections are computed, by using the results from the adjustment, from

$$v_u = u - u_0 \quad (7.237)$$

where  $u$  stands for the adjusted and  $u_0$  for the initial value of the parameter. Next one computes

$$\Sigma v^* P_l v_l + \Sigma v_{\alpha,\delta}^* P_{\alpha,\delta} v_{\alpha,\delta} + \Sigma v_u^* P_u v_u = \Sigma v^* P v \quad (7.238)$$

and in accordance with (7.193) the mean error of unit weight after adjustment  $s_0$  with

$$s_0 = \left[ \frac{\Sigma v^* P v}{n - u} \right]^{1/2} \quad (7.239)$$

The mean error of the computed parameters is obtained by multiplying  $s_0$  by the square root of the corresponding diagonal term in  $N^{-1}$  of (7.206). The mean errors of the given quantities result from dividing  $s_0$

by the square root of the weight assigned to the quantities.

The mean error of the camera constant (7.232) and the mean error of radial and decentering distortion are computed as mean errors of functions of quantities determined in the adjustment. In general, the mean error  $s_a$  of a quantity  $a$

$$a = F(u) \quad (7.240)$$

is

$$s_a = s_0 (\mathbf{f}_a^* \mathbf{N}^{-1} \mathbf{f}_a)^{1/2} \quad (7.241)$$

in which  $\mathbf{f}_a$  is the vector whose components are the partial derivatives  $\partial F(u)/\partial u$ , the components corresponding to parameters not present in (7.240) being zero. For the cases in question here,

Substituted in (7.241), the components computed with (7.242) now give the mean error of the camera constant  $c^*$ , with (7.243), of the radial distortion at the selected distances  $d$ , with (7.244), of the radial distortions corresponding to camera constants  $c^*$ , with (7.245), of the decentering distortion, and, with (7.246), of astronomic refraction as function of selected zenith distances.

This concludes the computations in connection with the reduction of the single camera.

In preparation for the next series of computations the orientation matrix  $\underline{R}'_y(\alpha, \omega, \kappa)^\dagger$  during the satellite pass must first be transformed from the local  $y'$  system into the final  $z$  or  $z'$  system that has been selected for the eventual spatial triangulation.  $\underline{R}'_y(\alpha, \omega, \kappa)^\dagger$  results from (7.79), either with the second group of elements of orientation in the

$$\mathbf{f}_{c^*}^* = \begin{array}{c|c|c|c|c} & \partial / & & & \\ \hline \partial c_x & \partial c_y & \partial K_1 & \partial K_2 & \partial K_3 \\ \hline \frac{1-K_0}{2} & \frac{1-K_0}{2} & -\frac{c_x+c_y}{2} \cdot d_0^2 & -\frac{c_x+c_y}{2} \cdot d_0^4 & -\frac{c_x+c_y}{2} \cdot d_0^6 \\ \hline \end{array} \quad (7.242)$$

$$\mathbf{f}_{\Delta R}^* = \begin{array}{c|c|c} & \partial / & \\ \hline \partial K_1 & \partial K_2 & \partial K_3 \\ \hline d^3 & d^5 & d^7 \\ \hline \end{array} \quad (7.243)$$

$$\mathbf{f}_{(\Delta R)}^* = \begin{array}{c|c|c} & \partial / & \\ \hline \partial K_1 & \partial K_2 & \partial K_3 \\ \hline d(d^2-d_0^2) & d(d^4-d_0^4) & d(d^6-d_0^6) \\ \hline \end{array} \quad (7.244)$$

$$\mathbf{f}_{\Delta T}^* = \begin{array}{c|c} & \partial / \\ \hline \partial K_4 & \partial K_5 \\ \hline d^2 & d^4 \\ \hline \end{array} \quad (7.245)$$

$$\mathbf{f}_T^* = \begin{array}{c|c|c|c} & \partial / & & \\ \hline \partial \tau_1 & \partial \tau_2 & \partial \tau_3 & \partial \tau_4 \\ \hline T^{1/2} W \tan \frac{\beta}{2} & T^{1/2} W \tan^3 \frac{\beta}{2} & T^{1/2} W \tan^5 \frac{\beta}{2} & T^{1/2} W \tan^7 \frac{\beta}{2} \\ \hline \end{array} \quad (7.246)$$

schematic of figure 7.36, or, in accordance with the principle of combination of (7.228), from a group of orientation elements, which also includes star recordings simultaneous with the satellite transit.

The necessary transformation is accomplished with (7.30) and (7.108) or (7.109), so that we have

$$\begin{aligned} \underline{R}'_z(\alpha, \omega, \kappa) &= \underline{R}(\lambda_{cast}), \\ &\begin{matrix} 3 \\ 2 \end{matrix} (90^\circ - \phi) \begin{matrix} 2 \\ 1 \end{matrix} \underline{R}(-x, -y) \begin{matrix} 2 \\ 2 \end{matrix} \underline{R}(270^\circ + \phi), \\ &\begin{matrix} 3 \\ 3 \end{matrix} (-\lambda_{cast}) \underline{R}'_y(\alpha, \omega, \kappa) \end{aligned} \quad (7.247)$$

and with (7.79), for example,

$$\left. \begin{aligned} \cos \alpha_{z'} &= r_{33} / \cos \omega_{z'} \\ \sin \omega_{z'} &= -r_{23} \\ \cos \kappa_{z'} &= r_{22} / \cos \omega_{z'} \end{aligned} \right\} \quad (7.248)$$

The reduction just described, of a single observation of stars, is on the one hand suitable for a camera calibration, and on the other represents one of the intermediate steps in the process of photogrammetric satellite triangulation.

We now list the intermediate results from the single camera program that will be needed in the next reduction step.

(1) The parameters set up to reconstruct the photogrammetric bundle and computed in the adjustment, namely, (a) the elements of exterior orientation  $(\alpha\omega\kappa)_{y'}$  referring to the local  $y'$  system and (b) in the general case, the parameters  $\epsilon, c_x, c_y, x_0, y_0, x_s, y_s, K_1, K_2, K_3, K_4, K_5, \phi_T, \tau_1, \tau_2, \tau_3, \tau_4$ .

(2) The elements of exterior orientation referred to the ultimate triangulation coordinate system, i.e., either  $(\alpha\omega\kappa)_z$  or  $(\alpha\omega\kappa)_{z'}$ .

(3) The mean error of unit weight  $s_0$ .

(4) The inverted normal equations system  $N^{-1}$ .

(5) Meteorological data at the observation site during the satellite observations.

(6) All data necessary for the identification of observation sites and instrumentation.

(7) All supplementary information needed for time determination of the satellite images.

## 7.4.7 Spatial Triangulation

### 7.4.7.1 Preliminary Computations

The principle problem of geometric satellite triangulation is the determination of three-dimensional rectangular coordinates for the observation sites, the triangulation being executed in either the  $z$  or the  $z'$  coordinate system introduced in section 7.4.6.2.6. In preparation for these computations the treatment of the single camera (as described at the end of section 7.4.6.4) includes, among other things, the transformation of the elements of exterior orientation to  $(\alpha\omega\kappa)_z$  or  $(\alpha\omega\kappa)_{z'}$ . Now, in order to triangulate, it is necessary to determine, at each of the stations which have recorded simultaneously a specific satellite pass, at least one direction associated with a specific satellite location in space. Just as the elements of exterior orientation of all photograms must refer to a consistent coordinate system, all the directions obtained with such an orientation must be with respect to unambiguously defined target points in space. This requirement is filled by reducing all measured image coordinates to a rigorous central perspective and then applying all the corrections explained in section 7.4.5.

Reduction of the plate coordinates  $l_x, l_y$  to a central perspective is accomplished with (7.141) and (7.142). The expressions for  $\Delta R_x, \Delta R_y, \Delta T_x, \Delta T_y$  are computed from (7.97), (7.98), and (7.103) with the use of (7.143) through (7.147) and with an iteration loop, as was indicated earlier. The coordinates  $l_{\bar{x}}$  and  $l_{\bar{y}}$  so obtained correspond in measuring to (7.138) and (7.139) and must still be reduced to a common scale factor. If in (7.138) we set  $c_{\bar{x}} = c$ , we obtain, in agreement with (7.212),

$$l_{x_c} = l_{\bar{x}} \quad (7.249)$$

and

$$l_{\bar{y}_c} = l_{\bar{y}} \cdot \frac{c_x}{c_y} \quad (7.250)$$

The image coordinates  $l_{\bar{x}_c}$ ,  $l_{\bar{y}_c}$  refer to the principal point and the scale factor  $c$ , i.e., to the idealized central perspective. Before these fictitious point images can be used in a spatial triangulation, they must be corrected for the influences cited in section 7.4.5. These corrections can be classified under the following groupings: (1) refraction, subdivided into astronomic and parallactic refraction; (2) eccentricity of the target; and (3) time corrections, subdivided into clock corrections and light propagation effects.

In the course of the reduction the influence of scintillation is largely eliminated, at the appropriate place, by smoothing the sequence of individual images of the satellite trail with the aid of polynomials.

The computation of some of these corrections requires an approximation to the distance between the camera site and the satellite. To effect these corrections, the coordinates  $l_{\bar{x}_k}$ ,  $l_{\bar{y}_k}$  (equations 7.249 and 7.250) and the  $R'_y(\alpha, \omega, \kappa)$  † matrix from the single camera are used to produce the unit vector  $y'_r$  from (7.81) and the corresponding standard coordinates  $\xi_r$ ,  $\eta_r$  with (7.23), and then the observed zenith distance  $z_r$  with (7.29). The astronomic refraction  $r_z$  follows from (7.40) by iteration. The unit vector  $y'$  corrected for astronomic refraction is computed with (7.42), where  $r_s$  is replaced with  $r_z$  or, alternatively, directly with

$$z = z_r + r_z \quad (7.251)$$

and (7.74), in the form

$$y' = \begin{bmatrix} \cos z & \cos A \\ \cos z & \sin A \\ \sin z & \end{bmatrix} \quad (7.252)$$

In this, the azimuth  $A$  is derived from (7.29). With  $y'$ , new values for  $\xi$  and  $\eta$  are derived from (7.28). With these and by using  $c = c_x$ , we compute image coordinates from (7.85) and (7.86), taking the direction cosines  $r_{jj}$  from  $R'_y(\alpha, \omega, \kappa)$  and substituting,  $\xi$ ,  $\eta$ , 1 for  $x - x_0$ ,  $y - y_0$ , and  $z - z_0$ , respectively. After all satellite images of a given photograph have been so reduced, the coefficients

for polynomials (7.48) are determined from an adjustment in accordance with (7.266) to (7.270). With these polynomials the  $l_{\bar{x}_c}$  and  $l_{\bar{y}_c}$  are expressed as functions of station clock time  $t$ . Omitting the subscript  $c$ , we have then, quite generally,

$$l_{\bar{x}} = f(t) \quad (7.253)$$

$$l_{\bar{y}} = g(t) \quad (7.254)$$

With the notation of figure 7.26 we obtain observation times referred to an unambiguous time designation by adding to each locally recorded time  $t$  the corresponding clock correction  $\Delta T$ , which rarely exceeds 10 msec. The normalized instants of time  $T_{j_{1,2}, \dots, m}$  recorded at stations  $j_{1,2}, \dots, m$  will then be

$$T_{j_{1,2}, \dots, m} = t_{j_{1,2}, \dots, m} + \Delta T_{j_{1,2}, \dots, m} \quad (7.255)$$

In order to obtain an instant of time that is as close as possible to the range of times recorded at each station, we form the arithmetic mean of the  $T$ 's and convert this mean to corresponding interpolated times referred to the individual station clocks. Thus

$$t_{j_{1,2}, \dots, m} = \frac{\sum T_{j_{1,2}, \dots, m}}{m} - \Delta T_{j_{1,2}, \dots, m} \quad (7.256)$$

On the basis of the relevant  $t$  value at each station,  $l_{\bar{x}}$ ,  $l_{\bar{y}}$  values are computed with (7.253), (7.254) for points along the satellite trail, which, since light propagation time has as yet been neglected, refer to simultaneous instants of exposure.

Next, approximate satellite positions are computed with these data. The camera-site coordinate approximations ( $\phi^0$ ,  $\lambda^0$ ,  $h^0$ ) are, with (7.111), (7.112), (7.113), transformed to rectangular coordinates in the  $z$  system, or, if necessary, by the additional transformation (7.36) are transferred to the  $z'$  system. With the  $R_x(\alpha, \omega, \kappa)$  or  $R_{z'}(\alpha, \omega, \kappa)$  orientation matrices mentioned previously and the interpolated  $l_{\bar{x}}$ ,  $l_{\bar{y}}$  coordinates, once these values are available for all stations, approxi-

mate satellite positions can be computed by using for an intersection with  $m$  rays

$$\begin{bmatrix} m & 0 & [a_x] \\ 0 & m & [a_y] \\ [a_x] & [a_y] & [a_x a_x + a_y a_y] \end{bmatrix} \begin{bmatrix} z_{s_1} \\ z_{s_2} \\ z_{s_3} \end{bmatrix} = \begin{bmatrix} + [b_x] \\ + [b_y] \\ + [a_x b_x + a_y b_y] \end{bmatrix} = 0 \quad (7.257)$$

The  $z_{s_1, 2, \dots, m}$  are the approximated coordinates of a point on the satellite orbit. As an auxiliary computation, one forms with (7.79)

$$a_x = - \frac{(r_{11} l_x) + (r_{21} l_y) + (r_{31} c)}{(r_{13} l_x) + (r_{23} l_y) + (r_{33} c)} \quad (7.258)$$

$$a_y = - \frac{(r_{12} l_x) + (r_{22} l_y) + (r_{32} c)}{(r_{13} l_x) + (r_{23} l_y) + (r_{33} c)} \quad (7.259)$$

$$b_x = - (a_x z_3^0 + z_1^0) \quad (7.260)$$

$$b_y = - (a_y z_3^0 + z_2^0) \quad (7.261)$$

where  $z_{1, 2, 3}^0$  are approximated rectangular station coordinates.

The distances between an observation station and the satellite positions are

$$d = [(z_{s_1}^0 - z_1^0)^2 + (z_{s_2}^0 - z_2^0)^2 + (z_{s_3}^0 - z_3^0)^2]^{1/2} \quad (7.262)$$

Instead of storing the large number of distances corresponding to the 500 to 600 satellite positions, it is preferable to express  $d$  as a function of  $t$ . As with the functions (7.253), (7.254), we again use (7.58), with, of course, just one expansion for the  $d$ . This results in one polynomial for each station or, expressed generally,

$$d = h(t) \quad (7.263)$$

We now resume the reduction of the results obtained with (7.249) and (7.250), computing first the satellite refraction  $r_s$  with (7.43) and using (7.263) along with the previously computed astronomic refraction  $r_x$ . Then follows the unit vector  $y'$  corrected for refraction, from the refracted vector  $y'$  by use of (7.42) or (7.252), where now

$$z = z_r + r_s \quad (7.264)$$

Reduction of the  $y'$  vector is continued with the elimination of the influence of eccentricity of the target point.

After the unit vector  $y'_0$  in the direction toward the Sun has been computed, in accordance with (7.54) and the Sun's right ascension and declination at the instant of observation and with the use of (7.20), (7.21), (7.23), and (7.24), one obtains the unit vector  $y'_{BM}$  to the center of the balloon with (7.52) and (7.49) in the form

$$y'_{BM} = y' - \frac{a}{d \sin \gamma} (y'_0 + \cos \gamma y') \quad (7.265)$$

in which the needed quantities are derived from (7.263), (7.50) or (7.51), and (7.46).

With the vector (7.265), corresponding  $\xi, \eta$  values are again computed with (7.28), as are  $l_x, l_y$  coordinates of the corresponding fictitious satellite images with the use of  $R_{y'}(\alpha, \omega, \kappa)$  matrix. With these values in (7.58) the final interpolation polynomials are set up, which, in complete analogy with the expressions (7.253) and (7.254), represent  $l_x$  and  $l_y$  as functions of  $t$  (see also sec. 7.4.8.1). Normal equations corresponding to (7.58) are set up in order to determine the polynomial coefficients, where, to simplify the numerical calculations, the  $t$  values, assumed free of error, are replaced with a sequence of integers whose increment corresponds to the greatest common divisor of the interval recorded at the various stations involved. The normal equations system for  $n$  images has the form

$$\sum_{i=1}^n \overbrace{[B_i^* P_i B_i]}^{N_c} c = \sum_{i=1}^n \overbrace{[B_i^* P_i I]}^{l_c} \quad (7.266)$$

in which  $P_i$  is expressed with sufficient accuracy in terms of the weight matrix assigned to the original coordinate measurements (cf. eq. 7.192). For an  $m^{\text{th}}$ -degree polynomial  $B_i$  is, from (7.58), for each of the  $n$  points



For discussion of the needed number of directions so introduced, see section 7.4.8.1. In any case, the selection of orbital times  $T$  should be such that one of these instants corresponds to a point of the orbit whose image on the several photograms is as close as possible to the principal point.

After these preliminary computations have been completed, a pair of image coordinates, representing fictitious observations, will be available for each selected point of the orbit. These image coordinates simulate images that would have been obtained had the following conditions been met:

(1) The photogrammetric camera reproduces a rigorous central perspective.

(2) The comparator has no linear scale errors and measures in two perpendicular directions.

(3) The origin of the image coordinate system coincides with the principal point.

(4) The observation was executed in vacuo, i.e., refraction and scintillation do not exist.

(5) The images correspond to the center of the balloon.

(6) Neither Earth nor satellite has a proper motion; i.e., there is no influence from aberration or time of light propagation.

(7) All station clocks run without error with respect to a reference time, and the recording times of the stars are rigorously UT1.

(8) The images at all stations observing a specific satellite pass correspond to uniquely defined positions on the satellite orbital curve.

After processing all observational data in the manner described, we have at our disposal for the execution of the spatial triangulation for each of the observing stations and for all satellite passes observed at such stations a photogram with a number of fictitious image point coordinates  $l_x, l_y$ , the relevant scale factor  $c$ , and either the  $\underline{R}_z(\alpha, \omega, \kappa)$  or the  $\underline{R}_{z'}(\alpha, \omega, \kappa)^\dagger$  orientation matrix. Since orientation matrices are referred to the same coordinate system, either the  $z$  or  $z'$  system, the spatial triangulation can now, with the

idealized image coordinates  $l_x, l_y$  mentioned above, be carried out in accordance with the geometrical principles of a rigorous central perspective. For this last adjustment step the covariance matrix associated with the computed image coordinates will also be needed.

With (7.274) a covariance matrix was obtained relating to the smoothing process of the orbital curve. The covariance matrix relating to the single camera reduction is computed, with the designations introduced in (7.188), from (7.195) and the results obtained with (7.206) and (7.239) of the single camera solution in the form

$$(\mathbf{s}_0)^2 = s_0^2 [\underline{B}_0 \underline{N}^{-1} \underline{B}_0^*] \quad (7.276)$$

Since the two error contributions are independent of each other, the total covariance matrix for the values  $l_x, l_y$  of a specific photogram is, with (7.274) and (7.276),

$$(\mathbf{s}_1)^2 = (\mathbf{s}_{1c})^2 + (\mathbf{s}_{10})^2 \quad (7.277)$$

with the proviso that all computations are with reference to a common mean error of unit weight (cf. sec. 7.4.8.1).

For each station to be triangulated and for all satellite passes observed at the station, the following information is now available:

(1) Approximate station coordinates

$$\phi^\circ, \lambda^\circ, \text{ and } h^\circ \quad (7.278)$$

(2) If given, the weight matrix of these coordinates

$$\underline{P}_\phi = \begin{bmatrix} p_\phi & p_{\phi,\lambda} & p_{\phi,h} \\ p_{\phi,\lambda} & p_\lambda & p_{\lambda,h} \\ p_{\phi,h} & p_{\lambda,h} & p_h \end{bmatrix} \quad (7.279)$$

(3) Corresponding rectangular coordinates  $z_{1,2,3}$  or  $z'_{1,2,3}$  derived from (7.111), (7.112), (7.113), and, if necessary, transformed with (7.36).

(4) The relevant weight matrices  $\underline{P}_z$  or  $\underline{P}_{z'}$  from (7.128).

(5) The elements of orientation  $(\alpha\omega\kappa)_z$  or  $(\alpha\omega\kappa)_{z'}$  from the single camera program (cf. eq. 7.248).

(6) The scale factor  $c$ .

(7) The fictitious image point coordinates  $l_{\bar{x}}, l_{\bar{y}}$  corresponding to the selected satellite positions and associated satellite orbit times.

(8) The covariance matrix (7.277) of these coordinates.

The information contained in points 1 to 8 above represents the input data for the spatial triangulation proper, whose solution and adjustment is treated in the next section as the final step in the evaluation.

The evaluation procedures of this section and, in addition, computations relating to alternative approaches to these problems are described in all details and with pertinent flowcharts in R. H. Hanson (unpublished papers, 1968). The treatment of the subject to this point has demonstrated that certain computer operations must be repeated frequently. For this reason the computer programs have been designed from the standpoint of optimal economic operation and the flowcharts (R. H. Hanson, unpublished paper, 1968) reflect a corresponding organization of the computations.

### 7.4.7.2 Adjustment

As was stated above, the spatial triangulation of the station coordinates can now proceed in accordance with the law of central perspective. The mathematical model on which the adjustment is based is given with (7.85) and (7.86), which, with the present nomenclature and in accordance with (7.148) and (7.149), are

$$F = \frac{c[(z_{s_1} - z_1)r_{11} + (z_{s_2} - z_2)r_{12} + (z_{s_3} - z_3)r_{13}]}{(z_{s_1} - z_1)r_{31} + (z_{s_2} - z_2)r_{32} + (z_{s_3} - z_3)r_{33}} - l_{\bar{x}} = 0 \tag{7.280} \ddagger$$

$$G = \frac{c[(z_{s_1} - z_1)r_{21} + (z_{s_2} - z_2)r_{22} + (z_{s_3} - z_3)r_{23}]}{(z_{s_1} - z_1)r_{31} + (z_{s_2} - z_2)r_{32} + (z_{s_3} - z_3)r_{33}} - l_{\bar{y}} = 0 \tag{7.281} \ddagger$$

The  $z_{s_{1,2,3}}$  denotes the coordinates of a satellite position and the  $z_{1,2,3}$  station coordinates. In case the exterior elements of orientation ( $\alpha_{\omega\kappa}$ ) † are referred to the  $z'$  system, the station coordinates are designated as  $z'$  without making any other changes in the algorithm.

With the nomenclature of table 7.6, the observation equations corresponding to expressions (7.280) and (7.281) are, according to (7.151) and (7.152) given in following inset.  $F^\circ$  and  $G^\circ$  are computed with approximations for the station coordinates  $z_{1,2,3}$  and for the satellite position coordinates  $z_{s_{1,2,3}}$  (cf. eq. 7.257). The definition of the coefficients in (7.282), (7.283) is given in (7.153) to (7.155). All pairs of coordinates  $l_{\bar{x}}, l_{\bar{y}}$  computed for a given photogram are correlated, since all directions to the satellite depend on the orientation matrix derived from the single camera solution. Furthermore, for a passive satellite all the coordinate pairs  $l_{\bar{x}}, l_{\bar{y}}$  of fictitious satellite images are correlated, since they are derived from the smoothing polynomials that are based on an adjustment involving all coordinate measurements of the original satellite images.

According to (7.277),  $(s_{i,j})^2$  is the covariance matrix associated with the  $n$  sets of  $l_{\bar{x}}, l_{\bar{y}}$  derived from the photogram taken at station  $i$  observing the event  $j$ . The corresponding weight matrix is, from (7.196),

$$P_{l_{i,j}} = m_0^2 [(s_{i,j})^2]^{-1} \tag{7.284}$$

If we now set up observation equations (7.282) and (7.283) for all the directions in-

$$\underbrace{\begin{bmatrix} \Delta z_{s_1} & \Delta z_{s_2} & \Delta z_{s_3} \\ -D_x & -E_x & -F_x \\ -D_y & -E_y & -F_y \end{bmatrix}}_{B_{z_s}} + \underbrace{\begin{bmatrix} \Delta z_1 & \Delta z_2 & \Delta z_3 \\ +D_x & +E_x & +F_x \\ +D_y & +E_y & +F_y \end{bmatrix}}_{B_z} - \underbrace{\begin{bmatrix} v_x & v_y \\ 1 & 0 \\ 0 & 1 \end{bmatrix}}_{A_i} + \underbrace{\begin{bmatrix} F^\circ \\ G^\circ \end{bmatrix}}_{-l} = \begin{bmatrix} 0 \\ 0 \end{bmatrix} \tag{7.282}$$

$$\tag{7.283}$$

troduced into the satellite triangulation net, i.e., for all the coordinate pairs  $l_x, l_y$  derived from measurements of the photograms, taking into account all existing correlations as expressed in the  $P_i$  matrices, we could form directly the corresponding system of normal equations. The unknowns of such a system would be the coordinates of the observing stations as well as of the orbital points. To make the solution economically more feasible, the corrections to coordinates of the orbital points are eliminated in the formulation of the normal equations, thus producing a final system of normal equations that contains only corrections to the camera station coordinates. The procedure, which is analogous to the elimination of relative pass points in numerical aerial photo triangulation, requires a formulation of partial systems of normal equations in the following manner.

As was stated above, the  $n$  pairs of coordinates  $l_x, l_y$  for a particular photogram are correlated by way of the associated  $P_i$  matrix. With (7.282), (7.283) the  $2n$  observation equations pertaining to station  $i$  and event  $j$  are formed. The normal equations system is then formed, which is, with appropriate use of the designations introduced in (7.282), (7.283),

$$\begin{matrix} \Delta z_{s_{j,1,2,3,\dots,n}} & \Delta z_i \\ \left[ \begin{array}{c|c} \underline{B}_{z_{s_j}}^* & \underline{P}_{l_{i,j}} & \underline{B}_{z_{s_j}}^* & \underline{B}_{z_{s_j}}^* & \underline{P}_{l_{i,j}} & \underline{B}_{z_i} \\ \hline \underline{B}_{z_i}^* & \underline{P}_{l_{i,j}} & \underline{B}_{z_{s_j}} & \underline{B}_{z_i} & \underline{P}_{l_{i,j}} & \underline{B}_{z_i} \end{array} \right] & = & \left[ \begin{array}{c} \underline{B}_{z_{s_j}}^* & \underline{P}_{l_{i,j}} & \underline{B}_{z_{s_j}}^* & \underline{B}_{z_{s_j}}^* & \underline{P}_{l_{i,j}} & \underline{B}_{z_i} \\ \hline \underline{B}_{z_i}^* & \underline{P}_{l_{i,j}} & \underline{B}_{z_{s_j}} & \underline{B}_{z_i} & \underline{P}_{l_{i,j}} & \underline{B}_{z_i} \end{array} \right] \end{matrix} \quad (7.285)$$

where

$$\Delta z_{1,2,3,\dots,n} = \begin{bmatrix} \Delta z_{s_1} \\ \Delta z_{s_2} \\ \cdot \\ \cdot \\ \Delta z_{s_n} \end{bmatrix} \quad (7.286)$$

Each of the partial vectors  $\Delta z_{s_{1,2,\dots,n}}$  is the vector of corrections for a specific satellite position;  $\Delta z_i$  is the correction vector for the coordinates of observation station  $i$ . The system of normal equations shown schemat-

ically in (7.285) must be set up as a unit for all the fictitious points computed for the photogram in question, since the associated  $P_{i,j}$  of dimension  $2n \times 2n$  is an indivisible unit. If a specific satellite event  $j$  has been observed from  $m$  stations, the partial systems (7.285) are set up individually for each of the  $m$  photograms and combined into the normal equations partial system representing the event  $j$  as shown on page 592 in the schematic arrangement in the inset.

With evident simplification, (7.287) can also be written in the form

$$\begin{bmatrix} \underline{A} & \underline{C} \\ \underline{C}^* & \underline{B} \end{bmatrix} \begin{bmatrix} \Delta z_{s_{j,1,2,\dots,n}} \\ \Delta z_{i,1,2,\dots,n} \end{bmatrix} = \begin{bmatrix} \Delta l_{s_j} \\ \Delta l_{z_{i,1,2,\dots,n}} \end{bmatrix} \quad (7.288)$$

Now the correction vector  $\Delta z_{s_{j,1,2,\dots,n}}$  for the satellite positions is eliminated, and a partial system of normal equations is left for corrections to coordinates of the stations that observed the satellite event  $j$ . This system is

$$(\underline{B} - \underline{C}^* \underline{A}^{-1} \underline{C}) \Delta z_{i,1,2,\dots,m} = (\Delta l_{z_{i,1,2,\dots,m}} - \underline{C}^* \underline{A}^{-1} \Delta l_{s_j}) \quad (7.289)$$

or simply

$$\underline{N}_{z_{i,1,2,\dots,m}} \Delta z_{i,1,2,\dots,m} = \underline{l}_{z_{i,1,2,\dots,m}} \quad (7.290)$$

When the partial systems (7.290) have been formed for all events, the final, complete system of normal equations for the corrections to coordinates of all stations involved in the satellite triangulation is formed by adding the individual systems (7.290) according to the station index. The resulting system is

$$\underline{N}_z \Delta z = \underline{l}_z \quad (7.291)$$

In the present form,  $\underline{N}_z$  of (7.291) is singular and not invertible, since no origin of coordinates or a scale has as yet been introduced (cf. sec. 7.4.2). To satisfy the first requirement, the introduction of an origin or the equivalent, at least three possibilities worthy of consideration present themselves.

$$\begin{array}{c}
 \Delta \mathbf{z}_{s_j, 1, 2, 3, \dots, m} \\
 \left[ \begin{array}{c|c|c|c|c}
 \sum_{i=1}^m (\underline{B}_{z_s}^* \underline{P}_{l_{i,j}} \underline{B}_{z_s})_i & \Delta \mathbf{z}_{i=1} & \Delta \mathbf{z}_{i=2} & \dots & \Delta \mathbf{z}_{i=m} \\
 \hline
 (\underline{B}_{z_t}^* \underline{P}_{l_{i,j}} \underline{B}_{z_s}^*)_{i=1} & (\underline{B}_{z_s}^* \underline{P}_{l_{i,j}} \underline{B}_{z_i})_{i=1} & (\underline{B}_{z_s}^* \underline{P}_{l_{i,j}} \underline{B}_{z_i})_{i=2} & \dots & (\underline{B}_{z_s}^* \underline{P}_{l_{i,j}} \underline{B}_{z_i})_{i=m} \\
 \hline
 (\underline{B}_{z_t}^* \underline{P}_{l_{i,j}} \underline{B}_{z_s})_{i=2} & \underline{0} & (\underline{B}_{z_t}^* \underline{P}_{l_{i,j}} \underline{B}_{z_i})_{i=2} & \underline{0} & \underline{0} \\
 \hline
 \vdots & \underline{0} & \underline{0} & \dots & \underline{0} \\
 \hline
 (\underline{B}_{z_t}^* \underline{P}_{l_{i,j}} \underline{B}_{z_s})_{i=m} & \underline{0} & \underline{0} & \underline{0} & (\underline{B}_{z_t}^* \underline{P}_{l_{i,j}} \underline{B}_{z_i})_{i=m}
 \end{array} \right] \\
 \\
 = \left[ \begin{array}{c}
 \sum_{i=1}^m (\underline{B}_{z_s}^* \underline{P}_{l_{i,j}} \underline{l}_{i,j})_i \\
 \hline
 (\underline{B}_{z_t}^* \underline{P}_{l_{i,j}} \underline{l}_{i,j})_{i=1} \\
 \hline
 (\underline{B}_{z_t}^* \underline{P}_{l_{i,j}} \underline{l}_{i,j})_{i=2} \\
 \hline
 \vdots \\
 \hline
 (\underline{B}_{z_t}^* \underline{P}_{l_{i,j}} \underline{l}_{i,j})_{i=m}
 \end{array} \right] \tag{7.287}
 \end{array}$$

The simplest is to assume that one of the stations of the net is given with its initial coordinates  $\mathbf{z}^\circ_{(1,2,3)_i}$  free of error. This assumption imposes on the system (7.291) the condition that the corresponding  $\Delta \mathbf{z}_i$  vector be a zero vector in the solution of the system. This is accomplished by assigning the approximation coordinates an infinite weight; i.e., the quantity  $10^n$  is introduced as weight in the relevant diagonal terms of (7.291),  $n$  being as large as the capacity of the computer allows. This step causes the  $\Delta \mathbf{z}_i$  vector to vanish for all practical purposes, since the corresponding entries in the  $\underline{N}^{-1}$  matrix will be multiplied by  $10^{-n}$ .

A second possibility exists, especially in connection with triangulation of a continental satellite net in which the observation stations are part of an established geodetic reference system. For such a case, weight matrices (7.279) and, after appropriate transformation, corresponding  $\underline{P}_z$  or  $\underline{P}_{z'}$  matrices (7.128) are available as input data. It is then necessary only to add these weight

matrices to the system (7.291) where called for.

A third possibility, which is especially attractive for error studies, is to introduce as origin of coordinates the centroid of all adjusted coordinates. This means adding to the system the supplementary condition

$$\Sigma (\mathbf{z}^\circ + \Delta \mathbf{z}) = \Sigma \mathbf{z} = 0 \tag{7.292}$$

This will result, although with modifications depending on the shape of the net, in a symmetrical distribution of mean errors for the net.

In order not to endanger the accuracy of the  $\underline{N}_z$  matrix inversion, it has been found advisable in practice to combine these various possibilities. Initially, one of the stations is held fixed at the origin. After the  $\underline{N}_z$  matrix inversion, the coordinate system is translated. The three condition equations (7.292) are replaced by the condition valid for each station

$$\hat{z}_i = z_i - \frac{\sum_{i=1}^s z_i}{s} \quad (7.293)$$

where  $s$  is the number of stations involved in the triangulation. The matrix of weight coefficients for the  $z$  values are obtained, since in this case  $\underline{F}^* = \underline{F}$  from

$$\hat{N}^{-1} = \underline{F} \underline{N}_z^{-1} \underline{F} \quad (7.294)$$

where the  $\underline{F}_z$  matrix is obtained as a symmetric quadratic matrix by differentiating the right side of (7.293). The coefficients of  $\underline{F}$  are  $(s-1)/s$  along the diagonal and  $-1/s$  in the spaces where the correlation between the individual components of the station coordinates should appear. A sequence of operations utilizing the symmetry of the  $\underline{F}$  matrix is described in detail in R. H. Hanson (unpublished paper, 1968).

The introduction of scale into the triangulation by means of measured distances between two or more stations of the net is of prime importance in satellite triangulation. Such distances can be derived, for example, from long-line traverses measured with, for instance, a geodimeter (cf. Meade, 1968; Wolf, 1967). If the two stations are designated  $i$  and  $j$  and the distance between them  $d$ , then obviously

$$d_{ij} = [(z_{i_1} - z_{j_1})^2 + (z_{i_2} - z_{j_2})^2 + (z_{i_3} - z_{j_3})^2]^{1/2} \quad (7.295)$$

the weight of the distance  $d_{ij}$  being expressed as

$$P_{d_{ij}} = \frac{m_0^2}{m_{d_{ij}}} \quad (7.296)$$

where  $m_{d_{ij}}$  is the mean error of the distance  $d_{ij}$  in meters. With the designation

$$\mathbf{f}^* d_{ij} = \frac{\partial d_{ij}}{\partial z_{ij}} = \begin{array}{|c|c|c|c|c|c|} \hline \partial z_{i_1} & \partial z_{i_2} & \partial z_{i_3} & \partial z_{j_1} & \partial z_{j_2} & \partial z_{j_3} \\ \hline z_{i_1} - z_{j_1} & z_{i_2} - z_{j_2} & z_{i_3} - z_{j_3} & z_{j_1} - z_{i_1} & z_{j_2} - z_{i_2} & z_{j_3} - z_{i_3} \\ \hline d^\circ & d^\circ & d^\circ & d^\circ & d^\circ & d^\circ \\ \hline \end{array} \quad (7.297)$$

it is merely necessary in the system (7.291) to add, at the locations corresponding to stations  $i$  and  $j$ , including location  $ij$ , on the left side, the appropriate portion of the matrix

$$(\mathbf{f}_d P_d \mathbf{f}_d^*)_{ij} \quad (7.298)$$

and on the right side

$$(\mathbf{f}_d P_d \Delta l_d)_{ij} \quad (7.299)$$

where

$$\Delta l_{d_{ij}} = d_{ij} - d_{ij}^\circ \quad (7.300)$$

and  $d_{ij}^\circ$  is computed with the approximations for  $z_{ij}^\circ$  from (7.295). Any number of scalars can thus be introduced into the adjustment. With the expected development in measuring distances with lasers it should be possible in the future to measure distances between the observing stations and the satellite, which can then be similarly introduced into the system of normal equations (7.288) before the satellite positions are eliminated with (7.289).

After the system (7.291) has been amended with the two steps described above (fixing the origin of coordinates and introducing scale), the vector of coordinate corrections for all the stations in the triangulation can now be computed as

$$\Delta z = \underline{N}_z^{-1} \underline{l}_z \quad (7.301)$$

and the final result of the satellite triangulation is

$$z = z^\circ + \Delta z \quad (7.302)$$

From (7.235), using the  $z$  vector and expressions (7.280), (7.281) we compute corrections  $v_l$ , followed by the determination of corrections for all additionally introduced observations. Thus, for example, for a priori given station coordinates

$$\mathbf{v}_{z_i} = \Delta \mathbf{z}_i \quad (7.303)$$

and for distances used as scale control

$$v_{d_{ji}} = \bar{d}_{ij} - d_{ij} \quad (7.304)$$

in which  $\bar{d}_{ij}$  is computed with the final coordinates of (7.295) and  $d_{ij}$  is the initially given measurement.

With these  $v$ 's and their weights the mean error of unit weight  $s_0$  for the whole triangulation is computed from

$$s_0 = \left[ \frac{(\mathbf{v}_1^* P_1 \mathbf{v}_1) + (\mathbf{v}_z^* P_z \mathbf{v}_z) + (\Sigma P_d v_d v_d)}{B + Z + D - S} \right]^{1/2} \quad (7.305)$$

where  $B$  is the number of observations,  $Z$  is the number of station coordinates, given a priori with their weights,  $D$  is the number of distances, given with their weights, and  $S$  is the number of all coordinates, station locations as well as satellite points.

If in the course of the observations, stations must be moved a relatively small distance, e.g., for meteorological or logistic reasons, such dual stations must be coupled. Corresponding conditions are introduced and their number is added in the denominator of (7.305), just as all extraneous metric conditions must be appropriately taken into account. With the covariance matrix (7.195), corresponding to the system of inverted normal equations, and the  $s_0$  of (7.305) the mean error of the individual  $z_{1,2,3}$  is obtained with the square roots of the diagonal terms of this covariance matrix and, with (7.198) to (7.200), the semiaxes of the error ellipsoid and their direction cosines.

This actually completes the result of the satellite triangulation, at least from the standpoint of photogrammetry. Further processing of the results reverts to a strictly geodetic point of view, such as the conversion of the computed  $z$  values into an ellipsoidal system, which can be accomplished with (7.114) to (7.119).

If the approximations  $\phi^\circ, \lambda^\circ, h^\circ$  were given coordinates, a correction vector could be computed with (7.126) as

$$\mathbf{v}_\phi = T_\phi^{-1} \mathbf{v}_z \quad (7.306)$$

and the corresponding station covariance in analogy with (7.128)

$$\mathbf{s}_\phi^2 = s_0^2 [T_\phi^{-1} Q_z (T_\phi^{-1})^*] = \begin{bmatrix} s_\phi^2 & s_{\phi,\lambda} & s_{\phi,h} \\ s_{\phi,\lambda} & s_\lambda^2 & s_{\lambda,h} \\ s_{\phi,h} & s_{\lambda,h} & s_h^2 \end{bmatrix} \quad (7.307)$$

in which  $Q_z$  is the appropriate  $3 \times 3$  matrix from  $N^{-1}$ . In principle, we can say that the measures of accuracy for all quantities derived from the  $z$  values are to be computed as mean errors of functions of the adjusted  $z$ 's in conformance with (7.241). In R. H. Hanson (unpublished paper, 1968) the structure of a computing program for spatial triangulation is described and the necessary flowcharts shown, and all supplementary computations and statistical controls that are needed for check and that are of significance to the computations in an extended triangulation program are explained.

## 7.4.8 Theoretical Considerations of Error

### 7.4.8.1 Error Budget of Geometric Satellite Triangulation

As is shown in section 7.1 and at the beginning of this section, the principle of the method of geometric satellite triangulation is based on combining a large number of individual directions to satellites in a three-dimensional triangulation. The satellite directions needed at the stations to be triangulated are obtained by interpolating the individual images of the chopped satellite trail into the framework of the star background present on the photograms.

Directions to the star images are first computed, basically as functions of the observing datum, the time of observation (UT1), and the instantaneous-pole coordinates. These directions are referred either to the astronomical right ascension-declination system for a specific epoch ( $x$  system) or, after appropriate rotation, to an Earth-fixed three-dimensional reference coordinate system ( $y$

or  $z$  system) in which the observation station locations are to be triangulated (see sec. 7.4.6.2).

The satellite images are recorded in an arbitrary time sequence that is, however, common for all stations observing an event. The satellite images are then interpolated into the directions to the stars, i.e., into the background of stars, and thus fixed in the same reference system to which the star images have been reduced. The three-dimensional position of the observing stations is found by assigning to them a location such that the satellite directions emanating from the various stations lead to the determination of the three-dimensional geometry of all observed satellite transits.

It is not necessary, aside from the practical requirements of the field observer, to know in advance the orbit of the satellite. The points of the orbit serve merely as elevated triangulation targets, and only the condition for intersection of corresponding rays is needed to fix the positions of the observation sites (cf. sec. 7.4.2). As a consequent requirement, such rays must satisfy the "geometric condition of simultaneity" explained in section 7.4.4. This condition is automatically met, for example, if the satellite trail is fixed by the recording of a sequence of flashes emitted by the satellite.

Since to date in practice not a sufficient number of such flashes can be generated to reduce the influence of scintillation adequately (cf. sec. 7.4.5), we photograph the satellite in the position of its orbit illuminated by the Sun. In this method the trace of the orbit is chopped by means of a rotating disk shutter in the camera (cf. sec. 7.3.2, figs. 7.12 and 7.13) into a series of time-dependent individual images. For physical as well as technical reasons it is, however, impossible to generate satellite images at the several observing stations that satisfy initially the geometric condition of simultaneity. Basically, it therefore becomes necessary to fit the bundle of directions to the satellite for a particular event as closely as possible to the satellite orbit, which is by its nature continuous. Since only a small portion of the orbit

(about 1–2%) is involved, the observed curve may be considered as part of an elliptical orbit, obeying the Keplerian laws of motion, which predicate that the satellite directions are referred to an inertial system as approximated for instance by the right ascension-declination system.

On the other hand, a solution based on satellite directions referred to an Earth-fixed coordinate system requires, because of the Earth's rotation, the assumption of a twisted space curve as a model for the satellite orbit.

In such a procedure, satellite triangulation is basically subject to five sources of error. The first source is the uncertainties associated with the star-catalog data; the second is the accidental errors in time determination for the star and satellite exposures. The third is the accidental errors in coordinate measurement of the star and satellite images; the fourth, the influence of shimmer acting as an accidental error source; and the fifth, the irregular distortion of the photographic emulsion. All these sources must be taken into consideration.

Such a presentation of the error budget assumes first, that the corresponding systematic errors are sufficiently small, and second, that the mathematical model used to reconstruct the photographic process is sufficiently close to reality. Furthermore, the photographed sections of the satellite orbit must be valid in a qualitative sense as a tool for interpolation. All these assumptions must hold within such accuracy limits that the influence of the remaining imperfections on the triangulation computations remains a magnitude smaller than the propagation of the five cited basic error sources.

Obviously, all further secondary corrections, such as pole displacement (see end of sec. 7.4.4), astronomic and parallactic refraction, satellite phase angle, and light travel time (for all these corrections see sec. 7.4.5), correspond to geometric-physical reality with such accuracy that the effect of remaining biases is negligibly small.

The rigorous theoretical treatment of errors of the satellite triangulation method leads, even from this point of view, to a

mutually correlated matrix schematic. The individual plates are essentially uncorrelated with respect to the photogrammetric reduction, so far as processing the measured star and satellite coordinates is concerned. However, for all plates introduced into a satellite triangulation system, only one set of reference stars, limited in number and distribution, is available.

Hence, not only does the same group of stars appear repeatedly on the same plate as a result of star registration before, during, and after the event, but also similar groups are recorded on a number of plates.

In the observations for the world net, stars up to eighth magnitude and with maximum mean position errors of  $0''.4$  were selected from the SAO star catalog. Thus, there were about 20,000 stars at our disposal (sec. 7.4). With an average frequency of about 100 stars per plate and approximately 3000 plates in the world net, this means that each star appears, on the average, on 15 plates. Since, strictly speaking, there can result only one pair of corrections for each observed star in the adjustment, the mathematical reconstructions of all the photogrammetric bundles and their orientations are correlated to such a degree that they really should be adjusted as a unit, even if, for lack of knowledge of existing correlations, one accepts for the star coordinates independent weight matrices.

In the spatial triangulation of the observing stations the satellite directions are now combined to reconstruct the geometry of the recorded satellite orbit curve. The intersection condition for the rays applied in the process—either direct or indirect by way of fitting to a spatial model of the orbit—contains additional orientation information, similar to the relative orientation in the classical photogrammetric restitution process. But, since all photogrammetric bundle parameters that determine directions to the satellite and their orientation quantities are correlated, there results a correlation between all recorded satellite events; i.e., the determination of observing station positions should, together with the determination of

all observed satellite orbital curves, be obtained from one common adjustment with the use of the covariance matrix involving all reconstructed photogrammetric bundles and their orientations.

Processing the approximately 3000 plates available in the world net requires the computation of nearly 60 000 interpolation parameters. For the approximately 1400 recorded events, more than 8000 orbital parameters would have to be determined. A simultaneous adjustment of such a large number of correlated unknowns is at present, even with the largest available computer, neither economically feasible nor, because of the required computational accuracy, capable of realization.

One has, therefore, to make concessions. From the error theoretical point of view probably the most serious compromise is the necessity of separately determining the photogrammetric interpolation parameters for each plate, since these parameters determine absolute directions to the interpolated satellite images and are therefore of decisive significance in fixing the spatial positions of the observation stations. In conformance with the weights given with the star data there is obtained in this procedure in each bundle reconstruction adjustment, independent of the number of images of the particular star, a pair of corrections for the star coordinates. On completion of all the bundle reconstructions under consideration there will therefore be for each star as many corrections available as the number of times such a star was recorded on the various plates. On the basis of the observation data in the world net, this averages out to 15 times. Arguing from the concept that every adjustment represents in principle a weighted arithmetic mean, the possibility presents itself of computing for each star a unique set of corrections in the form of the arithmetic mean of the individual pairs. Care need be taken only to ensure, by use of appropriate weights, that the mean error of unit weight after adjustment is the same for all the bundle reconstructions. One could then add this average of the corrections to the

original star data and repeat the bundle reconstruction computations. With an appropriate choice of weights for these corrected star data, these values could then be held correspondingly fixed in the repeated bundle reconstruction.

The justification for such an expensive iteration depends on how close the averaged star-coordinate corrections come to the solution from a rigorous adjustment. The significance of such a solution hinges, therefore, on the extent to which these "improved star coordinates" represent in their totality a reference system which is superior to the star catalog originally available. In the processing of the world net the improved star coordinates for the 20 000 stars being used were computed so that these amended right ascensions and declinations could be presented to the astronomers for critical evaluation. Repetition of the computations for bundle reconstructions was for financial reasons, not contemplated.

As was mentioned earlier, the accidental errors of time designations for the star and satellite recordings must be taken into consideration. In the adjustment for the single camera this is taken care of automatically by carrying corrections to the right ascensions. These corrections being geometrically equivalent to UT1, it is necessary only to compute weights for the introduced right ascension values, taking into account the uncertainties in time associated with the recorded instants of observation. For the instrumentation used in the world net, this accidental timing error amounts to less than a millisecond so far as the registration of the shutter action is concerned. Since the available UT1 is in itself scarcely better than  $\pm 2$  msec (which acts as a system error in the orientation for the individual plate), the assumption of a  $\pm 3$ -msec overall uncertainty in the determination of time for the star exposures seems reasonable. The inaccuracy of a direction corresponding to this time uncertainty is  $\pm 0''.045$ , a magnitude considerably less than the photogrammetric measuring accuracy with the BC-4 system and the 450-mm lens, and hence negligible.

A similar conclusion can be drawn about the influence of random errors of the synchronization procedure on the satellite images. By means of periodic control of timing (sec. 7.2.1), the instants of observation at the various stations are fixed relative to each other within at least  $\pm 100$   $\mu$ sec. The most critical situation would arise for the ECHO satellite, with a speed of 8 km/sec and a minimum distance of 1000 km, for which 100  $\mu$ sec corresponds to a change in direction of  $\pm 0''.16$ . With the PAGEOS satellite used in the world net, because of its greater distance and consequent slower speed, a timing error of  $\pm 100$   $\mu$ sec results in a maximal direction uncertainty of only  $\pm 0''.04$ . Although this error is negligible, a calculation employed in the adjustment discussed later (a calculation designed primarily to eliminate shimmer by polynomial curve fitting) serves to adjust as well any existing random timing errors in the synchronization.

Existing correlations between the separately reconstructed bundles of directions to stars are, as detailed above, neglected. Thus, for each single-camera computation, individual parameters are determined for the interpolation model, including, of course, the covariance matrix associated with these parameters, which is of basic significance for further evaluations.

In the step of the adjustment which now follows, the locations of the observing stations are computed. Their position in space is fixed by the condition that the bundles of directions to the satellite issuing from these stations must lead to the geometry of all satellite orbital curves that have been recorded. Since each bundle of directions is obtained basically by the interpolation of the corresponding satellite images into the relevant interpolation model and since these models are now no longer correlated, it follows that the individual satellite orbit determinations are also uncorrelated. This results in an essential simplification of the data processing, since the orbit determinations can be processed sequentially and care need be taken only that their cumulative effect bears on the station determination.

The condition of intersection on which, as was mentioned previously, the determination of the geometry of the observed satellite orbits was based, either directly or indirectly by way of a fit to a spatial orbital model, basically contains additional information for determining the parameters of the relevant interpolation models. It follows that not only the coordinates of the stations and the parameters specifying the geometry of the satellite orbit, but also all parameters of all interpolation models involved together with their individual variance-covariance matrices referred to above, must appear as unknowns in the adjustment.

The resulting system of normal equations is  $Bv = \Delta$  with a range in weights  $P$  from zero to infinity. If the vector of corrections to the measured satellite image coordinates is designated by  $v_i$ , the correction vector for the previously computed bundle interpolation parameters  $\bar{O}$  by  $v_o$ , the correction vector for the approximated satellite orbital positions by  $v_{x_s}$ , and finally the correction vector for the approximated station coordinates by  $v_x$ , the corresponding system of normal equations can be written as indicated in figure 7.37. The  $\bar{X}$  are supplementary conditions that may exist between the stations to be triangulated, such as, for example, measured distances for scale determination.

Figure 7.38 shows the system of normal equations after these functional relations have been introduced. The corresponding set of correlates is designated by  $K$ . The system reduced to satellite orbit and station coordinates is given in the lower part of figure 7.38.

Because the image coordinates can be expressed as functions of the interpolation

<table border="1" style="border-collapse: collapse; text-align: center;"> <tr><td style="padding: 2px;"><math>P</math></td><td></td><td></td><td></td><td style="padding: 2px;"><math>I</math></td></tr> <tr><td></td><td style="padding: 2px;"><math>O</math></td><td></td><td></td><td style="padding: 2px;"><math>B_o'</math></td></tr> <tr><td></td><td></td><td style="padding: 2px;"><math>O</math></td><td></td><td style="padding: 2px;"><math>B_{x_s}'</math></td></tr> <tr><td></td><td></td><td></td><td style="padding: 2px;"><math>O</math></td><td style="padding: 2px;"><math>B_x'</math></td></tr> <tr><td style="padding: 2px;"><math>I</math></td><td style="padding: 2px;"><math>B_o</math></td><td style="padding: 2px;"><math>B_{x_s}</math></td><td style="padding: 2px;"><math>B_x</math></td><td></td></tr> </table>	$P$				$I$		$O$			$B_o'$			$O$		$B_{x_s}'$				$O$	$B_x'$	$I$	$B_o$	$B_{x_s}$	$B_x$		=	<table border="1" style="border-collapse: collapse; text-align: center;"> <tr><td style="padding: 2px;"><math>O</math></td></tr> <tr><td style="padding: 2px;"><math>O</math></td></tr> <tr><td style="padding: 2px;"><math>O</math></td></tr> <tr><td style="padding: 2px;"><math>O</math></td></tr> <tr><td style="padding: 2px;"><math>\Delta_s</math></td></tr> </table>	$O$	$O$	$O$	$O$	$\Delta_s$	}	with	<p style="margin: 0;"><i>Additional Conditions</i></p> <p style="margin: 0;"><math>\bar{O}</math> is the solution vector of Single Camera adjustment</p> <p style="margin: 0;"><math>\bar{X}</math> may be given from independent surveys</p>	}	with	$P_x$
$P$				$I$																																		
	$O$			$B_o'$																																		
		$O$		$B_{x_s}'$																																		
			$O$	$B_x'$																																		
$I$	$B_o$	$B_{x_s}$	$B_x$																																			
$O$																																						
$O$																																						
$O$																																						
$O$																																						
$\Delta_s$																																						

FIGURE 7.37.—Basic normal equation system for  $Bv = \Delta, P = 0 \rightarrow \infty$ .

Introducing  $\Delta_o = \bar{O} - O'$  and  $\Delta_x = \bar{X} - X'$

<table border="1" style="border-collapse: collapse; text-align: center;"> <tr><td style="padding: 2px;"><math>P</math></td><td></td><td></td><td></td><td style="padding: 2px;"><math>I</math></td><td></td><td></td><td></td><td></td><td></td><td></td></tr> <tr><td></td><td style="padding: 2px;"><math>O</math></td><td></td><td></td><td style="padding: 2px;"><math>B_o'</math></td><td style="padding: 2px;"><math>I</math></td><td></td><td></td><td></td><td></td><td></td></tr> <tr><td></td><td></td><td style="padding: 2px;"><math>O</math></td><td></td><td style="padding: 2px;"><math>B_{x_s}'</math></td><td></td><td></td><td></td><td></td><td></td><td></td></tr> <tr><td></td><td></td><td></td><td style="padding: 2px;"><math>O</math></td><td style="padding: 2px;"><math>B_x'</math></td><td></td><td style="padding: 2px;"><math>I</math></td><td></td><td></td><td></td><td></td></tr> <tr><td style="padding: 2px;"><math>I</math></td><td style="padding: 2px;"><math>B_o</math></td><td style="padding: 2px;"><math>B_{x_s}</math></td><td style="padding: 2px;"><math>B_x</math></td><td style="padding: 2px;"><math>O</math></td><td></td><td></td><td></td><td></td><td></td><td></td></tr> <tr><td></td><td style="padding: 2px;"><math>I</math></td><td></td><td></td><td></td><td></td><td></td><td style="padding: 2px;"><math>\sigma_s</math></td><td></td><td></td><td></td></tr> <tr><td></td><td></td><td></td><td></td><td></td><td></td><td></td><td style="padding: 2px;"><math>I</math></td><td></td><td></td><td style="padding: 2px;"><math>\sigma_x</math></td></tr> </table>	$P$				$I$								$O$			$B_o'$	$I$								$O$		$B_{x_s}'$										$O$	$B_x'$		$I$					$I$	$B_o$	$B_{x_s}$	$B_x$	$O$								$I$						$\sigma_s$											$I$			$\sigma_x$	=	<table border="1" style="border-collapse: collapse; text-align: center;"> <tr><td style="padding: 2px;"><math>O</math></td></tr> <tr><td style="padding: 2px;"><math>O</math></td></tr> <tr><td style="padding: 2px;"><math>O</math></td></tr> <tr><td style="padding: 2px;"><math>O</math></td></tr> <tr><td style="padding: 2px;"><math>\Delta_s</math></td></tr> <tr><td style="padding: 2px;"><math>\Delta_x</math></td></tr> <tr><td style="padding: 2px;"><math>\Delta_x</math></td></tr> </table>	$O$	$O$	$O$	$O$	$\Delta_s$	$\Delta_x$	$\Delta_x$	}	with	<p style="margin: 0;"><math>\sigma_o = P_o'</math></p> <p style="margin: 0;"><math>\sigma_x = P_x'</math></p>
$P$				$I$																																																																																					
	$O$			$B_o'$	$I$																																																																																				
		$O$		$B_{x_s}'$																																																																																					
			$O$	$B_x'$		$I$																																																																																			
$I$	$B_o$	$B_{x_s}$	$B_x$	$O$																																																																																					
	$I$						$\sigma_s$																																																																																		
							$I$			$\sigma_x$																																																																															
$O$																																																																																									
$O$																																																																																									
$O$																																																																																									
$O$																																																																																									
$\Delta_s$																																																																																									
$\Delta_x$																																																																																									
$\Delta_x$																																																																																									

After elimination of  $v_i, v_o, k_s, k_o$  and  $k_x$

<table border="1" style="border-collapse: collapse; text-align: center;"> <tr><td style="padding: 2px;"><math>B_o'(\sigma_s \cdot B_o \sigma_s B_o')</math></td><td style="padding: 2px;"><math>B_{x_s}'(\sigma_s \cdot B_{x_s} \sigma_s B_{x_s}')</math></td></tr> <tr><td style="padding: 2px;"><math>B_x'(\sigma_s \cdot B_x \sigma_s B_x')</math></td><td style="padding: 2px;"><math>B_x'(\sigma_x \cdot B_x \sigma_x B_x')</math></td></tr> </table>	$B_o'(\sigma_s \cdot B_o \sigma_s B_o')$	$B_{x_s}'(\sigma_s \cdot B_{x_s} \sigma_s B_{x_s}')$	$B_x'(\sigma_s \cdot B_x \sigma_s B_x')$	$B_x'(\sigma_x \cdot B_x \sigma_x B_x')$	=	<table border="1" style="border-collapse: collapse; text-align: center;"> <tr><td style="padding: 2px;"><math>B_o'(\sigma_s \cdot B_o \sigma_s B_o')</math></td><td style="padding: 2px;"><math>(\Delta_s - B_o \Delta_s)</math></td></tr> <tr><td style="padding: 2px;"><math>P_x \Delta_x \cdot B_x'(\sigma_x \cdot B_x \sigma_x B_x')</math></td><td style="padding: 2px;"><math>(\Delta_x - B_x \Delta_x)</math></td></tr> </table>	$B_o'(\sigma_s \cdot B_o \sigma_s B_o')$	$(\Delta_s - B_o \Delta_s)$	$P_x \Delta_x \cdot B_x'(\sigma_x \cdot B_x \sigma_x B_x')$	$(\Delta_x - B_x \Delta_x)$
$B_o'(\sigma_s \cdot B_o \sigma_s B_o')$	$B_{x_s}'(\sigma_s \cdot B_{x_s} \sigma_s B_{x_s}')$									
$B_x'(\sigma_s \cdot B_x \sigma_s B_x')$	$B_x'(\sigma_x \cdot B_x \sigma_x B_x')$									
$B_o'(\sigma_s \cdot B_o \sigma_s B_o')$	$(\Delta_s - B_o \Delta_s)$									
$P_x \Delta_x \cdot B_x'(\sigma_x \cdot B_x \sigma_x B_x')$	$(\Delta_x - B_x \Delta_x)$									

FIGURE 7.38.—System of normal equations after introduction of functional relations. (Below) System reduced to satellite orbit and station coordinates.

parameters describing the photogrammetric bundle, of the coordinates of the satellite position, and of the relevant coordinates of the observing station, it is possible, since the individual bundle reconstructions are uncorrelated, to replace the correction vector to the interpolation parameters by a corresponding correction vector to the image coordinates, thus reducing decisively the number of unknowns to be carried.

As is apparent from the lower part of figure 7.38, this computational procedure is completely rigorous only when the expression  $\Delta_o$  is carried along on the right-hand side of the system of reduced normal equations, i.e., with the vector of absolute terms; hence a rigorous elimination of the  $O$  parameters is not possible. However, since in the first iteration loop the  $O$  values as obtained from the single camera adjustment are introduced into the triangulation adjustment as approximation values,  $\Delta_o$  is initially a zero vector. This means that the elimination of the  $O$  parameters is valid to within the first order of the  $\Delta_o$  terms. Moreover, because of the large number of absolute control points (in our case about 100 stars per plate), the influence of the orientation contribution resulting from the intersection condition is quite small, so that the considerable gain in simplicity derived from the elimination of these parameters in the triangulation adjustment justifies the procedure.

This leaves the unknowns that are to be determined by means of the condition of intersection of the rays: the coordinates of the observing station and the parameters describing the geometry of the satellite orbital curves. From a conceptual point of view, this means that the bundles of directions to a satellite assigned to a particular satellite pass must fit themselves as closely as possible in the sense of an adjustment to the orbital curve, which is subject first of all to the geometric consequences of Kepler's first law, according to which the orbit can be expressed, in an inertial system, by the equation of an ellipse.

Furthermore, the fitting process must do justice to the dynamic content of Kepler's second law, according to which the true anomaly is a function of time. It seems convenient in the application to develop the true anomaly as a series in the eccentricity and the mean anomaly. Basically speaking, one can say that Kepler's first law accomplishes the fit of the bundle perpendicular to the direction of the orbital curve, and the second law accomplishes the fit along the orbit curve. Kepler's third law cannot be used, because, in the first place, the orbital period of the observed satellite is not known. Moreover, the balloon satellite with its typically unfavorable mass-ratio is exposed to disturbing influences such as residual atmospheric pressure and the Sun's radiation pressure, so that the orbital period could yield only limited information in a geometrical sense. All computational schemes must, furthermore, take into account the fact that the recorded times for satellite imagery refer to the instants of exposure, and these data must therefore be corrected for light travel time and geometrically for Earth rotation during the light travel time before they can be further processed with the application of the principles of celestial mechanics.

The practical application of orbital determination by means of bundle fitting is faced with two further obstacles. As was stated at the end of section 7.4.5, a relatively large number of satellite images is needed in the adjustment to sufficiently reduce the shim-

mer effect. In the world net, the number of images averages 300 per plate. Since the corresponding 300 directions are derived from one and the same group of interpolation parameters, they are correlated, which means that for each of the satellite direction bundles to be introduced into the fit a  $600 \times 600$ , completely filled covariance-matrix must be taken into consideration. If the event has been observed by more than two stations, undesirably large demands are very soon made on the memory capacity of the computer. Even more decisive is the fact that the shimmer effect depends on the meteorological conditions during the event, which can be quite different at the contributing stations. To prevent this "noise" from being averaged between the contributing stations to an event in the triangulation adjustment, the appropriate weight matrices for the individual direction bundles must be computed by using the mean shimmer characteristic for each station. This quantity is, however, in the evaluation method under discussion and is not as yet available.

As an alternative to the bundle-fitting concept, one could also fix the satellite orbital curve by smoothing the spatial coordinates of the triangulated satellite points with polynomials as functions of time (Wolf, 1967). Such a solution assumes that the orbital curve is designated by a series of short-duration flashes emitted from the satellite, the time sequence of the flashes being sufficiently well known. Only then will images be recorded on the individual plates, which lead to the triangulation of the corresponding orbital points. On the other hand, if, as is necessary for practical reasons at this time, the satellite images are produced on the various plates by chopping the trail of the continuously illuminated satellite with a rotating disk shutter into separate points, then one would first have to compute the necessary light travel times iteratively with approximated satellite positions. In principle, this computation would give sufficient information to interpolate on each photograph for the event image points that satisfy the geometric condition of simultaneity.

From an error-theoretical standpoint, however, such interpolation is open to question, because the position of the individual images is influenced to a different and unknown extent by shimmer. From the computational standpoints, still another disadvantage accrues to this solution, in that all the satellite directions on the selected plates are correlated, leading to variance-covariance matrices whose consideration would require an intolerable amount of computer memory space.

The theoretical and practical difficulties of the above method of solution are circumvented by modifying the approach and evaluating each plate independently to the greatest extent possible.

This concept is also valid from the standpoint of error theory and is based on the fact that the measurements at a given observing station, i.e., the photogrammetric registration of the star images and satellite orbit, together with the relevant recordings of time, are self-sufficient in the sense that the information so obtained is completely independent of and not influenced by the fact that similar operations have been carried out at other stations. Transforming these measuring data into time-correlated satellite directions requires only the additional assumption that the satellite orbital curve is by nature continuous.

If the geometric-dynamic properties of the photographed portion of the satellite orbit as described above are known, it should be possible to postulate the form of this trail on the photogram, in the direction of the trail and at right angles to it, in terms of the central perspective laws, light propagation time, and the aberration due to the Earth's rotation. The formalization would lead to an infinite-series expansion in which higher-order terms could be neglected. The orbital projection could then be adjusted to this theoretical model by fitting the satellite images to it. Another possibility, the one adopted here, is to smooth the satellite images with polynomials. Just as the triangulated spatial coordinates of discrete orbital points can be fitted to polynomial functions

of time, the recorded sequence of time-related satellite images can be similarly smoothed, resulting in positions of the satellite on the photogram as a function of time. A polynomial fit is all the more justifiable from the standpoint of error theory inasmuch as the simplest conceivable projection model exists between the orbit, continuous by nature, and the corresponding satellite image sequence. The measured satellite image coordinates, by means of the bundle reconstruction parameters, as obtained from an adjustment based on reference stars and their images, are therefore first of all reduced to the concept of a rigorous central perspective, i.e., the concept of an ideal photograph. Then one applies the principle of an adjustment to compute best-fitting polynomials. To the extent that the central-perspective nature of the images of the satellite orbital points has been reproduced, this adjustment has the function of neutralizing the random errors of the comparator measurements, random emulsion shrinkage, and shimmer effects. In addition, it yields, in the form of statistical functions, an indication of the accuracy of the smoothing polynomials.

In order to verify the required degree for these polynomials, 380 satellite space coordinates for a simulated PAGEOS orbit at intervals of 0.8 sec were recorded, which corresponds to the average length of the PAGEOS arc observed with the BC-4 camera. The satellite orbit was integrated with a tenth-order Cowell-Störmer process. The Earth's gravitational field was introduced by means of an expansion in spherical functions to the fourth degree and fourth order by using the coefficients of the 1966 Smithsonian Institution Standard Earth (Lundquist and Veis, 1966). The radiation pressure of the Sun and the attraction of the Moon and Sun were also included in the integration computations. The resulting coordinates of satellite positions were then transformed into a geostationary system.

Six fictitious observing stations (fig. 7.39) were distributed relative to the computed orbit to simulate essentially the geometrical distribution of stations in practice. For each

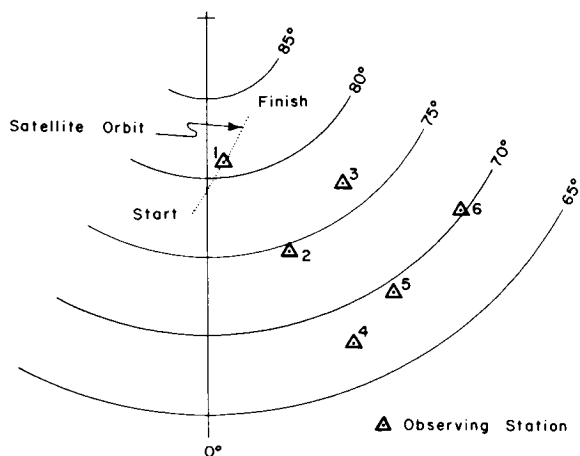


FIGURE 7.39.—Schematic representation of satellite orbit and positions of observing stations.

of the 380 fictitious points of the orbit, by applying the time of light propagation, corresponding plate coordinates were computed at each of the six stations to reproduce an exact, central-perspective mapping of the orbital geometry. These plate coordinates were then subjected to polynomial curve fits from the first to the eleventh degree in sequence. The resulting mean errors of the computed coordinates after adjustment are listed in table 7.7,  $\sigma_x$  referring to the coordinate component in direction of the trail and  $\sigma_y$  at right angles to the trail.

From table 7.7 it is seen that the required accuracy can be obtained with a polynomial of the fifth degree along the trail and of the fourth degree across the trail. At the same time no undesirable effect of oversmoothing is apparent with polynomials of higher degree, at least up to the eleventh degree. This degree is of consequence in that from an adjustment polynomial of the  $n$ th degree, only  $n+1$  computed values can be used; otherwise, the corresponding covariance matrix becomes singular, while the use of fewer values does not exhaust the available information content completely.

In processing the world net, polynomials of the sixth degree are used in smoothing both  $x$  and  $y$ , so that seven fictitious directions can be used in the final triangulation, provided that the trace of the portion of the

satellite orbit common with other stations extends over the whole plate. Thus, the polynomials provide the adjusted location of the satellite trace as a function of the recorded time. This relation is very useful, since it simplifies the application of the influence of time corrections, such as clock differences and light propagation. It is necessary, after a selected satellite orbital time has been transformed to a corresponding time of registration on the plate, merely to compute from the relevant polynomial with this transformed time the  $x$  and  $y$  coordinates for the corresponding fictitious plate image. By using this procedure on all photographs that have observed a common event, a fictitious image that satisfies the geometric condition of simultaneity is obtained on each photograph (see sec. 7.4.4). An approximate preliminary triangulation of the relevant orbital points will be needed to determine for each registered orbital image the variable propagation time of light. It should be noted in this connection that an error of 3 km in the approximated distance will create an error of only  $10 \mu\text{sec}$  in the time. Along with the coefficients of the curve-fit polynomials, one obtains the mean dispersion of the individual images and, hence, the variance-covariance of the polynomial parameters. Since the fictitious satellite-image positions corresponding to specified times are computed as functions of the polynomial parameters (cf. eqs. 7.58 and 7.270), the corresponding error propagation computation will produce their variance-covariance matrix, which displays rigorously the correlations among the individual satellite images resulting from the polynomial smoothing. If seven such fictitious satellite images are used, as, for example, in the world net, a  $14 \times 14$  covariance matrix for these points must also be computed.

At this stage the following evaluation data are available for each satellite orbit observation at a station:

(1) The bundle parameters describing the interpolation model, including the exterior elements of orientation, and the associated covariance matrix (in this case, of

dimension  $20 \times 20$ ) scaled to an a priori introduced error of unit weight.

(2) The pairs of coordinates for the selected fictitious satellite images (in the present case, seven pairs) together with their  $14 \times 14$  covariance matrix, also referred to the error of unit weight mentioned in (1) above.

The last processing step, computing the three-dimensional geometry of the observing stations, amounts basically to determining the spatial directions corresponding to the fictitious satellite images in order to triangulate the satellite orbit points and all the observation sites by means of an adjustment, subject to the condition that the sum of squares of weighted corrections to the fictitious satellite-image coordinates be a minimum. The weight matrices of the satellite direction bundles are compounded at each station by the joint influence of the covariances of the relevant interpolation parameters (statement 1 above) and the covariances of the plate coordinates of the fictitious satellite images (cf. statement 2 above).

Whenever additional a priori given information relative to the geometry of the observing sites, such as spatial distance between the sites (as for scale determination), position coupling between adjacent stations (eccentric reductions), or the like, is used as input data, such data can be introduced into the adjustment without difficulty after the necessary functional weights, referred of course to the a priori selected error of unit weight, have been computed. This is true also when additional geometric data become available through, for example, distance measurement by laser DME between satellite and station.

In the world net, such scalars are introduced in the form of measured distances of edges of the world net polygon in, primarily, the United States, Europe, Africa, and Australia, as shown in figure 7.5, section 7.3.

The basic ideas underlying the error budget of geometric satellite triangulation are presented here as explanation of the error theoretical considerations that lead to the

adjustment algorithm described in section 7.4.6. Moreover, by pointing out computational possibilities that differ from the present solution and lead eventually to completely rigorous adjustment and error propagation, it is hoped that impetus will be given to perfecting the developing method of geometric satellite triangulation.

In the next section will be reported some results on the accuracies in the various evaluation phases obtained in the processing of the observational data for the world net.

#### 7.4.8.2 Analysis of the Essential Sources of Error and the Error Propagation Into the Spatial Triangulation

In section 7.4.8.1 it was shown that, in essence, the method of geometric satellite triangulation is subject to five random error sources. The accidental errors from these sources arise in connection with:

- (1) Comparator measurements of star and satellite images.
- (2) Reference data from the star catalogs.
- (3) Designated times of the star and satellite recordings.
- (4) Atmospheric shimmer affecting the directions to the recorded star and satellite orbit points.
- (5) Accidental emulsion shifts generated in the process of developing the plate.

This idealized situation will, however, exist only to the degree that, during the field observations and in the data processing, sufficient precautions are taken to either model the following systematic error sources or eliminate them by corresponding operational procedures.

##### Observational Phase.—

- (1) Eliminating possible static instability of the camera during the average half-hour period of observation.
- (2) Eliminating systematic errors in recording the instant of shutter operation that is needed to within a few milliseconds of Universal Time and, relative to all involved cameras, to within  $1/10$  msec.

## Measurement Phase.—

- (1) Adhering strictly to the Abbe comparator principle.
- (2) Correcting for the lack of perpendicularity of the comparator axes.
- (3) Accounting for at least linear differences in the comparator scales.

## Adjustment Phase.—

- (1) Determining the elements of interior orientation existing in the operational environment.
- (2) Determining the comparator constants outlined necessary to correct for the lack of perpendicularity of the comparator axes and to account for the differences in comparator scales.
- (3) Modeling of astronomic and parallactic refraction, the latter being needed because of the finite distance of the satellite.
- (4) Modeling the phase angle of the satellite illumination as a function of size and shape of the satellite, its reflective property, and the geometric positions of the Sun, satellite, and observing station during the event.
- (5) Considering influence of light travel time on station synchronization and aberration.
- (6) Introducing with sufficient accuracy the spatial orientation of the instantaneous rotation axis of the Earth (pole wandering) with respect to individual camera orientations as well as with respect to the use of UT1 (true angle of Earth's rotation).
- (7) Reducing star places to time of observation, involving precession, nutation, proper motion, radial velocity, annual and diurnal aberration, as well as the influence of the spectral characteristics and magnitude of the star on the photogrammetric imagery.

Quantitative results will now be given with respect to the above random errors mentioned and their propagation into the end results of the spatial satellite triangulation, errors in time determination, as was previously mentioned, being considered negligible (Schmid, 1965b, 1966b, 1967a, b, 1969).

## 7.4.8.2.1 ACCURACY OF THE COMPARATOR MEASUREMENTS

We discuss first the result of measuring 1210 photograms, representing practically half of the observational data from the world net.

On each photogram, on the average, 100 fixed stars were recorded before and after the satellite transit and also during the event. With repeated exposure, 500 to 800 star images in all are registered. There are, in addition, about 300 satellite images, so that on each photogram at least 800 images must be measured. In order to complete these measurements in the time allotted to the world net program, six comparators of similar design were in operation. Of significance also is the fact that a group of operators was involved in the measurements. Each photogram was measured on the comparator in two positions differing by approximately 180 degrees (cf. sec. 7.3.2). By means of a two-component translation, two scale factors, and a rotation, the two sets of measurements were brought into coincidence by an adjustment. The internal accuracy of the measuring process (precision of the comparator measurements) can then be judged on the basis of residual differences from double measurements. From the selected photograms with their 1 291 744 double measurements there resulted a mean error for the arithmetic mean of a double measurement of  $\pm 1.63 \mu\text{m}$ . No significant differences between the precision of the  $x$  and  $y$  coordinates were detected.

It is of interest to group the measurement of plates by individual operators. The separately computed average measuring accuracy for each of the 34 comparator operators, arranged in sequence of increasing absolute amounts, is shown in figure 7.40. The number at the top of each arrow represents the number of photograms measured by the operator, and the ordinates of the arrowheads indicate the range over which the mean errors of the individual plate measurements vary for that operator.

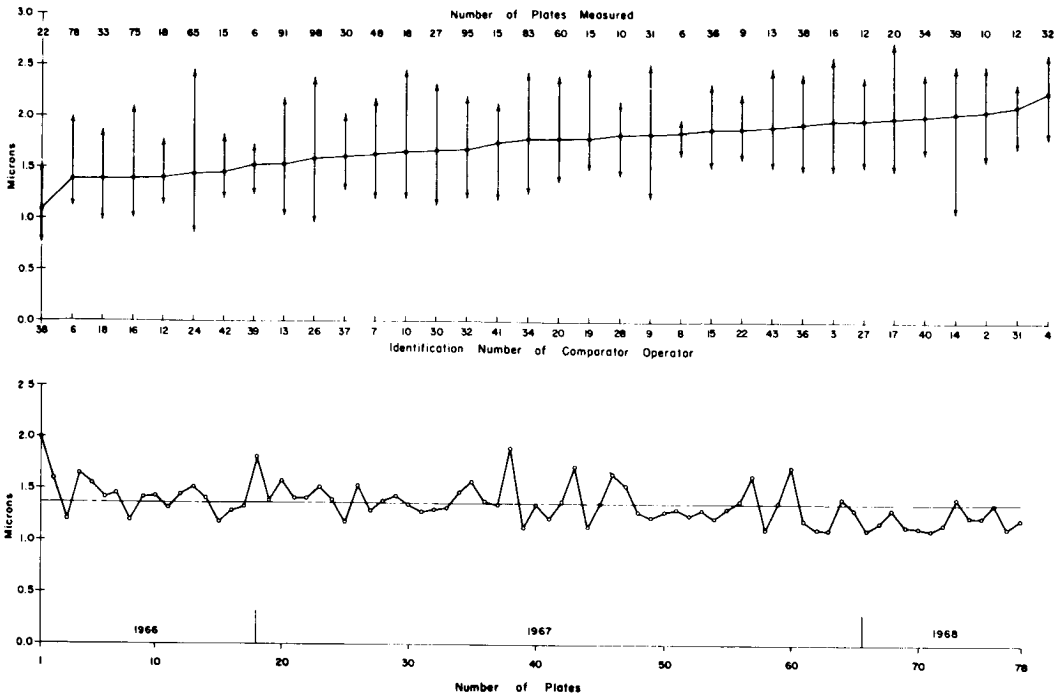


FIGURE 7.40.—Computed average measuring accuracies of 34 comparator operators. (Below) Performance of operator 6.

It can be seen that the mean measuring precision attained ranges from  $\pm 1.1 \mu\text{m}$  (for operator 38) to  $2.2 \mu\text{m}$  (for operator 4). The best single result was  $\pm 0.76 \mu\text{m}$  by operator 38, and the worst was  $2.66 \mu\text{m}$  by operator 20. As an explanation of these fairly surprising differences, one must assume not only the varying capabilities of the operators, but also the influence of environmental conditions on image quality. The lower diagram in figure 7.40 shows for operator 6 in chronological order the mean error of the 78 photograms measured by him over a period of 18 months. Although the average mean error for this operator of  $\pm 1.37 \mu\text{m}$  is relatively low, the dispersion is typical for the behavior of all operators with respect to the quality of their individual measuring results. In addition to displaying the variation in precision from plate to plate, the diagram indicates a steady though small improvement in the measuring operation.

Figure 7.41 shows the histogram of the 1 291 744 double measurements. From the

similarity of the histogram with the superimposed, theoretical, normal distribution, one can conclude a sufficiently close absence of bias errors, all the more so when the fact that the data for the histogram are composed of samples with differing mean errors is taken into consideration. On the basis of these results one can well imagine that these measurements were all made by one fictitious operator on one fictitious comparator, instead of by 34 operators on 6 comparators. Hence, for the further error theoretical studies we shall assume that the internal accuracy of image coordinates, meant from double measurement, is sufficiently well expressed in their totality by a mean error of  $\pm 1.63 \mu\text{m}$ .

The mean errors  $m_i$  computed separately for each photogram are plotted in figure 7.42 for 500 photograms selected for further study. The observational data selected are derived from 35 stations of the world net, plotted according to latitude. Table 7.8 shows the number of plates for each station. The location of the stations is shown in figures

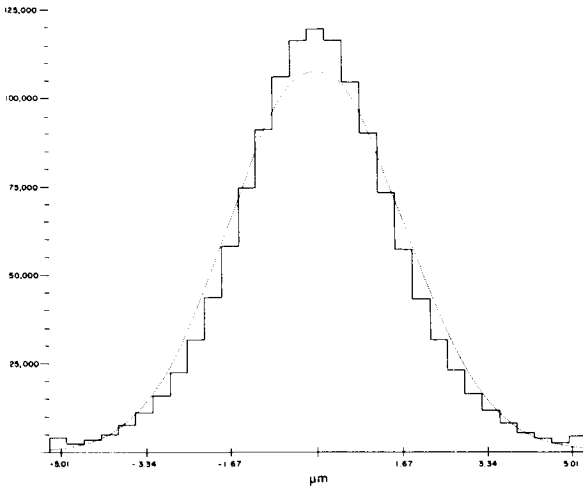


FIGURE 7.41.—Histogram of 1 291 744 double measurement differences.

7.6 through 7.11 of section 7.3. See also table 7.2 in section 7.1.2.

7.4.8.2.2 ACCURACY OF THE RECONSTRUCTIONS OF THE PHOTOGRAMMETRIC BUNDLES AND THEIR ORIENTATIONS

The parameters for reconstructing the bundle and its orientation are obtained by relating the measured star-image coordinates to the corresponding star-catalog data with an adjustment to a mathematical model. The total of these quantities, previously designated as interpolation parameters, includes, in addition to the purely photogrammetric parameters, a second scale factor and an angle for correcting for the a priori assumed

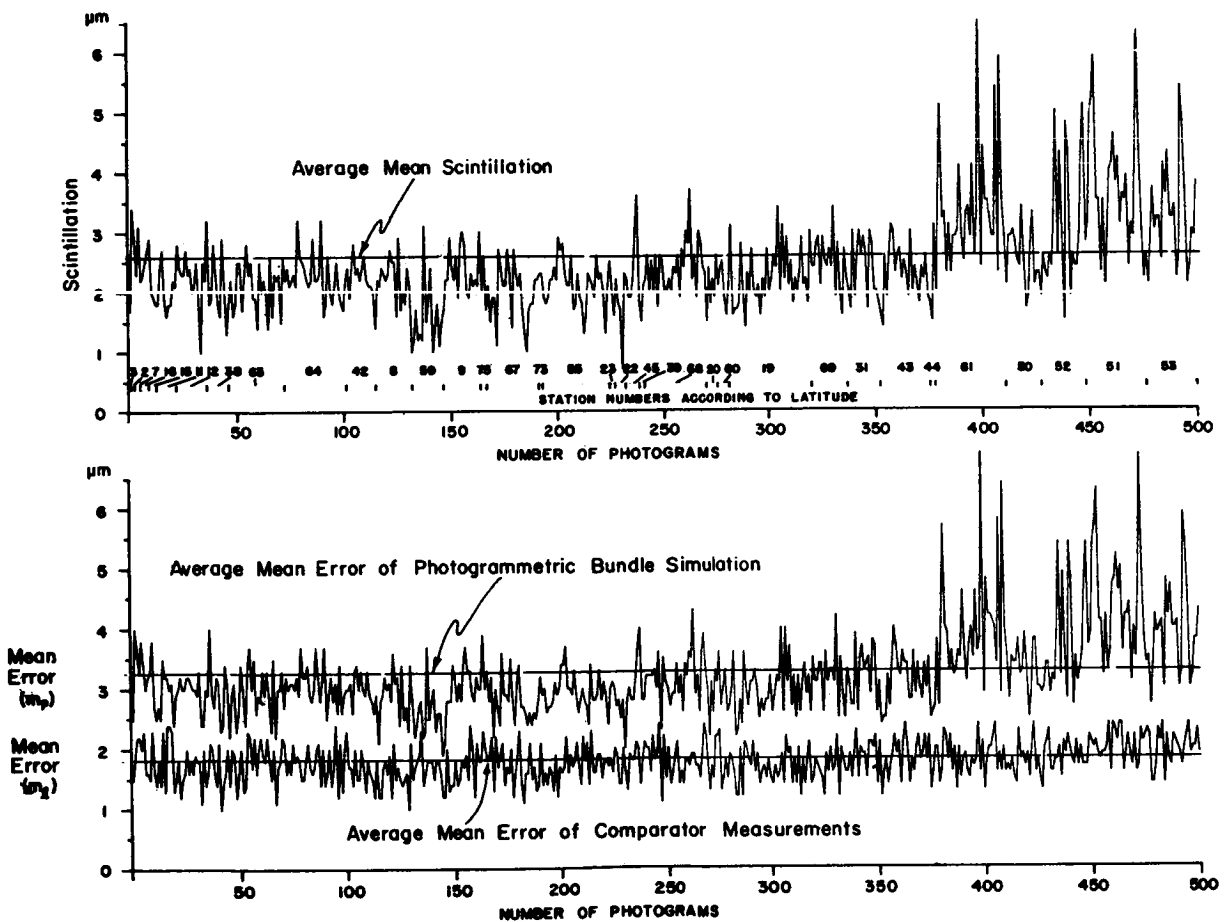


FIGURE 7.42.—Plot of mean errors for 500 photograms.

perpendicularity of the comparator spindles. The introduction of these extra parameters is justified insofar as one may assume that the homogeneity of the scale of the astronomic reference system (unit sphere) and the orthogonality of its coordinates are superior, with respect to systematic errors, to the corresponding mechanical components of the comparators. After the linear scale difference between the  $x$  and  $y$  spindles and the deviation from perpendicularity has been determined in this manner, the mean error of  $\pm 1.63 \mu\text{m}$ , computed as a measure of precision for the image coordinates, can be considered a measure of accuracy for the subsequent treatment. (Periodic screw errors are independently tested for in comparator calibrations.) If it is assumed that the error for the astronomic coordinate  $\alpha, \delta$  of FK-4 stars, reduced to the observation datum, is  $\pm 0''.3$ , and for all other stars  $\pm 0''.4$ , and that the mathematical model for simulation of the bundle is sufficient, then, since time errors are negligible, the mean error of coordinate corrections resulting from an adjustment executed with appropriate weights

will express the additive influence of the random errors produced by the comparator measurement, shimmer, and emulsion shift. Figure 7.42 shows for the 500 selected photographs the values for  $m_p$  and  $m_l$  and the rms for all the data,  $m_p$  being the mean error of the image coordinates for the photograph as obtained from the adjustment for the photogrammetric bundle reconstruction and  $m_l$  being the expression for the accuracy of the corresponding comparator measurements. A mean error of  $\pm 1.0 \text{ m}$  is assumed for the influence of random emulsion shift (Altman and Ball, 1961). Hence, the contribution to the total mean error

$$m_s = \pm (m_p^2 - m_l^2 - 1.0^2)^{1/2} \quad (7.308)$$

This error component is also shown in figure 7.42. The rms values for the 500 plates are  $m_p = \pm 3.31 \mu\text{m}$ ,  $m_l = \pm 1.81 \mu\text{m}$ , and  $m_s = \pm 2.58 \mu\text{m}$ .

Figure 7.43 shows the histograms of combined  $x$  and  $y$  coordinate corrections with corresponding normal distribution curves for 25 single camera adjustments. These were

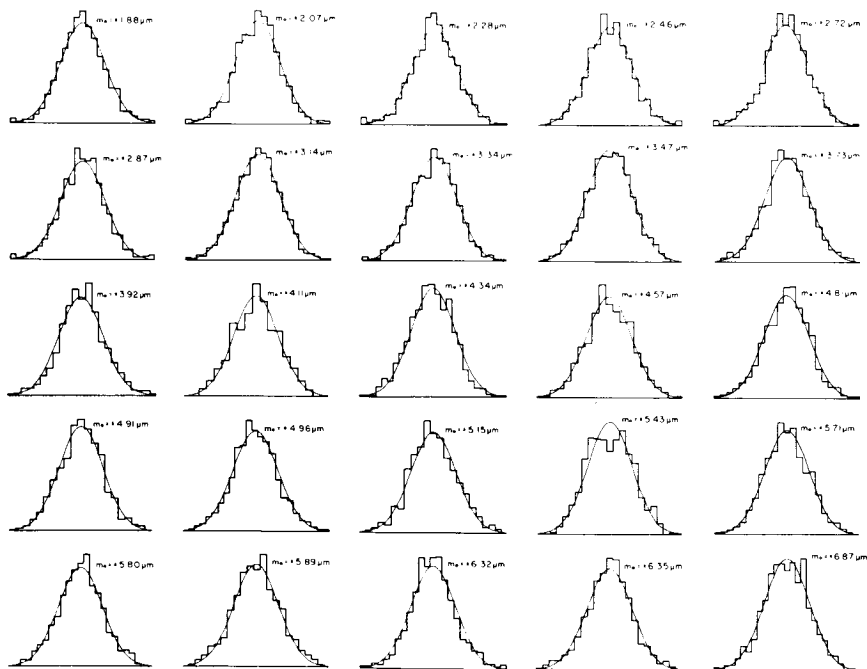


FIGURE 7.43

selected to cover uniformly the range of mean coordinate errors, after adjustment, actually obtained, i.e., the range from  $\pm 1.88$  to  $\pm 6.87 \mu\text{m}$ . The histograms illustrate the typical behavior of the totality of evaluated observational data.

### 7.4.8.2.3 ACCURACY OF THE TRACE OF THE SATELLITE ORBIT AFTER THE POLYNOMIAL FIT

The mean deviation of a measured satellite point from the smoothing polynomial of degree 6 varies between  $\pm 1.6$  and  $\pm 8.6 \mu\text{m}$ , with rms of  $\pm 3.75 \mu\text{m}$  for the fit in direction of the satellite trail and between  $\pm 1.3$  and  $\pm 9.3 \mu\text{m}$  with an rms of  $3.28 \mu\text{m}$  perpendicular to the trail (fig. 7.44). The corresponding  $x, y$ , mean value is  $3.52 \mu\text{m}$ .

The individual mean displacement is a measure of how well the satellite images on a given photogram fit the polynomial. These quantities are the sums of the superimposed random errors of the comparator measurements, the emulsion shifts, and, again, the shimmer. The mean deviation in direction

of the satellite trail is, on the average,  $0.47 \mu\text{m}$  larger than that at right angles to the trail. This difference is not so much due to random time errors of the recording sequence which operate in the direction of the trail, as to the fact that the comparator measurements of the trail images have a larger mean error in this direction than in the direction perpendicular to the trail, because of image blur from the satellite motion.

About 300 satellite image measurements are available per plate. From the double measurements, i.e., from their differences, the accuracy of the comparator measurements is again determined. This is on the average  $\pm 1.79 \mu\text{m}$  for the  $x$  and  $y$  measurements, or practically the same value as that for the star image measurements. Again, with the assumption of  $\pm 1.0 \mu\text{m}$  for the mean random emulsion shift, the opportunity is given to isolate the shimmer effect as

$$m_s = (3.52^2 - 1.79^2 - 1.0^2)^{1/2} = \pm 2.86 \mu\text{m} \tag{7.309}$$

The treatment of the shimmer as a random source of error is based on the fact,

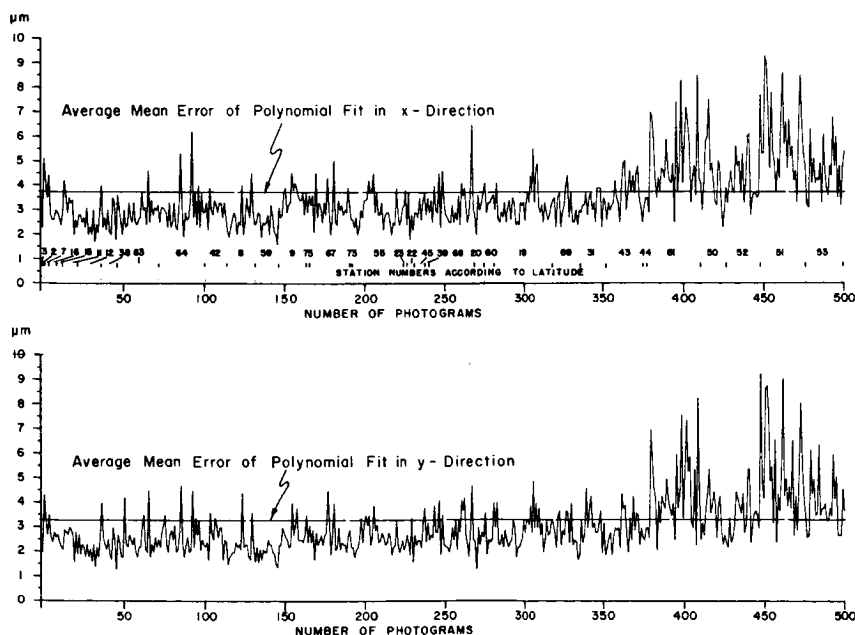


FIGURE 7.44.—Mean deviations after polynomial fit.

known from astronomical observations (Hynek, 1960), that the mean amplitude of shimmer operates as an irregular error source in all directions. When for each plate the shimmer effect on the star images is computed in accordance with (7.308) and these values are compared with the corresponding values obtained from the curve fit with (7.309), the correlation coefficient  $\rho = 0.81 \pm 0.02$  is obtained with the formula

$$\rho = \frac{\sum_{i=1}^{n=500} \Delta S_1 \cdot \Delta S_2}{\left[ \sum_{i=1}^{n=500} \Delta S_1^2 \right]^{1/2} \left[ \sum_{i=1}^{n=500} \Delta S_2^2 \right]^{1/2}} \quad (7.310)$$

where the  $\Delta$ 's represent deviations of the individual amounts of shimmer from their mean value, and the indices 1 and 2 refer to the shimmer computed from the bundle reconstructions and the polynomial fit, respectively.

Figure 7.45 shows the mean shimmer at each observing station, the stations arranged by latitude. From this figure it is seen that shimmer, with an overall mean for all stations of  $\pm 2.58 \mu\text{m}$  for the star images and  $\pm 2.86 \mu\text{m}$  for satellite images, represents a considerable error contribution to the total error budget. Also apparent is the increase in shimmer with increasing latitude, which is to be expected in consequence of the theory presented by Nettelblad (1953), according to which shimmer is least in warm ocean air masses and

greatest in cold continental climates. The amplitude of the shimmer depends, in addition, on the exposure time, which may be the cause for the fact that the mean shimmer for the star exposures of between 0.2 and 3.2 sec is  $\pm 2.58 \mu\text{m}$  and for the satellite images exposed from 1/15 to 1/30 sec is  $\pm 2.86 \mu\text{m}$ . Obviously, the use of short-duration flashes (1/1000 sec) will increase the shimmer effect for the individual flash, thus making it all the more desirable to have a considerable number of such flashes before an adequately accurate triangulation can be performed.

#### 7.4.8.2.4 ERROR PROPAGATION INTO THE SPATIAL TRIANGULATION

In sections 7.4.2.1 through 7.4.2.3, quantitative results were given for the significant random error contributions that must be considered in setting up an error budget for spatial triangulation. In table 7.9, average values from the processing of the selected 500 photograms are presented.

The figure in column 7 of table 7.9 indicates that an average uncertainty of  $1''.57$  in direction should be associated with a bundle reconstruction that is not overdetermined. Actually, this value is a function of the position of a ray within this bundle (Schmid, 1967a), and to be completely rigorous, in accordance with error theory, should be computed with the covariance matrix obtained

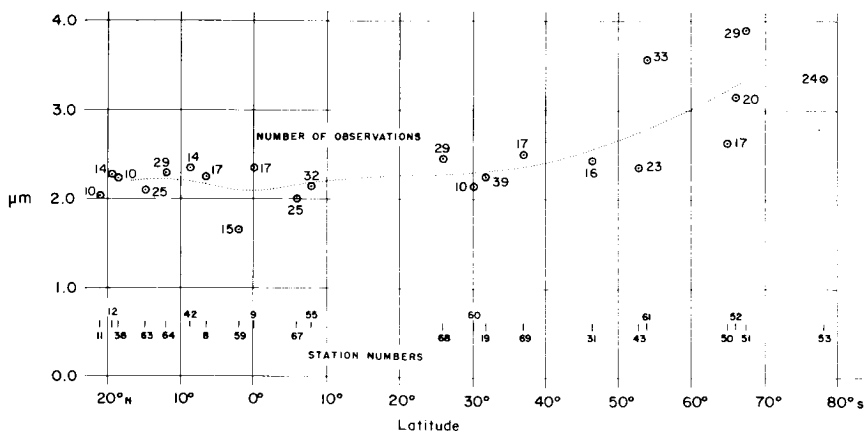


FIGURE 7.45.—Average shimmer versus latitude of observing station.

from the individual bundle reconstruction adjustment. Since the bundles under consideration here are relatively narrow, however (the angle of vision for the BC-4 camera is about 20 degrees), we can for the present ignore this fact in a general examination of the error propagation. In order to determine uniquely the 20 required interpolation parameters of an oriented bundle reconstruction, at least 10 reference stars are required, so that the use of an average of 100 stars per plate represents 10 solutions in the adjustment. Each star being, on the average, measured five times, it can be expected that the direction uncertainty for a central ray after adjustment of the bundle reconstruction will, from a combination of tabulated values in table 7.9, result as follows.

The error sources affecting the individual image coordinates add quadratically to

$$m_i = \pm (1.81^2 + 1.0^2 + 2.58^2)^{1/2} = \pm 3.31 \mu\text{m}$$

(cf. table 7.9, columns 2, 3, 4, and 5). If it is assumed that the five images for each reference star are combined into one fictitious image, then the coordinates will have an accuracy of  $3.31/\sqrt{5} = \pm 1.48 \mu\text{m}$ . Combining this with the mean star-catalog uncertainty of  $\pm 0.4 = \pm 0.87 \mu\text{m}$  (column 6), we have a mean uncertainty in direction  $\pm 1.72 \mu\text{m} = \pm 0.79$ . The combination of 10 independent solutions in one adjustment reduces this error approximately to  $0.79/\sqrt{10} = 0.25$ .

The figures of table 7.10 are results from a bundle reconstruction adjustment with a mean error of  $\pm 3.31 \mu\text{m}$  for the image coordinates after adjustment involving 648 star images of 105 reference stars distributed approximately evenly over the plate. The results shown are mean accuracies of directions corresponding to various image positions on the plate, which are assumed free of error (Schmid, 1967a).

The mean error  $\pm 0.23$  from this table for the central ray ( $x=y=0$ ) is in good agreement with the value  $0.25$  obtained before from general considerations. When the mean satellite image error figure of  $1.61$  from table 7.9, column 8, is used, the sixth-degree

polynomial fit over 300 satellite points will contribute an uncertainty in direction after adjustment of  $\pm 1.61/\sqrt{300/7} = 0.25$ . The error sources being uncorrelated, the total expected error in direction for the central ray is  $(0.25^2 + 0.25^2)^{1/2} = \pm 0.35$ .

The use of sixth-degree polynomials makes seven directions available for satellite triangulation in each photographed bundle. However, as we know, these directions are mutually correlated. One reason is that they are all obtained with a specific group of interpolation parameters from a single camera, and another is that they all derive from a single pair of smoothing polynomials. From a study of the relevant covariance matrices in a rigorous adjustment whose reproduction here would far exceed the available space, it becomes apparent that the use of seven directions distributed evenly over the satellite trail yields a gain of 32 percent for the geometry of the bundles, as opposed to the use of a single central direction. This means that the use of all seven directions has about the same information content that would be obtained from two central rays that are not correlated.

Hence, if we conceive the total information used in the evaluation of a specific photogram as being compressed to determine a central fictitious direction, we may expect for such a direction an accuracy of  $m_r = \pm 0.35 - 32\%$  ( $\pm 0.35$ ) =  $0.24$ .

According to section 7.4.7.1, the adjustment algorithm is based on the assumption that the results of bundle reconstructions at the individual stations are uncorrelated. Consequently, the directions to the satellite for a given event derived at the individual stations are also uncorrelated. To obtain a measure of the mean accuracy to be expected for the spatial triangulation of the observing sites, one can assume that the mean accuracy  $0.24$  of a direction computed above for a fictitious central direction containing all the information content is an uncorrelated function of the station. In the adjustment algorithm, this accuracy of triangulation directions associated with a specific evaluation of a photogram is expressed in the form of the

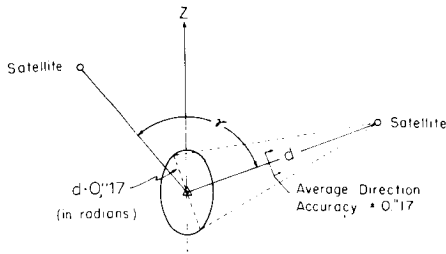


FIGURE 7.46

weight matrix associated with the coordinates of the seven fictitious satellite-images, the weight and matrix being computed from the corresponding covariance matrix derived with equation (7.277) of section 7.4.6. In section 7.4.8.1 it was mentioned that, in the mathematical formulation to be set up for the final triangulation, only the satellite and station positions were to be determined as unknowns. The basic triangulation geometry (fig. 7.14) implies that the accuracy of the triangulation in a direction perpendicular to the direction station-satellite is proportional to both the directional accuracy and the distance station-satellite. This is indicated schematically and reduced to two dimensions in figure 7.46.

The accuracy in direction of the  $z$  coordinate is obviously a function of the angle  $\gamma$  in which the station-satellite planes intersect. From analysis of the systems of inverted normal equations, which contain the geometry of the actual satellite observations, it follows, quite generally, that the mean error of the triangulated station in the direction of the geodetic latitude and longitude is, assuming errorless scale, proportional to the product  $m_R \cdot d$ , where  $m_R$  is the mean accuracy of the direction and  $d$  is the mean distance station-satellite; on the other hand, the average mean error in the direction of height is three times as large (Schmid, 1969). These relations are shown in figure 7.47, in which  $\sqrt{Q}$  is the error propagation factor (sometimes called the weight reciprocal) for the position coordinate.

The same result is shown schematically in another form in figure 7.48, from which, by comparison of antipodal stations, it is apparent that the uncertainty in height determination within a world triangulation eventually has the effect of an uncertainty in scale. One can expect, therefore, that additional scale control will have a particularly

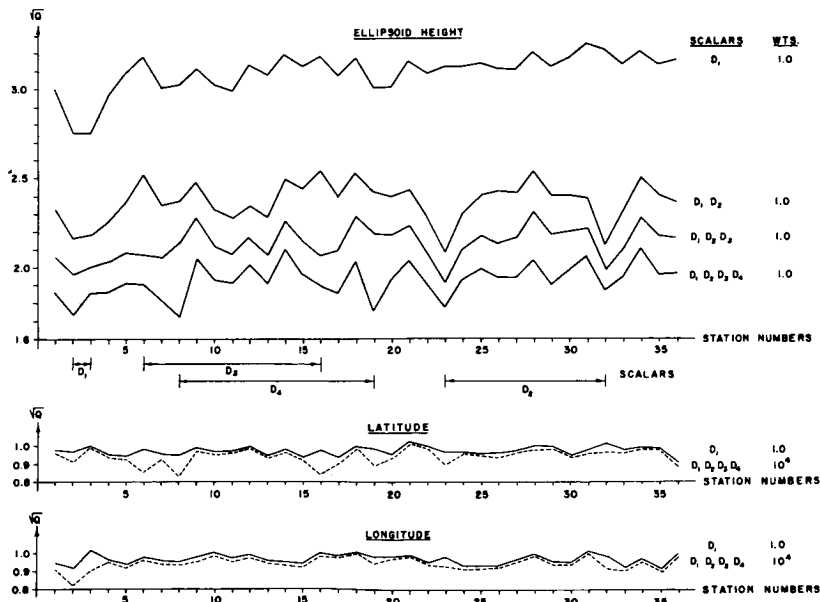


FIGURE 7.45.—Average shimmer versus latitude of observing station. using one to four scalars.

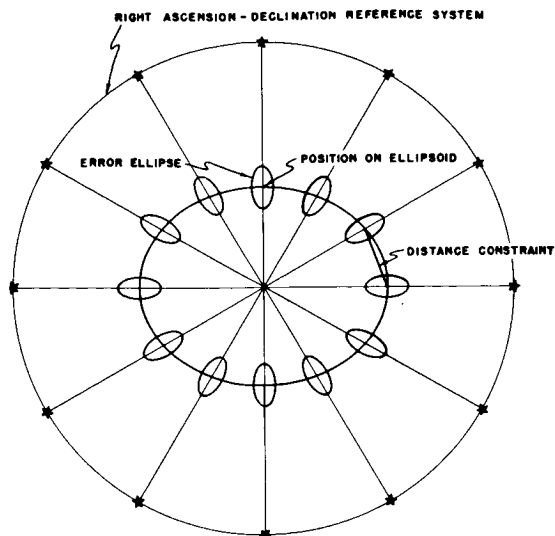


FIGURE 7.48.—Error propagation of the method of geometric satellite triangulation.

favorable influence on the accuracy of height coordinates, but will represent no real gain for the determination of the position coordinates  $\phi, \lambda$ . This fact is illustrated in figure 7.47, which shows the effect of from one to four scale determinations. The lower part of figure 7.47 shows that even under the assumption of errorless scalars (weight  $10^4$ ) only the stations directly involved in the scale determination show a gain in the determination of their latitude  $\phi$  and longitude  $\lambda$ . On the other hand, the error propagation coefficient for the height determination reduces from 3 to 1.8 with the use of four scalars, even when a more realistic weight of 1 is used in the scale determination (Schmid, 1969; Rinner, 1966).

In the world net, the PAGEOS satellite was observed almost exclusively. Its nominal circular orbit elevated about 4600 km above the surface of the earth resulted in an average distance station-satellite of 6000 km. With a mean direction accuracy of  $0'24$  and the propagation factors of figure 7.47, a triangulation solution based on two satellite transits or two events per triangle side, under the assumption of an errorless scale, produces position coordinates for the observing stations with mean errors  $m_\phi = m_\lambda = \pm 7.0$

m and  $m_h = \pm 21.0$  m. At this time, 2350 plates have been reduced for evaluation in the world net. The distribution of the corresponding events is shown in figures 7.6 through 7.11. These observations correspond to about five independent solutions. Therefore, adjusting all these events should yield an accuracy of  $m_\phi = m_\lambda = \pm 7.0/5 = \pm 3.1$  m and  $m_h = \pm 21.0/5 = \pm 9.4$  m. When the planned four scalars, measured independently with an accuracy of at least 1:1 000 000 are introduced, the expected mean error in height reduces to  $m_h = \pm 3.1 \text{ m} \times 1.8 = \pm 5.6$  m (cf. fig. 7.47) and the mean position error of a station

$$m = \pm \left( \frac{m_\phi^2 + m_\lambda^2 + m_h^2}{3} \right) = \pm 4.1 \text{ m} \quad (7.311)$$

or  $m$  is roughly 1:1 500 000 of the mean distance station-satellite.

In the next paragraphs the result of the worldwide geometric satellite-triangulation program is presented with an associated error analysis based on the statistical information obtained during the final triangulation adjustment.

## 7.5 RESULTS OF THE WORLDWIDE GEOMETRIC SATELLITE TRIANGULATION <sup>3</sup>

### 7.5.1 Statement of Results

The quantitative result of the worldwide geometric satellite-triangulation program consists of the three-dimensional positions of 45 stations. Their locations can be seen from figure 7.4 and table 7.2.

The corresponding Cartesian reference coordinate system has, as was explained before, one of its axes parallel to the rotation axis of the Earth for a certain epoch (CIO). The origin of the system and the selection of

<sup>3</sup> NGS used a left-handed coordinate system for its  $x, y, z$  coordinates. The values in tables 7.11 and 7.15 are given in a right-handed system, to permit comparison with coordinates in other chapters. Otherwise, the system is left-handed as noted. Great care should be exercised when values from this and other sections are taken.—[Editor]

the  $x$  direction is, for reasons inherent to the method of geometric satellite triangulation, arbitrary. It was fixed by enforcing for station 2, Beltsville, Maryland, the following coordinates, which are approximate values for a geometric position:

Spatial Coordinates (m)	
1 130 761.500	$x$
4 830 828.597	$y$
3 994 704.584	$z$

As is discussed in the analysis of the results in the next paragraph, it was decided to enforce all eight scalars with their measured values.

Table 7.11 lists the three-dimensional Cartesian coordinates for the 45 stations and their mean errors (one-sigma level) as obtained from the final adjustment. The coordinates refer to the projective center of the BC-4 cameras. The elevation of this point above the permanent station mark is in each case +1.5 m.

### 7.5.2 Analysis of the Triangulation Adjustment

The input of the triangulation adjustment refers to the information obtained from the evaluation of 2350 photographic plates. Specifically, observations from 856 two-station, 194 three-station, and 14 four-station satellite events were used. The 1064 satellite events chosen for evaluation required, in addition to the determination of the spatial positions of the tracking stations, the triangulation of 6604 satellite positions. The adjustment provided for 9162 degrees of freedom. Two station-to-station couplings were introduced as additional constraints in order to tie together stations 6111-6134 (California) and 6012-6066 (Wake Island), where, for technical reasons, satellite observations were collected from neighboring observation piers. Furthermore, eight scalars were rigorously introduced. They represent the spatial distances between the stations given in table 7.3, section 7.3.0. These scalars were

measured and computed by various national agencies. For references, see table 7.4.

In order to obtain a measure for the precision of the strictly photogrammetric triangulation, a first triangulation adjustment was executed with only the scalar between stations 6002-6003 enforced. This adjustment produced a sum of the squares of the weighted residuals in terms of plate coordinate corrections  $[p_{vv}] = (3.064 \pm 0.045) \times 10^{-8} (m^2)$ .

A comparison of the measured baselines with the corresponding triangulation results provides a first insight into the internal accuracy of the geometric world net. The differences between the computed and measured distances with a complete constraint on scalar (6002-6003) are shown in table 7.12.

The sum  $\Sigma d$  of the lengths of the measured scalars is 17 513 184 m, so that

$$\frac{\Sigma \Delta d}{\Sigma d} = 1:1\ 911\ 920$$

As can be seen from table 7.12, the difference  $\Sigma \Delta d$  is only about 0.6 of the standard deviation associated with the sum of the triangulated distances.

It was therefore concluded that the scalars, at least in their totality, are probably of higher accuracy than the geometric satellite triangulation itself, a conclusion which is further evidenced when the standard errors for these scalars computed by the various computing centers are considered.

An adjustment in which all scale lines were enforced with weights corresponding to an accuracy of one part in two million of their respective lengths gave the result shown in table 7.13.

The  $[p_{vv}]$  of this adjustment was  $3.068 \times 10^{-8}$ , or a value which is only  $0.004 + 10^{-8}$  unit larger when it is compared with the single scalar adjustment mentioned above. This difference is only  $\frac{1}{40}$  of the associated sigma. It can therefore be safely concluded that the scalars do not exercise undue constraint on the triangulation system.

If all eight scalars are rigorously enforced, the  $[p_{vv}]$  sum increases to  $3.071 \times 10^{-8}$ , a

solution which from a statistical standpoint is equally defensible.

The numerical solution was iterated on the CDC 6600 computer (generally three times) until the maximum increments to the triangulated coordinates became  $<1$  mm. When the normal equations matrix pertaining to the final iteration is multiplied by its corresponding inverse matrix, one obtains, as a check, the expected unit matrix to within a unit in the tenth decimal place.

The mean error of unit weight after adjustment is for all these solutions  $1.830 \pm 0.014$ , against the expectation of 1.0, indicating the presence of additional unmodeled error sources. If the increase in the overall error budget can be ascribed to additional random-error sources, then the effect is relatively harmless, resulting only in a corresponding increase in the mean errors of the triangulated station positions. But if the effect of systematic errors which are distributed in the adjustment in accordance with the least-squares principle is involved, the situation is more serious.

To gain some insight into the stability of the camera during the average half-hour period of operation, star photography taken immediately before and after the satellite transit was adjusted and sets of camera orientation parameters computed. Thus, for each plate the change in azimuth  $\Delta A$  and in

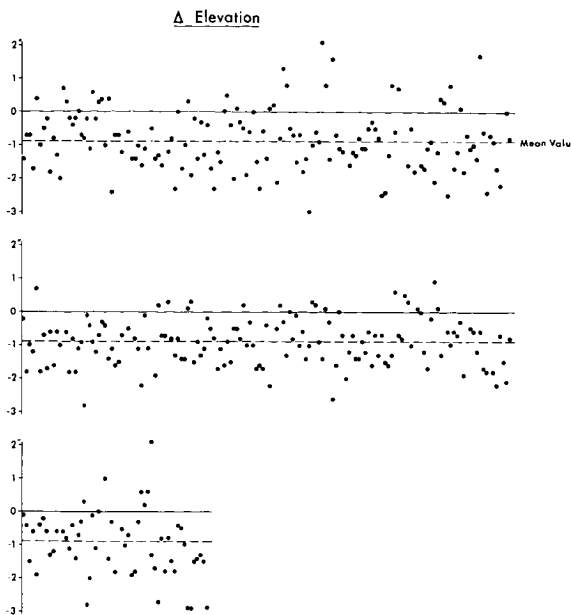


FIGURE 7.50

elevation  $\Delta h$  of the central ray with a corresponding rotation component  $\Delta \alpha$  was computed. The  $\Delta \alpha$  are random and completely within the range of their mean errors. The  $\Delta A \cos h$  and, especially, the  $\Delta h$  component, however, indicate the influence of a systematic error, as shown in figures 7.49 and 7.50. For an evaluation of these diagrams it should be added that the individual  $\Delta$  values shown have an average mean error of  $\pm 0''.5$ . Since star imagery is also available for the satellite transit period, it is possible to study these systematic changes in orientation over the period of observation. A roughly linear trend with time is indicated.

To eliminate this source of error, orientation parameters that were based solely on star images obtained during the period of actual satellite transit were used in the final adjustment, whenever possible. Still, we cannot entirely escape the conclusion that the instability of the camera creates an additional error which, as the diagrams show, has a systematic component and acts as a source of additional accidental errors.

For a further analysis of the results it is important to realize that, as consequence of

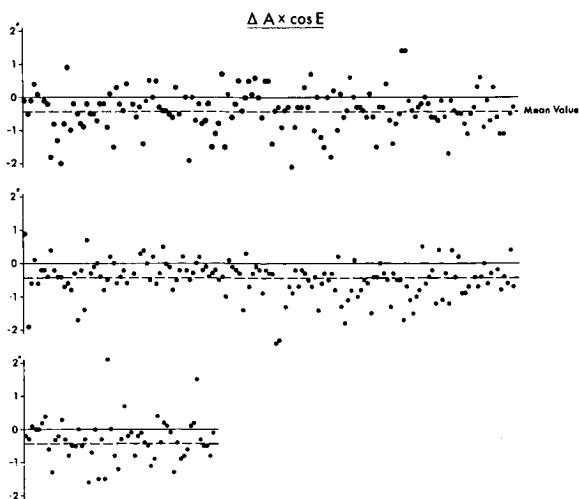


FIGURE 7.49

the interpolation of each event into the astronomical system, absolute directions are obtained. This means that it is possible to triangulate the direction of the chord joining two adjacent stations in the net independently, i.e., with only the satellite passes observed from these two stations. Such computations were made for all 170 lines of the world net. In these adjustments, as well as in the final solution, all covariance matrices resulting from the individual processing steps were included, so that all results can be considered as rigorously derived values. The line triangulations yield an average mean value for the ratio of mean error of unit weight before and after adjustment of 1:1.746, the range being from 1:0.706 to 1:2.429. The theoretical expected average value is, of course, 1:1. This means that the observational data do not completely fill the accuracy expectations computed in the partial analyses cited above, a fact which was mentioned in connection with the obtained mean error of unit weight after adjustment in the final triangulation.

However, it is gratifying to note that this value increases only slightly, from 1.746 for the average of all individual line adjustments, to 1.830 for an adjustment based on the combination of all observations. These figures indicate that the entire body of data is apparently free of perturbing systematic errors and satisfies with practically no constraint the three-dimensional geometrical closure condition of the world net.

In order to strengthen this conclusion, the directions derived from the individual line adjustments and those of the combined solution were compared. The resulting azimuth and elevation angle differences are shown in the diagrams with their three-sigma errors and combined in histograms of figures 7.51 and 7.52. Although these results do not fully meet ideal statistical expectations, it is not really possible to otherwise draw any conclusions regarding the presence of possible systematic error influences in the triangulations of the individual lines.

In order to analyze the accuracy of the shutter synchronization, the following argu-

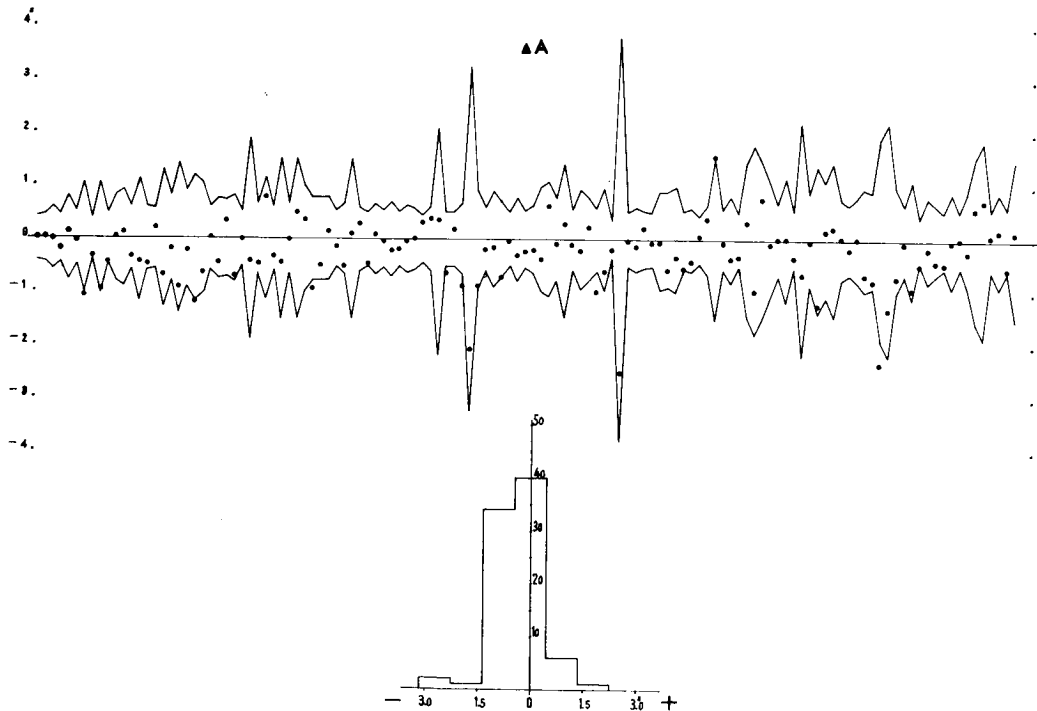


FIGURE 7.51

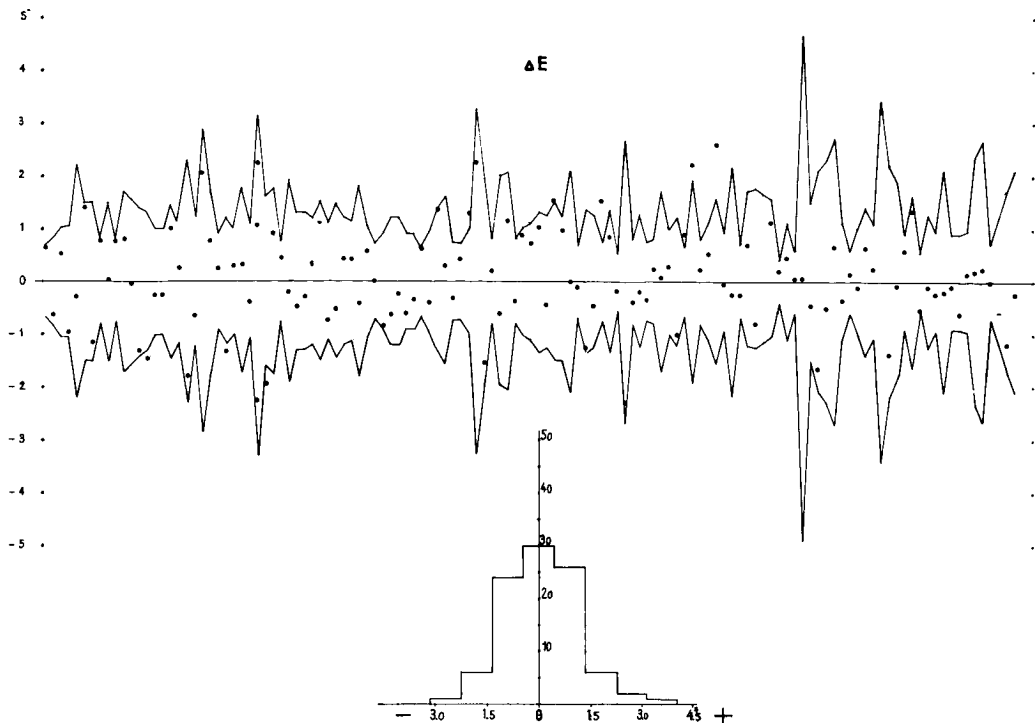


FIGURE 7.52

ment can be applied to the results of the individual line adjustments. Simple geometric considerations suggest that synchronization discrepancies will lead to larger residual errors in the spatial triangulation the larger the angle between the orbital plane of the satellite and the line to be triangulated. Because the PAGEOS satellite has an approximately polar orbit, it is sufficient to plot the mean error of unit weight after adjustment for the individual line adjustments versus the azimuth (respectively, azimuth—180 degrees) of the triangulated line. As figure 7.53 shows, the distribution of these values is circular, and no dependence on azimuth can be detected. This test at least does not indicate the influence of any synchronization errors.

An examination of the statistical distribution of the 29 104 residuals in the overall adjustment presents a further and obviously necessary opportunity to analyze the data. Figures 7.54 and 7.55 are histograms of the residuals in events that were observed from

two and three stations, respectively. In order to compare these distributions with their theoretical normal-distribution curves, the residuals would have to be normalized, requiring the computation of the covariance matrix:

$$\Sigma_v = \Sigma_\epsilon - AN^{-1}A^* \sigma_0^2 \quad (7.312)$$

This is, in the present case, a 29 104 × 29 104 completely filled, square matrix, an obvious impossibility. As a result, we are forced to neglect the geometric content of the second term of the expression (7.312) and to normalize the residuals  $v$  approximately by dividing each by the mean error of the corresponding observation before adjustment. The greater the number of observations available for the determination of the position of the satellites or, in other words, the greater the number of stations observing the satellite, the more acceptable is the proposed approximation for the normalization of the residuals. This may explain, at least in part, the fact

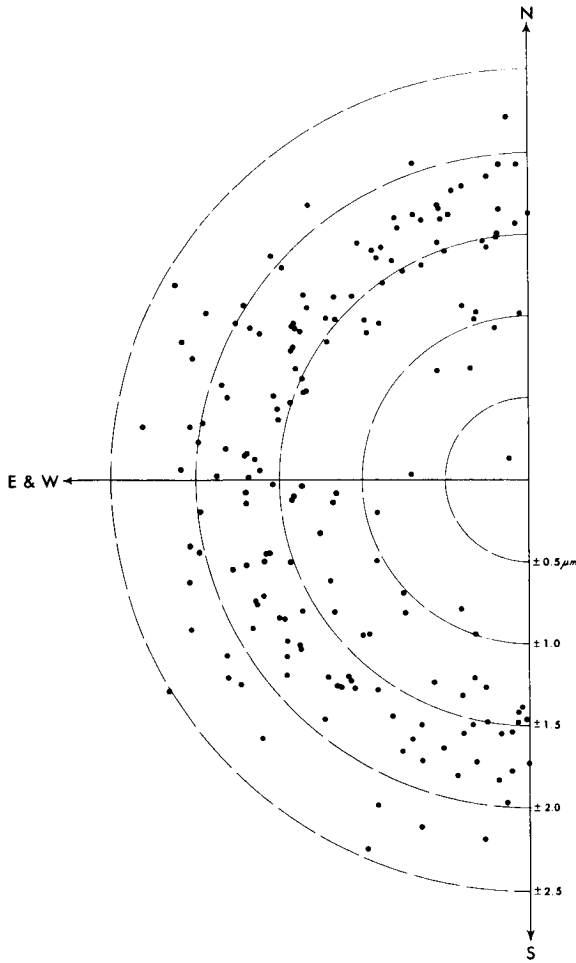


FIGURE 7.53.—Event  $\sigma$ 's versus line azimuths.

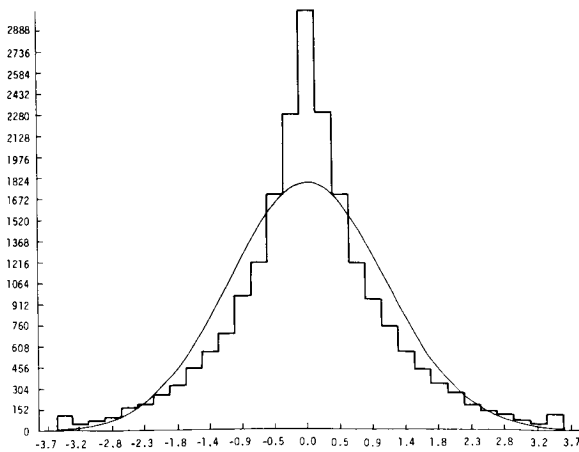


FIGURE 7.54.—Plate coordinate residuals for two-plate events.  $X+Y$  values.

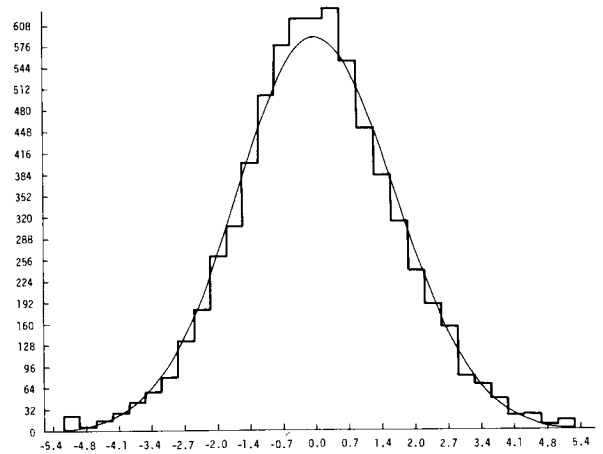


FIGURE 7.55.—Plate coordinate residuals for three-plate events.  $X+Y$  values.

that the fit of the normal curve to the histogram is better for the three-station events.

If one accepts the mean error of unit weight after adjustment as a significant measure for the inherent observational accuracy, we have mean coordinate errors for the triangulated stations as shown in figure 7.56. It should be noted that although, qualitatively, the material at all stations is uniform, the quantity varies somewhat, resulting in the variations of the coordinate errors.

### 7.5.3 A Combination Solution

Based on the principles of celestial mechanics, the interpretation of the orbital parameters of satellites as derived from time-correlated observations permits not only the determination of the parameters of a mathematical model of the Earth's gravitational field, but also the three-dimensional positions of the satellite-observing stations within a framework of coordinates referred to the Earth's mass center.

Satellite triangulation, on the other hand, is a measuring method in which the three-dimensional positions of a number of points on the Earth's surface are established by purely geometric means.

Quite generally, satellite triangulation produces coordinates for the camera stations which should, in principle, agree, except for

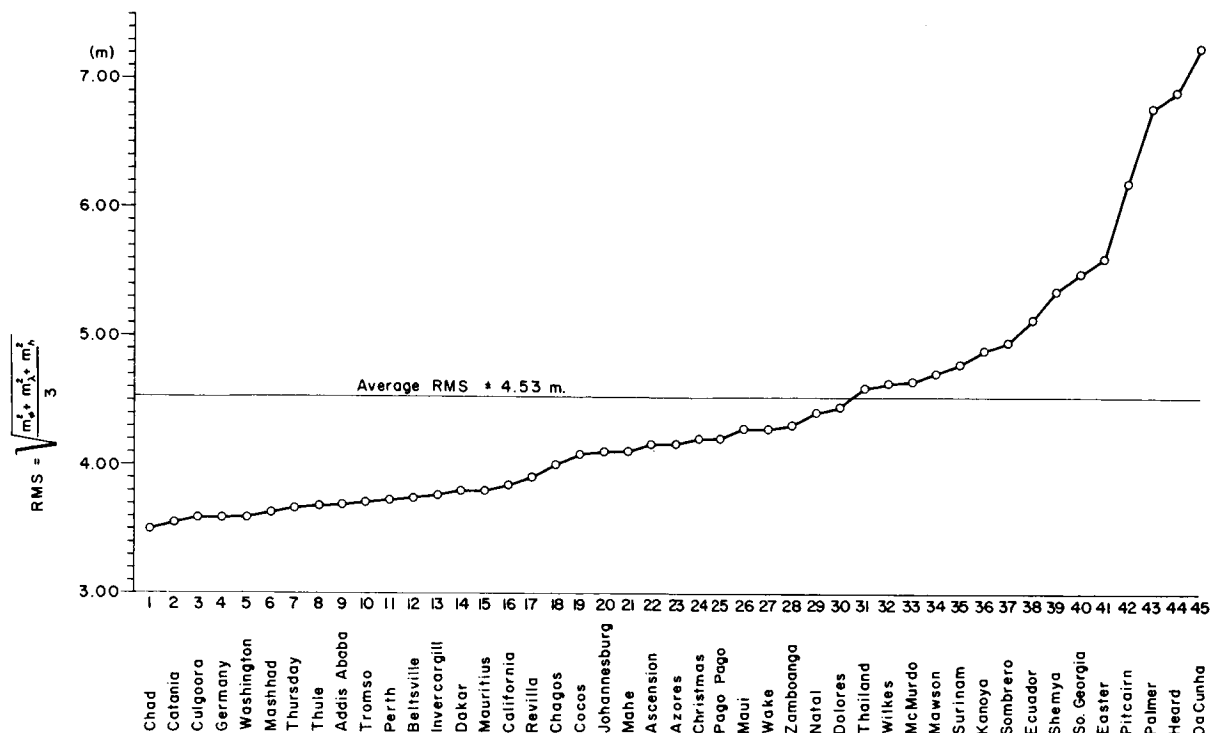


FIGURE 7.56.—Mean coordinate errors for triangulated stations.

a translation, with the corresponding results from dynamic satellite geodesy, even though the methods are completely different in conceptual approach. This difference extends as well to the determination of scale, which in geometric satellite triangulation is established by measuring the length of at least one side in the net by space traverse. In dynamic satellite geodesy the scale is determined from the physical quantity  $GM$  (gravitational constant  $\times$  mass of the earth).

The fundamental differences of the two methods provide the logical justification for the establishment of a worldwide geodetic system using both approaches, the method of dynamic satellite geodesy and the method of geometric satellite triangulation. The basic equivalence of the results with respect to spatial coordination of the observation stations suggests a comparison and combination of such solutions.

R. J. Anderle of the Naval Weapons Laboratory, Dahlgren, kindly furnished the National Geodetic Survey a list of three-

dimensional coordinates of 37 stations resulting from a dynamic solution and referred to the mass center of the Earth as origin. These stations are located in close vicinity to BC-4 stations, with the exception of five stations that are somewhat farther away. In each case, the relative positions of the two neighboring stations were determined by a local survey tie. In order to make a valid comparison of the two solutions, it is first necessary to translate the BC-4 coordinate system, which has an arbitrary origin, into the origin of the dynamic solution, the mass center, and to rotate the Doppler result about its  $z$  axis in order to make the two systems compatible with respect to longitude. However, in the comparison adjustment, two further rotations and a scale factor were modeled. These additional rotations give an indication to what extent the orientations of the conventional, pole-referenced rotation axes differ in the dynamic and the geometric solutions. Similarly, the scale factor reveals the difference in scale, which, as was pointed out

before, is derived in the one case from the product GM and in the other from the measured terrestrial baselines. The seven transformation parameters (three translations, three rotations, and a scale factor) were computed subject to a minimum condition on the sum of squares of residual coordinate differences, (in the following referred to as *xyz* fit).

The resulting mean-discrepancy vector is 14.4 m, a value which is influenced by discrepancies larger than 20 in five stations, as can be seen from the tabulation of the discrepancy vectors in table 7.14. Anderle gives for the precision of his positions the standard deviations  $\sigma_\phi = \pm 1.5$  m,  $\sigma_\lambda = \pm 1.2$  m, and  $\sigma_h = \pm 1.6$  m, resulting in a station rms of +1.44 m. Together with the average standard deviation of the BC-4 system for these stations, neglecting for this cursory consideration the influence of the standard errors of the transformation parameters, the expectation for a mean discrepancy vector is  $\pm 4.35$  m.

The difference between the actually obtained mean discrepancy vector of  $\pm 14.4$  m and the statistically expected value of  $\pm 4.35$  m shows that the two systems are not quite compatible within the range of their standard deviations.

We cite now the transformation parameters obtained in this adjustment.

Translation of BC-4 result into mass center (BC-4 +  $\Delta$  = mass centered BC-4 result) :

$$\begin{array}{lll} \Delta x = +19.590 & \Delta y = +17.684 & \Delta z = -14.344 \\ \pm 1.342 & \pm 1.325 & \pm 1.506 \end{array}$$

Rotations of Doppler data to conform to translated BC-4 results (left-handed system) :

<i>x</i> to <i>y</i>	<i>z</i> to <i>y</i>	<i>z</i> to <i>x</i>
+0°6135	+0°1478	+0°0638
±0°0451	±0°0572	±0°0563

Scale factor to be applied to original Doppler data to conform to BC-4 system scale :

$$s = 0.999\ 997\ 723\ 0 \pm 0.000\ 000\ 247\ 6$$

An adjustment with three scale factors, which was also executed :

$$\begin{array}{l} s_x = 0.999\ 997\ 389\ 3 \pm 0.000\ 000\ 356\ 0 \\ s_y = 0.999\ 997\ 092\ 3 \pm 0.000\ 000\ 369\ 2 \\ s_z = 0.999\ 998\ 972\ 0 \pm 0.000\ 000\ 439\ 7 \end{array}$$

The translation and rotation parameters were essentially the same as those obtained before.

As can be seen, the scale parameters in *x* and *y* agree with each other within the range of their standard deviations. The *z* scalar shows a significant deviation, which, however, reduces the average discrepancy vector after the *xyz* fit by only 0.9 m. Therefore the following results were based on the solution which features only one scale factor. For this solution, table 7.14 gives the remaining coordinate differences between the BC-4 system (table 7.11) plus the translation parameters and the rotated and scaled Doppler system given above. With the coordinate differences given in table 7.14 and the translations and rotations given before, it is a straightforward matter to compute backward, from the BC-4 result (table 7.11), the Doppler station data originally given. The translated BC-4 system itself represents the strictly geometric result referred to the mass center of the dynamic solutions.

The problem for a combined solution is now to average the coordinate values as obtained for the translated BC-4 system and the rotated and scaled Doppler system. In recognition that the two transformed systems differ, as expressed by a rms discrepancy vector of 14.4 m, more than three times the amount expected from the individual solution accuracy statements, a combination solution becomes a question of the weight ratio between the two solutions. To shed light on this question, the geometric satellite triangulation system was adjusted several times, introducing as constraints the transformed Doppler position coordinates for the given 37 stations with various weights. The critical evaluation of these adjustments was made in relation to the individually obtained sum of squares of the weighted residuals for

the geometric solution, a quantity which, because of its straightforward meaning, is believed to be a quite reliable indicator. Figure 7.57 shows the sum of the  $pvv$ 's versus the various weight assumptions made for the Doppler results covering a range from  $\pm 0.1$  to  $\pm 5.0$  m for each of the given Doppler-derived coordinates. On the left side is given the  $pvv$  sum as obtained from the strictly geometric solution (without any Doppler station constraint) for the one- and eight-scalar solutions mentioned earlier. The dotted line indicates the standard deviation associated with the  $pvv$  sum.

From the  $[pvv]$  curve, one can see, as was to be expected, that an essentially rigorous enforcement of the Doppler result (standard deviation of  $\pm 0.1$  m) increases the  $[pvv]$  drastically; in other words, the integrity of the geometric triangulation is impaired. On the other hand, a weighting in accordance with a standard deviation of  $\pm 5$  m results in a  $pvv$  sum identical to the one obtained from a strictly geometric adjustment using the eight scale lines as constraints.

It is now unquestionably a decision of personal preference which weighting factor for the dynamic solution to accept as defensible for a combination result, at least in the range from  $\pm 2.5$  to  $\pm 4.0$  m. On the other hand, the resulting differences in the mean station

coordinate-discrepancy vectors between these two solutions are rather small, amounting in latitude to 1.5 m, in longitude to 1.2 m, and in height to 1.6 m. In order to keep the increase in the  $[pvv]$  small, in comparison with the strictly geometric solution, a weighting in accordance with a standard deviation of  $\pm 3.5$  m for all Doppler coordinates was adopted. The solution was further constrained by the scalars, all weighted in accordance with a standard deviation of 1 part in 2 million. Table 7.15 gives the result of this adjustment and the associated standard deviations for the triangulated coordinates. Tables 7.16 and 7.17 show coordinate differences between the combined solution and the BC-4 and Doppler solutions, respectively.

The mean error of unit weight after adjustment is  $1.830 \pm 0.13 \mu\text{m}$ , the same as that for the purely geometric solution.

A comparison between the two sets of 29 104 residual errors from the purely geometric adjustment and the adjustment enforcing the Doppler results was made. These  $\Delta v$  values have a mean of  $0.001 \mu\text{m}$ . Their distribution is shown in figure 7.58. The maximum values encountered are  $-0.587 \mu\text{m}$  and  $+0.451 \mu\text{m}$ .

As a byproduct, the standard deviation for each event is computed in each triangulation adjustment. A comparison of these standard deviations between the purely geometric and the combined solution shows that the range

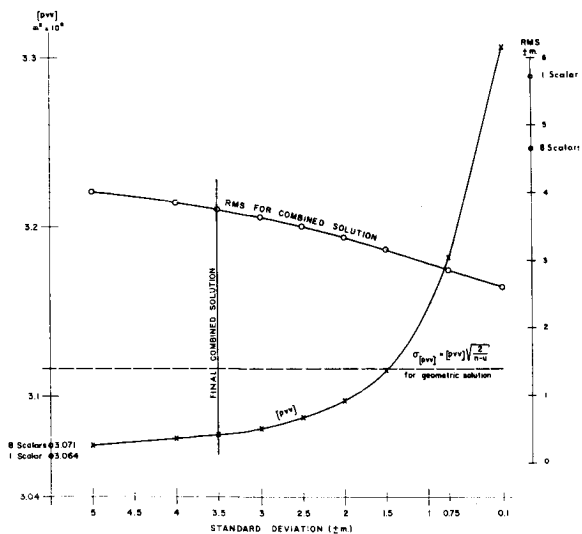


FIGURE 7.57.—Rationale for combined solution.

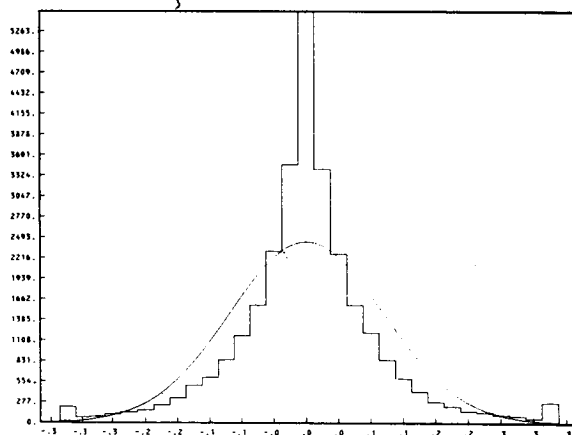


FIGURE 7.58.—Histogram of differences between two sets of residuals.

for these values in the geometric solution is from  $\pm 0.281 \mu\text{m}$  to  $\pm 3.462 \mu\text{m}$  and for the combined solution from  $\pm 0.251 \mu\text{m}$  to  $\pm 3.468 \mu\text{m}$ . The distribution of the differences of those values, which have a mean of  $-0.002 \mu\text{m}$ , is shown in figure 7.59.

This statistical information is presented to give evidence that in the combined solution no undue strain on the observational data of the geometric satellite triangulation is present.

#### 7.5.4 Derived Geodetic Parameters

The semimajor axis  $a$  and the flattening  $f$  of a reference ellipsoid may be regarded as the basic parameters for a geodetic world system, its center coinciding with the Earth's center of mass. The direction of the  $z$  axis, i.e., the Earth's rotation axis, is fixed by the conventionally adopted mean pole position at a specified epoch and the direction of the  $x$  axis through the null meridian by an identifiable point on the surface of the earth. It is also possible, although hardly practical, to postulate a triaxial ellipsoid.

With the establishment of such a reference system, the  $xyz$  coordinates of the combined solution as given in table 7.15 can be transformed into latitude, longitude, and ellipsoid height. Furthermore, classical geodetic results referred to individual datum ellipsoids can be transformed to such a world system.

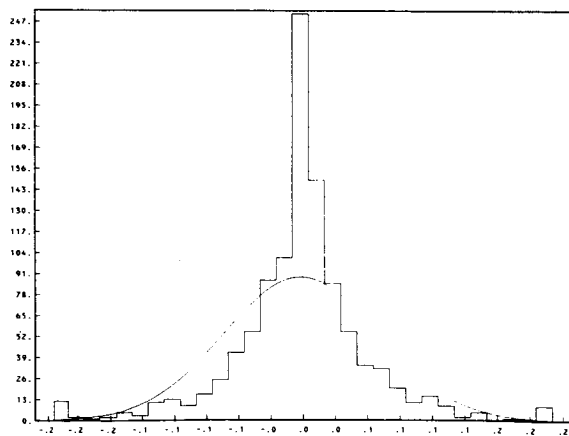


FIGURE 7.59.—Histogram of differences between two sets of event mean errors.

Using the values presented for the determination of these quantities, we arrive at the following results.

To begin with, the station coordinates obtained in the geometric satellite triangulation solution (table 7.11), reduced to sea level, were adjusted to a best-fitting ellipsoid of revolution. The significance of such a solution is somewhat dubious, in view of the fact that only 43 stations for which leveling heights were obtained are available, and that there is no a priori evidence that the mean of the corresponding geoid heights is close to zero. The result is shown in the first row of table 7.18 [left-handed coordinate system—Editor]. The resulting translations  $\Delta x$ ,  $\Delta y$ ,  $\Delta z$  on line 1, as well as those shown on lines 2, 6, 7, and 11 for other solutions, are not significant in themselves, because they depend entirely on the approximation values for the mass-centered coordinates, introduced for the origin of the geometric solution (compare beginning of sec. 7.5.1). Only their consistency in the various solutions is of interest.

The second solution is a repetition of the first, with the flattening  $f=1/298.250$  held fixed, a value which is derived by dynamic satellite-geodesy methods and is now considered to be reliable. This result is on the second line. Furthermore, ellipsoid fits were executed with the results of the combined solution resembling otherwise the solutions presented on lines 1 and 2. These results are given on lines 3 and 4, respectively. Here, as on lines 8 and 9, the  $\Delta x$ ,  $\Delta y$ ,  $\Delta z$  indicate to what extent the coordinate origin of the specific solution differs from the mass center of the dynamic solution. Still another computation was performed with the combined solution holding the original position of Anderle's mass-center fixed. In this solution, only the semimajor axis  $a$  was determined. This result is shown on line 5. With the same raw material these ellipsoid-fit solutions were repeated, incorporating the geoid heights as computed from raw data from Anderle. The corresponding results are shown on lines 6 to 10. On the eleventh line the result of the station-to-station least-

squares fit is shown, based on the matching of the positions of 37 stations as determined by the geometric and the dynamic methods.

From the information presented in table 7.18 it was concluded that a reference ellipsoid with  $1/f=298.250$  and a semimajor axis of 6 378 130 m would correspond best to the available information.

Table 7.19 gives the corresponding latitude, longitude (east), and ellipsoid heights with their respective standard deviations computed from the  $xyz$  coordinates of the combined solution (table 7.15).

In table 7.2, section 7.3, the survey data are given. A comparison of the results presented in table 7.19 with the results of astronomical position observations and the values of mean sea level observations, as given with the survey data, allows the computation of plumbline deflections and the determination of geoid heights. The corresponding results are tabulated in tables 7.20 and 7.21.

The  $\Delta\lambda$  values in table 7.20 refer, in accordance with the given geographic coordinates in table 7.19, to a system of positive east longitudes, with the conventional designation: astro-geodetic= $\Delta$ . The  $\Delta\phi$  values represent absolute position deflections in the meridian of the station, positive to the south. The computed  $\eta$  values, positive to the east, however, depend quantitatively on the chosen position of the null meridian of the combined solution. In order to average them out, an additional rotation in longitude would be necessary, which would have to be added as a constant to all longitudes tabulated in table 7.19.

Such a correction amounts to

$$\begin{aligned} \Delta\lambda &= \frac{\sum_i (\lambda_A - \lambda_G)_i \cos \phi_i}{\sum_i \cos \phi_i} \\ &= -0''.485 \text{ (east longitudes positive)} \end{aligned} \tag{7.313}$$

The significance of such a correction is, however, impaired by the relatively small number of plumbline deflections available.

Table 7.21 gives the geoid heights as computed from the combined solution (table

7.19) and the msl elevations of the survey data. For comparison, the geoid heights as obtained by Anderle from the dynamic solution are given in the second column and the corresponding differences in the third column, labeled  $\Delta N$ .

With the exception of stations 6011 (Hawaii), 6012 (Wake), 6013 (Japan), and 6043 (Sombrero), these  $\Delta$  values are well within the expected level of accuracy. Obviously, both sets of  $N$  values are also affected by the uncertainties in mean sea level for the various datums, to which the leveling data are referred.

A comparison between the  $xyz$  coordinates given in table 7.15 and the corresponding information computed from the survey data (table 7.2) results in the translations  $\Delta x$ ,  $\Delta y$ ,  $\Delta z$ . These translations transform, station by station, the survey data into a mass-centered system.

Table 7.22 shows these results, the stations grouped in terms of specific datums. Large differences in these translations for stations within a specific datum suggest distortions in such a datum.

In column  $N$  of table 7.22, the geoid height used for the computation of the station shift components is given. At stations where such information was not available from the collected survey data, the corresponding geoid heights from the combined solution (table 7.21) were used, indicated by an asterisk.

Furthermore, a set of station shift components was computed on the basis of astronomical positions of the BC-4 stations when no other survey data were available. Here again, the computations were based on geoid heights obtained from the combined solution; furthermore, an ellipsoid with  $f=1:298.25$  and an equatorial radius of 6 378 130 m were used. The resulting  $\Delta x$ ,  $\Delta y$ , and  $\Delta z$  of shifts [left-handed coordinate system—Editor] express therefore only the plumbline deflections tabulated in table 7.20.

For datums for which more than one station is available, datum shift parameters were computed, allowing for an additional scale factor and an additional rotation (in longitude) in addition to the conventional

three translations. These results are shown in table 7.23 [left-handed coordinate system—Editor]. The smaller the indicated coordinate differences, after datum shift, the more closely the survey result resembles the relative geometry as determined by satellite triangulation.

Because of the small number of stations belonging to a specific datum, it was not possible to compute meaningful datum shifts allowing an adjustment in the spatial orientation of the rotation axis of the individual datum ellipsoids, as desirable as such a test would be from the theoretical standpoint. Such a complete set of datum shift parameters will be computed for the NAD, when the results of the satellite densification program in the area of the North American continent are completed.

## 7.6 SUMMARY AND CONCLUSIONS

The BC-4 world net is the result of a strictly three-dimensional geometric triangulation, including a scale derived from classic geodetic surface measurements executed between several pairs of world net stations. Because the method of geometric satellite triangulation is based on absolute directions as obtained by interpolating the satellite position into the background of the surrounding field of fixed stars, the triangulation results can at best be only as accurate as the astronomical system of right ascension-declination itself. This situation holds for both the relative accuracy of the reference stars and the absolute accuracy of the astronomical reference system in its entirety. The photogrammetric triangulation, as a result of the high redundancy of data, should pro-

vide a result valid to about 1 part in 2 million in terms of the average station to satellite distance, in other words, station positions with an accuracy of  $\pm 3$  to  $\pm 4$  m in all three coordinates. The statistical information obtained as a by-product of the various data reduction steps indicates that the accuracy of the final result does not entirely fulfill the theoretical accuracy expectations. The statistically proven instability of the BC-4 camera system must be considered as a possible source of a slight systematic error, which in the adjustment algorithm is unavoidably distributed in accordance with the minimum principle for residual errors. The good agreement of the photogrammetric triangulation result with the measured baselines around the world indicates, however, that the final result is essentially free of significant bias errors. A comparison between the result of the geometric triangulation and the corresponding result obtained by dynamic satellite geodesy from Doppler data, as computed by the Navy, shows excellent agreement in an overall sense, but significant discrepancies in a few places on the globe. A combination of both results that respects fully the covariance of the photogrammetrically derived directions becomes possible by assuming a weighting of the dynamically determined coordinates in accordance with a station position mean error of  $\pm 3.5$  m. The only significant difference between the Navy-8D dynamically determined result and the geometric triangulation is in terms of scale, indicating that the dynamic solution is based on a scale larger by 2 parts in a million. The geometric solution suggests a value of 6 378 130 m for the equatorial radius  $a$  of a best-fitting ellipsoid.

## APPENDIX

TABLE 7.1

Images per second	Shutter speed (100% efficiency) (sec)	Optimal subdivision with third shutter	Accuracy of timing ( $10^{-6}$ sec)
20	1/120		$\pm 20$
10	1/60	:2, :3, :4, :5	$\pm 40$
5	1/30		$\pm 60$
2.5	1/15		$\pm 70$

TABLE 7.2.—Survey Coordinates of BC-4 Stations

BC-4 sta. no.	Station name	Geodetic coordinates		Astronomic coordinates		Elev. of ref. pt. above MSL (m)	N (m)	Datum	Ellipsoid
		$\phi_G$	$\lambda_G$ (west)	$\phi_A$	$\lambda_A$ (west)				
6001	Thule	76°30'05".3226N	68°32'33".1709	76°30'11".67N	68°32'48".91	206.0	+32.0	QORNOQ	Int'l.
6002	Beltsville	39°01'39".003N	76°49'33".058	39°01'37".73N	76°49'24".65	44.3	-0.4	NAD 1927	Clarke 1866
6003	Moses Lake	47°11'07".1324N	119°20'11".8815	47°11'03".24N	119°20'17".05	368.74	-16.0	NAD 1927	Clarke 1866
6004	Shemya	52°42'54".8940N	185°52'22".1299	52°43'03".48N	185°52'15".08	36.76	-46.0	NAD 1927	Clarke 1866
6006	Tromso	69°39'44".2901N	341°03'27".6743	69°39'43".24N	341°03'12".96	106.0	+12.6	European	Int'l.
6007	Azores	38°45'36".7250N	27°05'38".9360	38°45'43".28N	27°05'24".59	53.26	-----	S. W. Base	Int'l.
6008	Surinam	05°27'04".9824N	55°12'13".9921	05°26'48".96N	55°12'21".21	18.38	+3.0	Prov. S.A. 1956	Int'l.
6009	Quito	00°05'50".4680S	78°25'10".7875	00°05'53".09S	78°25'03".09	2682.1	+24.6	S.A.D. 1969	S.A.
6011	Maui	20°42'38".5610N	158°15'31".4711	20°42'21".86N	156°15'22".95	3049.27	-----	Old Hawaiian	Clarke 1866
6012	Wake	19°17'23".2275N	193°23'20".2197	19°17'24".40N	193°23'34".82	3.46	-----	1952 Astro	Int'l.
6013	Kanoya	31°23'30".13971N	229°07'35".14051	31°23'38".48N	229°07'34".29	65.90	+27.0	Tokyo	Bessel.
6015	Mashad	36°14'29".5269N	300°22'17".2712	36°14'27".82N	300°21'59".20	991.05	-38.0	Europe 1950	Int'l.
6016	Catania	37°26'42".3451N	344°57'12".3041	37°26'38".70N	344°56'56".81	9.00	-16.6	European	Int'l.
6019	Villa Dolores	31°56'33".9540S	65°06'18".658	-----	-----	608.18	+13.0	S.A.D. 1969	S.A.
6020	Easter Isl.	27°10'39".2132S	109°25'42".5051	27°10'39".21S	109°25'42".51	230.8	-----	1967 Astro.	Int'l.
6022	Pago Pago	14°20'12".216S	170°42'46".758	14°20'08".34S	170°42'52".15	5.34	+22.0	Am. Samoa 1962	Clarke 1866
6023	Thursday Isl.	10°35'08".0374S	217°47'24".5045	10°35'06".78S	217°47'25".11	59.6	-4.6	AND	AND
6031	Invercargill	46°25'03".4908S	191°40'28".8448	46°25'01".05S	191°40'25".10	0.95	-----	Geodetic 1949	Int'l.
6032	Perth	31°50'28".9922S	244°01'33".3824	31°50'24".57S	244°01'56".28	26.30	+15.4	AND	AND
6038	Revilla	18°43'44".93N	110°57'20".72	18°43'44".93N	110°57'20".72	23.20	-----	Is. Soc. Astro.	Clarke 1866
6039	Pitcairn	25°04'07".1461S	130°06'48".1184	25°04'07".15S	130°06'48".12	339.39	-----	1967 Pitcairn Astro.	Int'l.
6040	Cocos	-----	-----	12°11'57".91S	263°10'12".92	4.41	-----	1965 Anna 1 Astro	AND
6042	Addis Ababa	08°46'08".5013N	321°00'10".8355	08°46'05".74N	321°00'02".81	1886.46	-8.0	Adindan	Clarke 1880
6043	Cerro Sombrero	52°46'52".4683S	69°13'30".4273	52°46'50".74S	69°13'33".56	80.66	-----	1963 Prov. South Chile	Int'l.
6044	Heard Isl.	-----	-----	53°01'12".0309S	286°36'32".5846	3.771	-----	1969 Astro	Int'l.
6045	Mauritius	20°13'41".942S	302°34'52".339	20°13'37".48S	302°35'07".20	138.2	-----	Le Ponce Astro	Clarke 1880
6047	Zamboanga	06°55'26".132N	237°55'55".162	06°55'18".29N	237°55'53".55	9.391	-----	Luzon	Clarke 1886
6050	Palmer	-----	-----	64°46'33".98S	64°03'22".96	16.44	-----	1969 Palmer Astro	Clarke 1880
6051	Mawson	-----	-----	67°36'03".08S	297°07'35".59	11.3	-----	1969 Astro	-----
6052	Wilkes (Casey)	-----	-----	66°16'45".12S	249°27'55".39	18.0	-----	1969 Astro	-----
6053	McMurdo	77°50'46".2487S	193°21'52".4155	77°50'43".32S	193°21'46".14	19.09	-----	Camp Area Astro 1961-62 USGS	Int'l.
6055	Ascension	07°58'16".6342S	14°24'27".2363	07°58'18".27S	14°24'30".36	70.94	-----	Ascension Is. 1958	Int'l.
6059	Christmas Isl.	-----	-----	02°00'35".622N	157°24'38".038	2.75	-----	Christmas Is. 1967 Astro	Int'l.
6060	Culgoora	30°18'39".4182S	210°26'23".1079	30°18'36".14S	210°26'28".89	211.1	+0.7	AND	AND
6061	So. Georgia Isl.	-----	-----	54°16'39".5147S	36°29'17".4690	4.180	-----	Astro	Int'l.
6063	Dakar	14°44'39".8986N	17°28'57".5476	14°44'44".23N	17°29'04".41	26.28	+20.7	Adindan	Clarke 1880
6064	Ft. Lamy	12°07'51".7410N	344°57'53".7659	12°07'53".939N	344°57'51".044	295.41	+23.6	Adindan	Clarke 1880
6065	Hohenpeissenb.	47°48'07".009N	348°58'31".4263	47°48'09".54N	348°58'29".47	943.50	-0.6	European	Int'l.
6067	Natal	05°55'37".4136S	35°09'53".8003	05°55'37".74S	35°09'57".03	40.63	+26.14	S.A. 1969	S.A.
6068	Johannesburg	25°52'56".98S	332°17'34".83	25°52'50".06S	332°17'28".82	1523.8	-----	Buffelsfont	Clarke 1880
6069	Tristan	-----	-----	37°03'26".2572S	12°19'06".4452	24.83	-----	1968 Astro	Int'l.
6072	Chieng Mai	18°46'06".149N	261°01'44".877	18°45'47".50N	261°01'51".62	308.4	-----	Indian	Everest
6073	Diego Garcia	07°20'58".5270S	287°31'27".8444	7°20'58".53S	287°31'27".84	3.85	-----	I.S.T.S. 1969 Astro	Int'l.
6075	Mahé	04°40'11".614S	304°31'06".617	4°40'10".31S	304°31'06".02	588.98	-----	Mahé 1971	Clarke 1880
6111	Wrightwood	34°22'54".5368N	117°40'50".5161	34°23'00".80N	117°40'35".38	2284.41	-23.0	NAD 1927	Clarke 1866

TABLE 7.3.—*Baselines Used in Adjustment*

Stations between which scalars were measured	Spatial distances (m)	$\sigma_a$ (m)
6002-6003	3 485 363.232	$\pm 3.53$
6003-6111	1 425 876.452	$\pm 1.59$
6006-6065	2 457 765.810	$\pm 0.80$
6065-6016	1 194 793.601	$\pm 1.43$
<sup>a</sup> 6006-6016	3 545 871.454	$\pm 1.64$
6023-6060	2 300 209.803	$\pm 0.88$
6032-6060	3 163 623.866	$\pm 0.98$
6063-6064	3 485 550.755	$\pm 2.10$

<sup>a</sup> The scalar 6006-6016 is not a truly independent scalar.

TABLE 7.4.—*Documentation*<sup>a</sup>

Scalar between stations <sup>b</sup>	Measured by:	Computed by:	Documentation
002-003 and 003-111	National Geodetic Survey (USA)	National Geodetic Survey Triangulation Branch (USA)	Office memos from NGS Triangulation Br. to Geodetic Research & Development Lab. for 002-003—B. K. Meade dated 3/29/71, for 003-111 John G. Gergen dated 8/5/73.
006-065 065-016 006-016	Geodetic Agencies of Norway Sweden Denmark Federal German Republic Austria Italy	National Geodetic Survey (USA) Triangulation Branch	Office memo from NGS Triangulation Br. to GRDL—B. K. Meade dated 4/9/70. Office memo from NGS, New Datum Br. to GRDL—John G. Gergen dated 8/5/73. Further reference literature, the results of which were not used here: Computation of the European Baseline Tromsø-Catania by R. Kube and K. Schnädelbach, Deutsches Geodätisches Forschungsinstitut, München (1973).
023-060 032-060	Dept. of National Development Div. of National Mapping, Australia	Division of National Mapping, Australia	Dept. of National Development, Div. of National Mapping, Australia Technical Report No. 11 by K. Leppert, Canberra, Australia, March 1972, entitled "Two Australian Baselines for the Pageos World Triangulation."
063-064	Dept. of Defense, Defense Mapping Agency and Institutue Geographique Nationale (France)	Dept. of Army Commanding Officer US Army Engineer Topographic Production Center Code 14400 Army Topographic Stations Wash., DC 20315	Transmittal letters to Dr. H. H. Schmid, GRDL, NGS, NOAA, Rockville, Md. 20852 USA dated June 4, 1971, and July 22, 1971.

<sup>a</sup> The measuring and computation of these scalars were executed by various national agencies. For reference, the above information is given.

<sup>b</sup> Add 6000 to station numbers.

TABLE 7.5.—*Number of Successful Observations<sup>a</sup>*

Station-to-station line <sup>b</sup>	Number of successful events		Station-to-station line <sup>b</sup>	Number of successful events	
	L	R		L	R
1 to 2	7	16	11 to 22	1	2
3	9	18	38	13	2
4	4	2	59	21	21
6	17	15	12	4	20
7	5	1	111	15	5
°11	0	1	12 to 13	1	11
°15	1	0	22	2	5
°16	2	1	23	7	9
°38	1	2	59	9	2
°65	3	6	°60	1	0
2 to 3	14	19	°13 to 15	2	0
°6	1	1	23	0	0
7	4	5	47	8	5
8	16	8	72	4	1
9	3	3	15 to 16	31	37
38	4	10	°40	7	3
111	6	11	42	28	15
3 to 4	0	4	°45	9	1
11	7	16	°64	2	12
38	7	13	65	0	5
°12	0	2	72	4	10
111	24	20	73	12	7
°4 to 6	0	2	75	11	1
11	0	3	16 to 42	5	0
13	5	5	63	0	13
12	0	8	64	22	9
6 to 7	2	4	65	7	12
15	9	7	19 to 20	7	2
16	9	13	43	19	30
65	5	8	61	4	14
7 to 8	0	0	67	6	9
16	18	11	°69	0	2
°55	0	2	20 to 38	11	2
63	23	7	39	1	2
°64	3	1	43	4	11
65	6	0	22 to 23	2	3
°67	2	2	31	14	4
8 to 9	7	1	39	2	5
19	7	15	59	9	10
°61	0	1	60	15	4
63	0	1	78	0	3
67	2	3	°23 to 31	2	8
9 to 19	4	12	32	19	4
20	2	3	°40	1	1
38	4	6	47	6	3
°43	2	2			

TABLE 7.5.—(Cont'd)

Station-to-station line <sup>b</sup>	Number of successful events		Station-to-station line <sup>b</sup>	Number of successful events	
	L	R		L	R
°23 to 60	20	32	44 to 45	1	1
°72	0	4	51	3	4
78	6	1	52	1	1
			68	1	0
°31 to 32	10	10	°45 to 51	2	5
39	3	0	68	13	7
°51	0	1	73	13	18
52	6	4	75	22	11
53	10	12			
°59	0	1	°47 to 60	0	2
60	31	25	72	5	11
78	2	2	°78	1	0
			50 to 51	0	1
32 to 40	26	6	°52	2	0
44	4	4	53	4	0
°45	4	0	61	2	7
47	9	4			
°51	5	0	51 to 52	18	19
52	5	5	53	13	11
°53	1	1	61	5	1
60	17	39	68	8	12
°72	0	1			
			52 to 53	15	13
38 to 39	3	2	60	2	6
59	1	5			
111	3	8	°53 to 60	3	8
			°61	1	0
39 to 59	6	2			
			55 to 63	21	8
40 to 44	2	0	64	7	8
45	26	8	67	13	7
47	4	3	68	0	2
°60	0	3	69	6	4
72	1	4			
73	9	4	61 to 67	3	0
°75	6	2	68	1	2
			69	2	2
°42 to 45	7	8			
64	16	4	63 to 64	9	5
68	8	30	67	10	3
°73	6	0	°69	0	2
75	2	15			
			64 to 68	3	25
43 to 50	3	8	67 to 69	1	0
61	4	9			
			68 to 69	4	0
			75	0	3

<sup>a</sup> For station positions compare figure 7.8.

<sup>b</sup> Add 6 000 to all numbers

<sup>c</sup> Skip lines.

TABLE 7.6.—*Partial Derivatives of F and G With Respect to u*

$u$	$\alpha \ \omega \ \kappa \ X_0 \ Y_0 \ Z_0 \ c_x \ c_y \ x_0 \ y_0 \ X \ Y \ Z \ K_1 \ K_2 \ K_3 \ x \ y \ K_4 \ K_5 \ \phi \ \epsilon \ l_x \ l_y$
$\frac{\partial F}{\partial u}$	$A_x \ B_x \ C_x \ D_x \ E_x \ F_x \ G_x \ -H_x \ I_x \ J_x \ K_x \ L_x \ M_x \ N_x \ O_x \ P_x \ Q_x \ R_x \ S_x \ T_x \ U_x \ Z_x \ -$
$\frac{\partial G}{\partial u}$	$A_y \ B_y \ C_y \ D_y \ E_y \ F_y \ -G_y \ H_y \ I_y \ J_y \ K_y \ L_y \ M_y \ N_y \ O_y \ P_y \ Q_y \ R_y \ S_y \ T_y \ U_y \ -Z_y$

TABLE 7.7.—*Curve Fit of 380 Fictitious Satellite Images With Polynomials of Degree 1 Through 11 (x in Direction of the Trail, y Normal to It)*

	Degree of polynomial <sup>a</sup>	$\sigma_x$ [ $\mu m$ ]	$\sigma_y$ [ $\mu m$ ]		$\sigma_x$ [ $\mu m$ ]	$\sigma_y$ [ $\mu m$ ]
Observation sta. 1	1	404 166	215 720	Observation sta. 4	494 437	57 121
	2	53 445	1 853		53 362	0 209
	3	1 267	0 289		1 571	0 039
	4	0 090	0 006		0 099	0 000
	5	0 003	0 001		0 004	0 000
	6	0 000	0 000		0 000	0 000
Observation sta. 2	1	461 861	133 736	Observation sta. 5	356 618	82 163
	2	54 919	0 964		51 751	0 223
	3	1 479	0 166		1 116	0 077
	4	0 099	0 004		0 085	0 001
	5	0 004	0 000		0 003	0 000
	6	0 000	0 000		0 000	0 000
Observation sta. 3	1	226 233	169 385	Observation sta. 6	145 585	157 387
	2	50 510	0 229		48 951	0 476
	3	0 709	0 204		0 458	0 184
	4	0 076	0 002		0 070	0 000
	5	0 002	0 000		0 001	0 000
	6	0 000	0 000		0 000	0 000

<sup>a</sup> For polynomials of seventh to eleventh degree all entries are zero, as they are for the sixth degree.

TABLE 7.8

Seq. no.	Observ. sta. no. <sup>a</sup>	No. of processed plates
1	2	1
2	3	1
3	7	3
4	8	17
5	9	17
6	11	10
7	12	14
8	15	3
9	16	4
10	19	39
11	20	1
12	22	5
13	23	2
14	31	16
15	38	10
16	39	2
17	42	14
18	43	23
19	44	2
20	45	7
21	50	17
22	51	29
23	52	20
24	53	24
25	55	32
26	59	15
27	60	10
28	61	33
29	63	25
30	64	29
31	67	25
32	68	29
33	69	17
34	73	2
35	75	2
Sum:		500

<sup>a</sup> Add 6000 to station numbers.

TABLE 7.9

Photogrammetric camera: Wild BC-4. lens: Cosmotar  $f = 450\text{mm}$ , aperture 132mm  
 Target: PAGEOS balloon satellite for 496 photograms and ECHO satellite for 4 photograms  
 Program: World Net  
 Period of observation: October 1966-September 1969  
 Observation material: 500 selected photograms with corresponding time recordings from 35 stations in the World Net

	(1) Type of imagery	(2) Mean errors of comparator measurements $m_1$ ( $\mu\text{m}$ )	(3) Assumed mean of irregular emulsion shift ( $\mu\text{m}$ )	(4) Average of mean shimmer		(5) Mean coordinate error after adjustment in photogrammetric bundle simulation $[(2)^2 + (3)^2 + (4)^2]^{1/2}$ ( $m_1$ )( $\mu\text{m}$ )	(6) Introduced mean error of reduced star catalog data ( $\mu\text{m}$ )	(7) Total noise in photogrammetric bundle simulation adjustment		(8) Mean error of polynomial smoothing $[(2)^2 + (3)^2 + (4)^2]^{1/2}$ ( $\mu\text{m}$ )
				( $\mu\text{m}$ )	( $''$ )			( $\mu\text{m}$ )	( $''$ )	
Average values	<i>a</i> Stars	$\pm 1.81$	$\pm 1.00$	$\pm 2.58$	$\pm 1.18$	$\pm 3.31$	$\pm 0.87$	$\pm 3.42$	$\pm 1.57$	-----
	<i>b</i> Satellite	$\pm 1.79$	$\pm 1.00$	$\pm 2.86$	$\pm 1.31$	-----	-----	-----	-----	$\pm 1.61$
Minimal values	<i>c</i> Stars	$\pm 0.97$	$\pm 1.00$	$\pm 1.01$	$\pm 0.46$	$\pm 1.88$	$\pm 0.87$	$\pm 1.93$	$\pm 0.88$	-----
	<i>d</i> Satellite	$\pm 0.87$	$\pm 1.00$	$\pm 1.07$	$\pm 0.47$	-----	-----	-----	-----	$\pm 1.46$
Maximal values	<i>e</i> Stars	$\pm 2.45$	$\pm 1.00$	$\pm 6.46$	$\pm 2.96$	$\pm 6.87$	$\pm 0.87$	$\pm 7.03$	$\pm 3.22$	-----
	<i>f</i> Satellite	$\pm 2.68$	$\pm 1.00$	$\pm 6.84$	$\pm 3.14$	-----	-----	-----	-----	$\pm 8.96$

TABLE 7.10

Image coordinates										
$x$ (mm)/ $y$ (mm)	-----	0/0	10/10	20/20	30/30	40/40	50/50	60/60	70/70	
Mean accuracy of direction	-----	$\pm 0'23$	$\pm 0'25$	$\pm 0'23$	$\pm 0'19$	$\pm 0'21$	$\pm 0'25$	$\pm 0'44$	$\pm 2'77$	

TABLE 7.11.—*Three-Dimensional Cartesian Coordinates*

No.	Station name	X (m)	$\sigma_x$ $\pm$ (m)	Y (m)	$\sigma_y$ $\pm$ (m)	Z (m)	$\sigma_z$ $\pm$ (m)
6001	Thule	546 567.862	2.297	-1 389 990.609	3.447	6 180 239.602	3.960
6002	Beltsville	1 130 761.500	0	-4 830 828.597	0	3 994 704.584	0
6003	Moses Lake	-2 127 833.613	.790	-3 785 861.054	2.976	4 656 034.740	2.906
6004	Shemya	-3 851 782.861	4.888	+396 404.016	5.654	5 051 347.586	6.673
6006	Tromso	2 102 925.118	3.663	+721 667.562	4.772	5 958 188.868	4.748
6007	Azores	4 433 636.070	4.737	-2 268 143.467	4.362	3 971 656.223	4.945
6008	Surinam	3 623 227.823	4.563	-5 214 231.698	4.502	601 551.302	5.716
6009	Quito	1 280 815.597	4.338	-6 250 955.436	5.800	-10 793.013	5.717
6011	Maui	-5 466 020.732	5.045	-2 404 435.198	4.352	2 242 229.885	4.703
6012	Wake	-5 858 543.398	5.308	+1 394 489.166	5.281	2 093 807.584	5.391
6013	Kanoya	-3 565 865.509	5.200	+4 120 692.866	6.694	3 303 428.249	6.131
6015	Mashhad	2 604 346.389	3.988	+4 444 141.147	5.513	3 750 323.381	4.974
6016	Catania	4 896 383.234	4.080	+1 316 167.822	4.463	3 856 673.791	4.698
6019	Dolores	2 280 603.832	4.190	-4 914 545.588	4.789	-3 355 412.286	6.839
6020	Easter	-1 888 616.886	4.845	-5 354 892.780	6.246	-2 895 739.444	7.217
6022	Pago Pago	-6 099 954.446	5.392	-997 367.321	4.710	-1 568 567.088	5.883
6023	Thursday Is.	-4 955 371.694	4.671	+3 842 221.799	5.689	-1 163 828.451	5.852
6031	Invercargill	-4 313 815.856	4.687	+891 322.098	5.238	-4 597 238.676	6.398
6032	Perth	-2 375 397.874	4.579	+4 875 524.035	5.746	-3 345 372.936	6.170
6038	Revilla	-2 160 983.561	2.008	-5 642 711.612	3.653	2 035 371.417	4.062
6039	Pitcairn	-3 724 766.403	6.502	-4 421 236.249	6.480	-2 686 072.609	7.288
6040	Cocos	-741 969.205	4.859	+6 190 770.789	6.606	-1 338 530.638	5.843
6042	Addis Ababa	4 900 734.926	4.844	+3 968 226.427	5.481	966 347.675	5.103
6043	Sombrero	1 371 358.188	4.171	-3 614 760.271	4.969	-5 055 928.396	8.156
6044	Heard	1 098 896.432	6.448	+3 684 591.597	7.801	-5 071 838.356	9.919
6045	Mauritius	3 223 422.870	4.472	+5 045 312.452	6.019	-2 191 780.736	6.065
6047	Zamboanga	-3 361 946.845	4.909	+5 365 778.338	6.501	763 644.128	6.121
6050	Palmer	1 192 659.730	5.174	-2 450 995.361	7.275	-5 747 040.896	10.171
6051	Mawson	1 111 335.585	5.189	+2 169 243.189	5.456	-5 874 307.692	8.002
6052	Wilkes	-902 598.435	4.912	+2 409 507.607	5.700	-5 816 527.805	7.901
6053	McMurdo	-1 310 841.759	4.993	+3 111 248.105	5.500	-6 213 251.231	7.886
6055	Ascension	6 118 325.238	5.260	-1 571 746.070	4.816	-878 595.457	5.507
6059	Christmas	-5 885 331.078	5.213	-2 448 376.867	4.435	221 683.837	5.446
6060	Culgoora	-4 751 637.577	4.552	+2 792 039.266	5.653	-3 200 142.319	5.866
6061	So. Georgia	2 999 903.036	4.896	-2 219 368.228	6.055	-5 155 246.454	8.547
6063	Dakar	5 884 457.561	4.898	-1 853 492.773	4.257	1 612 863.206	5.072
6064	Chad	6 023 375.533	4.690	+1 617 924.383	4.242	1 331 742.422	4.834
6065	Hohenpeissenberg	4 213 552.554	3.730	+820 823.968	4.444	4 702 787.513	4.620
6067	Natal	5 186 398.560	5.260	-3 653 936.203	4.854	-654 277.651	5.569
6068	Johannesburg	5 084 812.984	5.229	+2 670 319.559	5.065	-2 768 065.639	6.586
6069	De Cunha	4 978 412.958	8.167	-1 086 867.619	6.918	-3 823 159.761	9.443
6072	Thailand	-941 692.348	5.593	+5 967 416.884	6.919	2 039 317.530	5.461
6073	Chagos	1 905 130.320	4.345	+6 032 252.624	6.702	-810 711.562	5.751
6075	Mahe	3 602 810.169	4.910	+5 238 217.287	6.393	-515 928.653	5.650
6111	Wrightwood	-2 448 854.721	2.088	-4 667 988.213	3.367	3 582 758.969	3.185

TABLE 7.12

Scalar <sup>a</sup>	$\Delta d =$ meas. - comp. (m)	$\sigma$ of scalar as obtained from the triang. adjust. (m)
002-003	0	0 held fixed
003-111	-7.3	$\pm 2.8$
006-065	<sup>b</sup> -2.0	$\pm 4.9$
065-016	+9.3	$\pm 5.1$
023-060	+5.8	$\pm 3.9$
032-060	+8.5	$\pm 4.6$
063-064	-5.1	$\pm 5.2$
Sum	+9.2	$\pm 15.6$ ( $\sigma$ of $\Sigma d$ )

<sup>a</sup> Add 6000 to station numbers.

<sup>b</sup> The German Geodetic Research Institute gives, for the baseline 006-065, a value which is 1.9 m larger than the one used here. The corresponding  $\Delta$  values would then be only one decimeter.

TABLE 7.13

Scalar <sup>a</sup>	Assumed mean error (m)	Correction from the adjustment (m)
2-3	$\pm 1.75$	-0.06
3-111	$\pm 0.72$	+1.50
6-16	$\pm 1.78$	-0.26
6-65	$\pm 1.23$	+0.10
16-65	$\pm 0.60$	+0.42
23-60	$\pm 1.15$	-0.98
32-60	$\pm 1.58$	-2.76
63-64	$\pm 1.75$	+2.60

<sup>a</sup> Add 6000 to station numbers.

TABLE 7.14.—Coordinate Differences Between Transformed Doppler Solution and Translated BC-4 Solution After XYZ Fit ( $\Delta = BC-4 - \text{Doppler}$ )

No. <sup>a</sup>	Station name	$\Delta\phi$ (m)	$\Delta\lambda$ (m)	$\Delta h$ (m)	Resultant (m)
1	Thule .....	10.198	-2.216	10.464	14.779
2	Beltsville .....	-1.254	1.201	-4.516	4.839
3	Moses Lake .....	-3.072	5.628	-3.670	7.388
4	Shemya .....	5.711	13.780	15.061	21.198
6	Tromso .....	-1.451	-17.014	7.566	18.677
7	Azores .....	-10.097	-5.716	4.377	12.401
8	Surinam .....	.002	1.959	-8.694	8.912
9	Quito .....	6.507	10.573	-7.272	14.388
11	Maui .....	4.162	-2.037	8.789	9.935
12	Wake .....	-14.550	-10.924	-24.453	30.479
13	Kanoya .....	6.458	.116	3.956	7.574
15	Mashhad .....	3.600	4.048	1.256	5.561
16	Catania .....	1.740	-1.638	3.341	4.107
19	Dolores .....	-18.425	15.163	-4.296	24.245
20	Easter .....	7.924	13.930	3.152	16.333
22	Pago Pago .....	4.227	-6.107	-5.317	9.134
23	Thursday .....	-1.735	-7.291	-15.435	17.159
31	Invercargill .....	-7.362	-9.689	-5.584	13.389
32	Perth .....	3.261	.162	.665	3.332
38	Revilla .....	-5.298	.445	3.129	6.169
40	Cocos .....	3.360	.864	2.135	4.073
42	Addis Ababa .....	14.086	-1.952	5.724	15.329
43	Sombrero .....	-20.140	3.173	24.247	31.680
45	Mauritius .....	3.838	5.642	1.044	6.903
47	Zamboanga .....	3.162	3.466	-9.571	10.659
50	Palmer .....	-19.872	-5.176	12.703	24.147
53	McMurdo .....	-18.103	-1.576	-4.321	18.678
55	Ascension .....	-7.126	-10.677	.245	12.838
59	Christmas .....	4.404	-4.747	-4.207	7.722
60	Culgoora .....	-12.420	-9.048	-2.916	15.641
63	Dakar .....	.998	5.593	.304	5.690
64	Chad .....	5.889	2.226	5.226	8.182
65	Hohenpeissenberg .....	5.497	-8.304	6.434	11.856
67	Natal .....	-10.375	-5.277	3.692	12.212
68	Johannesburg .....	1.352	2.525	-8.008	8.504
72	Thailand .....	3.350	6.659	-8.712	11.466
75	Mahe .....	8.413	.122	-6.102	10.394
	rms values	$\pm 8.916$	$\pm 7.179$	$\pm 8.697$	$\pm 14.376$

<sup>a</sup> Add 6000 to station numbers.

TABLE 7.15.—*Three-Dimensional Cartesian Coordinates From Combined Final Solution*

No. <sup>a</sup>	Station name	X (m)	$\sigma_x$ ± (m)	Y (m)	$\sigma_y$ ± (m)	Z (m)	$\sigma_z$ ± (m)
1	Thule	546 588.043	2.524	-1 389 976.770	2.442	6 180 221.157	3.191
2	Beltsville	1 130 783.206	2.464	-4 830 812.170	2.853	3 994 691.260	2.979
3	Moses Lake	-2 127 810.402	2.337	-3 785 844.188	2.610	4 656 021.673	2.896
4	Shemya	-3 851 759.714	3.610	396 416.742	3.622	5 051 324.861	4.235
6	Tromso	2 102 943.362	2.365	721 679.260	2.697	5 958 170.871	3.090
7	Azores	4 433 652.575	3.091	-2 268 128.968	2.686	3 971 641.629	3.327
8	Surinam	3 623 251.037	3.166	-5 214 216.431	3.288	601 536.293	3.489
9	Quito	1 280 842.366	3.158	-6 250 939.190	3.947	-10 807.932	3.487
11	Maui	-5 466 002.263	3.288	-2 404 414.762	2.767	2 242 214.785	3.235
12	Wake	-5 858 531.333	3.287	1 394 513.654	2.966	2 093 798.651	3.211
13	Kanoya	-3 565 848.055	3.138	4 120 713.101	3.636	3 303 409.134	3.581
15	Mashhad	2 604 363.535	2.345	4 444 158.701	2.711	3 750 306.588	2.712
16	Catania	4 896 401.374	2.357	1 316 181.910	2.316	3 856 657.080	2.572
19	Dolores	2 280 628.090	2.674	-4 914 528.492	2.950	-3 355 416.607	3.163
20	Easter	-1 888 587.555	3.790	-5 354 875.392	3.952	-2 895 751.980	3.784
22	Pago Pago	-6 099 939.342	3.122	-997 345.983	2.730	-1 568 582.700	3.208
23	Thursday Is.	-4 955 355.561	2.613	3 842 245.988	2.427	-1 163 843.516	2.534
31	Invercargill	-4 313 799.508	2.680	891 345.724	2.588	-4 597 253.294	2.833
32	Perth	-2 375 382.732	2.505	4 875 545.638	2.621	-3 345 387.849	2.728
38	Revilla	-2 160 960.225	2.510	-5 642 694.520	3.078	2 035 358.416	3.176
39	Pitcairn	-3 724 745.647	6.280	-4 421 218.035	5.694	-2 686 087.346	5.255
40	Cocos	-741 953.040	3.161	6 190 790.099	3.069	-1 338 547.676	2.752
42	Addis Ababa	4 900 753.422	2.762	3 968 244.643	2.626	966 329.417	2.552
43	Sombroero	1 371 383.334	2.724	-3 614 745.095	3.157	-5 055 927.530	3.641
44	Heard	1 098 912.818	5.747	3 684 612.693	6.212	-5 071 853.727	7.780
45	Mauritius	3 223 440.444	2.656	5 045 332.006	2.739	-2 191 798.454	2.698
47	Zamboanga	-3 361 931.463	2.812	5 365 800.248	3.094	763 627.375	3.330
50	Palmer	1 192 684.033	3.433	-2 450 986.983	4.323	-5 747 037.701	4.672
51	Mawson	1 111 352.024	4.285	2 169 264.675	3.238	-5 874 322.862	4.844
52	Wilkes	-902 583.987	3.525	2 409 530.660	3.232	-5 816 542.503	4.730
53	McMurdo	-1 310 828.143	3.356	311 271.145	3.073	-6 213 265.956	3.958
55	Ascension	6 118 342.544	3.108	-1 571 732.245	2.883	-878 608.379	3.089
59	Christmas	-5 885 315.086	3.027	-2 448 357.151	2.732	221 669.643	3.145
60	Culgoora	-4 751 621.039	2.483	2 792 063.383	2.372	-3 200 156.628	2.442
61	So. Georgia	2 999 924.593	3.745	-2 219 357.041	4.232	-5 155 247.563	4.886
63	Dakar	5 884 475.772	2.853	-1 853 478.486	2.307	1 612 848.261	2.930
64	Chad	6 023 393.960	2.749	1 617 940.871	2.236	1 331 726.674	2.508
65	Hohenpeissenberg	4 213 570.222	2.356	820 837.313	2.346	4 702 769.262	2.758
67	Natal	5 186 415.778	3.301	-3 653 921.575	3.208	-654 288.938	3.072
68	Johannesburg	5 084 832.837	3.146	2 670 338.698	2.580	-2 768 083.655	3.248
69	Da Cunha	4 978 430.027	7.231	-1 086 856.181	5.644	-3 823 164.893	7.581
72	Thailand	-941 678.219	3.661	5 967 438.461	3.337	2 039 300.514	2.969
73	Chagos	1 905 147.827	2.911	6 032 272.479	3.482	-810 729.775	3.001
75	Mahe	3 602 828.788	3.024	5 238 237.170	3.096	-515 947.433	2.773
111	Wrightwood	-2 448 831.364	2.679	-4 667 972.160	3.052	3 582 744.578	3.162

<sup>a</sup> Add 6000 to station numbers.

TABLE 7.16.—Coordinate Differences Between Translated BC-4 Solution and Combined Solution After XYZ Fit ( $\Delta = BC-4$  Solution - Combined Solution)

No. <sup>a</sup>	Station name	$\Delta\phi$ (m)	$\Delta\lambda$ (m)	$\Delta h$ (m)	Resultant (m)
1	Thule	4.905	-0.684	3.289	5.945
2	Beltsville	0.185	2.209	-1.853	2.889
3	Moses Lake	-1.735	4.091	0.269	4.452
4	Shemya	1.505	4.864	9.935	11.164
6	Tromso	-1.757	-5.547	4.648	7.447
7	Azores	-0.822	-4.204	1.007	4.400
8	Surinam	0.515	2.110	-3.960	4.517
9	Quito	0.156	7.501	-2.580	7.933
11	Maui	0.582	-2.418	1.395	2.852
12	Wake	-2.316	-4.665	-8.936	10.343
13	Kanoya	5.430	-0.159	0.670	5.474
15	Mashhad	0.712	1.603	2.850	3.347
16	Catania	0.101	-3.388	3.223	4.677
19	Dolores	-10.566	4.851	3.581	12.165
20	Easter	-0.379	10.325	4.284	11.185
22	Pago Pago	0.561	-3.868	-2.642	4.718
23	Thursday	-0.403	-3.230	-5.313	6.231
31	Invercargill	-2.236	-5.096	-1.787	5.845
32	Perth	-2.256	1.600	-3.654	4.583
38	Revilla	-1.674	4.430	0.880	4.816
39	Pitcairn	0.968	1.486	1.936	2.625
40	Cocos	1.943	2.522	-1.498	3.518
42	Addis Ababa	3.113	0.599	1.303	3.427
43	Sombrero	-13.364	5.306	10.147	17.598
44	Heard	-1.623	3.003	-1.282	3.646
45	Mauritius	2.317	1.935	-1.021	3.187
47	Zamboanga	2.878	0.990	-4.290	5.260
50	Palmer	-17.711	1.139	12.169	21.519
51	Mawson	-1.968	3.462	-0.566	4.022
52	Wilkes	-5.689	1.977	-1.901	6.315
53	McMurdo	-5.707	-3.880	-0.698	6.936
55	Ascension	-2.133	-4.243	1.390	4.948
59	Christmas	-0.003	-2.663	-1.335	2.978
60	Culgoora	-2.556	-4.203	-3.594	6.092
61	So. Georgia	-13.290	-3.515	8.088	15.950
63	Dakar	-0.078	-3.618	0.264	3.628
64	Chad	0.396	-1.160	1.656	2.060
65	Hohenpeissenberg	0.397	-4.163	4.660	6.261
67	Natal	-3.810	-3.519	0.459	5.207
68	Johannesburg	1.930	0.627	-2.082	2.908
69	Da Cunha	-7.851	-6.563	6.722	12.243
72	Thailand	3.621	4.358	-2.717	6.284
73	Chagos	3.124	1.925	-1.213	3.865
75	Mahe	3.651	1.386	-1.143	4.069
78	Vila Efate	0.192	-4.949	-3.148	5.868
111	Wrightwood	-0.250	4.706	0.827	4.784
123	Point Barrow	-0.378	6.691	4.322	7.974
rms values		$\pm 4.817$	$\pm 3.974$	$\pm 4.183$	$\pm 7.516$ n = 47

<sup>a</sup> Add 6000 to station numbers.

TABLE 7.17.—*Coordinate Differences Between Transformed Doppler Solution and Combined Solution After XYZ Fit ( $\Delta$  = Combined Solution - Doppler)*

No. <sup>a</sup>	Station name	$\Delta\phi$ (m)	$\Delta\lambda$ (m)	$\Delta h$ (m)	Resultant (m)
1	Thule -----	4.948	-1.690	7.309	8.987
2	Beltsville -----	-2.044	-0.855	-2.602	3.418
3	Moses Lake -----	-1.540	1.573	-3.619	4.236
4	Shemya -----	4.433	8.980	5.727	11.537
6	Tromso -----	-0.062	-11.187	3.029	11.590
7	Azores -----	-10.072	-1.351	3.282	10.679
8	Surinam -----	-1.574	0.269	-4.707	4.970
9	Quito -----	5.469	3.704	-4.496	7.991
11	Maui -----	3.717	0.755	8.146	8.986
12	Wake -----	-11.845	-6.005	-14.576	19.718
13	Kanoya -----	1.320	0.417	4.100	4.327
15	Mashhad -----	2.605	2.585	-1.262	3.881
16	Catania -----	0.976	1.908	0.143	2.148
19	Dolores -----	-9.064	11.106	-7.536	16.195
20	Easter -----	7.860	4.731	-0.514	9.188
22	Pago Pago -----	4.182	-1.580	-1.630	4.758
23	Thursday -----	-0.665	-3.988	-8.993	9.860
31	Invercargill -----	-4.103	-4.126	-2.665	6.400
32	Perth -----	6.200	-1.870	5.400	8.432
38	Revilla -----	-4.009	-3.528	2.629	5.953
40	Cocos -----	1.678	-2.067	4.543	5.265
42	Addis Ababa -----	10.339	-2.729	4.697	11.679
43	Sombrero -----	-7.959	-1.174	14.647	16.711
45	Mauritius -----	1.132	3.045	2.671	4.206
47	Zamboanga -----	0.682	2.454	-4.308	5.004
50	Palmer -----	-3.410	-5.423	1.174	6.512
53	McMurdo -----	-11.079	2.695	-2.663	11.709
55	Ascension -----	-6.249	-6.384	-1.088	9.000
59	Christmas -----	4.643	-1.483	-1.990	5.265
60	Culgoora -----	-8.968	-4.719	1.850	10.302
63	Dakar -----	0.028	9.353	-0.024	9.354
64	Chad -----	4.612	3.340	3.648	6.763
65	Hohenpeissenberg ---	4.508	-3.934	1.788	6.244
67	Natal -----	-7.821	-1.469	3.266	8.602
68	Johannesburg -----	-1.506	1.312	-5.527	5.876
72	Thailand -----	-0.145	2.282	-5.246	5.723
75	Mahe -----	4.334	-1.677	-4.459	6.441
	rms values	$\pm 5.588$	$\pm 4.436$	$\pm 5.339$	$\pm 8.911$

<sup>a</sup> Add 6000 to station numbers.

TABLE 7.18

Input	Additional data	Type of solution	$a$ 6 378 ... (m)	$1/f$	$\Delta X$ (m)	$\Delta Y^a$ (m)	$\Delta Z$ (m)
(1) } BC-4 result, (2) } 43 stations	{ MSL elevations	Unconstrained ellipsoid fit	130.17	298.377	+16.20	-14.82	-16.40
	{ The same	Ellipsoid fit constrained to dynamically determined $1/f$	132.80	298.250	+16.29	-15.32	-16.74
(3) } Combined solution, (4) } 43 stations	{ The same	Unconstrained ellipsoid fit	133.98	298.246	+1.373	+2.434	-1.844
	{ The same	Ellipsoid fit constrained to dynamically determined $1/f$	133.90	298.250	+1.370	+2.453	-1.835
(5) }	{ The same	Ellipsoid fit constrained to dynamically determined $1/f$ and to Anderle mass center position	134.02	298.250	0	0	0
(6) } BC-4 result, (7) } 37 stations	{ MSL elevations and Anderle geoidal heights $N$	as in (1) above	126.47	298.409	+14.702	-19.482	-13.816
	{ The same	as in (2) above	129.45	298.250	+15.140	-20.181	-15.252
(8) } Combined solution, (9) } 37 stations	{ The same	as in (3) above	128.83	298.322	-1.900	-0.378	+1.183
	{ The same	as in (4) above	130.21	298.250	-1.756	-0.764	+0.721
(10) }	{ The same	as in (5) above	130.22	298.250	0	0	0
(11) BC-4 result, Doppler result, for 37 stations	None	XYZ fit between Doppler and BC-4 result	130.48 $\pm 1.58$	-----	+19.590 $\pm 1.34$	-17.684 $\pm 1.33$	-14.344 $\pm 1.51$

<sup>a</sup> Left-handed system: reverse signs.

TABLE 7.19.—*Geographic Coordinates From Combined Solution Computed With  $a = 6378130$  m and  $f = 1:298,250$  m*

Station no. <sup>a</sup>	Station name	Latitude			$\sigma_\phi$ (m)	Longitude (east)			$\sigma_\lambda$ (m)	Ellipsoid height (m)	$\sigma_h$ (m)
		deg	min	sec		deg	min	sec			
1	Thule	N 76	30	4.8627	2.184	291	27	59.4280	2.675	219.379	3.236
2	Beltsville	N 39	01	39.3318	2.540	283	10	27.9765	2.440	-1.458	3.264
3	Moses Lake	N 47	11	6.6534	2.424	240	39	43.5760	2.308	336.069	3.069
4	Shemya	N 52	42	48.9705	3.782	174	7	26.0462	3.475	39.745	4.193
6	Tromso	N 69	39	44.4978	2.361	18	56	27.5273	2.535	133.357	3.211
7	Azores	N 38	45	36.0847	2.864	332	54	25.2813	2.652	108.829	3.546
8	Surinam	N 05	26	53.4378	3.457	304	47	40.6928	2.880	-20.115	3.585
9	Quito	S 0	5	51.7281	3.504	281	34	47.4488	3.163	2694.047	3.937
11	Maui	N 20	42	26.9218	3.045	203	44	38.3808	2.696	3075.656	3.522
12	Wake	N 19	17	28.2961	2.947	166	36	39.4948	2.896	4.297	3.589
13	Kanoya	N 31	23	42.5648	3.278	130	52	16.2716	3.390	83.416	3.694
15	Mashhad	N 36	14	25.5340	2.441	59	37	43.9207	2.459	963.436	2.860
16	Catania	N 37	26	38.5025	2.158	15	2	44.8491	2.240	45.972	2.800
19	Dolores	S 31	56	35.5287	2.992	294	53	38.5873	2.579	627.599	3.203
20	Easter	S 27	10	36.4176	3.317	250	34	22.7515	3.544	219.755	4.554
22	Pago Pago	S 14	19	54.4748	3.141	189	17	8.7112	2.701	35.347	3.223
23	Thursday Is.	S 10	35	2.9982	2.511	142	12	39.5544	2.341	119.259	2.718
31	Invercargill	S 46	24	58.1142	2.542	168	19	31.6698	2.588	-0.007	2.949
32	Perth	S 31	50	24.9112	2.482	115	58	31.8154	2.420	-8.327	2.927
38	Revilla	N 18	43	58.2071	3.020	249	2	41.4901	2.515	-14.701	3.235
39	Pitcairn	S 25	4	6.8403	3.686	229	53	12.6661	4.975	317.220	7.817
40	Cocos	S 12	11	44.0207	2.682	96	50	3.0512	3.132	-29.827	3.163
42	Addis Ababa	N 8	46	12.5193	2.574	38	59	52.1902	2.607	1872.647	2.766
43	Sombrero	S 52	46	52.5872	3.472	290	46	33.7413	2.662	95.214	3.378
44	Heard	S 53	1	9.0693	6.472	73	23	35.2173	6.032	39.662	7.314
45	Mauritius	S 20	13	53.1132	2.586	57	25	32.4106	2.634	137.814	2.869
47	Zamboanga	N 6	55	20.7741	3.324	122	4	8.8287	2.696	71.335	3.215
50	Palmer	S 64	46	26.7693	4.870	295	56	53.4936	3.289	26.028	4.184
51	Mawson	S 67	36	4.8017	3.925	62	52	23.3298	3.829	39.813	4.690
52	Wilkes	S 66	16	44.9811	3.267	110	32	7.4526	3.359	10.755	4.808
53	McMurdo	S 77	50	41.6571	3.445	166	38	30.7416	3.006	-41.095	3.907
55	Ascension	S 7	58	15.4065	3.058	345	35	34.4179	2.943	83.939	3.092
59	Christmas	N 2	0	18.3902	3.148	202	35	16.2920	2.593	24.514	3.157
60	Culgoora	S 30	18	34.2631	2.339	149	33	41.0676	2.275	235.088	2.666
61	So. Georgia	S 54	17	1.1326	3.750	323	30	20.9006	4.454	19.203	4.659
63	Dakar	N 14	44	42.1988	2.847	342	31	0.2512	2.306	55.378	2.945
64	Chad	N 12	7	54.5921	2.520	15	2	7.0547	2.223	306.766	2.756
65	Hohenpeissenberg	N 47	48	3.9953	2.184	11	1	25.0048	2.296	977.952	2.928
67	Natal	S 5	55	39.0642	3.061	324	50	4.6598	3.199	38.288	3.328
68	Johannesburg	S 25	52	59.1717	2.975	27	42	23.5867	2.587	1536.885	3.402
69	Da Cunha	S 37	3	53.6135	6.418	347	41	5.3077	5.714	45.432	8.227
72	Thailand	<sup>a</sup> N 18	46	10.5737	2.770	98	58	2.9441	3.622	259.580	3.545
73	Chagos	S 7	21	6.6304	2.994	72	28	21.1236	2.969	-72.915	3.446
75	Mahe	S 4	40	14.6759	2.753	55	28	48.1258	2.830	545.382	3.298
111	Wrightwood	N 34	22	54.4315	2.628	242	19	6.1310	2.757	2252.261	3.457

<sup>a</sup> Add 6000 to station numbers.

TABLE 7.20.—*Components of Vertical Deflections ( $\Delta = \text{Astro} - \text{Geodetic}$ )*

Station no. <sup>a</sup>	$\Delta\phi''$	$\Delta\lambda''$	$\eta'' = \Delta\lambda'' \cos\phi$	$\cos\phi$
001	6.81	-48.34	-11.28	0.2334
002	-1.60	7.37	5.72	0.7768
003	-3.41	-0.63	-0.43	0.6796
004	14.51	18.87	11.43	0.6058
006	-1.26	19.51	6.78	0.3475
007	7.20	10.13	7.90	0.7797
008	-4.48	-1.90	-1.89	0.9955
009	-1.36	9.46	9.46	1.0000
011	-5.06	-1.33	-1.24	0.9353
012	-3.90	-14.31	-13.51	0.9439
013	-4.08	9.44	8.06	0.8537
015	2.29	16.88	13.62	0.8066
016	0.20	18.34	14.56	0.7939
020	-2.79	-5.26	-4.68	0.8896
022	-13.87	-0.86	-0.83	0.9689
023	-3.78	-4.66	-4.58	0.9830
031	-2.94	3.23	2.23	0.6894
032	0.34	-28.10	-23.87	0.8496
038	-13.28	-2.21	-2.09	0.9470
039	-0.31	-0.79	-0.72	0.9058
040	-13.89	-15.97	-15.61	0.9774
042	-6.78	5.00	4.94	0.9883
043	1.85	-7.30	-4.42	0.6048
044	-2.96	-7.80	-4.70	0.6016
045	15.63	-39.61	-37.17	0.9383
047	-2.48	-2.38	-2.36	0.9927
050	-7.21	-16.45	-7.01	0.4260
051	1.72	1.08	0.41	0.3811
052	-0.14	-2.84	-1.14	0.4022
053	-1.66	-16.88	-3.55	0.2105
055	-2.86	-4.78	-4.73	0.9903
059	17.23	5.67	5.66	0.0994
060	-1.88	-9.96	-8.60	0.8633
061	21.62	21.63	12.63	0.5838
063	2.03	-4.66	-4.51	0.9670
064	-0.65	1.91	1.87	0.9777
065	5.54	5.53	3.71	0.6717
067	1.32	-1.69	-1.68	0.9946
068	9.11	7.59	6.83	0.8997
069	27.35	-11.75	-9.38	0.7981
072	-23.07	5.44	5.15	0.9468
073	8.10	11.04	10.95	0.9918
075	4.37	5.85	5.83	0.9967
111	6.37	18.49	15.26	0.8253

<sup>a</sup> Add 6000 to station numbers.

TABLE 7.21.—*Height of Geoid Above Ellipsoid (N) = Ellipsoid Height (h) Minus Mean Sea Level Elevation (H)*

Station no. <sup>a</sup>	(1) N Combined solution based on 6378130 (m)	(2) N Anderle solution (m)	(3) $\Delta N$ (m)
1	13.379	7.30	+6.08
2	-45.758	-43.7	-2.05
3	-32.671	-29.70	-2.97
4	2.985	-3.40	+6.38
6	27.357	24.16	+3.20
7	55.569	51.87	+3.70
8	-38.495	-34.25	-4.25
9	11.947	15.90	-3.95
11	26.386	15.81	+10.58
12	0.837	15.08	-14.24
13	17.516	27.80	-10.28
15	-27.614	-26.80	-0.81
16	36.972	36.42	0.55
19	19.419	26.44	-7.02
20	-11.045	-11.20	0.16
22	30.007	30.83	-0.82
23	59.659	67.88	-8.22
31	-0.957	0.95	-1.91
32	-34.627	-40.30	5.68
38	-37.901	-41.20	3.30
39	-22.170	-----	-----
40	-34.237	-39.40	5.16
42	-13.813	-18.90	5.09
43	14.554	-0.65	15.20
44	35.891	-----	-----
45	0.336	-3.54	3.15
47	61.944	65.56	-3.62
50	9.588	7.84	1.75
51	28.813	-----	-----
52	-7.245	-----	-----
53	-60.185	-58.20	-1.98
55	12.999	13.72	-0.72
59	21.764	22.95	-1.19
60	23.988	21.37	2.62
61	15.023	-----	-----
63	29.098	28.75	0.35
64	11.356	7.35	4.01
65	34.452	34.06	0.39
67	-2.342	-6.09	3.75
68	13.085	17.70	-4.62
69	20.002	-----	-----
72	-48.820	-44.12	-4.70
73	-76.766	-----	-----
75	-43.598	-39.18	-4.42
111	-32.140	-----	-----
			$\Sigma = +3.33$
			RMS = $\pm 5.57$

<sup>a</sup> Add 6000 to station numbers.

TABLE 7.22.—Station Shifts ( $\Delta$  = Combined Solution - Survey)

Station <sup>a</sup>	Datum	$\Delta X$ (m)	$\Delta Y^b$ (m)	$\Delta Z$ (m)	$N$ (m)	Ellipsoid
002	North American	-15.464	-175.238	+170.683	-0.4	Clarke 1866
003		-15.073	-168.389	+176.173	-16.0	
004		-14.839	-224.661	+125.460	-46.0	
111		-14.909	-156.030	+174.079	-23.0	
023	Australian	-124.696	+59.448	+145.870	-4.6	AND
032		-122.122	+61.380	+148.912	+15.4	
060		-120.584	+58.544	+140.350	+0.7	
006	European	-95.289	+87.386	-130.319	+12.6	International
015		-102.814	+116.573	-157.106	-38.0	
016		-94.780	+97.941	-128.373	-16.6	
065		-98.045	+94.773	-130.038	-0.6	
042	Adindan	-175.031	+22.702	+207.848	-8.0	Clarke 1880
063		-159.895	+18.666	+211.616	+20.7	
064		-162.790	+18.035	+201.089	+23.6	
009	S.A.D. 1969	-62.026	-30.896	-38.650	+24.6	South American
019		-84.870	-10.993	-28.779	+13.0	
067		-79.113	+2.203	-44.415	+26.14	
001	QORNOQ	+193.755	-152.336	-179.116	+32.0	International
007	S.W. Base on Int.	-146.464	-189.307	-85.530	+55.569	International <sup>c</sup>
008	Prov. S.A. 1956	-285.742	-124.472	-364.343	+3.0	International
011	Old Hawaiian	+89.609	+272.174	-204.940	+26.28	Clarke 1866
012	1952 Astro on Int.	+297.342	+62.206	+118.723	+0.837	International <sup>c</sup>
013	Tokyo	-112.208	-476.369	+643.232	+27.0	Bessel
022	Am. Samoa 1962	-75.859	-125.169	+431.583	+22.0	Clarke 1866
031	Geodetic 1949	+86.529	+29.100	+204.364	-0.957	International <sup>c</sup>
043	Prov. S. Chile 1963	+4.265	-209.046	+104.397	+14.554	International <sup>c</sup>
045	LePonce Astro on 1880	-750.581	-159.580	-507.541	-0.386	Clarke 1880 <sup>c</sup>
047	Luzon	-72.235	+115.447	-115.971	+61.944	Clarke 1886 <sup>c</sup>
055	Ascension Is. 1958	-231.471	-111.769	+48.248	+12.999	International <sup>c</sup>
068	Buffelsfont	-153.391	+130.351	-283.829	+13.085	Clarke 1880 <sup>c</sup>
072	Indian	+230.419	-827.968	+291.150	-48.820	Everest <sup>c</sup>
075	Mahe 1971	+60.571	+197.879	-140.513	-43.598	Clarke 1880 <sup>c</sup>
007	Astro	+12.302	+280.978	-173.013	+55.569	Comb. Solution <sup>c</sup>
012	Astro 1952	-58.951	+415.588	+113.310	+0.837	$a = 6378130^c$
020	Astro 1967	+123.534	+85.205	+76.460	-11.045	$f = 1:298.25^c$
038	Astro Is. Soc.	+107.336	-99.244	+386.616	-37.901	$f = 1:298.25^c$
039	Astro 1967	+14.216	+17.322	+8.608	-22.170	$f = 1:298.25^c$
040	Astro Anna 1 1965	-490.078	-32.066	+417.173	-34.237	$f = 1:298.25^c$
044	Astro 1969	-118.468	-111.631	+55.102	+35.891	$f = 1:298.25^c$
045	Astro LePonce	-1058.365	-479.038	-451.105	-0.386	$f = 1:298.25^c$
050	Astro 1969	+283.896	+86.525	+95.174	+9.588	$f = 1:298.25^c$
051	Astro 1969	-11.130	+49.721	-20.296	+28.813	$f = 1:298.25^c$
052	Astro 1969	-34.580	+8.773	+1.786	-7.245	$f = 1:298.25^c$
053	Astro Camp Area 1961/62	-74.517	+95.634	+10.908	-60.185	$f = 1:298.25^c$
059	Astro Christmas Is. 1967	-84.514	-154.619	-528.955	+21.764	$f = 1:298.25^c$
061	Astro	-669.022	-8.101	-390.231	+15.023	$f = 1:298.25^c$
069	Astro 1968	-434.607	-392.099	-672.974	+20.602	$f = 1:298.25^c$
073	ISTS Astro 1969	+313.175	+132.303	-246.794	-76.765	$f = 1:298.25^c$

<sup>a</sup> Add 6000 to station numbers.

<sup>b</sup> Left-handed system; reverse signs on  $\Delta Y$

<sup>c</sup>  $N$  obtained from combined solution (table 7.21, col. 1) because of lack of corresponding survey data.

TABLE 7.23.—Datum Shifts

Datum	Stations	Residual coordinate differences after datum shift			Datum shift parameters					
		$\Delta\phi$ [m]	$\Delta\lambda$ east [m]	$\Delta h$ [m]	Scalar	$\Delta\lambda$ rotation + $\lambda$ east X to Y	Translations			
							$\Delta X$ (m)	$\Delta Y$ (m)	$\Delta Z$ (m)	
NAD	002	-1.9	-1.9	-2.4	1.000 000 065 6	-7680	-31.6	+171.1	+173.4	
	003	+6.1	-0.5	-2.2						
	111	-2.6	+2.1	+4.6						
AUS	023	+1.2	+1.4	+1.6	0.999 999 939 9	+70730	-124.1	-61.0	+144.9	
	032	+2.8	+0.3	-2.8						
	060	-4.8	-1.9	+1.1						
Europe	006	-0.1	-0.3	+0.2	0.999 999 172 0	+7563	-96.4	-78.9	-125.6	
	016	-0.2	-0.3	+0.9						
	065	+0.4	+0.4	-1.1						
South American 1969	009	+5.4	+10.4	-3.4	0.999 994 906 7	+7101	-43.5	-1.9	-44.1	
	019	-2.3	-13.5	-0.4						
	067	-3.3	+1.1	+3.7						
Adindan	042	+1.3	+0.6	-2.2	0.999 999 979 4	-5231	-162.6	-34.0	+206.9	
	063	+5.1	-0.2	-0.6						
	064	-6.5	-0.4	+2.8						